

Electromagnetic properties of DBSA-doped polyaniline

Baćani, Mirko

Doctoral thesis / Disertacija

2014

Degree Grantor / Ustanova koja je dodijelila akademski / stručni stupanj: **University of Zagreb, Faculty of Science / Sveučilište u Zagrebu, Prirodoslovno-matematički fakultet**

Permanent link / Trajna poveznica: <https://um.nsk.hr/um:nbn:hr:217:107232>

Rights / Prava: [In copyright](#)/[Zaštićeno autorskim pravom.](#)

Download date / Datum preuzimanja: **2024-11-25**



Repository / Repozitorij:

[Repository of the Faculty of Science - University of Zagreb](#)





UNIVERSITY OF ZAGREB
FACULTY OF SCIENCE
PHYSICS DEPARTMENT

Mirko Baćani

**Electromagnetic properties
of DBSA-doped polyaniline:
from fundamentals towards application**

doctoral thesis

Zagreb, 2014



SVEUČILIŠTE U ZAGREBU
PRIRODOSLOVNO – MATEMATIČKI FAKULTET
FIZIČKI ODSJEK

Mirko Baćani

**Elektromagnetska svojstva
polianilina dopiranog s DBSA:
od temelja prema primjeni**

doktorska disertacija

Zagreb, 2014.



UNIVERSITY OF ZAGREB
FACULTY OF SCIENCE
PHYSICS DEPARTMENT

Mirko Baćani

**Electromagnetic properties
of DBSA-doped polyaniline:
from fundamentals towards application**

doctoral thesis

supervisor:
Dr Dinko Babić

Zagreb, 2014

BASIC DOCUMENTATION CARD

University of Zagreb
Faculty of Science
Physics Department

Doctoral Thesis

Electromagnetic properties of DBSA-doped polyaniline: from fundamentals towards application

MIRKO BAĆANI

Faculty of Science, University of Zagreb

We have carried out a comparative experimental study of the dc electrical conductivity σ and magnetic susceptibility χ of own-made polyaniline (PANI) pellets doped with dodecylbenzenesulphonic acid (DBSA), a long molecule with surfactant properties. For all samples, we find that σ at low temperatures (T) is governed by the variable-range hopping (VRH) in a homogeneously disordered three-dimensional (3D) system of coupled one-dimensional (1D) chains. Depending on the doping and the corresponding disorder level, the VRH exponents are either $1/2$, $2/5$, or $1/4$. At higher T , in all samples, we find an exponent 1 that signifies nearest-neighbour hopping. All these exponents are predicted in a model by Fogler, Teber, and Shklovskii for the charge transport in quasi-1D Anderson-Mott insulators, and conditions for their appearance depend on disorder and T . We identified the presence of a soft (Coulomb) gap in our samples, which signifies a long-range Coulomb interaction.

Change from one exponent into another in $\sigma(T)$ appears at a crossover temperature T^* where there are also noticeable features in $\chi(T)$. This coupling of charge and spin is discussed in the spirit of $k_B T^*$ being the thermal energy which causes an enhancement of the density of delocalised (Pauli) spins at the expense of localised (Curie) spins as T rises above T^* . Utilising the observed correlation between spin dynamics and electronic transport, we estimate the energy scales in the electronic structure of PANI-DBSA.

Utilising a property that both PANI-DBSA and multiwall carbon nanotubes (MWCNT's) are soluble in chloroform, we have produced bulk blends of these two materials, the achieved mass fraction of MWCNT's being up to 40 %. This is as remarkable as the accompanying effective loss of the temperature dependence of σ : it decreases by only 3 times from room temperature to 10 K, whereas this decrease for pure PANI-DBSA is by a factor of 10^6 . Thus, our blends simultaneously offer a solution to the problem of applications of MWCNT's in bulk form, as well as to that of

poor conductivity of PANI–DBSA at low T . It is also possible to make thin films, both of PANI–DBSA and of the blends, on a commercial plastic substrate (FR4).

(168 pages, 239 references, original in English)

Keywords: Polyaniline, Electrical conductivity, Hopping transport, Coulomb gap, Magnetic susceptibility, Carbon nanotubes, Blends

Supervisor: Dr Dinko Babić, Institute for Medical Research
and Occupational Health, Zagreb

Committee:

1. Prof Ivan Kokanović, University of Zagreb
2. Dr Dinko Babić, senior research associate, IMI Zagreb
3. Prof László Forró, EPFL Lausanne, Switzerland
4. Dr Osor Barišić, research associate, IF Zagreb
5. Prof Hrvoje Buljan, University of Zagreb

Replacements:

1. Dr Eduard Tutiš, senior scientist, IF Zagreb
2. Prof Krešo Zadro, University of Zagreb

Thesis accepted: 08 April 2014

TEMELJNA DOKUMENTACIJSKA KARTICA

Sveučilište u Zagrebu
Prirodoslovno-matematički fakultet
Fizički odsjek

Doktorska disertacija

Elektromagnetska svojstva polianilina dopiranog s DBSA: od temelja prema primjeni

MIRKO BAĆANI

Prirodoslovno-matematički fakultet, Sveučilište u Zagrebu

Provedeno je komparativno eksperimentalno istraživanje temperaturne (T) ovisnosti istosmjernje električne vodljivosti σ i magnetske susceptibilnosti χ na tabletama polianilina (PANI) dopiranog s dodecilbensulfonskom kiselinom (DBSA), koja je dugačka molekula sa surfaktantskim svojstvima. Niskotemperaturno ponašanje u svim uzorcima karakterizirano je skočnom vodljivošću promjenjivog dosega (VRH) u homogeno neuređenom trodimenzionalnom (3D) sustavu vezanih jednodimenzionalnih (1D) lanaca. Ovisno o dopiranju i pripadnom stupnju nereda u materijalu, VRH eksponenti su $1/2$, $2/5$ ili $1/4$, dok je na višim T u svim uzorcima nađen eksponent 1, koji ukazuje na redukciju srednjeg dosega skokova na prve susjede. Svi ti eksponenti anticipirani su u teoriji Foglera, Tebera, i Shklovskiija za transport naboja u kvazi-1D Anderson-Mott izolatorima, a uvjeti za njihovo pojavljivanje ovise o neredu i T . Utvrdili smo prisustvo mekog (kulonskog) procijepa, što ukazuje na postojanje dugodosežne kulonske interakcije u našim uzorcima.

Promjene s jednog eksponenta na drugi zbivaju se u $\sigma(T)$ na temperaturama prijelaza T^* , gdje su također zamjetne i promjene u $\chi(T)$ krivuljama, što ukazuje na vezanje naboja i spina. Diskutirano je kako $k_B T^*$ ima ulogu termičke energije koja uzrokuje povećanje gustoće delokaliziranih (Paulijevih) spinova na račun lokaliziranih (Curiejevih) spinova pri porastu T iznad T^* . Uočena korelacija između spinske dinamike i elektronskog transporta omogućila nam je procjenu energijskih skala u elektronskoj strukturi PANI-DBSA.

Koristeći svojstvo topivosti u kloroformu, koje je zajedničko i PANI-DBSA polimeru i višezidnim ugljikovim nanocjevčicama (MWCNT), načinili smo volumne kompozite ta dva materijala. Postignut je značajan maseni udio MWCNT od do 40 %. Značajan je i prateći efektivni gubitak temperaturne ovisnosti σ : smanji se svega 3 puta od sobne temperature do 10 K, dok je to smanjenje za čisti PANI-DBSA za faktor 10^6 . Tako

naši blendovi istovremeno nude rješenje problema primjene MWCNT u volumnom obliku, te problema loše vodljivosti PANI–DBSA na niskim T . Također je moguće raditi tanke filmove, i od PANI–DBSA i od blendova, na komercijalnom plastičnom supstratu (FR4).

(168 stranica, 239 literaturnih navoda, jezik izvornika engleski)

Ključne riječi: polianilin, električna vodljivost, skočna vodljivost, kulonski procijep, magnetska susceptibilnost, ugljikove nanocjevčice, kompoziti

Mentor: Dr. sc. Dinko Babić, Institut za medicinska istraživanja
i medicinu rada, Zagreb

Ocjenjivači: 1. Izv. prof. dr. sc. Ivan Kokanović, Sveučilište u Zagrebu
2. Dr. sc. Dinko Babić, viši znanstveni suradnik, IMI Zagreb
3. Prof. dr. sc. László Forró, EPFL Lausanne, Švicarska
4. Dr. sc. Osor Barišić, znanstveni suradnik, IF Zagreb
5. Prof. dr. sc. Hrvoje Buljan, Sveučilište u Zagrebu

Zamjene: 1. Dr. sc. Eduard Tutiš, znanstveni savjetnik, IF Zagreb
2. Prof. dr. sc. Krešo Zadro, Sveučilište u Zagrebu

Rad prihvaćen: 08. travnja 2014.

Acknowledgments

I would like to thank my supervisor Dr Dinko Babić (Sveučilište u Zagrebu & Institut za medicinska istraživanja Zagreb) for introducing me to this exciting field of research. I am immensely honoured to have had his guidance in my formal education as a physicist. His characteristically level-headed remarks have oriented our discussions and debates towards producing light, not heat. His persistence upon the paradigm of “you don’t understand it if you can’t explain it to your granny”, a paradigm that I recognise as his own version of the Epstein law [1], has often been demanding but always rewarding. I am also grateful for his patience and friendly support, which were most helpful in difficult moments — sometimes even key ingredients of disentanglement.

My sincere gratitude goes to Prof Ivan Kokanović (Sveučilište u Zagrebu & University of Cambridge) for sharing his knowledge and kindness, and particularly for performing the measurements of magnetic susceptibility at the Cavendish Laboratory, University of Cambridge. I am grateful to Dr Mario Novak (Sveučilište u Zagrebu & Osaka University) for helping me to solve many problems, especially during long lab hours. Without his involvement, this work would not have been possible.

The work presented in this thesis has been funded by the Croatian Ministry of Science, Education and Sports under grant No. 119-1191458-1008. I also acknowledge Helmholtz-Zentrum Dresden-Rossendorf for awarding me the scholarship for the 3rd EuroMagNET Summer School.

I would like to acknowledge the following experts for their involvement in experiments on my samples. Dr Stjepko Fazinić (Institut Ruđer Bošković Zagreb) provided results of elemental analysis of my samples, our collaboration was fruitful and indispensable in the early stage of my research. Dr Krunoslav Prša (ETH Zürich & EPFL Lausanne) and Dr Mirta Herak (Institut za fiziku Zagreb) took part in measurements of magnetic susceptibility. Dr Ognjen Milat (Institut za fiziku Zagreb) determined the thickness of the films by high-resolution optical microscopy. Prof Antun Tonejc (Sveučilište u Zagrebu) performed X-ray diffraction measurements. Dr Matthew D. Steinberg (GoSense Wireless Ltd Cambridge) provided first test specimens of FR4.

I have benefited from discussions and insightful suggestions from Prof Sofian Teber (Université Pierre-et-Marie-Curie Paris), Prof Bertram Batlogg (ETH Zürich), Dr Krunoslav Prša (ETH Zürich & EPFL Lausanne), Prof Emil Babić (Sveučilište u Zagrebu), Dr Andrzej Sienkiewicz (EPFL Lausanne), Dr Osor S. Barišić (Institut za fiziku Zagreb), Prof Eric Beaugnon (LNCMI Grenoble), Prof James S. Brooks (NHMFL Tallahassee), Prof Damir Pajić (Sveučilište u Zagrebu), Prof Jean-Paul Pouget (Université

Paris-Sud Orsay), Dr Eduard Tutiš (Institut za fiziku Zagreb), Prof Natasha Kirova (Université Paris-Sud Orsay), Prof Frederic Mila (EPFL Lausanne), and Prof Ivana Murković Steinberg (Sveučilište u Zagrebu). I would also like to thank Academician Slaven Barišić (Sveučilište u Zagrebu), former director of Doctoral Studies in Condensed Matter Physics at the University of Zagreb, for his support.

I also appreciate occasional discussions — usually not related to my research but rather to condensed matter physics in general — with my colleagues in Zagreb, particularly those with Marko Bosiočić and Dr Marinko Jablan.

Various technical assistance provided by departmental administration staff — Mrs Marina Kavur, Mrs Gordana Stubičan-Ladešić, Mr Ivan Gladović, Mrs Jasna Čorko, Mrs Marina Pavičić, Mrs Sandra Požar, Mrs Dijana Turkalj, Mr Tomislav Sermek and Mr Marko Šušak — is gratefully acknowledged.

Prof Miguel Monteverde (Université Paris-Sud Orsay) most kindly introduced me to the physics of Dirac fermions. Although this field was not related to my PhD research project, it reconvinced me of the general importance of the interrelation between fundamental and applied research.

Inspiration has been an important driving force during my research. I have particularly been inspired by the attitude towards science enunciated by Prof George M. Whitesides (Harvard University), whose lecture I heard at a conference in Lyon, then by the vim and vigour of Prof Davor Pavuna (EPFL Lausanne), and by the vision of Prof László Forró (EPFL Lausanne). The latter two I would like to thank for their hospitality during my visit to Lausanne.

The support and encouragement of my friends were indispensable in completion of this thesis. I am indebted to them all for their help, particularly to Branimir, Marko, Hrvoje, Ivica, Luka, Sanja, Karlo, Tomica, Marinko, Ivan, Silvije, Sanjin, Zlatko, Ana and Nina. I cherish moments spent with you, particularly those spent at the seaside.

I am grateful to my friends in my hometown Varaždin, my friends in Dubrovnik, my friends in Split, dudes in Čakovec, folks at the American Institute of Zagreb, my friends from Palermo, and my friends from Naples. Forza Napoli! Ho il cuore azzurro.

I am also grateful to colleagues I befriended during the summer school at the island of Rügen: Steven Reichardt (Universität Leipzig), Samuel F. Blake (University of Oxford) and Fabrice Iacovella (Université Toulouse 3). Our illuminating discussions convinced me that physicists can have a touch of real life. Even when the dart machine offers cricket ☺

Ich möchte Altprior P. Gebhard Grünfelder OSB (Benediktinerstift Admont) für seine Gastfreundschaft, Großzügigkeit sowie für seine Gebete danken. Die Harmonie zwischen der benediktinischen Geistlichkeit und der obersteiermärkischen Natur war ein einzigartiges Erlebnis für mich.

Na kraju, želio bih zahvaliti svojoj obitelji koja je najviše osjetila uspone i padove tijekom izrade disertacije. Ponajviše želim zahvaliti svojoj majci Katarini na podršci i ljubavi. ♪ *Su zrnnon soli, su mrvu kruva i puno duše...* ♪

Stay hungry. Stay foolish.

Steve Jobs

(in a commencement address at Stanford in 2005 [2])

Contents

Acknowledgments	xi
Contents	xv
Introduction	1
1 Overture	3
1.1 Complexity and simplicity	3
1.1.1 In favour of simple and cheap	3
1.2 Materials science of strongly correlated systems	5
1.3 Stemming from real life	6
2 Complex matter	9
2.1 Disordered solids	9
2.2 Low-energy excitations	10
2.3 Soft matter	12
2.3.1 Overview	12
2.3.2 Conjugated polymers	13
2.4 Conducting polymers	14
2.4.1 Materials science of conducting polymers	14
2.4.2 Processibility of conducting polymers	17
2.4.3 Application of conducting polymers	18
2.5 Polyaniline	19
3 Synthesis, doping, and sample characterisation	23
3.1 Synthesis of polyaniline	23
3.2 Equilibrium doping of polyaniline in aqueous DBSA solution	24
3.2.1 Preparation of aqueous DBSA solutions	25
3.2.2 Doping	26
3.3 Characterisation of the obtained PANI–DBSA	28
3.3.1 Elemental analysis by nuclear spectroscopy	28
3.3.2 Magnetic susceptibility	34
3.3.3 Electrical conductivity	35
3.4 X-ray diffraction analysis	37
3.5 Concluding remark	39

4	Electronic transport in PANI–DBSA	41
4.1	Introductory remarks on electrons in solids	41
4.2	Localisation of electrons	43
4.3	Anderson localisation	44
4.3.1	Scattering by weak random potential	44
4.3.2	Strong localisation	46
4.3.3	Localised and extended states in Anderson insulator	48
4.4	Effects of interaction and dimensionality	49
4.5	Electronic transport in low-dimensional systems	50
4.6	Hopping transport	50
4.6.1	Introduction	50
4.6.2	Nearest-neighbour hopping	53
4.6.3	Mott’s law of variable-range hopping	54
4.6.4	Beyond the Mott law	56
4.6.5	Efros - Shklovskii model	56
4.6.6	Fogler - Teber - Shklovskii model	58
4.7	Electronic transport in conducting polymers	60
4.8	Dc electrical conductivity of PANI–DBSA	61
4.8.1	Putting into context	61
4.8.2	Measurements	63
4.8.3	Results	63
4.8.4	Verification of the Fogler - Teber - Shklovskii model	66
4.8.5	Further inferences and the Coulomb gap	68
4.9	Concluding remarks	72
5	Magnetic properties of PANI–DBSA	73
5.1	A complementary approach	73
5.2	Magnetisation and magnetic susceptibility	74
5.3	Magnetic susceptibility in the regime of linear $M(H)$	75
5.3.1	Diamagnetism of atoms and ions	76
5.3.2	Curie paramagnetism	77
5.3.3	Pauli paramagnetism	78
5.4	Kamimura model	80
5.4.1	Basic notions	80
5.4.2	Spin susceptibility	81
5.4.3	Comment on Coulomb interactions	83
5.5	Magnetism in conducting polymers	84
5.6	Magnetic susceptibility of PANI–DBSA	87
5.6.1	Measurements	87
5.6.2	Results	87
5.6.3	Diamagnetic susceptibility of PANI–DBSA	90
5.6.4	Inferences	91
5.7	Cusps	97
5.8	Coupling of spin and charge in PANI–DBSA	99
6	... towards application	103

7	Blending PANI–DBSA with carbon nanotubes	107
7.1	Treating PANI–DBSA with chloroform	107
7.2	Carbon nanotubes	109
7.3	Fabrication of blends and measuring their electrical conductivity	110
7.3.1	Initial steps	110
7.3.2	Systematic study of the blends	113
7.4	Concluding remarks towards application	116
8	Outlook	117
9	Conclusion	121
	Appendices	123
A	Calculation of Coulomb gap from crossovers	125
	Prošireni sažetak	127
	Polimeri	127
	Vodljivi polimeri	130
	Procesibilnost i topivost vodljivih polimera	134
	Primjena vodljivih polimera	134
	Polianilin	136
	Mottov model skočne vodljivosti	137
	Fogler - Teber - Shklovskii model	139
	Karakterizacija uzoraka PANI–DBSA	141
	Elektronski transport u PANI–DBSA	142
	Magnetska svojstva PANI–DBSA	145
	Vežanje spina i naboja u PANI–DBSA	147
	Kompoziti od PANI–DBSA i ugljikovih nanocjevčica	150
	Zaključak	151
	References	153
	Curriculum Vitæ	165

Introduction

This thesis presents a comprehensive experimental study of the conducting polymer polyaniline (PANI) doped with dodecylbenzenesulphonic acid (DBSA), a long molecule with surfactant properties. Utilising a novel doping method, we produced PANI–DBSA that exhibits both strongly correlated behaviour of electrons and potential for application.

The thesis is organised as follows:

- Chapter 1 presents the motivation for studying conducting polymers (CP's). We discuss the interrelation between complexity and simplicity, which appears in science and technology as well as in everyday life, and which has been decisive in setting up the aims of our study.
- Chapter 2 gives an overview of soft matter, particularly regarding CP's.
- Chapter 3 provides a description of the synthesis, doping, and characterisation of our PANI–DBSA. Solid understanding of the properties of PANI–DBSA sets foundations for the research presented in the rest of the thesis. Results presented in this chapter have been published in [3].
- Chapter 4 is dedicated to electrical conductivity σ of PANI–DBSA. We give an extensive outline of theoretical concepts used in the analysis of our experimental data. We confirm the importance of the Coulomb interaction in PANI–DBSA. A large part of this work has been published in [4] and [5].
- Chapter 5 is dedicated to magnetic susceptibility χ of PANI–DBSA. We observe a strong correlation between spin dynamics and electronic transport, and utilise this to estimate the energy scales in the electronic structure of PANI–DBSA.
- Chapter 6 explains how the complexity of PANI–DBSA has been reduced to simplicity in our application-oriented study of this material.
- Chapter 7 brings results of our studying of solid blends that were cast from solutions of PANI–DBSA and multiwall carbon nanotubes (MWCNT's) in chloroform (CHCl_3). Application potential of these blends has been identified.

- Chapter 8 presents the process of deposition — from the CHCl_3 solution — of films of both the blends and pure PANI–DBSA onto a commercial plastic substrate. Promising results of this procedure may serve as a starting point for future work in this direction.

The main results of the thesis are the following:

1. Utilising an own-invented method of doping, that circumvents micellisation of DBSA in aqueous solutions, we produce a form of doped PANI with a good potential for application.
2. Our variant of PANI–DBSA permits a comprehensive testing of models of electronic transport in CP's. Good agreement with the Fogler-Teber-Shklovskii model is found, which represents the first comprehensive verification of this hopping-transport theory.
3. We identify a coupling of spin and charge in PANI–DBSA, and estimate energy scales in the electronic structure of this material.
4. Solid blends of PANI–DBSA and MWCNT's, with the mass fraction of MWCNT's of up to 40%, are prepared from their solution in CHCl_3 for the first time. These blends simultaneously offer a solution to a problem of application of MWCNT's in bulk form, as well as to that of poor conductivity of doped PANI at low temperatures.

Basically, we started this (ad)venture with three flasks, each containing a different liquid. We mixed the liquids together and obtained PANI. Then we took the fourth flask, dissolved its content in water, added PANI, and obtained PANI–DBSA. After studying physical properties of PANI–DBSA extensively, we successfully dissolved it in a flask containing CHCl_3 . Then we took another flask with CHCl_3 and dissolved MWCNT's in it. We mixed the contents of the latter two flasks together and cast an interesting blend from the solution. We also used our solutions in flasks to deposit films of both the blend and PANI–DBSA on a commercial plastic substrate.

This is our story in short. The specificities of the procedures used in this (ad)venture, and the challenges encountered along the way, are described in the thesis. We hope that someone might find our (ad)venture interesting enough to continue it.

Chapter 1

Overture

§ 1.1 Complexity and simplicity

Science increasingly focuses on studying various complex systems. Partly, this is because society continuously increases the demand for materials and technologies that can help to make a better world. However, due to the **complexity** of these materials and related technologies, the related achievements do not meet the expectations readily. Complexity itself cannot be circumvented, but one can attempt to build up complexity as **stacked simplicity** once one knows the basic properties of stacked elements. It could be a good way to mitigate or avoid vicissitudes on the path towards application.

Hence, my thesis consists of both fundamental and application-oriented research. Albeit more demanding, I believe that such an approach is much more rewarding in the long run. The final product of my research — a film of a blend of a conducting polymer and carbon nanotubes, which has been deposited onto a commercial plastic substrate (see Fig. 8.1) — may seem complex at first, but it merely represents a product of stacked simplicity.

1.1.1 In favour of simple and cheap

G. M. Whitesides, an American chemist and a University Professor at Harvard University, claims that academics like complexity and emergence*, whereas the world

*Phenomenon that cannot be predicted by studying the behaviour of constituent particles alone is dubbed emergent. Emergent properties are properties of solutions that are not readily apparent from the equations.

puts up with it reluctantly and really wants simplicity [6]. The current state of science is such that complexity is highly developed whereas simplicity is almost not pursued at all, at least not in the academic world. Whitesides says: “We academics love complexity. You can write papers about complexity, and the nice thing about complexity is it’s fundamentally intractable in many ways, so you’re not responsible for outcomes”.

Whitesides advocates another class of simple things: things that are **simple in function** but not at all simple in their underlying structure. They may be perceived as complexity, but actually represent simplicity. An example is the cell phone, which is a complexity but also a user-friendly device. Another example is the Internet. Both are complex systems but reside on layers of simplicity: binary arithmetic (the simplest possible way of representing numbers) and the transistor. The transistor is so simple (because it is reliable) that many of them can be combined together in an integrated circuit (IC). Then, the IC is also simple in the sense that it works very well despite its complex inner structure. So, there are layers of simplicity that stack to build up a complexity that is simple by itself, in the sense that it is completely reliable. We recognise that kind of stacked simplicity when we see it. For instance, the Google search engine on the Internet functions extremely reliably. We can quantify simplicity as something that:

- is predictable - we have to know the basic properties of a simple thing
- is cheap - “If you have things that are cheap enough, people will find uses for them, even if they seem very primitive. For example: stones. You can build cathedrals out of stones.” - G. M. Whitesides
- has a good enough performance/cost ratio
- is stackable - should be able to fit into a more complex structure without losing its reliability.

We witness that the world is by far more complex than science can grasp. Many problems are intractable, it is tricky to deduce the basic laws that govern them. Therefore, it is wise to allocate some energy for the alternative approach which consists of a search for simple and inexpensive scientific systems. Such an approach engages the construction of systems of interacting components which exhibit complex behaviours whilst being as simple as possible in their function [7].

An example of a remarkable success of such an approach is found in paper diagnostic systems with almost zero cost [8], based on microfluidic lab-on-a-chip devices [9]. It provides affordable health care for the developing world, completely circumventing the class issue usually associated with the solutions for the developing world.

The concept of stacked simplicity can also be recognised in the pattern by which technology evolves: new elements are constructed from the ones that already exist,

and then these newly constructed and reliable elements represent possible building blocks for the construction of more complex elements. Technologies seldom come into being just by exploiting a novel phenomenon, but rather as a response to societal need [10]. This is largely in accordance with the Darwinian mechanism of natural selection [11].

§ 1.2 Materials science of strongly correlated systems

Materials science expands rapidly because novel materials are increasingly sought after. Perhaps the most studied classes of materials in the preceding decades have been conducting polymers (CP's) and high- T_c superconductors (HTSC's). Both classes have been rewarding, yet both science and society have expected much more from them. Let me outline the present status of both classes.

The origin of superconductivity in HTSC's remains one of the major unsolved problems of condensed matter physics. The mechanism of the formation of Cooper pairs in HTSC's is not known [12]. Despite exceedingly large amount of experimental and theoretical work, and many promising leads [13, 14], explanation of the phenomenon has so far eluded physicists, and we might be in the wake of a new theory of HTSC's [15]. One reason for this elusion is that HTSC's are generally very complex materials. Anyhow, incomplete understanding of the underlying physics appears as a hindrance to application. Additionally, HTSC's face a number of technical barriers in application, which are almost equally important.

In contrast, CP's are more promising for both understanding complex systems and their application. A number of technologies based on CP's are nowadays in service [16–19]. Current research programmes are mostly concerned with improving morphology (through improvement of syntheses), with characterisation, and with focusing on fabrication of blends and nanocomposites [20, 17]. But too many of these efforts are associated with relentless striving for materials of superior performance. Along with the inherent complexity of CP's, this approach marginalises experimental investigations of the fundamental properties of CP's. Lacking a solid fundamental knowledge could reduce research to just tweaking the properties that are presently accessible and utilised, without the possibility to nurture the application potential of a material to full fruition.

As we see, complex materials can be complicated in many respects. On the other hand, physical properties of simple materials (like ordinary metals), which we understand well [21, 22], are sturdy. They prove to be very difficult to manipulate with in order to meet requests of modern technology. Complex materials can offer a better perspective with regard to that.

However, many advanced functional materials, including CP's and HTSC's, are examples of strongly correlated electron systems [23] which call for nontrivial theoretical description. Electrons in these materials experience **strong Coulomb interaction** that dominates their properties. Spatial confinement may be the cause (e.g., in the Anderson insulator) or the consequence (e.g., in the Mott insulator) of the strong Coulomb interaction, or a combination of both. In strongly correlated materials, the mean-field approximation is broken; the behaviour of electrons cannot be described effectively in terms of non-interacting particles. Strong interactions between particles produce emergent phenomena. The issues of **dimension** and **disorder** even further contribute the multiplicity of effects at play in real materials.

Despite the mentioned difficulties, both theoretical and experimental research keep yielding results, so nowadays physics can offer to engineering a large body of strongly correlated materials for which a sufficient understanding has been achieved. Many CP's are in that group. Since properties of CP's can depend on fabrication and processing strongly, one cannot easily predict the properties of a CP just by knowing its chemical composition. Therefore, in this thesis, I investigate the role of the Coulomb interaction in a CP I have chosen to study.

Complexity of CP's is both a hindrance (regarding complete understanding of their properties) and an advantage (regarding the opportunity for realisation of different physical properties), so it has to be managed wisely. Despite being a blatant example of complex systems, CP's can be reduced to simplicity, as I show by this thesis.

§ 1.3 Stemming from real life

As opposed to academic science, in engineering, in business, and in many other human activities related to science, simplicity is actively sought after. So, there is a societal need for a more practical approach in science. Function should replace structure as the objective of research in modern science. Structure is now relatively easy to define and manipulate with, whereas function is still a challenge, especially if attempted to be achieved by designing. Function usually emerges from empiricism and serendipity [24], as emergent laws do as well [25]. Society is interested only in function, not in the structure of a functional element. If overhauled, science of the 21st century could provide for this. The overhaul should take into account economic factors because modern science of the 21st century ought to be **immersed into the real world** — stemming from it and upgrading it. Such a pattern has already been proven very successful, as I briefly review below.

The 20th century and the beginning of the 21st century witnessed a major betterment in the way the vast majority of people lived [26–29]. The primary reason that eco-

conomic well-being, i.e., living standard is higher today than it was a century ago is that technological knowledge (society's understanding of how the world functions, which are the best ways to produce goods and services) has advanced [30]. A breakthrough in science and technology has been taking place over the course of the last 100-odd years. Inventions were those new values which led to a vast improvement of the ability to produce goods and services.

Among the spate of inventions that have so improved our lives, one holds a special position. The invention of the transistor in 1948 [31] affected the society unprecedentedly. Along with other important inventions, notably those of the IC in 1958 [32] and the World Wide Web in 1990 [33], the invention of the transistor and its broad applications have led to the pervasiveness of personal computers, cell phones, and the Internet. Equipped with Google's web search engine, the Internet has profoundly changed the society. So, we can see that exactly those complexities that represent stacked simplicity, played a major role in attaining prosperity. And their impact was enormous.

The salient ingredient of this impact has been **low cost** of production of the IC. This feature of simplicity restructured whole economies, and upgraded our lives. And an IC, the fundamental building block of information technology, costs about the same as one printed newspaper character nowadays [34].

Knowledge, the underlying basis of prosperity, is not any more merely about information, because pieces of information have become available promptly and freely. Nowadays, when the pace of the growth of human knowledge is increasing swiftly, the true value is in distinguishing between the important and the unimportant. One can find a support for such a stance in a description of characteristics sought after in potential employees [35].

Hence, this thesis is conceived with a conviction that, beside performances, the cost also plays a critical role on the path towards the application of functional materials in real life. This conviction, drawn from successful historical patterns, is implemented in pivotal points of the thesis. The specificities that pertain to the materials investigated in the thesis are explicated in more detail in Chapter 6. As such, the thesis aspires to take part in a perennial contest between those who push forward and a timid ignorance obstructing world's progress.

Chapter 2

Complex matter

§ 2.1 Disordered solids

Disordered solids are ubiquitous natural or engineered systems. Disorder represents deviations from long-range periodicity, and can be related to either impurities or intrinsic imperfections of the crystal structure. Impurity atoms deliberately placed in a material are called dopants.

Disordered solids are usually subdivided into amorphous solids and glasses. The term amorphous implies the presence of a short-range atomic order in a material, along with the absence of a long-range repeatability of this short-range order. An amorphous solid could mathematically be constructed from a crystal by continuous deformations, viz, an atom in the amorphous solid has the same number of nearest neighbours as in the crystalline case, and the neighbours are located approximately the same distance away from said atom. However, distorted bond lengths and angles preclude any long-range periodicity. Glasses could, on the other hand, be imagined as formations originating from topological deformations of crystals, thence they are more disordered than amorphous solids. Glassy solids contain imperfections such as interstitial atoms or lattice vacancies. The terms disordered and amorphous are often used interchangeably, and precise distinction is not universally agreed upon.

Polymers can be both disordered or crystalline. But not all polymers crystallise and — even in those that do — there are always some remaining non-crystalline regions. Non-crystalline polymers are usually termed “amorphous polymers”. Disorder level in amorphous polymers can be significantly more pronounced than in non-polymeric solids, due to different conformations and configurations of polymer chains in a bulk polymer material. Most of the polymers in practical applications are amorphous, but

can also often comprise a combination of amorphous and crystalline regions [36, 37]. Regarding our PANI–DBSA, it is completely amorphous (see Section 3.4).

Among disordered solids, disordered semiconducting materials (to which a vast majority of CP’s also belongs) are of particular interest because of their application potential. Many of the formalisms used to describe crystalline semiconductors work well in describing disordered semiconductors as well. Most notable are the concepts of conduction and valence bands with the forbidden energy gap in between. The difference in the descriptions of crystalline and amorphous semiconductors arises exactly from the properties of the gap in a disordered state.

In a crystalline semiconductor, there is a complete lack of states within the gap, and the delocalising conduction and valence bands begin somewhat abruptly at the band edges. In a disordered semiconductor, there is a smooth transition between the localised states and the states which extend throughout the lattice (see Subsection 4.3.3 for more details). Thus, it is more common to speak of a “mobility gap” in amorphous solids [38]. That is, in crystalline semiconductors, there are no states below the mobility edge (the upper edge of the gap), whereas in disordered semiconductors, electrons can become trapped in localised states below the mobility edge. Thus, an undoped disordered semiconductor, though chemically pure, is electronically impure since it has states within the gap.

In addition to the band tails extending into the gap, in disordered semiconductors it is also common to find narrow bands of localised states within the gap. These are called impurity bands or **disorder bands**. In this thesis, we shall examine the properties of the disorder band (composed of dopant states) of our PANI–DBSA material. In order to do that, we first address the ways in which a disordered system can be excited by external probes at long wavelengths and low frequencies.

§ 2.2 Low-energy excitations

Solids, as quantum systems, have a ground state and a number of excited states above. In many contexts, only low-lying excited states, with energies close to the ground state, are relevant for the properties of a solid. This is due to the Boltzmann distribution, which implies that very-high-energy thermal fluctuations are unlikely to occur at any T the solids might be utilised at. Most important types of such low-energy excitations are the following [39]:

- Nambu–Goldstone modes. Nambu–Goldstone bosons, such as phonons or magnons, are a necessary concomitant of spontaneously broken continuous symmetries. The concept of spontaneous symmetry breaking [40] has perhaps

been the most influencing physical concept of the 20th century.

- **Critical fluctuations.** When critical fluctuations at a second-order phase transition are excited, the system moves towards one or another competing phases.
- **Fractional quantum Hall quasiparticles.** In topological phases, a system of strongly-correlated electrons supports excitations which have fractional quantum numbers for electrons. Fractionally charged quasiparticles are neither bosons nor fermions. The fractional quantum Hall state is not adiabatically deformable to any noninteracting electron state. Consequently, these states represent a distinct state of matter [41].
- **Localised excitations.** Spatially localised low-energy excitations are a consequence of a static disorder, such as that caused by impurities in a solid.

We shall be concerned exclusively with the last of the four types of excitations. The phases associated with **localised excitations**, in which the presence of disorder plays a dominant role, can only be rather loosely grouped together. An ordinary metal at low T is an example of such a phase: its finite conductivity is a consequence of the interaction between electrons and imperfections. If the disorder level in a metal is high enough, or the effective dimension low enough, the presence of the disorder can turn the metal into an insulator. This insulator will have low-energy excitations, but these will be localised. An even more exotic example is spin glass, in which the spins are frozen in randomly oriented directions. Such a state also has low-energy excitations, associated with local rearrangements of spins [39].

Disorder has interesting effects on the electronic states in a solid. In general, many-body systems tend to form energy gaps as means of lowering their energy. One might be tempted to conclude that, consequently, their low-energy properties are trivial and that interesting physics occurs only when they are gapless, either because their ground state spontaneously breaks a symmetry, or because they are tuned to a critical point. However, the presence of disorder can engender low-energy excitations even without any tuning.

For a qualitative understanding of why this should be so, let us suppose that — in the absence of disorder — there is a gap related to the creation of a quasiparticle, as in the case of a semiconductor. However, in the presence of imperfections, there are states within the gap. If there is a random distribution of imperfections, we expect a distribution of bound-state energies within the gap. In other words, there will generically be states at E_F , unlike in a crystalline system, although the density of these states will depend on impurity density or/and disorder level.

Electronic transport comprising localised states within disorder band, which is of a particular interest for our PANI-DBSA, will be discussed in Chapter 4.

§ 2.3 Soft matter

2.3.1 Overview

Soft condensed matter (or soft matter, for brevity) is a term which encompasses materials that are neither simple liquids nor crystalline solids of the type studied in other branches of solid state physics [42]. Many such materials are familiar from everyday life (e.g., glues, paints, soaps, biological matter) while others are important in industrial processes, such as the polymer melts that are moulded and extruded to form great diversity of plastics.

Soft matter comprises polymers, surfactants, liquid crystals and colloids [43]. These apparently disparate materials have a number of common features. These include:

- **Universality.** For instance, many aspects of the behaviour of polymers derive not from the particular chemical structure of the building blocks (monomers) that make up the polymer chain. They derive simply from the topological implications that follow from the fact that polymer macromolecule resembles a long curve in space, as if tracked by random walk. Moreover, soft matter systems should be visualised as being in a constant state of random motion — polymer chains are continually writhing and turning, especially in solutions.

Individual monomers are bound together by covalent bonds, about which rotations are usually possible. Therefore, long polymer chains have a very large number of internal degrees of freedom, which leads to an enormous number of spatial conformations of the chain, and hence a very large entropy. On distances that are large compared to the size of a monomer, the chemical structure of the building block plays only a minor role, and the properties of the chain are mainly determined by the statistical mechanics of the chain, i.e. essentially by the entropy of a chain. As a consequence, on large distance scales, or for a large number of monomers, Ω , one expects that polymer properties, will be universal, depending only on the nature of the chain that the monomers form, i.e. whether flexible or semi-flexible, self-intersecting or self-avoiding [44]. The simplest example of such a law is the scaling behavior is the relation between the size of a polymer (measured by its average end-to-end distance) and the physical length of the polymer is (determined by Ω):

$$\sqrt{\langle R_{\text{end-to-end}}^2 \rangle} \propto \Omega^\nu, \quad (2.1)$$

where $\nu = 1/2$ in all dimensions for a self-intersecting, completely flexible chain. For a self-avoiding chain, $\nu = 1, 3/4,$ and 0.5886 in 1D, 2D, and 3D, respectively. Similar scaling relations appear in other examples of soft matter [44]. Their derivation and elucidation played an important role in polymer theory [45, 46].

- **Responsiveness.** A hallmark property of soft matter is its mutability and responsiveness to its surroundings. The response may be large even for small changes of outer parameters such as magnetic field, temperature, concentration of different molecules, pH, pressure. We shall see how a small change in the concentration of the dopant can cause a large change in the electrical conductivity of our PANI–DBSA.

Both PANI and the dopant DBSA are examples of soft matter. The latter is a surfactant, and can form molecular aggregates in aqueous solutions. This property — which is otherwise useful in many technological application of surfactants — can pose an obstacle for the doping in aqueous solutions that we employ. The intricacy of this issue and its resolution are explained in Section 3.2.

2.3.2 Conjugated polymers

Polymers are subdivided into saturated polymers and non-saturated polymers. Saturated polymers comprise common plastics such as polyethylene, polypropylene, polytetrafluoroethylene, polystyrene, poly(ethyleneglycol), poly(ethyleneglycol-terephthalate), poly(methylmethacrylate), poly(vinylacetate), poly(vinylchloride), nylon, etc. In saturated polymers, all four valence electrons of each C atom are used up in covalent bonds. Hence, saturated polymers are hard insulators. On the contrary, non-saturated polymers can be interesting from the point of view of electronic materials. Yet, not all non-saturated polymers can become conducting, only conjugated polymers can. This property arises from a particular electronic configuration of conjugated polymers. Below, we outline interrelation between structural and electronic properties of conjugated polymers, utilising [47].

In conjugated polymers, chemical bonding leads to one unpaired electron (π electron) per each C atom. Moreover, π bonding (in which the orbitals of C atoms are in the sp^2p_z configuration and the orbitals of successive C atoms along the polymer backbone overlap) leads to electron delocalisation along the backbone of the polymer chain. Such a delocalisation provides for charge mobility along this backbone.

A classic example of a conjugated polymer is *trans*-polyacetylene (PA), $(-\text{CH}-)_n$, in which each C atom is σ -bonded to only two neighboring C atoms and one H atom, with one free (delocalised) π electron per C atom. If the C–C bond lengths were all equal, the chemical formula $(-\text{CH}-)_n$, with one unpaired electron per formula unit, would imply a metallic state. Alternatively, if the electron-electron interaction were strong, $(-\text{CH}-)_n$ would be an antiferromagnetic Mott insulator (due to the half-filling of the molecular orbital composed of all π electrons of the polymer backbone). However, the easy conversion to the metallic state upon doping together with a variety of studies of the undoped PA have eliminated the antiferromagnetic Mott insulator as a possibility. This does not yet imply that PA is metallic.

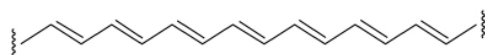


Figure 2.1: *trans* isomer of polyacetylene.

Namely, the structure of real PA is dimerised (see Fig. 2.1) as a result of the Peierls instability. Consequently, two C atoms constitute the repeat unit, $(-\text{CH}=\text{CH}-)_n$. Thus, the pre-dimerisation π band (i.e., the π molecular orbital) is — after dimerisation — divided into π and π^* bands. Since each band can hold two electrons per atom (spin up and spin down), the π band is filled and the π^* band is empty. The energy difference between the highest occupied state in the π band and the lowest unoccupied state in the π^* band is the energy gap E_g . The structure of alternating single and double bonds, a hallmark of PA, is also characteristic of all conjugated polymers, and thus also of CP's (see Fig. 2.2). Consequently, since there are no partially filled bands, conjugated polymers are typically insulators or semiconductors. Conjugated polymers can be turned into CP's by means of doping.

§ 2.4 Conducting polymers

2.4.1 Materials science of conducting polymers

PA was for a long time viewed as a wide-gap semiconductor ($E_g \approx 1.4$ eV) with low intrinsic $\sigma \approx 10^{-4}$ S/m [48]. As E_g depends on molecular structure of the repeat unit, synthetic chemists focused on synthesising other conjugated polymers with narrower band gaps, in order to achieve σ higher than in PA. All of that was done in hope for a future replacement of metals with these cheaper and lighter non-corrosive materials.

It had been recognised for many years before the discovery of electrical conductivity of conjugated polymers (this was actually the discovery of electrical conductivity of PA) that a very long linear conjugated PA might have various interesting electrical, optical, and magnetic properties [49]. It was found already in 1968 that σ of pressed pellets of PA can be varied from 10^{-7} to 1 S/m by exposure to various strong Lewis acids [50]. Physicist and chemists gradually realised that doping of conjugated polymers is more rewarding than trying to control the width of E_g via design at the molecular level.

Two pivotal points were critical in the attainment of the possibility to synthesise such a PA that could have been turned conducting upon doping. The first point was the possibility to synthesise long enough linear (not branched or grafted) polymers. This was achieved by the invention of the Ziegler catalysts. The second point was the invention of the Ziegler-Natta catalysts in 1958, which enabled syntheses of stereoregular polymers. In the case of polyacetylene, this leads to the product of synthesis

Figure 2.2: Molecular structures of a few of important CP's. Note the bond alternation in structures. (Reproduced from [16].)

being pure *trans*-polyacetylene (without the presence of the *cis* isomer* in the macromolecule), and that it is a long linear macromolecule.

The second pivotal point was the synthesis of free-standing films of PA in 1974 [51]. In 1976, A. G. MacDiarmid, H. Shirakawa, and A. J. Heeger, together with a group of graduate students and postdoctoral researchers, succeeded to dope these films over a range from $\sigma = 10^{-4}$ S/m to $\sigma = 10^5$ S/m [52]. This was particularly exciting because it created a new field of research on the boundary between chemistry and condensed matter physics, and because it created a number of opportunities [47]:

- CP's opened a route to progress in understanding the fundamental chemistry and physics of π -bonded macromolecules.
- CP's provided an opportunity to address questions that had been of fundamental interest to quantum chemistry for decades: Is there a bond alternation in long-chain PA? What is the relative importance of the electron-electron and electron-lattice interactions in π -bonded macromolecules?
- CP's provided an opportunity to address fundamental issues of importance to condensed matter physics as well, including, for example, the metal-insulator transition (MIT) as envisioned by N. F. Mott and P. W. Anderson, and the instability of 1D metals discovered by R. Peierls.
- Finally — and perhaps most importantly — CP's offered an opportunity of achieving a new generation of polymers: Materials which exhibit the electrical and optical properties of metals or semiconductors and simultaneously retain attractive mechanical properties and processing advantages of polymers.

In 1987, σ of the order of 10^6 S/m was reported for films of PA [53, 54]. By further improvement of the material, σ was increased in 1990 by another order of magnitude, to 10^7 S/m [55, 56], which is comparable to the room-temperature σ (σ_{RT}) of Cu (6×10^7 S/m). Stimulated by these terrific results, much of academic and industrial research on CP's has been done in the following years.

Although CP's were initially built upon the foundations of quantum chemistry and condensed matter physics, it soon became clear that entirely new concepts were involved in the science of CP's. The discovery of nonlinear excitations in CP's, solitons in systems in which the ground state is degenerate, and confined soliton pairs (polarons and bipolarons) in systems in which the ground-state degeneracy has been lifted by the molecular structure, opened entirely new directions in the study of the interconnection of chemical and electronic structure. The spin-charge separation characteristic of solitons and the reversal of the spin-charge relationship (relative to that expected for electrons as fermions) in PA gained much attention (see Section 5.5 for more details).

**cis*-polyacetylene has a much wider E_g than PA, and consequently its intrinsic σ is four orders of magnitude lower than that of PA.

The study of solitons in PA and other CP's dominated the first half of the 1980s [57]. Its theoretical background is known as the Su-Schrieffer-Heeger (SSH) model. The SSH model is a model of the electronic structure of conjugated polymers, and consequently a model of their conductivity. The model is based on quasi-1D tight-binding approximation (Q1D TBA), in which π -electrons are coupled to a distortion of the polymer backbone through electron-phonon interaction. The core of the model was formulated in the early 1970s [58]. The SSH model found many experimental verifications, but was not on the route towards possible wider technological application of CP's.

Reversible doping of CP's is a major achievement. Reversible control of σ over several orders of magnitude can be accomplished either by chemical doping or by electrochemical doping. Concurrent with the doping, the Fermi energy E_F is moved, either by a redox reaction or an acid-base reaction (which is also actually a redox reaction), into a region of energy with a high density of electronic states. Charge neutrality is maintained by the presence of counterions. CP's are, therefore, salts. Their electrical conductivity results from the existence of charge carriers (through doping) and from the ability of those charge carriers to move both along the polymer backbone and from one backbone to another. Disorder, however, limits the carrier mobility and consequently the electrical conductivity as well.

2.4.2 Processibility of conducting polymers

Magnificent results of fundamental research on PA [57, 59] were of little use for possible wider technological application of CP's. There are two main reasons for that. The first one is that the SSH model pertains to crystalline CP's whereas real CP's are highly disordered and usually not fully crystalline. The second reason is that PA is both rather unstable and unprocessable, and as such unsuitable for technological applications despite the achieved high σ .

The problem of instability of PA was solved by the synthesis of another CP — poly-paraphenylene (PPP) [60]. This CP was the first aromatic CP (see Fig. 2.2). Aromaticity makes PPP resistant against oxidation and thermal degradation [61], but does not ensure the processibility of PPP.

The first processible (and stable) CP was synthesised in 1991 [62]. It was PANI (also an aromatic CP) doped with surfactant acids such as DBSA, CSA (camphorsulphonic acid), DBNSA (dibutyl-naphthalene sulphonic acid), AMPSA (2-acrylamido-2-methyl-1-propanesulphonic acid). These surfactant dopants enable the solubility of PANI in common weakly-polar organic solvents such as chloroform, xylene, *m*-cresol. The synthesis of a CP that is well-conducting, stable and processible has been a giant leap towards application of CP's.

Even PA itself can be made processible. PA can be synthesised by ring-opening

metathesis polymerisation (ROMP) from cyclooctatetraene, a material easier to handle than the acetylene monomer. This synthetic route generally provides a facile method for adding solubilising functional groups to the polymer backbone while maintaining the conjugation [63]. R. H. Grubbs and co-workers synthesised a variety of PA derivatives with linear and branched alkyl chains. PA derivatives with linear groups such as *n*-octyl had high conductivity but low solubility, whereas highly branched *tert*-butyl groups increased solubility but decreased conjugation. Conjugation is decreased because of the twisting of the polymer in order to avoid steric crowding. Both soluble and well-conducting PA was obtained with *sec*-butyl and neopentyl groups [63].

If CP's can be made soluble, and can be cast from a solution, this solves a crucial problem on the path towards their application. Let us outline the underlying mechanism of (in)solubility, relying on [63].

Delocalisation of electrons throughout the backbone of a CP requires the adjacent monomer units along the backbone to be coplanar. The coplanarity tends to make the CP's inflexible and, consequently, insoluble. This insolubility can be attributed to a combination of a small positive entropy of dissolution (due to the lack of a conformational mobility in the solution) and a small negative enthalpy of dissolution (due to efficient molecular packing in the solid state). Structural modifications can, however, render a CP soluble. For example, the attachment of long, flexible, pendant alkyl or alkoxy chains to a rigid chain can induce solubility of PT, PANI, PPV and PPP. The conformational mobility of the side chains which act as "bound solvent", provides enough entropic driving force to carry the rigid polymer chain into solution. Moreover, these side chains can also assist solubility by disrupting the packing forces in the solid state.

2.4.3 Application of conducting polymers

Applications of CP's are numerous indeed. Just as science drives technological applications, technology drives scientific research by a feedback effect. Nowadays, CP's as functional materials hold a prominent position in the field of materials science. Their excellent electrical and mechanical properties, low production cost and increased processibility make them increasingly attractive. This particularly holds for novel, nanostructured forms of CP's. Here, we list major applications of CP's relying on [16, 17, 64–66].

Light-emitting diodes can be fabricated from CP's. Therefore, CP's have been incorporated into commercial displays made from arrays of such light-emitting diodes. CP's are also used as light-emitting electrochemical cells, as laser materials, as photovoltaic cells, and as field effect transistors. CP's are used as protecting coatings against metal corrosion and electrostatic discharge, and can even be printed using desktop inkjet printer. They find application as supercapacitors, in batteries, as chemical and biological sensors, as electrochemomechanical devices (e.g. artificial muscles), in actuators, etc. CP's are used in printed circuit board manufacturing, as con-

ducting resists for optical and e-beam lithography, even as substitutes for metal wires. They find another use as microwave-absorbent coatings, particularly radar-absorptive coatings on stealth aircrafts.

Currently, photovoltaic cells and supercapacitors are regarded as the most promising applications of CP's.

§ 2.5 Polyaniline

Within the class of CP materials, PANI is of a special interest because of its excellent stability under ambient conditions. Consequently, it is one of the most studied and most widely applied CP's. PANI exists in two basic chemical forms: in the form of a base (undoped and non-conducting PANI) and in the form of a salt (doped and conducting PANI). PANI is formed by a process of oxidative polymerisation of aniline (aminobenzene).

Figure 2.3: Isolated variations of poly(*p*-phenyleneamineimine) bear the following names: leucoemeraldine, protoemeraldine, emeraldine, nigraniline and pernigraniline, with $y = 0$, $y = 1/4$, $y = 1/2$, $y = 3/4$ and $y = 1$, respectively.

Fig. 2.3 shows fully reduced mer of PANI base (left two rings), and fully oxidised mer of PANI base (right two rings). PANI base is a copolymer comprising any variation of these two mer units, and is properly referred to as poly(*p*-phenyleneamineimine). The form corresponding to $y = 1/2$ is known as emeraldine base (EB), and is the most common variant of poly(*p*-phenyleneamineimine) [67]. Henceforth we shall consider and refer only to this form of both PANI base and salt (doped EB). EB base can be dissolved in N-methyl-2-pyrrolidinone, but finding a proper solvent for a doped EB required much effort (see Subsection 2.4.2).

Conversion of EB into a salt is obtained by means of doping by some protonic acid (actually any Lewis acid can be used). Most commonly, EB is doped with HCl, which results in the salt emeraldine-hydrochloride (or emeraldinium-chloride). Hydronium ions bound to the lone pair of electrons on N atoms give rise to emeraldinium polycation (which is a conjugate acid of EB base). Counterions Cl^- ensure the charge neutrality. Imine atoms are stronger bases than amine atoms, so — according to

the Brønsted-Lowry theory — only the former ones should be protonised. This is confirmed experimentally [68]. Fully protonated and half-protonated emeraldinium-chloride are depicted in Fig. 2.4 and Fig. 2.5, respectively.

Figure 2.4: 100% protonated emeraldinium-chloride.

Figure 2.5: 50% protonated emeraldinium-chloride.

Fully protonated emeraldinium polycation (see Fig. 2.4) is thermodynamically the most stable form of possible polycations of poly(*p*-phenyleneamineimine) (see Fig. 2.3) in an aqueous acidic medium. This structure is stabilised by the resonance of its four equivalent structures [69]. The resonance produces a state in which all rings in Fig. 2.4 are between benzene and quinone, all N atoms are between amine and imine ones, all N atoms carry charge $+e/2$, and all N-C bonds are of equal length. Such a resonant structure enables large polarons (large localisation length of the electron wavefunctions). This picture explains why polymerisation in an acidic medium always produces emeraldinium polycation, and not polycation(s) of other oxidation forms (see Fig. 2.3). It also reverts us from trying to perform polymerisation in media other than aqueous acidic solutions, lest result in a product of oxidation state(s) different from that of emeraldinium ion. However, this resonant structure does not suffice to explain the conductivity of PANI. The mechanism that turns PANI conducting is explicated below.

EB is turned into a conducting form by protonation. This protonation is an acid-base chemical reaction which accomplishes p-doping without changing the number of electrons in the polymer backbone [70], which makes PANI unique among CP's. The doping mechanism, explained in Fig. 2.6, does not depend on the type of counterions. Yet, the doping level and conductivity do depend on counterions. For the complete protonation, we obtain poly(semiquinone) radical cation (see Fig. 2.6d), i.e., the mer unit is halved in comparison with that of EB (see Fig. 2.6a). Poly(semiquinone) radical cation has one unpaired spin per mer and thus has a charge of $+e$. The consequence of this unpairing of spin is the formation of a half-filled polaronic band, which accounts for the conductivity of doped PANI.

Figure 2.6: p-doping of EB by protonation. Transition from insulating to conducting form is accomplished without the change in the number of electrons. (a) EB (b) Protonation of imine atoms gives rise to one bipolaron per mer of emeraldinium polycation. (c) Quinone ring transforms into the benzene one — two polarons are produced. This is an internal redox reaction. (d) Redistribution of charge and spin. There is one polaron per mer unit of poly(semiquinone) radical cation.

Doped PANI is conjugated polymer which does not have a doubly degenerated ground state (as, e.g., PA does), and consequently, does not exhibit a soliton conductivity. Positive charge of poly(semiquinone) radical cation is equally distributed between both N atoms in the mer unit, and also partially delocalised through both of its C_6H_4 benzene rings [71]. However, this model of conductivity of doped PANI does not account for the disorder present in real PANI samples which consist of entangled polymer chains. Nevertheless, it has served as a starting point in understanding this exciting and promising CP.

PANI has found numerous applications, which have already been mentioned in Subsection 2.4.3. We aspire to contribute to the palette of doped PANI and its applications by our PANI-DBSA, the synthesis and doping of which we describe in Chapter 3.

Chapter 3

Synthesis, doping, and sample characterisation

In general, in all the procedures used to obtain results presented in this thesis, we have attempted to maintain simplicity, bearing in mind that (only) such an approach can pave a way towards application.

§ 3.1 Synthesis of polyaniline

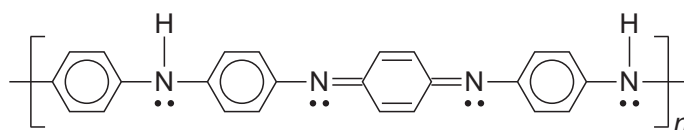
Chemicals were acquired either from Merck (aniline) or Alfa Aesar (ammonium peroxydisulfate, DBSA). Since our results could be of interest for research in different fields (e.g. physics, chemistry, materials science), we pursued simplicity by avoiding any untraceable post-processing of the bought chemicals (which is often done prior to syntheses of PANI [17]).

The starting undoped PANI (EB) powder was produced using a standard method [72]. We first synthesised PANI-HCl through the oxidative polymerization of aniline $C_6H_5NH_2$, using ammonium peroxydisulfate $(NH_4)_2S_2O_8$ as the oxidant, in a ~ 1 M aqueous HCl solution, and then converted it — by a deprotonation in a ~ 1 M aqueous NH_4OH solution — into undoped PANI powder ready for subsequent controlled doping by DBSA as described below.

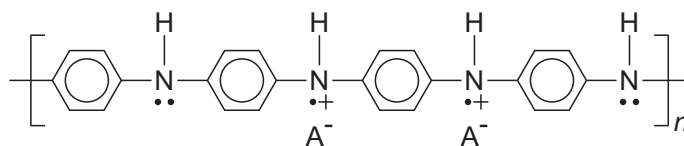
§ 3.2 Equilibrium doping of polyaniline in aqueous DBSA solution

Although direct polymerisation of aniline in an aqueous DBSA solution can yield PANI–DBSA in a one-step procedure [73], it is difficult to control the doping this way. Instead, in our work we employ another method, i.e., equilibrium DBSA doping of independently synthesised EB powder. More precisely, we use the term "equilibrium" in connection with the following procedure: EB powder and aqueous DBSA solution are equilibrated for two weeks, the only perturbation being occasional stirring. Due to the prolonged reaction time and absence of external disturbances, the system can reach a state close to its thermodynamic equilibrium. This method is standard in doping of EB by HCl, and we have deliberately avoided any further modifications because the effects of these can be elucidated only if the simplest approach is understood well enough.

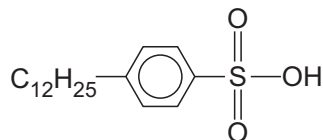
For clarity of the discussion, we show schematically in Fig. 3.1: (a) one mer of EB, (b) this mer fully protonated by an acid H^+A^- [47], and (c) the DBSA molecule.



(a) EB (undoped PANI)



(b) fully protonated PANI- H^+A^-



(C) DBSA molecule

Figure 3.1: (a) Mer of EB (undoped PANI). The dots represent electron lone pairs on the N atoms. (b) Fully protonated mer of EB. The protonation by an acid H^+A^- results in PANI- H^+A^- . The "+" symbols on the protonated N atoms depict holes. (c) DBSA molecule. The $C_{12}H_{25}$ - "tail" points outwards from the polymer backbone and causes a surfactant effect in an appropriate solvent.

3.2.1 Preparation of aqueous DBSA solutions

Preparation of the doping solutions required a consideration of the complexity of DBSA. As shown in Fig. 3.1(c), DBSA molecule consists of a $-\text{C}_6\text{H}_4\text{SO}_3\text{H}$ "head" and a long $\text{C}_{12}\text{H}_{25}-$ "tail". Being an anionic surfactant, DBSA shares common properties with these materials in aqueous solutions. For temperatures $T < T_K$, where T_K is the Krafft temperature, there are no micelles regardless of the surfactant concentration, so single surfactant molecules dispersed in water aggregate only as crystalline hydrates if the amount of the former exceeds the value given by the solubility curve. For $T > T_K$, at surfactant concentrations above the critical micelle concentration (CMC), which depends on T only weakly, micelles appear [74]. Since the most efficient doping of EB by DBSA is expected to occur by single DBSA molecules, their aggregation should be suppressed but — as we argue below — this mainly applies to the formation of micelles.

Namely, at a low binding degree of H^+ counterions to a micelle of DBSA, H^+ can protonate EB, and the resulting PANI-H^+ can then attract the charged micelle. This attraction is strong, as it originates in the electrostatic force. Since micellisation is a fast and reversible reaction [75], the mere presence of micelles should not be an obstacle to the doping, but the chains may wrap around the micelles, forming different complex structures, etc., which would impede protonation of the other available protonation sites. On the other hand, the binding degree in crystalline hydrates is $\sim 100\%$, hence they can interact with EB only via van der Waals interaction — which is much weaker — and the danger of adhering crystalline hydrates to the chains (to form crystal-chain complexes) is not severe. Therefore, according to this picture, it is more important to keep T below T_K than to maintain the concentration low.

Little information on the phase diagram of DBSA dissolved in water is available in the literature, so we must estimate its main features by using data for similar molecules — of which sodium dodecylbenzene sulfonate (SDBS) seems to be appropriate for this purpose. The binding degree of counterions in SDBS micelles in aqueous solutions at $25\text{ }^\circ\text{C}$ is only around 38% [76], which implies that the H^+ counterions dissociation will most probably take place in micelles of DBSA as well, together with the consequences discussed above. Regarding T_K , in SDBS it depends on the isomerism, and falls within the range $\sim 30 - 65\text{ }^\circ\text{C}$ [77]. DBSA also exhibits isomerism, and is commercially available as a molecular mixture containing $\text{C}_{10} - \text{C}_{16}$ homologous hydrocarbon tails (each of the homologues comprising different isomers) [78]. Thus, it is difficult to determine T_K precisely, but we believe that it should not be much lower than $\sim 20 - 25\text{ }^\circ\text{C}$.

Since T_K is thought to be the decisive parameter in the doping kinetics, in our procedure, we put the main emphasis on ensuring $T < T_K$ by preparing all aqueous DBSA solutions at $4 - 8\text{ }^\circ\text{C}$ prior to using them as described in Section 3.2.2. For SDBS, the CMC at $30\text{ }^\circ\text{C}$ is (depending on the isomer) $1.2 - 1.6\text{ mol/m}^3$ [79], but — as argued above — such a possibly low value in DBSA poses less of a problem. The viability

of this somewhat intuitive approach is supported by the results presented henceforth.

3.2.2 Doping

The doping is realised by equilibrating EB powder with aqueous DBSA solution (of a volume V of H_2O) at a selected

$$P = \frac{n_{\text{DBSA}}}{n_{\text{EB}}} \quad , \quad (3.1)$$

where n_{Σ} is the amount of substance Σ (for EB, this refers to one mer). This method permits the doping to occur under conditions that are as close to equilibrium as reasonably possible, and defines a starting point for an approach to achieving a desired material property by establishing an out-of-equilibrium situation. The molar ratio

$$Q = \frac{4n_{\text{S}}}{n_{\text{N}}} \quad , \quad (3.2)$$

which accounts for the doping level in the resulting material*, is determined experimentally by a nuclear spectroscopy (proton scattering) as described in Subsection 3.3.1. In the simplest, idealised picture where all DBSA participates in the protonation, $Q(P \leq 2) = P$, and $Q(P > 2) = 2$ because $Q = 2$ corresponds to 100 % protonation. However, our results show that $Q > 2$ is also possible for DBSA doping of PANI.

Doping of the prepared EB powder by DBSA was carried out for 8 values of P , roughly equidistant in their logarithms, between ~ 0.003 and ~ 30 . The H_2O volume for this series was always $V = 80 \text{ cm}^3$, so we could investigate the effect of P at constant V . For another series of doping, $P \approx 10$ was fixed, whereas two solutions with $V = 200 \text{ cm}^3$ and $V = 800 \text{ cm}^3$ were used. Hence, three values of V for $P \approx 10$ permitted a study of the influence of the DBSA concentration,

$$c_{\text{DBSA}} = \frac{n_{\text{DBSA}}}{V} \quad , \quad (3.3)$$

on the doping at constant, high P . For numerical values of P and c_{DBSA} , see Table 3.1.

EB was added to cold aqueous DBSA solutions (see Subsection 3.2.1) which were then stirred manually every $\sim 1/2$ hour for the next 3 – 4 hours. The reason for this was to enable that the contact between the EB and DBSA was as homogeneous as possible, at the same time avoiding a serious external disturbance to the initial doping. However, attempts to continue with the doping by keeping the solutions cold did not give satisfactory results, presumably due to the weak activity of DBSA in its bonding to the polymer chains when T was low. Better results were obtained through a compromise between the activity enhancement and the inhibition of micellar aggregation. After initiating the doping, the solutions were left to slowly warm up to RT where they were kept for the next two weeks. During this period, the solutions

*We sometimes use Q to quantify the doping level in PANI-HCl. In this case, $n_{\text{S}} \rightarrow n_{\text{Cl}}$.

Table 3.1: Numerical values of important parameters of our PANI–DBSA material.

V [cm ³]	c_{DBSA} [mol/m ³]	P	Q	σ_{RT} [S/m]	χ_{RT} [10 ⁻⁴ emu/mol]
80	134.8	29.90	3.385	931.4	-3.203
80	44.51	9.532	2.918	337.3	-2.460
200	19.19	9.781	2.595	217.7	-2.248
80	26.52	3.085	2.095	73.86	-1.790
800	4.950	10.14	2.067	70.65	-1.735
80	8.941	1.054	1.104	19.18	-0.325
80	2.855	0.3454	0.3766	0.8765	-0.878
80	0.8903	0.1103	0.1282	9.235×10^{-4}	-0.825
80	0.2072	0.03987	0.0536	1.352×10^{-6}	
80	0.05760	0.01107	0.0248	2.241×10^{-7}	
80	0.02878	0.002920	0.0117	1.871×10^{-8}	

were only stirred manually every ~ 24 hours. Finally, the liquid was decanted and the material thoroughly dried.

It will be presented in Section 3.3 that the method described above leads to a good control over the doping level and its consequences. We believe that the reason for this is as follows. The doping starts at $T < T_K$, where the solution with c_{DBSA} above the solubility curve contains DBSA as single molecules and crystalline hydrates. The initial doping involves single molecules, the concentration of which becomes depleted as the doping progresses. The total c_{DBSA} decreases as well, and a shifted equilibrium is established by creating single molecules at the expense of crystalline hydrates. This lowering of c_{DBSA} by the doping also suppresses the formation of micelles, and — depending on a particular case — might prevent their formation even if T increases to moderately above T_K . Therefore, the doping by single molecules remains effective until it is complete under the given conditions, in spite of a high initial c_{DBSA} .

§ 3.3 Characterisation of the obtained PANI–DBSA

In this Section, we present our characterisation of the PANI–DBSA produced as described in Section 3.2. First we turn to the elemental analysis by means of nuclear spectroscopy which leads to a quantitative determination of Q . The related conclusions are supported by measured $\chi_{RT}(Q)$ and $\sigma_{RT}(Q)$ characteristics.

Although, for brevity, we do not discuss T dependences of σ and χ (which will be addressed in Chapters 4 and 5, respectively), we stress that both $\sigma(T)$ and $\chi(T)$ were reproducible in thermal cycling between RT and cryogenic temperatures, which holds even for $Q > 2$ where we observed specks of DBSA precipitated at the sample surface after the exposure to vacuum. This suggests stability of the material, since the reproducibility would not be possible in the presence of any structural feature that might depend irreversibly on temperature and/or pressure. On the other hand, the appearance of specks implies that a further increase of the DBSA content in the bulk is probably not feasible.

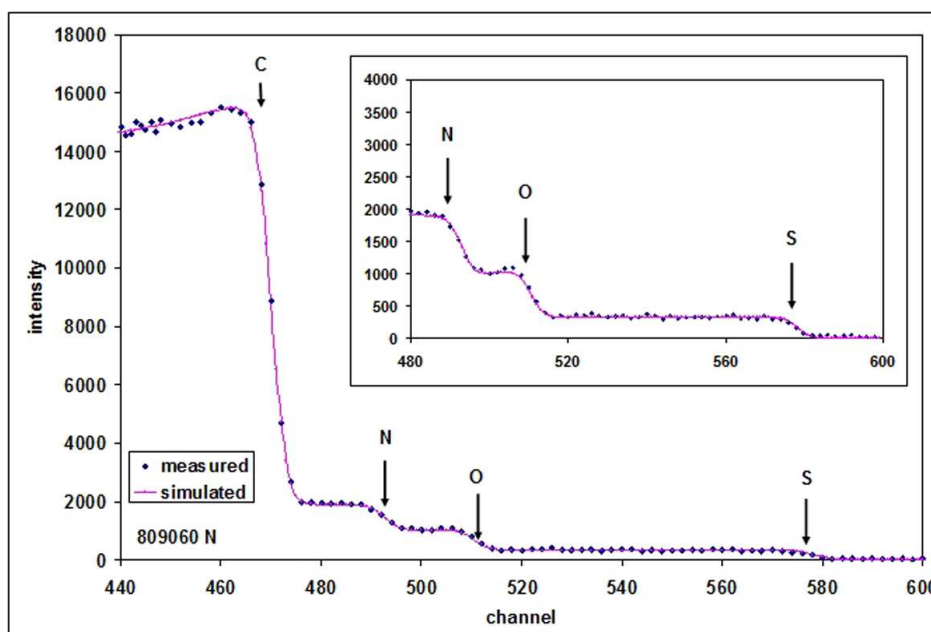


Figure 3.2: Measured and simulated EBS spectrum of the $P = 1$ sample.

3.3.1 Elemental analysis by nuclear spectroscopy

Elemental analysis was performed by the Elastic Backscattering Spectroscopy (EBS) technique using 1.6 MeV protons — produced by the Tandetron electrostatic accelerator — as probing ions. Owing to the large probing depth of protons and high cross sections due to the nuclear component of the interaction, this is a well established tool in the analysis of light elements in materials, the basic principles being equivalent to

the widely known Rutherford Backscattering Spectroscopy [80]. In particular, this method is appropriate for quantifying the content of light elements such as S and N (by using evaluated elastic backscattering cross sections available through the online SIGMACALC calculator [81]), which is of importance for our work. A full account of the amounts of all elements present in our samples — including impurities — was obtained by combining the above method with the Particle Induced X-Ray Emission (PIXE) technique [82]. PIXE is based on the effect of radiative inelastic scattering. PIXE spectra were analysed using GUPIXWIN software. Since PIXE is more appropriate for quantifying the content of heavy elements, it is complementary to EBS. Therefore, EBS and PIXE are often used simultaneously, as in the elemental analysis of our PANI-DBSA.

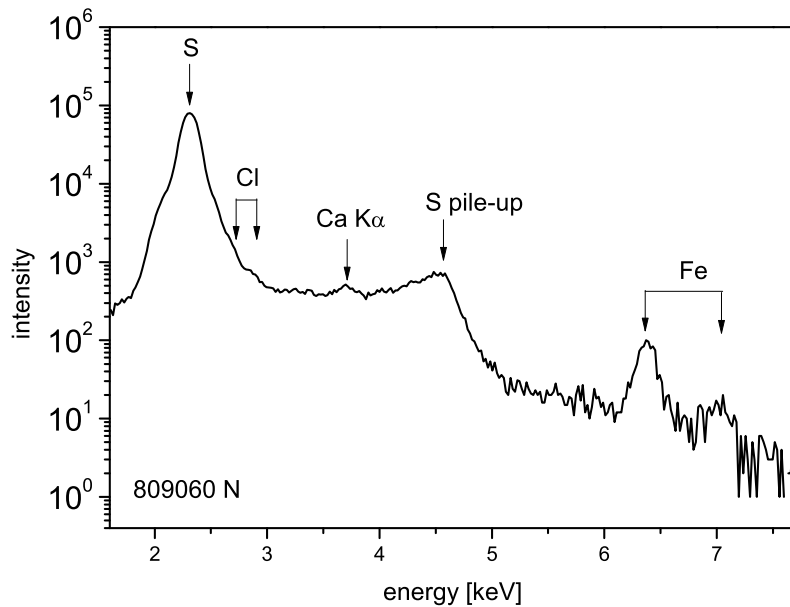


Figure 3.3: Measured PIXE spectrum of the $P = 1$ sample.

Figs. 3.2, 3.4, and 3.6 exemplify both the measured and simulated EBS spectra of PANI-DBSA samples with respectively high, moderate, and low portion of S. On horizontal axes are given channel numbers of the detector electronics, which are (quasicontinuously) proportional to the energy of recoiled protons. There are 1024 channels in total, and they represent discrete voltage ranges of the signal from detector. Although it is possible, we do not show the actual values of energy because these always depend on the selected energy of incident projectiles. In this particular case, the incident protons energy of 1.6 MeV was selected in order to avoid the resonant structure in elastic cross sections for C above 1.6 MeV [83], strong resonance related to N at 1742 keV [84], and to enable the use of evaluated EBS cross sections for S which are available for proton energies above 1506 keV [85].

Steps (which are actually superimposed peaks) corresponding to C, N, O i S are easily discernible in Figs. 3.2, 3.4, and 3.6. Different chemical elements are positioned in different channels because kinematic factors differ between the elements (with the protons of the same energy used as projectiles). In EBS spectra of low-doping-level samples, $P \leq 1/10$, it is not possible to distinguish between the contribution of S and Cl. In these cases, the related PIXE spectra were used to estimate the individual contribution of each of these two elements.

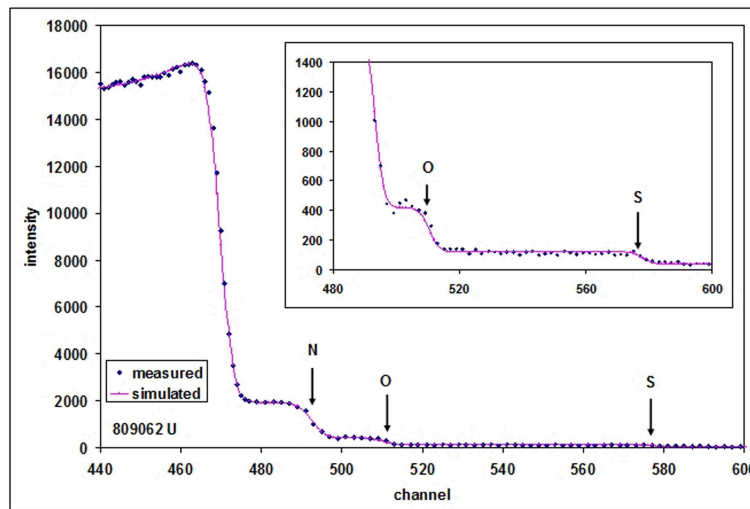


Figure 3.4: Measured and simulated EBS spectrum of the $P = 1/10$ sample.

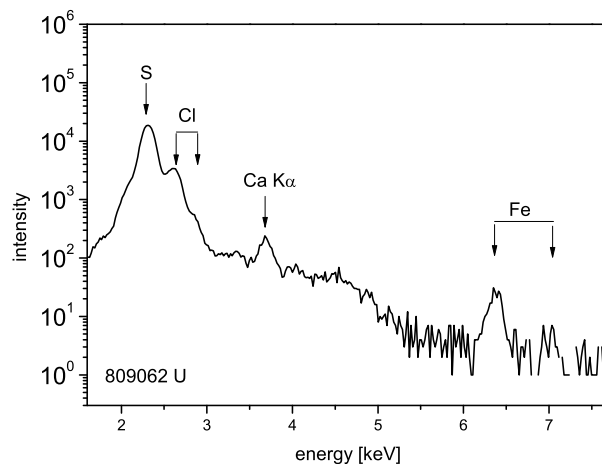


Figure 3.5: Measured PIXE spectrum of the $P = 1/10$ sample.

The PIXE spectra related to EBS spectra in Figs. 3.2, 3.4, and 3.6) are shown in Figs. 3.3, 3.5, and 3.7, respectively. In Fig. 3.3, traces of Fe, Ca and Cl are observable in the $P = 1$ sample, at the level of several tens of ppm, and are therefore negligible.

Traces of S and Cl detected in the undoped sample (see Fig. 3.7) are ascribed to remnants of chemicals used in the synthesis of PANI (see Section 3.1). The results of elemental analysis, obtained by a combination of EBS and PIXE, are summarised in Table 3.2. These data were used to calculate the values of Q . Uncertainties for C, H, N and O in all the samples are estimated to 8% of the given values. Uncertainties for S are also estimated to 8% in all the samples except in $P = 1/10$ and $P = 1/30$ where the uncertainties are 10%, and in $P = 1/100$, $P = 1/300$, and $P = 0$ where the uncertainties are 20%.

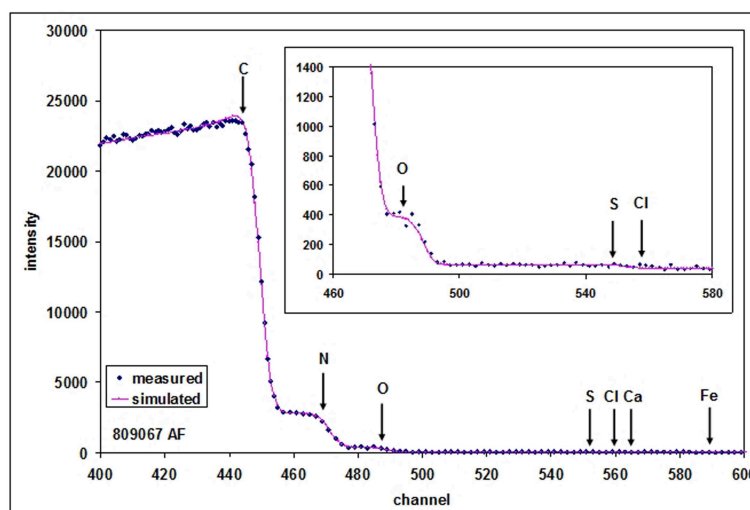


Figure 3.6: Measured and simulated EBS spectrum of the undoped sample ($P = 0$).

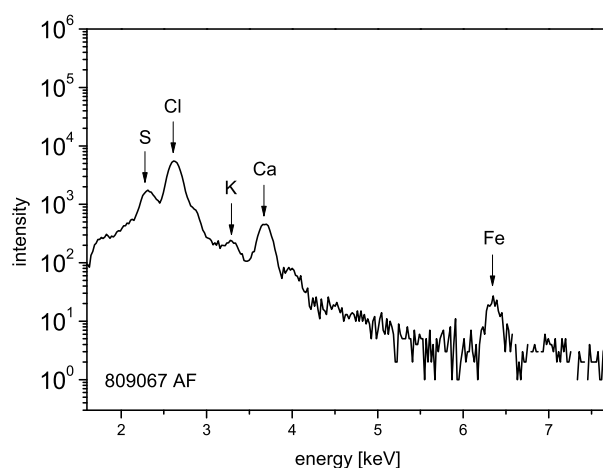


Figure 3.7: Measured PIXE spectrum of the undoped sample ($P = 0$).

Fig. 3.8 is a plot of Q against P on a log-log scale for the doping series at $V = 80 \text{ cm}^3$. The dashed line delineates the "ideal" doping: $Q = P$ for $P \leq 2$, and $Q = 2$ for

Table 3.2: Molar portions of chemical elements in PANI–DBSA samples determined by EBS and the related PIXE spectra. All the data are results of experiment, except the data for H, which are calculated by normalisation. One can see that for the first six samples (which possess a substantial content of dopant) the ratio of molar portions of O and S, $x_O/x_S \approx 3$, as expected from the formula of DBSA dopant (Fig. 3.1c).

molar portion [%]	C	H	N	O	S	Cl
$P = 30$	35.1	56.1	2.0	5.1	1.7	-
$P = 10 \ V = 80$	36.3	54.7	2.25	5.1	1.65	-
$P = 10 \ V = 200$	36.3	55.2	2.3	4.7	1.5	-
$P = 10 \ V = 800$	36.0	56.1	2.5	4.1	1.3	-
$P = 3$	38.4	52.6	2.8	4.7	1.5	-
$P = 1$	42.0	48.5	4.3	4.0	1.2	-
$P = 1/3$	46.4	43.5	6.6	2.8	0.7	-
$P = 1/10$	49.4	40.5	7.9	1.85	0.29	0.03
$P = 1/30$	50.3	39.5	8.4	1.6	0.16	0.04
$P = 1/100$	51.0	39.1	8.6	1.2	0.062	0.058
$P = 1/300$	51.5	38.3	8.7	1.4	0.024	0.076
$P = 0$	51.6	38.3	8.7	1.34	0.016	0.044

$P > 2$. However, the experimental $Q(P)$ continues to increase with increasing P even for $P > 2$, albeit much slower than at low P , which suggests the formation of a **two-phase system** comprising fully protonated PANI–DBSA and (chemically) unbound DBSA between the chains.

The error bars are shown only for three points below $P \approx 0.1$, where they are larger than the symbol size. These low- P points are displayed for the sake of completeness but are of limited interest, because (as shown later) $P \geq 0.1$ covers σ_{RT} between $\sim 10^{-3}$ S/m and $\sim 10^3$ S/m, i.e., most of the range where conductivity of PANI–DBSA is of practical value. The horizontal error bars represent estimates of the main traceable experimental uncertainties in preparing the doping solutions. These are important in cases where small amounts of DBSA are used, and refer to inaccuracies in calculating the molar mass of DBSA — since the hydrocarbon tail is not dodecyl for every molecule — and in the weighing of small masses of DBSA. The vertical error bars account for the precision of the nuclear spectroscopy when the amount of an element is so small that its experimental signature is close to the noise threshold.

Although the molar portion x_N of N (which is at the level of 5 %) introduces some error as well, most of the vertical error bar size is influenced by the uncertainty in x_S . For example, x_S at the lowest $P \approx 0.003$ is around 0.025 %, which can only give an indication of the correct order of magnitude in the measured Q . Hence, Q for $P < 0.1$ should be understood as a qualitative indicator — of a restricted quantitative

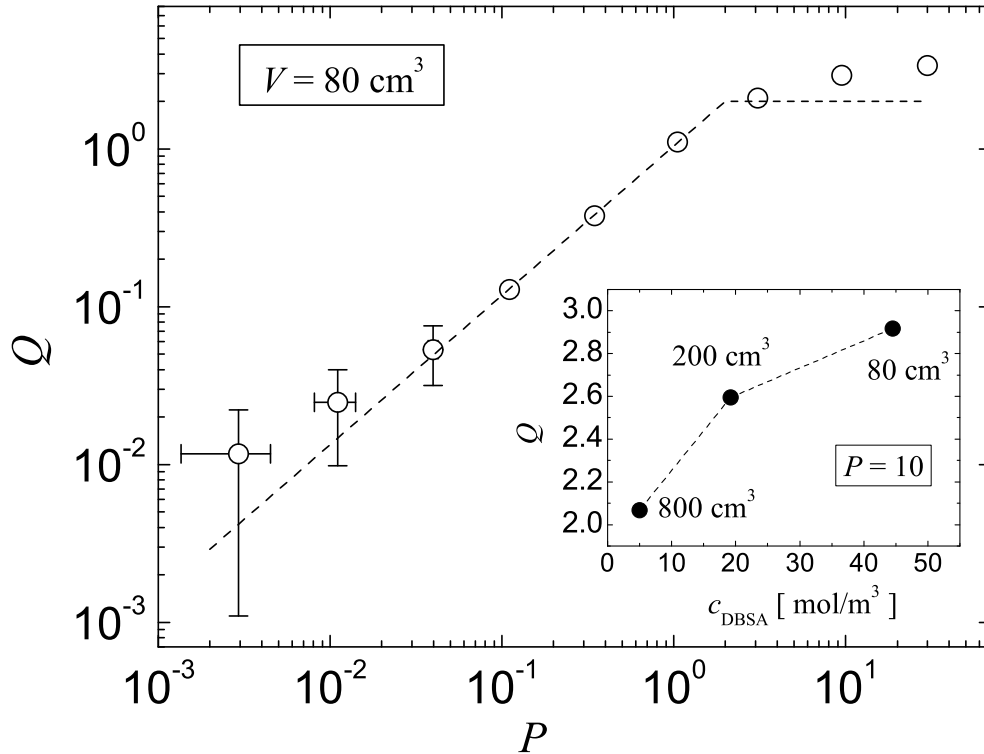


Figure 3.8: Q against P for the doping series at $V = 80 \text{ cm}^3$, plotted by the symbols and with error bars shown for $P < 0.1$ where they exceed the symbol size. The dashed line depicts the "ideal" doping (all DBSA being involved in the protonation). For large error bars at $Q < 0.1$, see the discussion in the text. Inset: Q vs c_{DBSA} for $P \approx 10$ and three doping-solution volumes, as indicated.

reliability — for the increase of the DBSA content with increasing P . One should also not overlook that even very small amounts of residual sulfur (originating from ammonium peroxydisulfate, or impurities from other chemicals used) can affect x_S , which then cannot be assigned solely to DBSA and hence the measured value of Q overestimates the DBSA content. Above $x_S \sim 0.25 \%$, which corresponds to $P \approx 0.1$, Q is a fairly precise measure of the DBSA content. At this level of x_S , the signal is sufficiently above the noise threshold, and any sulfur other than that from DBSA poses only a marginal alteration of the true Q .

For intermediate P values, i.e., excluding the first two (discussed above) and the last two (to be discussed below) endpoints, Q follows the dashed line quite well. For the points below $P = 2$, this suggests that all DBSA in the solution protonates EB because there are more available protonation sites than dopant molecules. The measured $Q \approx 2$ can, on the other hand, imply either that the protonation is partial and the rest of the DBSA remains (chemically) unbound in the interchain space, or that the protonation is essentially complete and there is little unbound DBSA.

Results presented in Subsections 3.3.2 and 3.3.3 support the scenario of the full proto-

nation not only for $Q \approx 2$ but also whenever $Q \geq 2$. In the inset to Fig. 3.8, we present Q vs c_{DBSA} for $P \approx 10$, corresponding to different V as explained in Section 3.2.2. It can be seen that Q decreases by diluting the solution. At the lowest $c_{\text{DBSA}} \approx 5$ mol/m³, Q is close to 2, which suggests - by the arguments presented above - full protonation with no unbound DBSA if the doping solution is dilute enough. One can therefore control Q both through P and c_{DBSA} , in contrast to PANI-HCl where solely pH of the doping solution determines the doping level.

3.3.2 Magnetic susceptibility

In Fig. 3.9, we plot the experimental $\chi_{\text{RT}}(Q)$ with open circles for selected samples doped at $V = 80$ cm³, the solid circle corresponds to the doping at $P \approx 10$ and $V = 200$ cm³, and the cross to that at $P \approx 10$ and $V = 800$ cm³. The dotted horizontal line is a guide to the eye, separating paramagnetic and diamagnetic regimes. It can be seen that $\chi_{\text{RT}} < 0$ over the entire doping range but it is nonmonotonic. Diamagnetic $\chi_{\text{core}}(Q)$, calculated as explained in Subsection 5.6.3, is plotted by the lower solid line. If a constant paramagnetic contribution of around 1.75×10^{-4} emu/mol is added to $\chi_{\text{core}}(Q)$, this line is shifted upwards and then fits the high- Q data reasonably well.

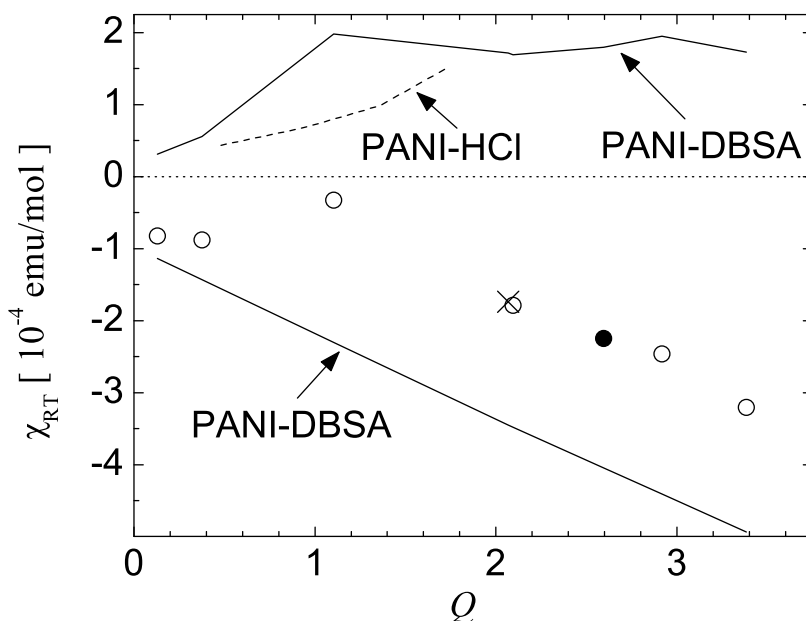


Figure 3.9: Symbols represent measured $\chi_{\text{RT}}(Q)$, for the doping series at $V = 80$ cm³ (open circles), for the doping at $V = 200$ cm³ and $P \approx 10$ (solid circle), and at $V = 800$ cm³ and $P \approx 10$ (cross). The calculated diamagnetic χ_{core} is shown by the lower solid line, and the extracted paramagnetic susceptibility by the upper solid line. The dashed line corresponds to the extracted paramagnetic susceptibility of PANI-HCl, whereas the horizontal dotted line is a guide to the eye, separating paramagnetic and diamagnetic regimes.

This means that the paramagnetic part of $\chi_{\text{RT}}(Q)$ is constant at high Q , i.e., the protonation is complete, whereas $|\chi_{\text{core}}(Q)|$ continues to increase with increasing Q due to the unbound DBSA. The overall magnitude of the paramagnetism as a function of Q can be inferred by subtracting the calculated $\chi_{\text{core}}(Q)$ from the measured $\chi_{\text{RT}}(Q)$, which results in a curve nonlinear in Q and displayed by the upper solid line. We also plot — by the dashed line — the paramagnetic contribution in PANI–HCl, obtained by carrying out the same procedure for the corresponding measured $\chi_{\text{RT}}(Q)$.

It can be seen that the paramagnetic part of $\chi_{\text{RT}}(Q)$ in PANI–HCl (where $Q = 2$ is the maximum dopant content in fully dry samples) differs from that in PANI–DBSA. This is, however, not entirely surprising, because the protonation level is not the only parameter which determines the paramagnetic response. For instance, the delocalisation of electrons is affected by local properties (through the Hubbard energy) [86] and extended disorder (through the Coulomb gap) [87], which are both material dependent and may have a stronger effect on χ than on σ . More importantly, the magnitudes of paramagnetism in PANI–HCl and in PANI–DBSA are of the same order, which in turn proves the viability of the protonation picture for PANI–DBSA and additionally supports the main conclusions of Subsection 3.3.1.

3.3.3 Electrical conductivity

In Fig. 3.10, on a log-log scale we plot σ_{RT} against Q . The open circles correspond to the doping series at $V = 80 \text{ cm}^3$, the solid circle to the doping at $P \approx 10$ and $V = 200 \text{ cm}^3$, and the cross to that at $P \approx 10$ and $V = 800 \text{ cm}^3$. The error bars of $Q < 0.1$ are large — for the reasons discussed in Subsection 3.3.1 — but a monotonic increase of σ_{RT} with increasing Q is clearly visible. The dashed lines delineate $\sigma_{\text{RT}} = 102 \text{ S/m}$ for 94 % protonated PANI–HCl, whereas $\sigma_{\text{RT}}(Q \approx 2)$ of PANI–DBSA is around 70 S/m. This similarity would not be possible if the protonation level in the two materials were not rather close, together with other parameters that influence the charge transport [4]. As before, this is in favor of $Q \approx 2$ corresponding to most of the DBSA being involved in the protonation, with little unbound DBSA remaining in the inter-chain space.

It can be seen that $\sigma_{\text{RT}}(Q)$ increases with increasing Q even when $Q > 2$, i.e., in the two-phase system. This increase is not small: $\sigma_{\text{RT}}(Q \approx 2)$ is roughly an order of magnitude smaller than the maximum obtained $\sigma_{\text{RT}}(Q \approx 3.4)$. There are two possible reasons for the monotonic increase in $\sigma_{\text{RT}}(Q)$ at $Q > 2$. The first is related to a simple geometrical consideration of the two-phase system. σ is extracted from the measured sample resistance R as $\sigma = L/SR$, where L is the distance between the voltage probes and S the cross-sectional area of the pellet. In the two-phase system, L and S do not correspond to (conducting) PANI–DBSA only, since some of the volume is occupied by the (insulating) unbound DBSA. Hence, it is certain that S and L are not true measures for the PANI–DBSA phase, but it is also questionable to what extent the geometrical correction can explain such a large increase in $\sigma_{\text{RT}}(Q)$ when Q in the two-phase system changes by less than twice.

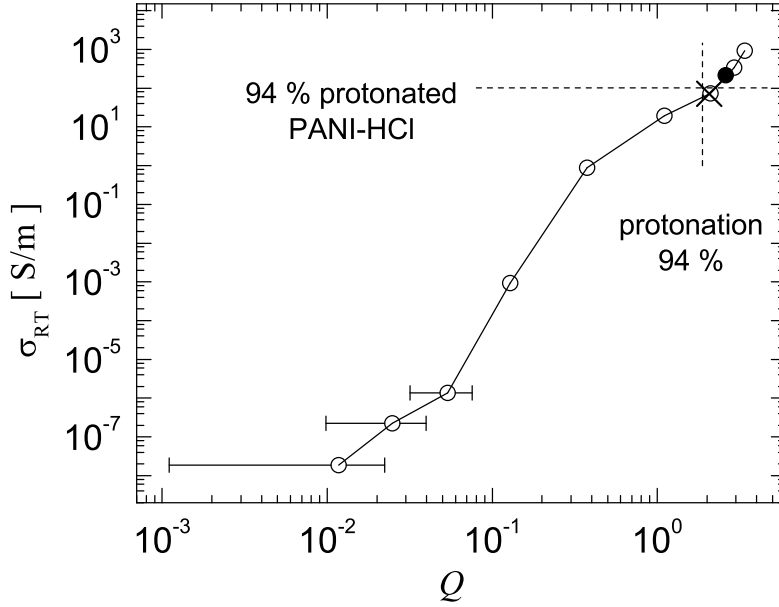


Figure 3.10: σ_{RT} vs Q for the doping series at $V = 80 \text{ cm}^3$ (open circles), for the doping at $V = 200 \text{ cm}^3$ and $P \approx 10$ (solid circle), and at $V = 800 \text{ cm}^3$ and $P \approx 10$ (cross). For large error bars of $Q < 0.1$, see the discussion in the text. The dashed line depicts σ_{RT} of 94 % protonated PANI-HCl.

This motivates us to address a second possible cause, that is, how the charge propagates at the microscopic level. Electrical conductivity in doped PANI is related to the hopping transport of charge carriers in a three-dimensional network of coupled one-dimensional conductors [88, 4]. This is manifested by σ decreasing with decreasing T as $\ln \sigma = \text{const.} - (T/T_0)^\alpha$, with α and T_0 carrying information on the microscopic processes involved [87]. While avoiding extensive discussion on details of α and T_0 , we note that α provides information on the effective dimensionality d of the charge transport as well as on the density of states for charge excitations, T_0 is related mainly to the localisation potential for charge carriers, whereas their combinations point to some other relevant energy and length scales [88, 87]. All these parameters and scales depend crucially on the nature of the chain entanglement [87], hence σ is influenced by much more than the bare density of mobile charge carriers that is created by the protonation — and which saturates at $Q = 2$.

Detailed analysis of $\sigma(T)$ of PANI-HCl suggests $d = 3$ [88], and this method applied to PANI-DBSA leads to the same conclusion — in particular with nearly the same α and T_0 for the two materials when the doping level is close to $Q = 2$ [4]. The effective $d = 3$ can, however, be achieved by moderate interchain coupling, which does not mean that the coupling cannot be enhanced further. A stronger interchain coupling implies a larger σ , as the charge carriers can more easily find energetically favoured

paths for their propagation. Notably, there is a change from $T_0 \approx 39000$ K at $Q \approx 2$ to $T_0 \approx 14000$ K at $Q \approx 2.9$ [4], suggesting that the localisation potential becomes shallower in the two-phase system because more easy-motion paths are created. This implies that — although being an insulator — DBSA can introduce additional spots for interchain charge jumps, possibly by affecting the entanglement of chains in a way that enhances their effective coupling in charge transport. These arguments offer at least a qualitative explanation for the increase of $\sigma_{\text{RT}}(Q \approx 3.4)$ so much above $\sigma_{\text{RT}}(Q \approx 2)$, which cannot be viably explained by geometrical considerations alone.

§ 3.4 X-ray diffraction analysis

X-ray diffraction on disordered polymers does not provide much information on the influence of structure on the electronic transport. Therefore, we use it only as a means of qualitative observation of the changes of morphology of samples with doping. All our samples (of different doping level) were subjected to X-ray diffraction analysis. Measurement was performed in Bragg-Brentano configuration [89] at RT, in the range of diffraction angles $10^\circ < 2\Theta < 60^\circ$. Here, we discuss the main findings using results for three representative PANI–DBSA samples.

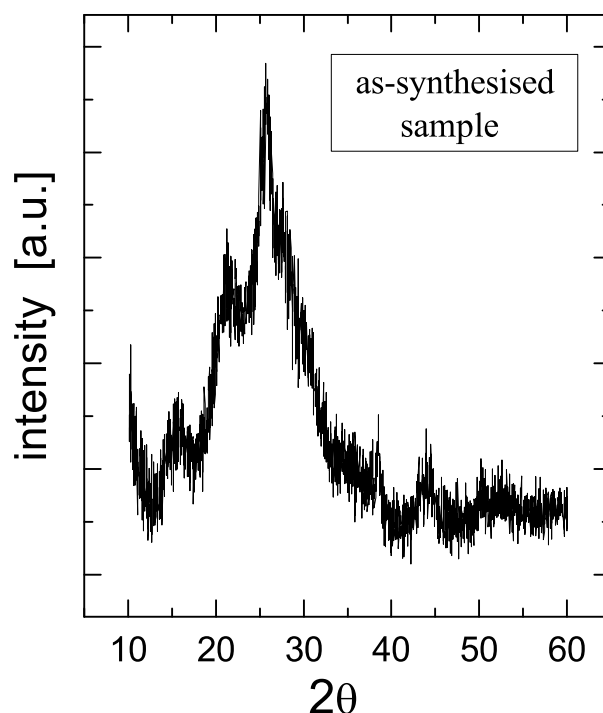
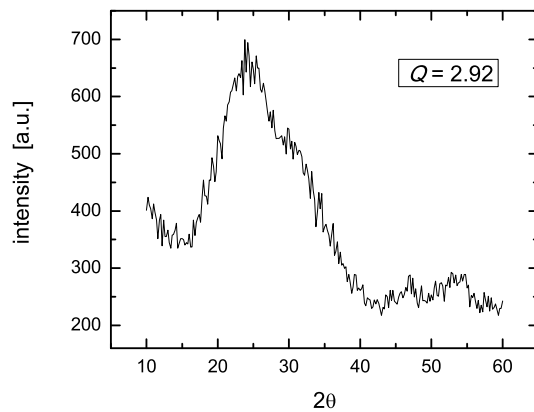
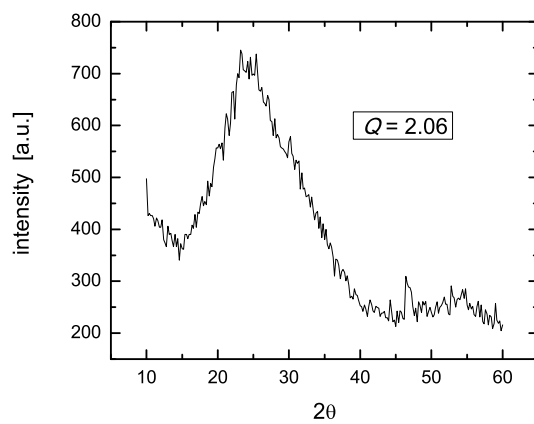
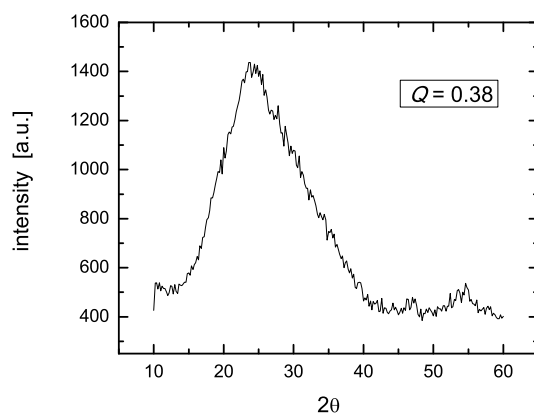


Figure 3.11: Diffractogram of the as-synthesised sample (PANI–HCl).

Figure 3.12: Diffractogram of the $Q = 2.92$ sample.Figure 3.13: Diffractogram of the $Q = 2.06$ sample.Figure 3.14: Diffractogram of the $Q = 0.38$ sample.

In Fig. 3.11, we first show the diffractogram of the as-synthesised sample. This is PANI–HCl material obtained as a direct product of the synthesis of PANI (see Section 3.1). One can see a broad amorphous signal with superimposed broad Bragg maxima which suggest structural ordering of polymer chains.

Results of X-ray diffraction measurements on PANI–DBSA samples (Figs. 3.12, 3.13 and 3.14) suggest a fully amorphous entanglement of the polymer chains over the entire doping range. This is in contrast to PANI–HCl, produced from the same generic PANI, where there are Bragg peaks (which become more pronounced as the doping level increases) superimposed onto a continuous background of the intensity vs diffraction angle plots [90, 88].

§ 3.5 Concluding remark

Having our PANI–DBSA properly characterised, we can now set off for exploring its fundamental properties (in Chapters 4 and 5), which will be followed by exploring its application potential (in Chapters 7 and 8).

Chapter 4

Electronic transport in PANI–DBSA

§ 4.1 Introductory remarks on electrons in solids

The study of the conductivity of electrons lies at the very heart of condensed matter physics. The early, Drude-Sommerfeld, model of electronic conductivity [21] relies on the idea of free electrons which scatter on ionic cores (fixed in points of the Bravais lattice of a metal), and on nothing else. The model disregards interactions between the electrons and the ionic cores, except as a source of instantaneous collisions. It also disregards electron-electron interaction. Given its simplicity, the Drude-Sommerfeld model is surprisingly successful in explaining many experimental phenomena, most notably the Ohm law

$$\mathbf{j} = \sigma \mathbf{E} \quad , \quad (4.1)$$

where \mathbf{j} is the current density, and \mathbf{E} the macroscopic electric field. The proportionality factor σ is the dc electrical conductivity given by

$$\sigma = \frac{n_e e^2 \tau}{m_e} \quad , \quad (4.2)$$

where n_e is the electron density, e the electron charge, m_e the free electron mass, and τ the average time between subsequent collisions.

Despite its numerous successes, the Drude-Sommerfeld model has flawed in some respects. For instance, it cannot explain the fact that some materials are insulators and semiconductors, i.e., that they are not metals. Complete disregarding of interactions is the underlying cause of the difficulties mentioned. The failures of the

Drude-Sommerfeld model can be remedied if one introduces interactions between free electrons and ionic cores, i.e., the periodic potential of a solid. An important apprehension arises from the introduction of a periodic potential V . Electrons do not scatter at all on ionic cores if the cores occupy points of a regular Bravais lattice.

Both very weak and very strong V give rise to a qualitatively similar result: an appearance of atomic-levels-like structure of energy bands (in the scheme reduced to the first Brillouin zone), with gaps in between. Organisation of electronic energy levels into the band structure is in fact a general property of an electronic energy spectrum in the presence of a periodic potential [91].

As already mentioned, periodic potentials do not scatter electrons. They determine their constant velocity, which asserts that there are stationary Bloch levels, which solutions of the Schrödinger equation for an electron in a periodic potential. So, in spite of the interaction of an electron with ionic cores, due to the translational symmetry of the potential of these ionic cores, the electron moves forever without any degradation of its (group) velocity. Consequently, in an ideal (i.e. perfectly periodic) crystal, electrons suffering no collisions would have $\sigma = \infty$ i.e. zero resistivity. Finite resistivity would appear only when electrons scatter on deviations from the periodicity of a crystal*.

Deviations of long-range periodicity — usually referred to as disorder — are identified either as impurities or intrinsic imperfections of the crystal structure. The motion of electrons in a disordered system is diffusive rather than ballistic; an electron experiences a series of random scatterings on imperfections, which results in a random walk.

The above discussion pertains to the Fermi gas, i.e. to non-interacting electrons. It is interesting to see what happens when one takes electron-electron interaction into consideration, which leads to the concept of Fermi liquid. Its remarkable result is that not much changes when interactions are present; properties of the system remain similar to those of free electrons. However, within the Fermi liquid theory, individual electrons are replaced by quasiparticles of finite lifetime — electrons dressed by the density fluctuations around them. But, even after the inclusion of electron-electron interaction, Eq. (4.2) of the Drude-Sommerfeld model may remain valid by replacing m_e with the effective mass of the electron.

The band structure determines characteristic properties of a solid, among which are those of the electronic transport. That is, from the band structure of a solid, one can infer (provided the possible effects of disorder and interactions are not severe)

*The resistivity of an ideal crystal would never be strictly zero because of the Heisenberg uncertainty relations smearing out the perfect periodicity of a crystal even at $T = 0$. At a finite T , electrons in an ideal crystal scatter on phonons, which lowers their conductivity. On the contrary, in disordered systems, scattering on phonons enables delocalisation of electrons at low T , which will be discussed later in more detail.

whether the medium is a conductor, an insulator, or a semiconductor, the CP's belonging to either the last or penultimate category. An important consequence of the band theory is that a fully occupied band cannot carry an electric current [91]. This “drawback” is usually circumvented by means of doping.

§ 4.2 Localisation of electrons

For deep bands, electrons can hardly move, spending most of the time bound to ionic cores, and only occasionally jumping from one atom to another. A very strong V can be realised in ideal crystals but can also appear due to imperfections, the latter being the case in real CP's.

The more the imperfections, the smaller the mean free path of electrons — and consequently the lower the conductivity. But how low can conductivity be? P. W. Anderson discovered that beyond a critical amount of scattering on imperfections, the diffusive motion of an electron is not just attenuated, it can come to a complete halt [92]. The electron becomes trapped and the conductivity vanishes. This is the Anderson localisation, also known as the strong localisation, and is addressed in more detail in Section 4.3.

This phenomenon is to be distinguished from the weak localisation — an enhanced backscattering of electrons which appears due to quantum interference of electronic Bloch waves that propagate through a disordered medium. Coherent treatment (adding the amplitudes by first summing and then squaring) of all the possible paths an electron can take travelling from a point A to a point B, increases the electron's probability of returning to the starting point A. Quantum interference thus lowers conductivity. But it was shown [93] using a fractal model of the Bethe lattice (infinite homogeneous Cayley tree), in which it is impossible for an electron to return to the same lattice site except by retracing exactly the same path, that weak localisation cannot eventually localise an electron around a lattice point, although it is regarded as a precursor effect of Anderson localisation.

Anderson localisation is also to be distinguished from the Mott localisation, where the transition from metallic to insulating behaviour is not due to disorder but due to a strong mutual Coulomb repulsion of electrons. When the density of charge carriers is commensurate with the lattice, the system can become an insulator. The longer the range of interaction, the higher the commensurability for which one can have a Mott insulator [94]. The Wigner crystal is an example of the Mott insulator. Another canonical example is given by the Hubbard model.

Many real materials cannot be neatly classified as being either Anderson or Mott insulators. While they might be metallic in the absence of disorder and electron-electron interaction, their insulating behavior can be related to an interplay of Anderson and Mott mechanisms [95]. Therefore, they are referred to as the Anderson-Mott insulators.

§ 4.3 Anderson localisation

A qualitatively correct description of the transition from metallic to insulating behaviour of electrons in disordered systems (i.e., when the crystal potential V is not periodic) can be given in terms of non-interacting electrons [96]. Anderson localisation, like any other phase transition, strongly depends on the dimension of the system. Unlike in 1D systems where all states are localised [97], the 3D case is more complex, as we shall see in this section. Anderson constructed a localisation model within the framework of TBA, retaining the periodic arrangement of potential wells but randomising their depths [98, 99, 92].

4.3.1 Scattering by weak random potential

We first wish to consider the case of a weak random potential. This is the weak-disorder limit of the Anderson localisation which is presented in Subsection 4.3.2.

As we already know from section 4.1, that a degenerate electron gas can move freely in the presence of an ordered periodic V_1 , i.e., of a crystalline array of potential wells of the same depth [as in Fig. 4.1(a)]. The corresponding one-electron wavefunctions $\psi_{\mathbf{k}}$, which are solutions of the Schrödinger equation

$$\nabla^2\psi + \frac{2m}{\hbar^2} [E - V_1(\mathbf{r})] \psi = 0 , \quad (4.3)$$

are Bloch waves. According to a corollary of Bloch theorem, any Bloch wave can be written as

$$\psi_{\mathbf{k}}(\mathbf{r}) = \frac{1}{\sqrt{M}} \sum_{j=1}^M e^{i\mathbf{k}\cdot\mathbf{R}_j} \Phi(\mathbf{r} - \mathbf{R}_j) , \quad (4.4)$$

where, when interpreted within TBA, functions $\Phi(\mathbf{r})$ stand for Wannier functions which are linear combinations of (a small number of) atomic orbitals $\phi(\mathbf{r})$. \mathbf{R}_j denotes the points of the Bravais lattice, i.e., of the potential wells. We assume to have M wells in total.

In other words, when an electron is allowed to hop from one well to another (the wells being in a periodic arrangement), a band containing M Bloch states is formed

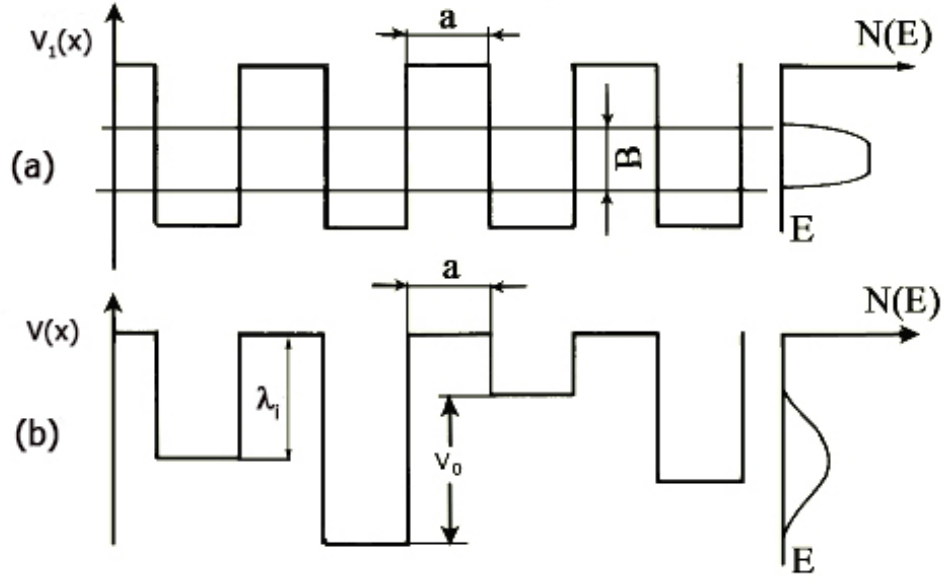


Figure 4.1: (a) An ordered potential $V_1(x)$ of a periodic arrangement of potential wells with a lattice constant a and a bandwidth B . (b) A disordered, random potential $V(x)$ of a periodic arrangement of potential wells, considered in the Anderson localisation model. The corresponding densities of states $N(E)$ are also shown.

from each bound state of a single well. One often wants to consider only one energy band. Bandwidth B is given by

$$B = 2zI \quad , \quad (4.5)$$

where z is the coordination number, and I the energy transfer integral between nearest neighbours (only they overlap substantially) given by

$$I = - \langle \phi(\mathbf{r} - \mathbf{R}_{j+1}) | \Delta V(\mathbf{r}) | \phi(\mathbf{r} - \mathbf{R}_j) \rangle \quad , \quad (4.6)$$

where $\Delta V(\mathbf{r})$ contains all corrections to the atomic potential required to produce an ordered periodic crystal potential V_1 .

In the Anderson localisation model, the array of potential wells is still periodic, but with random terms $-V_0/2 \leq U_i \leq V_0/2$ added to the wells [see Fig. 4.1(b)]:

$$V(x) = V_1(x) + \sum_i U_i \quad , \quad U_i \in \left[-\frac{1}{2}V_0, \frac{1}{2}V_0 \right] \quad \forall i \quad . \quad (4.7)$$

V_0 is the energy difference between the deepest and the shallowest of the wells. For $V_0 = 0$, there is no randomness, so the electronic states are simply Bloch waves. For $V_0 \ll I$ the system is metallic. Bloch waves are weakly changed by the random potential. This change causes the Bloch waves to lose phase coherence on a length scale of the mean free path l . Nevertheless, provided that V_0 is small, the wavefunction remains extended throughout the sample [see Fig. 4.2(a)], and is given in terms

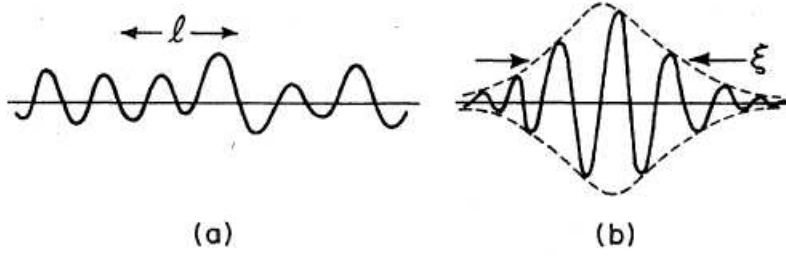


Figure 4.2: (a) Typical wave function of an extended state with the mean free path l . (b) Typical wave function of a localised state with the localisation length ξ . (Reproduced from [99].)

of atomic orbitals ϕ :

$$\psi(\mathbf{r}) = \frac{1}{\sqrt{M}} \sum_{j=1}^M C_j e^{i\gamma_j} \phi(\mathbf{r} - \mathbf{R}_j) , \quad (4.8)$$

where C_j and γ_j are random numbers. For a small V_0 , the effect is to introduce, for energies near the middle of the band, a finite l , which can be calculated from the perturbation theory within the Born approximation. The result is [100]:

$$\frac{l}{a} = 32\pi \left(\frac{I}{V_0} \right)^2 = \frac{8\pi}{z^2} \left(\frac{B}{V_0} \right)^2 . \quad (4.9)$$

So, if $z = 6$, then $l \gtrsim a$ when $V_0/B \cong 0.8$.

4.3.2 Strong localisation

The one-band Hamiltonian exhibiting Anderson localisation model is given by

$$\mathcal{H} = \sum_i \lambda_i c_i^\dagger c_i + \sum_{i \neq j} I_{ij} c_i^\dagger c_j + \text{h.c.} , \quad (4.10)$$

where λ_i are random depths of potential wells, I_{ij} the matrix element for hopping from well i to well j , and c_i the electron ladder operators. Spin is considered to be an inessential complication, so the electrons are taken to be spinless. In real systems, which are disordered and do not have translational symmetry, I_{ij} are random variables. In the Anderson model, all randomness is accounted for in the λ_i 's. This is a drastic simplification, yet the model yields rich physics, as we shall see. Anderson simplified the problem further by restricting the matrix elements I_{ij} in Eq. (4.10) to hopping integrals between nearest neighbours only [given by Eq. (4.6)],

$$I_{ij} = I \delta_{i,j-1} . \quad (4.11)$$

For $I = 0$, all of the eigenstates of (4.10) are localised at individual sites. In other words, the eigenstates are $|i\rangle$, with eigenvalues λ_i . The system is insulating. But the transition between $I/V_0 = \infty$ (the limit of no disorder) and $I/V_0 = 0$ (limit of enormous disorder) occurs at a finite I/V_0 . The electronic wavefunction in a random potential may be profoundly altered provided the randomness is sufficiently strong — it becomes localised and the envelope of the wavefunction decreases exponentially away from a point in space [see Fig. 4.2(b)]. Thus, in the strong disorder limit, the wavefunction will not be anymore of the form (4.8) but exponentially localised instead:

$$\psi(\mathbf{r}) = \frac{1}{\sqrt{M}} e^{-|\mathbf{r}-\mathbf{R}_m|/\xi} \sum_{j=1}^M C_j e^{i\gamma_j} \phi(\mathbf{r}-\mathbf{R}_j) , \quad (4.12)$$

where \mathbf{R}_m is the point (of the Bravais lattice) the wavefunction is centred about, and ξ is the localisation length.

The existence of a localised state can be easily understood if we address the limit of a very strong disorder. Then a zeroth-order description of the eigenstate would be a bound state or a localised orbital in the random potential. In this case, we can consider the admixture between different orbitals as a perturbation:

$$|i\rangle + \sum_j \frac{I}{\lambda_i - \lambda_j} |j\rangle . \quad (4.13)$$

The main point is that such admixtures will not produce an extended state composed of linear combinations of infinitely many localized orbitals [99]. The reason is that orbitals that are close to one another in space, so that their wavefunctions overlap significantly, are in general very different in energy, so that the admixture is small because of the large energy denominator in (4.13).

On the other hand, states that are nearly degenerate are generally very far apart in space, so that the overlap is exponentially small. Yet this is not a foolproof argument because λ_i and λ_j are random variables. Thus, there is always some finite probability for $\lambda_i - \lambda_j$ being exceedingly small. Nevertheless, it can be shown [101] that perturbation theory converges in the thermodynamic limit.

Hence, there is a regime where electronic states are localised and the system is insulating (Anderson insulator), by which we mean that the dc conductivity vanishes at $T = 0$. No diffusion or conductivity is then possible without thermal activation. It is not surprising that there are localised states in a disordered system. What is surprising is that if the disorder strength is sufficient, all the states will become localised collectively, i.e., the entire band will consist of localised states. Localisation occurs when the parameter V_0/B exceeds certain critical value [96]:

$$\frac{V_0}{B} > \left(\frac{V_0}{B}\right)_{\text{crit}} \approx 2 . \quad (4.14)$$

4.3.3 Localised and extended states in Anderson insulator

Electronic states will be localised if the criterion (4.14) is satisfied, and extended if it is not. This is in agreement with a principle enunciated by Ioffe and Regel [102], which states that as the extent of disorder is increased in a metallic system, there is a limit to metallic-conductivity-like behavior which corresponds to $k_F l \gg 1$, \mathbf{k}_F being the Fermi wavevector. When the mean free path becomes shorter than the interatomic spacing, coherent metallic transport is not possible. Thus, the Ioffe–Regel criterion for localisation is defined as

$$k_F l \approx 1 \quad . \quad (4.15)$$

When the strength of a random disorder potential is large in comparison with B , all states of a degenerate electron gas become localised and the conductor becomes a Fermi glass, that is, a continuous density of localized states occupied according to the Fermi-Dirac distribution. Although the Fermi glass is not gapped in energy, it behaves as an insulator because the states at E_F are spatially localised [103].

If the Anderson criterion (4.14) is not satisfied, we can apply perturbation theory to the random potential. In perturbation theory, the states will be Bloch waves, weakly changed by the random potential and given by Eq. (4.8). Perturbative analysis is correct for states in the centre of the band. But near the band edges, however, perturbative analysis breaks down and states are localised [104]. The corresponding density of states has the so-called Lifshitz tails [105]: instead of a van Hove singularity at the band edge, at which $\frac{dN}{dE}$ would diverge, one rather has an essential singularity (neither a removable singularity nor a pole) at which $\frac{dN}{dE}$ vanishes.

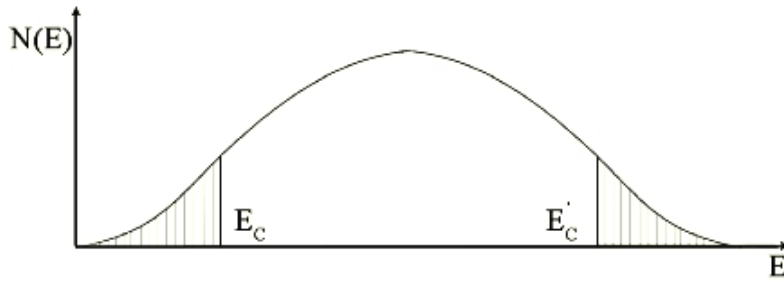


Figure 4.3: Density of states in an Anderson band, with the two mobility edges E_C and E'_C . States in the tails are localised.

Thus, in the weak disorder limit, there are extended states near the band centre, and localised states near the band edges. There is a critical energy E_C (the mobility edge) separating localised from extended states (see Fig. 4.3). The simplest definition of E_C in terms of the behaviour of σ is as follows:

$$\text{sgn} \left[\lim_{T \rightarrow 0} \sigma(T, E_F) \right] = \begin{cases} 0 & \forall E_F \leq E_C \\ +1 & \forall E_F > E_C \end{cases} ,$$

If, by changing the composition of a material or due to the effects of a strain or an applied magnetic field, E_F can be made to cross the value of E_C , a transition is expected from a metallic state, with finite values of $\sigma(T \rightarrow 0)$, to a non-metallic state for which $\sigma(T \rightarrow 0)$ vanishes. Bestowing Anderson's work, Mott called this kind of metal-insulator transition the Anderson transition. This is a sharp transition at $T = 0$. There is another, successful and famous formulation of the Anderson localisation - the scaling theory of localisation [106]. In any case, Anderson localisation belongs to the cornerstones of condensed matter physics.

In our PANI-DBSA we do not observe an Anderson transition. The system is insulating in the entire T range of our measurements (10 - 300 K), viz, E_F is within the disorder band, and only localised states take part in conduction. Hence, the conduction is of the hopping type (see Section 4.8).

§ 4.4 Effects of interaction and dimensionality

In the preceding analysis, we introduced a disorder-induced insulating state of non-interacting electrons. But what about the effects of electron-electron interactions? At high density, we expect the electrons to screen the Coulomb potentials, which then acquire the Yukawa form, and this should consequently enhance the metallic behavior. However, when the density of electrons is sufficiently low, the screening effect is too weak to prevent localisation [39]. Unscreened Coulomb interactions can strongly influence the properties of the insulating state, as we shall see for our samples. Of course, electron-electron interactions can have other effects beside the screening, e.g., they can lead to ordered states such as superconductivity or ferromagnetism, but neither of this is the case in our samples.

Electronic systems which do not follow the very successful Landau's Fermi liquid theory of interactions in solids are loosely referred to as strongly correlated systems. They are at the heart of the contemporary research in condensed matter physics. The effects of interactions should be greatly enhanced by reduced dimensionality. In 1D, the effects of interactions are at their maximum; and the Fermi liquid is replaced by a new state of matter, the Luttinger liquid with radically different properties [107]. Among low-dimensional electronic systems, organic conductors have a special place. Indeed, because of their abundance and intrinsic 1D nature, they provide not only exotic 1D electron subsystems but also a large number of 1D systems coupled together to form systems of higher dimensionalities [94, 108]. Depending on the coupling strength between the 1D subsystems, macroscopic samples can exhibit either predominantly 1D or 3D properties, including crossovers between the regimes. For CP's this coupling leads to 3D systems which consist of intrinsic 1D subsystems.

§ 4.5 Electronic transport in low-dimensional systems

Issues related to transport in low-dimensional electronic systems are challenging, the main difficulties being to take into account the disorder and interactions [109]. In some cases, one faces an interplay between the two. It is known that for strictly 1D systems, any amount of disorder leads to localised states [97].

Furthermore, a case with the presence of electron-phonon coupling has been studied [110], showing that 3D phonons provide a delocalisation mechanism for electrons at T low enough that the scattering is mainly elastic, i.e., $\tau_{\text{in}}(T) \gg \tau_{\text{el}}$, where τ_{in} is the inelastic phonon scattering time and τ_{el} the elastic scattering time on static defects. This delocalisation mechanism leads to a power-law in $\sigma(T)$ that originates in hopping between localised states, but it does not pertain to lowest T , i.e., it is valid only above $T_b \propto 1/\tau_{\text{el}}$.

Subsequent studies [107, 111] aimed at exploring the effects of electron-electron interactions in 1D Anderson insulators. It is worth noting that the presence of electron-electron interactions causes the power-law of hopping to acquire non-universal exponents. More recently was addressed [112] a low- T situation in a disordered system where the coupling to phonons is absent and electron-electron interactions are present. It was demonstrated that electron–electron interactions alone cannot lead to finite σ at a finite but small T . In the absence of phonons and extended one-electron states, a system of interacting electrons has exactly $\sigma = 0$ below a certain temperature T_s , and a power-law hopping conductivity above T_s .

Less explored, from the point of view of microscopic techniques, is the low- T regime where $T \ll T_b \propto 1/\tau_{\text{el}}$ and both electron–electron and electron phonon interactions are present. In this case, it is generally believed that the electronic transport is of variable-range hopping type, which is addressed in much detail in Section 4.6.

§ 4.6 Hopping transport

4.6.1 Introduction

Electrical conductivity in semiconducting materials (to which CP’s also belong) can be intrinsic and extrinsic, and is expressed as a superposition of the contributions of all types of charge carriers, that is,

$$\sigma = \sum_m q_m \mathcal{L}_m \mu_m \quad , \quad (4.16)$$

where m denotes the charge type, q_m its value, μ_m its mobility, and \mathcal{L}_m its concentration. Intrinsic conduction is due to thermal activation of electrons across the energy gap, from the valence band into the conduction band. This type of conduction is substantial only at very high T , and there it vanquishes extrinsic conduction should there be dopants present. So, in case of intrinsic conduction, (4.16) effectively turns into:

$$\sigma = e \mathcal{L}_e \mu_e + e \mathcal{L}_h \mu_h \quad , \quad (4.17)$$

where the first term refers to intrinsic electrons in the conduction band, and the second term to intrinsic holes in the valence band. In the steady state, \mathcal{L}_e and \mathcal{L}_h depend on T predominantly exponentially [22, 113]:

$$\mathcal{L}_e = \mathcal{L}_h = \frac{(2\pi\sqrt{m_e m_h} k_B T)^{3/2}}{4\pi^3 \hbar^3} \exp\left(-\frac{E_g}{2k_B T}\right) \quad , \quad (4.18)$$

where m_e and m_h are effective masses of electrons and holes, respectively, and E_g is the width of the gap. Due to the large activation energy, $E_g/2$, \mathcal{L}_e and \mathcal{L}_h decrease rapidly with decreasing T . At a sufficiently low T , \mathcal{L}_e and \mathcal{L}_h become smaller than the concentration of charge carriers contributed by dopants. In this T regime, σ is entirely determined by the nature and concentration of dopants, and is therefore called extrinsic [114].

We can distinguish between two types of extrinsic conduction:

1. **band conduction** (takes place within conduction band or valence band)

Band conduction occurs at T which is relatively high but satisfies $k_B T \ll E_g$. If we are dealing with shallow donors/acceptors, the ionisation energy of which is much lower than E_g , a majority of donors/acceptors will be ionised, viz, charge carriers originating from dopants will populate the conduction band or the valence band. $\sigma(T)$ for the band conduction is given by an Arrhenius law [113, 114], e.g., the conductivity of dopant electrons in a conduction band is given by

$$\sigma(T) \propto \exp\left(-\frac{E_C - E_D}{k_B T}\right) \quad , \quad (4.19)$$

where E_C is the lower edge of the conduction band, and E_D the dopant (donor) level within gap.

Further decrease in T results in a gradual freezing-out of charge carriers, i.e., electrons are recaptured by donors (and holes are recaptured by acceptors). Decreasing T eventually leads to a situation in which the main contribution to electrical conduction comes from electrons hopping directly between dopant states within the gap, without any excursion to the conduction band. This is called hopping conduction.

2. hopping conduction (takes place within a disorder band)

Electrons hop within a disorder band, from occupied dopant sites to empty ones. The hopping mechanism of conduction corresponds to a very low mobility, since the electron hops are associated with a weak overlap of the wavefunction tails from different dopants. Nevertheless, at low T , hopping conduction overcomes band conduction because only an exponentially small number of free carriers can participate in the latter [114]. Hopping conduction is particularly important for disordered systems, much more than for (doped) crystalline ones.

If E_F falls within the disorder band, dc conductivity will vanish at $T = 0$. At finite but low T , electronic transport in this kind of insulators takes place by hopping between localised sites. Through a sequence of hops, the insulator can conduct electricity. Such electronic transport is generally a very nontrivial competition of inelastic scattering with thermal activation and long-range Coulomb interaction [115].

In our PANI–DBSA, we have detected only hopping conduction, which holds for the entire T range investigated (10 - 300 K). However, different varieties of hopping transport have been identified. Therefore, I address hopping conduction in more detail below, relying on [115–118, 39, 100].

Hopping conduction happens among randomly placed dopant states (in a disorder band), which do not involve a superlattice within the host lattice. An important postulate of the concept of hopping conduction is the assumption that practically all the states have different energies: two states with equal energies are an infinite distance apart. Hence, hopping is generally accompanied by an emission or absorption of a phonon.

Let us consider two electron states, i and j , in disorder band. The states are a distance R apart, and their eigenenergies are E_i and E_j . We can, without any loss of generality, take that $W \equiv E_j - E_i > 0$. An electron can hop from site i to site j by the absorption of a phonon of energy W . The corresponding hopping probability is given by

$$P_{ij} = e^{-2R/\xi} f_i (1 - f_j) b_W \quad , \quad (4.20)$$

where ξ is the localisation length of the electron wavefunction, b_W the Bose-Einstein distribution for phonons of energy W , and f_i the Fermi-Dirac distribution for state i :

$$b_W = \frac{1}{e^{W/k_B T} - 1} \quad , \quad f_i = \frac{1}{e^{(E_i - \mu_i)/k_B T} + 1} \quad , \quad (4.21)$$

where μ_i is the local chemical potential in the presence of an electric current [119]. f_i in (4.20) denotes the probability that state i is full, whereas $(1 - f_j)$ denotes the probability that a state j is empty. The term $e^{-2R/\xi}$ represents quantum-mechanical tunnelling, which is underlying to the hopping process and which depends on how much the states i and j overlap. In a 1D system, ξ simply describes the exponential

decay of an electron wavefunction in a potential barrier and is directly related to the height of the potential barrier. In systems of higher dimensions, the meaning of ξ is less obvious. It is determined by an integration over all possible tunnelling paths between two sites, thus reflecting the potential landscape surrounding a particular hopping site.

The reverse hopping probability, for a hop from site j to site i , is given by

$$P_{ji} = e^{-2R/\xi} f_j (1 - f_i) (b_W + 1) \quad , \quad (4.22)$$

and it is accompanied by the emission of a phonon of energy W . The corresponding hopping rates are

$$\frac{1}{\tau_{ij}} = \omega_0 P_{ij} \quad , \quad \frac{1}{\tau_{ji}} = \omega_0 P_{ji} \quad , \quad (4.23)$$

where ω_0 is the attempt frequency given by a typical phonon frequency.

Assuming no correlations among the occupation probabilities of different localised states, the net flow of electrons between the two states is [120]

$$\mathcal{J}_{ij} = eR \left(\frac{1}{\tau_{ij}} - \frac{1}{\tau_{ji}} \right) \propto \omega_0 e^{-2R/\xi} \frac{\sinh \frac{\mu_j - \mu_i}{2k_B T}}{\sinh \frac{W}{2k_B T} \cosh \frac{E_i - \mu_i}{2k_B T} \cosh \frac{E_j - \mu_j}{2k_B T}} \quad . \quad (4.24)$$

This expression can be simplified (by expanding it into a series up to linear terms) if one assumes that all energy differences in (4.24) are larger than or comparable to $k_B T$. In the low-electric-field regime, which pertains to a small voltage drop over a hopping distance ($\mu_j - \mu_i \ll k_B T$), the above assumption results in the following expression for electrical conductivity [119] ($\Delta\mu \equiv \mu_j - \mu_i$):

$$\sigma_{ij} \equiv \lim_{\Delta\mu \rightarrow 0} \frac{\mathcal{J}_{ij}}{\Delta\mu} \propto \exp \left[-\frac{2R}{\xi} - \frac{|E_i - \mu| + |E_j - \mu| + W}{2k_B T} \right] \quad . \quad (4.25)$$

with $\Delta\mu \ll \mu_i, \mu_j$.

4.6.2 Nearest-neighbour hopping

The simplest form of hopping involves nearest neighbours. The density of states (DOS) in the disorder band at low dopant concentration is maximum at E_D . When the initial and final points of a hop comprise nearest neighbours, it is most probable that the energy levels of these points are in the vicinity of the maximum of DOS. The hopping event takes place only if the terminating site is free. The probability that it is free depends on its energy with respect to μ , and is proportional to [117]

$$\exp \left(-\frac{E_D - \mu}{k_B T} \right) \quad . \quad (4.26)$$

This is the smallest factor entering (4.25), and thus represents the crucial feature determining the conduction between nearest neighbours. The term $\exp(-W/2k_B T)$, which determines the probability that phonons of energy W participate in the hop, is

larger because $W \ll E_D - \mu$. It also holds that $\exp(-2R/\xi) \gg \exp[-(E_D - \mu)/k_B T]$ since R now represents the distance between nearest neighbours. Therefore, the T dependence of the nearest-neighbour-hopping (NNH) conductivity is given by the following Arrhenius-law form:

$$\sigma_{\text{NNH}}(T) = \eta_1 e^{-A/k_B T} \quad , \quad (4.27)$$

where $A = E_D - \mu$ is the activation energy, and η_1 a prefactor which weakly depends on T . Indeed, the physics of NNH is predominately determined by the fact that $A \gg W$.

A necessary condition for the realisation of NNH is the abundance of pairs of neighbouring sites with one of the sites in the pair being free. A decrease in T , such that $k_B T \ll E_D - \mu$, makes the number of empty sites among the nearest neighbours (the majority of which have energy E_D) too small, and hopping to the spatially nearest sites gradually diminishes. In turn, this increases the importance of hopping between the sites with energies lying in some vicinity of E_F where empty sites certainly exist [117]. We deal with this case in Subsection 4.6.3.

4.6.3 Mott's law of variable-range hopping

Variable-range hopping (VRH) is a model widely used in describing low- T conductivity in strongly disordered systems with Anderson-localised charge-carrier states, such as our PANI–DBSA is. It was developed by N. F. Mott [121, 122]. The model earned its fame through the plethora of experimental evidence supporting its validity in systems like doped crystalline semiconductors, amorphous semiconductors [123, 96], or CP's [16]. I shall present here a plain and intuitive derivation of the Mott law of VRH, in continuation to the above considerations on hopping transport.

One might (erroneously) imagine that electrons will only hop to the nearest neighbouring states since the matrix element to hop to a more distant state will be exponentially smaller (in distance). However, a state which is further away might be closer in energy, and therefore exponentially (in thermal energy) easier to reach [39]. The key insight of Mott was the proper balance in a competition between the two effects, and this eventually led to the concept of VRH.

Actually, VRH can be regarded as the nearest-neighbour hopping in a 4D hopping space of coordinates and energy [124]. In a system of localised states with random eigenenergies, the probability distribution function for all hops originating from one site is always dominated by the hop to a site which is the nearest-neighbour in the 4D hopping space of coordinates and energy. In such a 4D hopping space, the range between two states i and j is — due to the exponential dependence of the hopping conductance (4.25) — defined as

$$\mathcal{R}_{i \rightarrow j} = -\ln(P_{ij} - P_{ji}) \quad . \quad (4.28)$$

As introduced in the previous subsection, Mott's approach assumes that the dominant contribution to the hopping current is through states within $k_B T$ of the chemical potential $\mu \equiv E_F$. Thence, the Miller-Abrahams expression (4.25) reduces to

$$\sigma_{ij} \propto e^{-W/k_B T} e^{-2R/\xi} . \quad (4.29)$$

At low T , there is a scarcity of phonons, so the electronic transport favours longer hops of variable range.

The number of available electron states per unit energy within distance R from an electron state in the vicinity of E_F is, using the Fermi sea approximation, equal to $\frac{4\pi}{3} R^3 N_F$, where N_F is the DOS at E_F . Hence, the typical smallest energy difference between a given state and the other one, within a distance R , is given by:

$$W = \left(\frac{4\pi}{3} R^3 N_F \right)^{-1} . \quad (4.30)$$

In real materials, N_F will be an effective DOS. The electrical conductivity associated with such a hopping process is given by

$$\sigma_{ij} \propto \exp \left[-\frac{W(R)}{k_B T} - \frac{2\bar{R}}{\xi} \right] , \quad (4.31)$$

where $\bar{R} = 3R/4$ is the average hopping distance. So, we can infer that the VRH conductivity depends on the (squared) matrix element between two states involved in a hop, which we take to decay as $\propto \exp(-2\bar{R}/\xi)$, and on the probability that an electron hops over a barrier by thermal activation, which is accounted for by the Boltzmann term $\propto \exp[-W(R)/k_B T]$. The prefactor of the exponential dependence (4.31) contains various comparatively weak dependences in R ; for instance, there should be a factor of R corresponding to the fact that a longer hop constitutes a larger contribution to the electric current [39].

There are many such hopping processes available to an electron. The electron could hop a short distance with a relatively large matrix element, but the activation energy would probably be high in such a case. It could instead hop a long distance and find a state with a low activation energy, but the matrix element would be then very small. The optimal route is for the electron to hop a distance which maximises the exponential in (4.31), i.e.,

$$\frac{d\sigma_{ij}}{d\bar{R}} = 0 . \quad (4.32)$$

The above condition leads to [100, 39]

$$R_{\text{optimal}} = \left(\frac{3\xi}{2\pi k_B T N_F} \right)^{1/4} . \quad (4.33)$$

Hence, as T is decreased, the electron makes longer and longer hops. The resulting T dependence of the VRH conductivity is:

$$\sigma_{\text{VRH}}(T) = \sigma_0 \exp \left[-\left(\frac{T_0}{T} \right)^{1/4} \right] , \quad (4.34)$$

where σ_0 is relatively weakly dependent on T (e.g., a power-law dependence), and

$$k_B T_0 = \frac{24}{\pi N_F \xi^3} . \quad (4.35)$$

In d dimensions, the **Mott law** of VRH generalises to

$$\sigma_{\text{VRH}}(T) = \sigma_0 \exp \left[- \left(\frac{T_0}{T} \right)^{\frac{1}{1+d}} \right] . \quad (4.36)$$

For strictly 1D systems the above formula takes a different form [125], but for quasi-1D systems, such as CP's, its validity is restored [126, 127].

4.6.4 Beyond the Mott law

The Mott law (4.36) assumes a constant DOS in the vicinity of E_F , and an isotropic system. Coulomb interaction is not taken into account in its derivation. However, neglecting the Coulomb interaction (either electron-electron or electron-hole interaction) is often an oversimplification in real systems, such as CP's. Namely, in a disordered material, the Coulomb interaction is not screened at long wavelengths and low frequencies because there is a scarcity of mobile charge (since charge carriers are localised). Furthermore, this scarcity is particularly pronounced at low T since the charge transport in disordered materials is phonon-assisted. Thus, in systems with localised electrons, the Coulomb interaction remains both strong and long-ranged.

Following the work of Mott, an apprehension emerged [128, 129] that, in insulators, the DOS for charge excitations (DOSCE) around E_F will be suppressed in the presence of long-range Coulomb interaction. In a metal, electrons screen the Coulomb interaction so that the electric field of a charge does not extend beyond the Thomas-Fermi screening length, thus making the DOSCE around E_F a constant [115].

The basic physics of including the effects of Coulomb interaction in hopping is as follows. Suppose that there are two Anderson-localised single-particle states, one just below E_F and one just above. The single-particle energy cost associated with moving an electron from the lower state to the higher one would be at least partially offset by the negative Coulomb energy associated with the resulting particle-hole pair. If the distance between the states is small, this Coulomb energy will be large and will overcompensate the single-particle energy. Hence, the states must be far apart, and therefore, the single-particle DOSCE must be small [39]. So, due to unscreened Coulomb interaction, the DOSCE vanishes at E_F , and is suppressed near it. This mechanism introduces the concept of the **Coulomb gap** or the soft gap.

The effect is more quantitatively explained in the Subsection 4.6.5.

4.6.5 Efros - Shklovskii model

As we saw in the previous subsection, when the Coulomb interaction was taken into account, the states involved in a hop had to be far apart. Therefore, the Efros-Shklovskii (ES) model [129] assumes $\xi \ll R$, so the overlap term $\exp(-2R/\xi)$ can

be safely omitted from our consideration, and the energy of the system can be written in the form

$$\mathcal{H} = \sum_i \Psi_i n_i + \frac{1}{2} \sum_i \sum_{j \neq i} e_{ij} n_i n_j \quad , \quad (4.37)$$

where Ψ_i is the energy of the electronic state i not taking into account the contribution of electron-electron interaction, $e_{ij} = e^2/\kappa R$ is the energy of electron-electron interaction, κ the dielectric constant, and n_i the fermionic occupation number ($n_i = 0, 1$). The energies of single-particle excitations are given by

$$E_i = \Psi_i + \sum_{j \neq i} e_{ij} n_j \quad . \quad (4.38)$$

At $T = 0$, $n_i = 1$ for $E_i < E_F$ and $n_i = 0$ for $E_i > E_F$. The ground state of the system should also satisfy another condition. Let us consider states i and j , which in the ground state are occupied and vacant, respectively. The transfer of an electron from i to j should increase the energy of the system. Using (4.37), we find that the energy increase is

$$\Delta\mathcal{H}(i \rightarrow j) = E_j - e_{ij} - E_i > 0 \quad . \quad (4.39)$$

The term $-e_{ij}$ in (4.39) describes a quasi-excitonic effect, i.e., the Coulomb interaction of the electron-hole pair created by the electron transfer from i to j . The electron and the hole in the pair do not constitute an exciton, viz, the electron is not bound to the hole and they do not move together. The electron just feels a drag due to the hole left behind.

In the ground state, any two energies E_i and E_j close to the Fermi level must satisfy the inequality (4.39). It can be shown [129, 114] that this constraint causes a depletion of the DOSCE, $N(\varepsilon \equiv E - E_F)$, in the vicinity of E_F . Exactly at E_F , $N(\varepsilon)$ should vanish, i.e., $N(\varepsilon = 0) = 0$. It is important to note that $N(\varepsilon)$ is the DOSCE, it is not a thermodynamic DOS which does not vanish at E_F and is not altered by the inclusion of Coulomb interactions in the hopping transport story.

So, the described Coulomb interaction opens a Coulomb gap centred at E_F , and suppresses the DOSCE in the energy interval of a width 2ε centred at E_F . The DOSCE within the Coulomb gap is given by

$$N_{3D}(\varepsilon) \propto \varepsilon^2 \quad , \quad N_{2D}(\varepsilon) \propto |\varepsilon| \quad . \quad (4.40)$$

For energies farther away from E_F , the DOSCE value is restored to the constant value of the DOS, N_0 , the one that is assumed in the Mott model. So, the width of the Coulomb gap, Δ_C , is given by

$$N(\varepsilon = \Delta_C) = N_0 \quad . \quad (4.41)$$

The Coulomb gap plays an important role in the dc conductivity at low T , where thermal energy is of the order of Δ_C . Electrical conductivity in this T range is given

by the Efros-Shklovskii (ES) law,

$$\sigma_{\text{VRH}}(T) \propto \exp \left[- \left(\frac{T_{\text{ES}}}{T} \right)^{\frac{1}{2}} \right], \quad (4.42)$$

where $T_{\text{ES}} = e^2/\kappa\xi$. The ES law has a universal form, viz, the exponent is the same regardless of the dimension. The influence of the Coulomb gap can be neglected once $k_{\text{B}}T > \Delta_{\text{C}}$, and the Mott law (4.36) is restored.

It is important to note that the Coulomb gap exists only in a single-particle spectrum of energies E_i . This spectrum corresponds to the withdrawal of one electron or its addition to the system. There are other low-energy excitations in the system, but they do not contribute to dc conductivity [129, 130].

Just as for the Mott model, there is a plethora of experimental evidence [114] supporting the validity of the ES model. Yet, some experimental results could have not been explained by either of them, which called for further theoretical investigations.

4.6.6 Fogler - Teber - Shklovskii model

The ES model takes the Coulomb interaction into account but it pertains to isotropic systems, as well as the Mott model does. Since bulk CP's are on the microscopic scales highly anisotropic 3D systems, we expect a more complex model of VRH conductivity to describe the physics of CP's more appropriately. The Fogler - Teber - Shklovskii (FTS) hopping-transport model [87, 109], which pertains to coupled 1D systems and also includes the Coulomb interaction in the sense of the ES model seems to be a good candidate.

The central feature of the FTS model is a non-universal exponent α in the stretched exponential dependence of dc electrical conductivity, $\sigma(T) \propto \exp \left[- (T_{\alpha}/T)^{\alpha} \right]$. α implicitly depends on the Coulomb interaction and disorder. This is a generic property of incommensurate Q1D Anderson-Mott insulators and is absent for usual doped semiconductors and even for other (hypothetical) collective structures of interest, such as the pinned Wigner crystal [109].

So, strongly anisotropic screening of the Coulomb potential predicts unusual VRH laws, viz, the exponent α takes different discrete values: 1/2, 2/5, 1/4 and 1 (in 3D Q1D case [87]), and 1/2, 3/5, 5/11, 1/4 and 1 (in 2D Q1D case [109]). The exponent 1 signifies NNH, whereas the other exponents are related to VRH. Thus, we see that the FTS model accounts for the Mott case, the ES case, and the NNH case, and introduces some additional, intermediate-regime exponents.

It is worth mentioning that such intermediate (in T) regimes — between the ES-VRH regime and the NNH regime — were first discussed by Larkin and Khmel'nitskii for disordered thin films and wires [131], though not in the form of different exponents of the stretched exponential dependence of $\sigma(T)$. However, they also ascribed their unusual transport laws to a peculiar screening of the Coulomb interaction.

Coulomb interaction plays a major role in determining the transport properties of Q1D electron systems, and the FTS model addresses this issue. Q1D systems are those in which the transverse matrix elements of hopping (in CP's this corresponds to interchain transport) are finite but strongly attenuated in comparison with the longitudinal matrix elements (intrachain transport in CP's). In the FTS model, just as in the ES model, exists a Coulomb gap in DOSCE in the vicinity of E_F . In the case of a 3D Q1D system, the DOSCE exhibits a power-law dependence on energy ε for single-particle excitation (measured from E_F):

$$N_V(\varepsilon) \propto |\varepsilon|^{\nu} \quad , \quad (4.43)$$

with $\nu = 0, 1, 2$ which correspond to the cases of no gap, linear Coulomb gap, and quadratic Coulomb gap, respectively. Consequently, the FTS model yields the following VRH laws, parameterized by α :

$$\sigma_{\text{VRH}}(T) = \eta_{\alpha} \exp \left[- \left(\frac{T_{\alpha}}{T} \right)^{\alpha} \right] \quad , \quad \alpha = \frac{1 + \nu}{1 + \nu + d} \quad . \quad (4.44)$$

In the case of 3D Q1D system, $d = 3$. Depending on the shape of the Coulomb gap (4.43), $\alpha = 1/2$, $2/5$ or $1/4$. Beside different values of α , the FTS model also predicts regions of their validity depending on disorder level and T , as depicted in Fig. 4.4. The borders between different regions of validity are derived simply by equating the expressions of the FTS law (4.44) for two different α . Therefore, the borders should not be perceived as very strict ones but rather as lines roughly indicating positions of different regions of validity of the values of α [132].

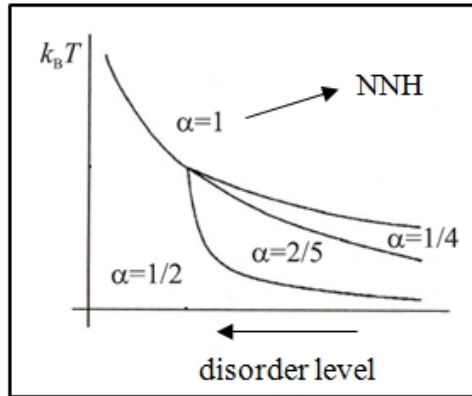


Figure 4.4: Different regimes of hopping charge transport depending on disorder level and T , as predicted by the FTS model for a 3D Q1D disordered system.

§ 4.7 Electronic transport in conducting polymers

Here we outline experimental research on electronic transport in CP's, relying on [133, 20]. Related theoretical models of Mott, and Efros and Shklovskii — that have been explicated in Section 4.6 — have found a strong support in the vast amount of experimental work on CP's.

The initial impetus for the study of electronic transport in CP's was generated by the discovery of the increase, by 9 orders of magnitude, in σ of PA upon doping with I_2 or other acceptors [52]. σ as high as that of a typical metal has been achieved (see discussion in Subsection 2.4.1), and CP's were seen as a great hope — as synthetic metals that could replace ordinary metals in many respects. Evidence of a Pauli spin susceptibility, a quasilinear T -dependence of thermopower, and a linear term in specific heat suggested a continuous DOS at E_F , which is characteristic of metals.

However, true fingerprints of a metallic behaviour were not observed in the first generation of CP's. For example, these include finite σ as $T \rightarrow 0$, a positive temperature coefficient of the logarithmic derivative W ,

$$W = \frac{\partial \ln \sigma}{\partial \ln T} , \quad (4.45)$$

and metallic (Drude-like) reflectivity in the infrared part of the electromagnetic spectrum.

On the insulating side of the MIT, $\sigma \rightarrow 0$ as $T \rightarrow 0$, and W shows a negative temperature coefficient [$\sigma(T)$ usually decreases rapidly upon decreasing T]. $\sigma(T)$ is typical of a hopping transport, and is given by the stretched exponential dependence, $\ln \sigma \propto T^{-\alpha}$ [see Eq. (4.44)], where α is determined by the effective dimensionality of the system and by the level of disorder [disorder is intricately related to morphology and (in)homogeneity].

Most of the electronic transport measurements on CP's are performed on materials in the insulating regime. Strong disorder masks a possible metallic behaviour; the results are typical of those expected for highly disordered media. Even on the metallic side of the MIT (which is observed only occasionally and in limited T ranges), $\sigma(T)$ is at low T nevertheless dominated by an interplay between localisation and Coulomb interaction.

New generations of CP's have made possible detailed studies of the critical regime of the MIT [134], previously unexplored in doped CP's. When the level of disorder is near the critical disorder for the Anderson transition, $\sigma(T)$ follows a power law over a substantial range of T , $\sigma_{\text{crit}} \propto T^{-\beta}$, and W is T -independent [135, 131], $W = \beta$. This power-law behaviour is universal near the critical regime of the MIT and does not depend on the details of the system.

However, the reversal does not hold — power-law dependence is not necessarily an indication of the critical regime. Namely, VRH conductivity of Q1D systems can deviate at low T from the usual formula, Eq. (4.44), if the chains are short [136]. Such a power-law dependence has recently been observed in a number of systems, among them polymer nanofibers [137, 138] and polymer films [139, 140].

After nearly three decades of the development of CP's, a hallmark of metallic conductivity — monotonic decrease of σ with increasing T — was finally obtained between RT and 5 K [141]. Moreover, the frequency-dependent conductivity, $\sigma(\omega)$, was found to be in agreement with the Drude-Sommerfeld model which is typical of metals. These measurements were performed on free-standing films of PANI-CSA of a typical thickness of about 30 μm . The films were cast from a solution in *m*-cresol. Prior to doping with CSA, the EB was prepared using self-stabilised dispersion polymerisation [142]. Despite the fact that the above remarkable features were observed (only) for samples having $\sigma_{\text{RT}} > 10^5$ S/m, truly metallic polymers have been produced indeed.

These achievements represent an insight into an exclusive and rather exotic regime of electrically conducting organic matter. This thesis, on the other hand, deals with the most common regime of CP's, that is, their properties on the insulating side of the MIT.

§ 4.8 Dc electrical conductivity of PANI–DBSA

In this section, we present results of our measurements of the dc electrical conductivity of our PANI–DBSA samples. When possible, we compare these results with those for PANI–HCl samples produced from the same starting undoped PANI. Both similarities and differences have been found.

Since this section represents the core part of the Thesis, it has been shaped as a fairly self-contained text. Therefore, we begin by summarising the theoretical concepts described in previous sections and put them into context, bearing in mind their applicability to CP's.

4.8.1 Putting into context

Particle transport through a disordered potential consisting of deep, localising potential wells has for decades been puzzling. This transport usually occurs via thermally assisted hopping from one localized site to another, good examples being electron transport in strongly disordered conductors [100], and vortex creep in type-II superconductors [143]. If the well depth varies in space strongly, a particle hops to a site determined by the most favourable balance between the hop length and the energy difference between the localized states involved. When thermal activation is

strong enough to diminish the importance of the spatially varying well depth, the above mechanism — called variable-range hopping (VRH) — is replaced by nearest-neighbour hopping (NNH). The most suitable observable for investigating these phenomena is electrical conductivity, which is a linear-response quantity that can contain enough information on the nature of a hopping electron transport (HET). This approach has been dominant ever since the early works of Anderson [92] and Mott [122] on localised electron states in solids and their thermally assisted delocalisation. Mott argued [100] that HET electrical conductivity σ generally depends on T as

$$\sigma(T) = \eta_\alpha \exp \left[- \left(\frac{T_\alpha}{T} \right)^\alpha \right], \quad (4.46)$$

where η_α , T_α , and $\alpha \leq 1$ contain information on the underlying microscopic mechanisms. These parameters may depend on dimensionality (d), interactions relevant for the transport, disorder level, localisation length of electrons, etc. For VRH, $\alpha < 1$, whereas NNH obeys the Arrhenius law ($\alpha = 1$).

VRH of noninteracting electrons results in the Mott law $\alpha = (1 + d)^{-1}$. Coulomb interaction leads to an $|E - E_F|^\nu = |\varepsilon|^\nu$ energy (E) dependence of the electron density of states (DOS) close to the Fermi energy E_F , with ν being a constant. This opens a soft (Coulomb) gap in the DOS, and results in the Efros-Shklovskii (ES) law where $\alpha = 1/2$ is universal [129, 114]. The above models address isotropic systems, e.g., disordered semiconductors. However, HET occurs in other materials as well, of which we pay attention to CP's. For many of them, Eq. (4.46) accounts for experimental data remarkably well [144], with $\alpha = 1/4$ and $\alpha = 1/2$ appearing often. Other $\alpha < 1$ have been found as well [145–147, 88, 4], including $\alpha = 2/5$ that cannot be explained neither by the traditional models (Mott, ES) nor by similar approaches [148–150]. NNH is, on the other hand, much less common in CP's, and $\alpha = 1$ is observed [151, 152] infrequently, probably because conditions for its occurrence are seldom established at T lower than the material degradation temperature.

A model with a potential to account for the complexity of $\sigma(T)$ in CP's was developed by Fogler, Teber and Shklovskii (FTS) [87]. They studied the HET in coupled chain-like conductors in the presence of disorder-dependent Coulomb interaction potential that affected DOS similarly as in the ES model. The FTS model predicts $\alpha = (1 + \nu) / (1 + \nu + d)$, which for strongly coupled chains ($d = 3$) and $\nu = 0, 1, 2$ leads to $\alpha = 1/4, 2/5, 1/2$, respectively. At low T , highly disordered samples should exhibit $\alpha = 1/2$, and more ordered samples $\alpha = 2/5$. In the former case, the transition to NNH as T increases should be direct, i.e., $\alpha = 1/2 \rightarrow 1$, whereas in the latter case, one should observe $\alpha = 2/5 \rightarrow 1/4 \rightarrow 1$. On the basis of these considerations, FTS proposed a $d = 3$ diagram where crossover temperatures between different α values were plotted vs suitably parameterized disorder level.

A support to the FTS predictions has come from recent experiments on VRH in polyaniline (PANI) [88, 151] which is a well-known polymer that becomes conducting when doped via protonation by an acid [68, 47]. In HCl-doped samples

(PANI–HCl), α exhibited crossovers between $1/4$, $2/5$, and $1/2$ [88], but the transition from VRH to NNH below room temperature (RT) was identified only occasionally [151]. Hence, the FTS diagram — which is in many respects central to the model — could not have been constructed from the experimental data. A similar VRH behavior has been found in samples of PANI–DBSA [4]. In this case, however, VRH-to-NNH transition occurs well below RT over a wide doping range, and this opens a possibility to explore the viability of the FTS diagram.

4.8.2 Measurements

Resistance measurements were carried out in a closed-cycle refrigerator, from the lowest achievable temperature of ~ 10 K up to RT, using a constant dc bias current and a nanovoltmeter with a 10 G Ω input resistance and a maximum input voltage of 12 V. Reproducibility of the results was confirmed by examining several identically doped samples for a number of Q . Polymer powder was pressed into $\sim 8 \times 5 \times 1$ mm³ pellets under ~ 90 MPa. Electrical contacts in the four-point configuration were made by first depositing a thin graphite layer onto the contact area and then applying a silver paste. This resulted in contact resistances that did not exceed the sample resistance irrespective of its value. For the applied currents ($0.01 - 10$ μ A; typically 0.1 A/m²) used in our experiment, we confirmed ohmicity of the current-voltage response over the whole T range of measurement for each sample.

4.8.3 Results

Experimental $\sigma(T)$ curves for the obtained range of Q are in Fig. 4.5(a) plotted by the symbols as $\log \sigma$ vs $T^{-1/2}$, which provides good insight into low- T data. Below the dashed line, the plots are obviously straight. Above the dashed line, the symbols and the corresponding straight solid lines (guides to the eye) do not match well, hence there is no linear dependence. These data are in Fig. 4.5(b) plotted by the symbols as $\log \sigma$ vs $T^{-2/5}$, which results in linear plots. From Figs. 4.5(a) and 4.5(b), we can conclude that Eq. (4.46) accounts for low- T data adequately, with $\alpha = 1/2$ for low Q , and $\alpha = 2/5$ for high Q . A similar behavior was found for PANI–HCl (in which $Q = 2$ cannot be exceeded[†]) but the change from $\alpha = 1/2$ to $\alpha = 2/5$ occurred at a Q lower than here [88].

It is difficult to note in Figs. 4.5(a) and 4.5(b) that the above low- T values of α do not hold for the high- T data in narrow ranges on the left-hand side of the plots. As we show later, the proper exponent in this case is $\alpha = 1$ irrespective of the low- T value, indicating that NNH is the mechanism that underlies the HET in this regime. Moreover, for the sample with the highest $Q = 3.39$, there is a narrow T range ($\sim 110 - 145$ K) where $\alpha = 1/4$, as shown in the inset to Fig. 4.5(b). Therefore, as T increases, α of this sample changes as $2/5 \rightarrow 1/4 \rightarrow 1$, in contrast to the other samples where this

[†]For PANI–HCl, Q is calculated by replacing n_S with Cl concentration n_{Cl} . In fully dry samples, no extra HCl can be intercalated between PANI chains.

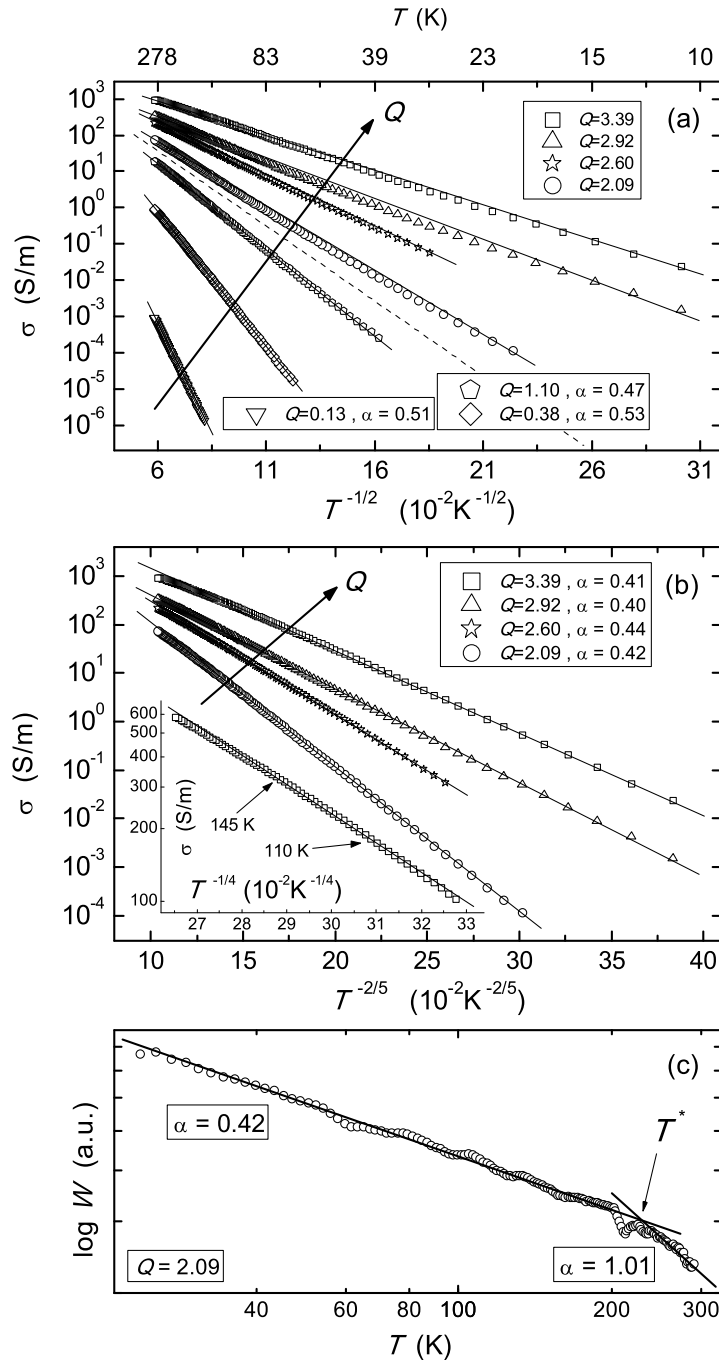


Figure 4.5: (a) Experimental $\log \sigma$ vs $T^{-1/2}$ (symbols). The solid lines are [here and in (b)] guides to the eye. (b) Data above the dashed line in (a), plotted as $\log \sigma$ vs $T^{-2/5}$ (symbols). Inset to (b): $\log \sigma$ vs $T^{-1/4}$ for $Q = 3.39$, exhibiting linearity for $110 \lesssim T \lesssim 145$ K. The corresponding α determined numerically [as exemplified in (c)] is 0.27. (c) $\log W$ vs $\log T$ of a selected sample (symbols), displaying two distinct ranges of linearity with a crossover at T^* . The solid lines represent linear fits that yield α numerically. α resulting from this procedure is listed in the legends to (a) and (b).

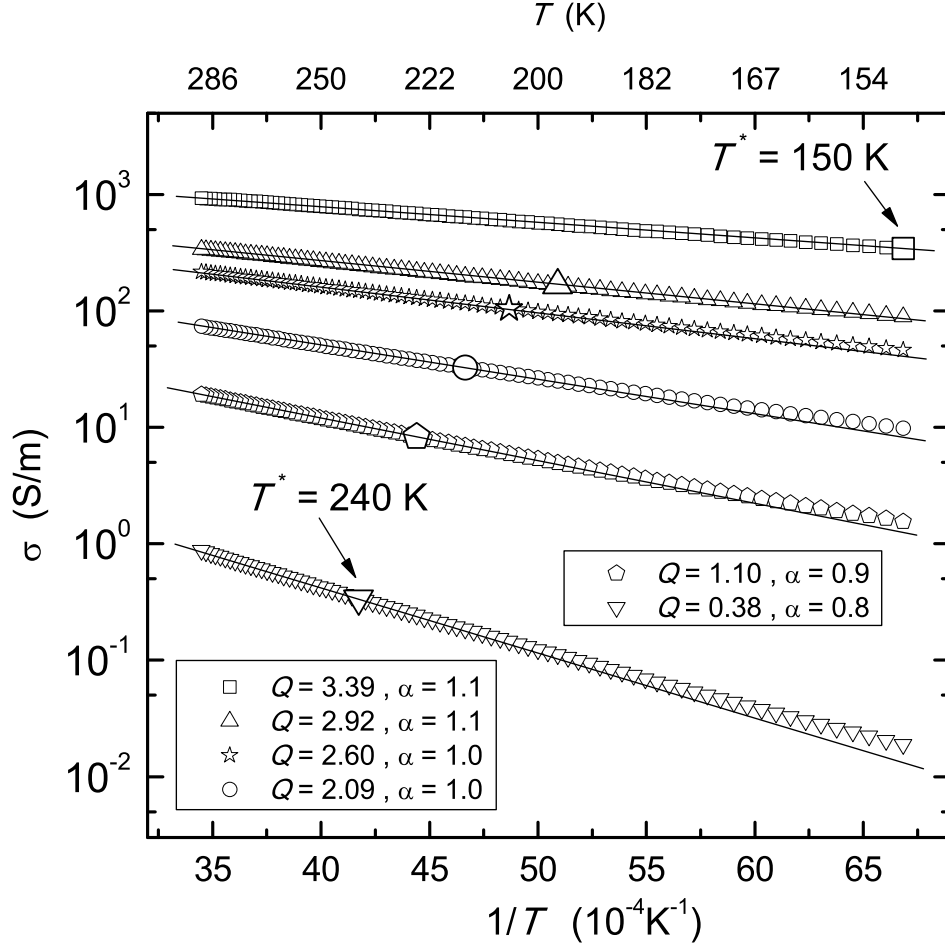


Figure 4.6: Experimental $\log \sigma$ vs T^{-1} (symbols) at $Q \geq 0.38$, for which T^* is below RT. The solid lines are guides to the eye. T^* for each sample is marked by a larger symbol. Numerical values of α extracted numerically are listed in the legends.

change is either $1/2 \rightarrow 1$ or $2/5 \rightarrow 1$.

Although $\log \sigma$ vs $T^{-\alpha}$ plots are indicative with regard to α , we carried out an alternative analysis as well. Application of the logarithmic derivative [Eq. (4.45)] to Eq. (4.46) leads to $-\alpha$ being the slope in the resulting linear $\log W$ vs $\log T$ dependence, which enables a more precise extraction of α from experimental $\sigma(T)$ [153]. This is demonstrated in Fig. 4.5(c) for a selected sample. Two distinct ranges of linearity are discernible, corresponding to VRH ($\alpha = 0.42$) and NNH ($\alpha = 1.01$), as indicated (for all our data, error in thus determined α is $\lesssim 10\%$). T^* is a crossover temperature between the VRH and NNH. Crossover at T^* is generally not sharp, and the T range between regimes of well defined low- T and high- T values of α can be up to ~ 40 K wide. A large crossover width can be an obstacle for identifying $\alpha = 1/4$, because this VRH behavior should — according to the FTS model — take place only in a narrow T range below T^* . Our result for the $Q = 3.39$ sample, where $\alpha = 1/4$

appears only over 35 K below T^* , supports this prediction. Moreover, we cannot rule out that $\alpha = 1/4$ in some other samples might be hidden due to a large width of the transition at T^* .

In Fig. 4.6, we use $\log \sigma$ vs T^{-1} plots to show the high- T part of $\sigma(T)$ at $Q \geq 0.38$, for which T^* is lower than RT. Larger symbols mark T^* which decreases with increasing Q . We also note that magnetic susceptibility χ of the samples undergoes a significant change (see Section 5.6), similar to that described in [154] for PANI–HCl, at basically the same $T^*(Q)$ as here. The fact that T^* leaves a signature both in σ and χ implies a qualitative change in the electronic system at T^* .

4.8.4 Verification of the Fogler - Teber - Shklovskii model

From the above analysis, it is rather clear that several predictions of the FTS model agree with our experimental results. The remaining issue is whether we can construct the FTS diagram — the proposed shape of which is sketched in the inset to Fig. 4.7 — from our data. This diagram maps areas of different α in a T versus disorder level plane. VRH exponents $1/4$, $2/5$, and $1/2$ can all appear only for $d = 3$ [87], and this dimensionality should hence apply to our samples. Since data on crossovers between different α are available from our $\sigma(T)$, constructing the FTS diagram reduces to parameterising the disorder level. This is, however, not straightforward. Disorder in CP's arises from a combination of molecular-scale disorder [134] and structural inhomogeneities at mesoscopic scale lengths [155]. Thus, information on averaged structural ordering (e.g., from X-ray diffraction) can be instructive but not conclusive in inferring what level of disorder a hopping electron experiences, particularly in the case of our PANI–DBSA samples which are fully amorphous. Having this in mind, we approach the problem by using a macroscopic property of σ as a parameter accounting for disorder.

We believe that η_α for $\alpha = 1$, i.e., experimental η_1 , can be used as an appropriate measure of the disorder level in our samples. This plausible assumption, as we show later, leads to our results reproducing the FTS diagram, and the reasoning behind choosing η_1 is as follows. Generally, the exponential part in Eq. (4.46) pertains mainly to thermal aspects of σ while η_α is related to non-thermal effects — in which disorder plays a crucial role. Since $\sigma \propto \eta_\alpha$, as disorder level decreases, η_α should increase. This holds although η_α also contains a contribution of the charge injected by the doping. Protonation not only increases the charge-carrier density (which also affects the screening of the Coulomb interaction and thus influences T_α [88]) but also reduces disorder in the hopping landscape [156]. This occurs because the Coulomb interaction energy between dopant anions — which are bound to the protonated sites together with the potential wells — is lowered in a more ordered configuration. Another possible effect of adding a dopant is enhancement of the interchain hopping [4], which is also a process that homogenises the potential. Of all η_α , we focus on η_1 because it accounts for the described processes in the same way for all the samples which exhibit NNH, regardless of the low- T value(s) of α .

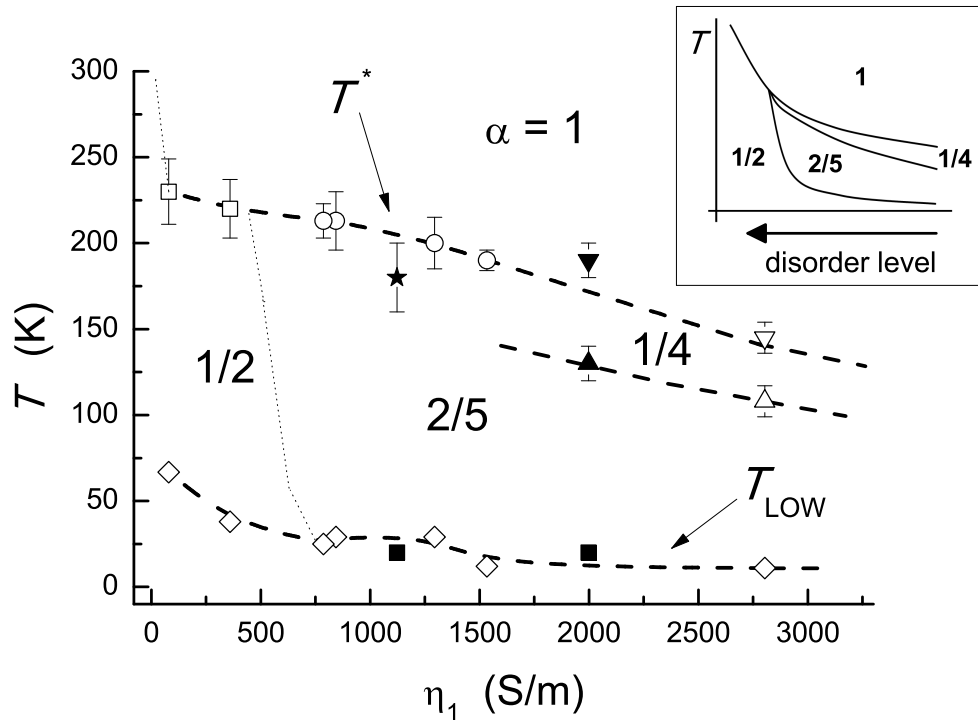


Figure 4.7: Areas of different values of α , shown in a T vs η_1 plane. The open symbols correspond to the PANI-DBSA samples, and the solid ones to two PANI-HCl samples that exhibit $\alpha = 1$ below RT. The lines are guides to the eye. The uppermost symbols correspond to T^* , whereas the bottom symbols show T_{LOW} which is the lowest temperature at which σ was measured. The intermediate symbol for the two highest η_1 values mark crossover between $\alpha = 2/5$ and $\alpha = 1/4$. A sketch of the theoretically predicted diagram [87] is shown in the inset.

In Fig. 4.7, we plot areas of different values of α in a (η_1, T) plane, as indicated. Each η_1 value is related to one sample, and the symbols have been extracted from the corresponding $\sigma(T)$. The vertical distance between two symbols for a given η_1 is the T range of the appearance of the indicated VRH α . The open symbols correspond to the PANI-DBSA samples, and the solid symbols to the only two of our PANI-HCl samples (both with $Q \lesssim 2$) that exhibit well defined T ranges of $\alpha = 1$ below RT (their undoped PANI being the same as for the PANI-DBSA samples). The uppermost symbols correspond to T^* (the error bars indicate the crossover widths), whereas the bottom symbols represent the lowest temperature T_{LOW} at which σ was measured (the low- T limit of the cryogenic system, or T at which σ is immeasurably small). For the two samples with the highest η_1 , the intermediate symbol represents crossover between $\alpha = 2/5$ and $\alpha = 1/4$. The dashed lines are guides to the eye, depicting characteristic temperatures extracted from $\sigma(T)$, whereas the dotted lines mimic other lines from the theoretical diagram.

The similarity of the experimental and theoretically predicted diagrams is obvious. Furthermore, the two PANI–HCl samples show the same behavior as the PANI–DBSA samples. We believe that this is not a coincidence, because the starting undoped PANI has been the same for both classes of samples and every processing (set by the choice of the dopant and the doping method) modified the same starting material. On the other hand, a particular processing leaves a distinct signature in η_1 . For instance, both PANI–HCl samples are almost fully protonated but they were processed differently and hence do not display the same properties [151]. The sample with $\eta_1 \sim 2000$ S/m exhibits $\alpha = 1/4$ while this regime is absent for the sample with $\eta_1 \sim 1100$ S/m. Moreover, the PANI–HCl samples are partly crystalline [88] while the PANI–DBSA samples are amorphous, which additionally supports the conclusion that degree of crystallinity is not a proper measure of the (dis)order in a potential that hopping electrons experience.

It seems, however, that the doping-induced ordering of the hopping potential must be strong enough for different classes of doped PANI to show the same HET behavior quantitatively, since our less ordered PANI–HCl samples from the same starting material do not exhibit NNH below RT [88]. That is, the $\eta_1 < 1000$ S/m parts of the FTS diagrams for PANI–HCl and PANI–DBSA differ quantitatively although the corresponding VRH properties are similar [88]. In contrast to PANI–HCl, T^* for PANI–DBSA does not increase above RT until η_1 decreases below ~ 75 S/m. This increase is depicted by the dotted line for $\eta_1 \rightarrow 0$, which can be drawn thus because there is no NNH below RT for the least conducting of the PANI–DBSA samples (see Fig. 4.5).

In developing their model, FTS primarily had in mind systems such as stripe phases, quantum wire arrays, carbon-nanotube films, compounds like Bechgaard salts and Fabre salts, etc. They also mentioned [109, 87] CP's as candidates since VRH has been reported extensively for these materials. Yet, FTS were seemingly not fully confident in the applicability of their model in this case, possibly because of the intricate underlying morphology. It turns out, however, that the model is robust enough to account for these complex HET conductors as well.

4.8.5 Further inferences and the Coulomb gap

Precise low- T and high- T values of α , determined from (4.45) as explained above, are presented in Fig. 4.8 as functions of Q . It is discernible that high- T α is grouped around 1, whereas low- T α is grouped around 1/2 for t low Q , and around 2/5 for high Q . This is consistent with two hypotheses incorporated into the FTS diagram. The first hypothesis is on a crossover from $\alpha = 1/2$ to $\alpha = 2/5$ by reduction of disorder (here, increase in Q), and the second one on a crossover from low- T α (either $\alpha = 1/2$ or $\alpha = 2/5$) to high- T $\alpha = 1$ by increasing T .

We can now fix low- T α to either 1/2 or 2/5, extract the corresponding T_α , and check whether $T_\alpha(Q)$ agrees with the FTS expectation too. We recall our conclusion that doping reduces disorder in the hopping landscape, hence in increase in Q means a

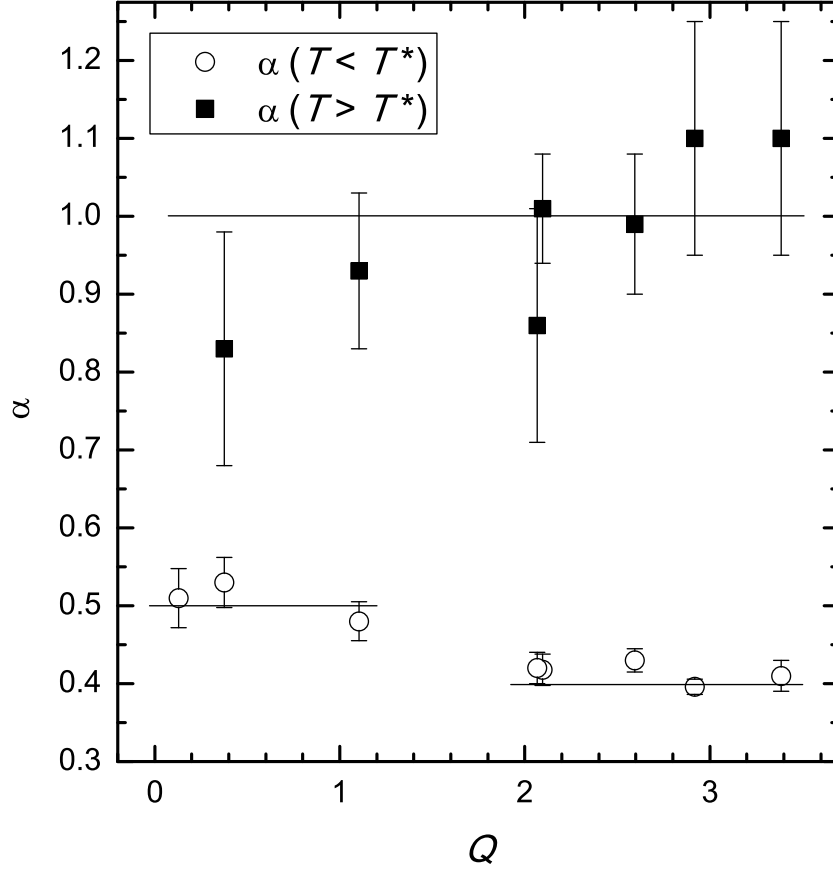


Figure 4.8: Low- T (open symbols) and high- T (solid symbols) α of PANI-DBSA samples, determined by the logarithmic-derivative method. Three long horizontal lines represent the theoretical values $\alpha = 1/2$, $2/5$ and 1 .

reduction of disorder. As displayed in Fig. 4.9, $T_{1/2}(Q)$ decreases with increasing Q . Hence, the FTS prediction on $T_{1/2}$ is confirmed, i.e., $T_{1/2}$ decreases with the weakening of disorder [87]. However, Fig. 4.9 shows that $T_{2/5}$ also decreases with the weakening of disorder, which is not in agreement with the FTS prediction that $T_{2/5}$ is being dependent of Q [87]. Since $T_{2/5}(Q)$ corresponds to fully doped and overdoped samples, the reason for this deviation could perhaps be related to a stronger screening of the Coulomb interaction at high doping [57], because $T_{2/5} \propto 1/\kappa$ [87].

The steep jump of T_α at the crossover $1/2 \rightarrow 2/5$ is of no significance, because only the Q dependence of T_α for a given α [i.e., for given $N(\epsilon)$] counts.

High- T α is not analysed along with its low- T counterpart because high- T α is actually scaled Coulomb gap, and it is therefore analysed separately below.

We proceed by considering some energies that are relevant to FTS VRH and can be estimated from our data. The first important energy scale in FTS VRH is a T -dependent energy range $|\epsilon|$, extending symmetrically around E_F , which represents the effective width of the disorder band, i.e., the portion of accessible states within

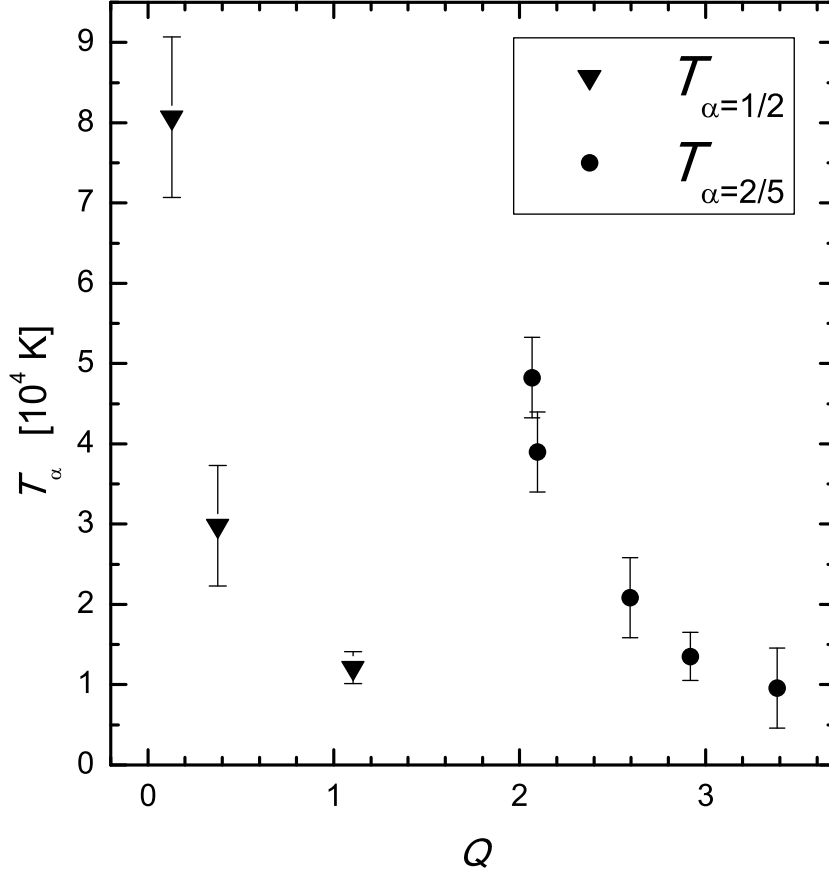


Figure 4.9: Corresponding T_α for low- T α in PANI-DBSA samples.

the disorder band at a given T [‡]. The second important energy scale in FTS VRH is the Coulomb gap Δ_C , representing the energy at which the density of states for charge excitations around E_F , $N(\varepsilon)$, saturates at a constant N_0 . If $|\varepsilon| \geq \Delta_C$, then $N(\varepsilon) \approx N_0$ effectively and $\sigma(T)$ should display either the Mott law ($\alpha = 1/4$) or the Arrhenius law ($\alpha = 1$).

Since all our PANI-DBSA samples undergo a crossover to $\alpha = 1$ at $T = T^*(Q)$, Δ_C can be estimated using this property. At crossovers to $\alpha = 1$, ε becomes equal to Δ_C :

$$\Delta_C = \varepsilon^* = \varepsilon(T = T^*) \quad . \quad (4.47)$$

As shown in Appendix A, using

$$\varepsilon(T) = \alpha k_B T \left(\frac{T_\alpha}{T} \right)^\alpha \quad , \quad (4.48)$$

the formula for determining Δ_C straightforwardly becomes the following:

$$\Delta_C(\alpha \rightarrow 1) = k_B T_1 \quad , \quad \forall \alpha \quad . \quad (4.49)$$

[‡]The energy ε is referred to as the activation energy at a given T [114]. For any hopping law of the form (4.46), ε monotonically decreases with decreasing T as $T^{1-\alpha}$ (see Appendix A for details).

So, to determine the Coulomb gap by using Eq. (4.49), one has to know T_1 , which is determined from linear fits $\ln \sigma(T)$ vs T^{-1} . However, there is another, independent, method for calculating Δ_C . This second method uses the fact that $\varepsilon(T)$ can be written as

$$\varepsilon(T) = k_B T W = k_B T \frac{\partial \ln \sigma}{\partial \ln T} . \quad (4.50)$$

Evaluating $\varepsilon(T)$ given by (4.50) at $T = T^*$, one obtains Δ_C directly from raw measurements without even assuming α . The two methods show a remarkable agreement, as demonstrated in Fig. 4.10. Decrease of the Coulomb gap with decreasing disorder level (increasing Q) is observed. This is consistent with the FTS model. Furthermore, Eq. (4.49) implies that Δ_C plays the role of the potential that defines the Arrhenius $\sigma(T)$ dependence in the NNH regime. This is also plausible; in the absence of energy restrictions for hops, which underlie VRH, electron-hole attraction is the only potential an electron must overcome to perform a hop by thermal activation.

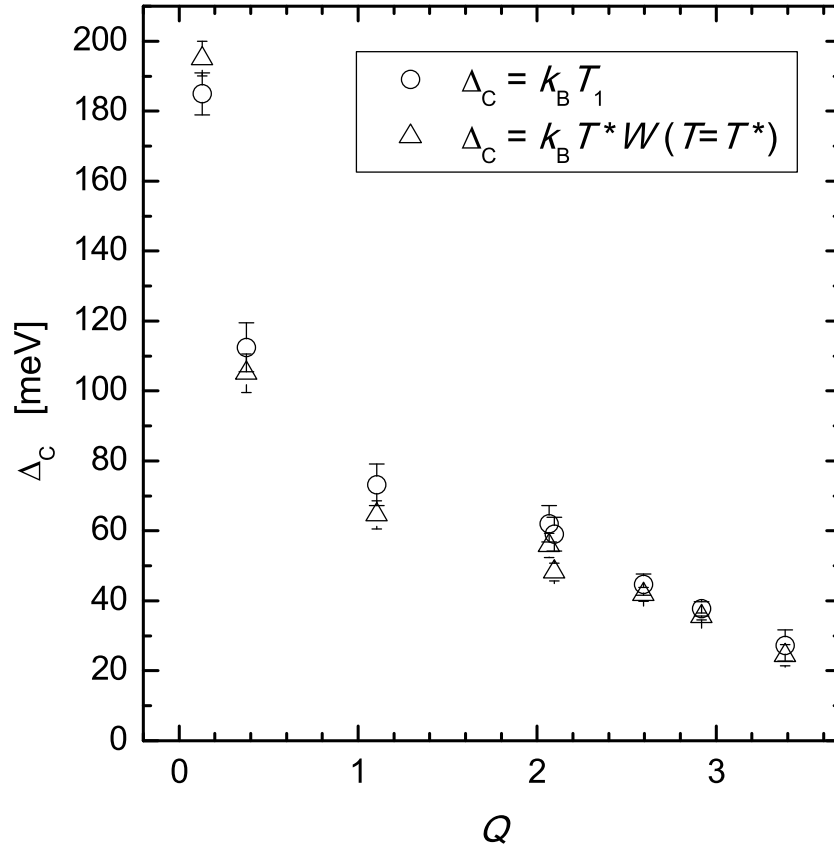


Figure 4.10: Coulomb gap in PANI-DBSA samples, determined by two independent methods as explained in the text.

§ 4.9 Concluding remarks

The $\sigma(T)$ curves (between 10 K and RT) of our doped PANI–DBSA pellets reveal both VRH and NNH. The two HET mechanisms extend over T ranges that are sufficiently large to permit studying of the full complexity of the FTS diagram. We determine crossover temperatures between regimes of different HET exponents. When we plot these temperatures against a measure of the disorder level, that is, prefactor of the NNH Arrhenius plots, we obtain a remarkable agreement with the predicted shape of the FTS diagram. This implies that the FTS model is both correct and applicable to CP's.

From the electronic transport measurements in the linear (Ohmic) response regime we have inferred the importance of the Coulomb interaction in PANI–DBSA. This Coulomb interaction is a quasi-excitonic electron-hole interaction (QEEHI), and is a consequence of disorder. Namely, the presence of disorder causes a strong, Anderson localisation of protonation-induced charge, and consequently the absence of metallic screening. This absence leaves the Coulomb interaction both strong and long-ranged. Because of the long-range nature of the Coulomb interaction, a depletion of the DOS for charge excitations appears around E_F . This effect is presented in terms of a soft gap around E_F . The quasi-excitons that emerge in the system (the Coulomb drag that electrons feel in their transport) are of the Mott-Wannier type, not of the Frenkel type.

The width of this soft gap, Δ_C , is a measure of QEEHI. Δ_C decreases with increasing Q from ≈ 170 meV to ≈ 30 meV.

If one can tune the disorder level (e.g., by means of doping) and reduce it sufficiently, a transition from VRH to NNH can be achieved at a T lower than the material degradation temperature. We have managed to accomplish such a weak, homogeneous disorder by choosing a suitable dopant — DBSA. Furthermore, exactly because of the homogeneous disorder, as T increases above T^* , all of our PANI–DBSA samples except one (the $Q = 3.4$ sample) directly cross over from the VRH regimes characterised by the importance of the Coulomb interaction ($\alpha = 1/2$ or $2/5$) to the NNH regime ($\alpha = 1$). The Mott VRH regime ($\alpha = 1/4$) is thus skipped in a manner much similar to ordinary sublimation process where one phase is jumped across.

Besides the Coulomb interaction accounted for in the FTS model, there are other types of Coulomb interaction that are present in PANI–DBSA, some of these being addressed in the Kamimura model (see Section 5.4).

Chapter 5

Magnetic properties of PANI–DBSA

§ 5.1 A complementary approach

Measurements of the electronic transport have confirmed the importance of the Coulomb interaction in our PANI–DBSA material below a certain temperature T^* that depends weakly on the doping level Q : $T^* = T^*(Q)$.

As described in Chapter 4, our study of the temperature (T) dependence of the dc electrical conductivity σ of PANI–DBSA pellets has revealed a stretched exponential dependence in $\sigma(T)$, with a non-universal and discrete stretching exponent $-\alpha$. The appearance of different exponents α is a consequence of different shapes of the density of states $N(E)$ for charge excitations around the Fermi energy [87]. Different shapes of $N(E)$ arise from the dependence of the Coulomb interaction on disorder level. The crossovers from $\alpha < 1$ to $\alpha = 1$, found systematically in $\sigma(T)$ of our PANI–DBSA samples, suggest that the effects of the Coulomb gap are not the same for $T < T^*$ and $T > T^*$, since $\alpha = 1$ has been found for all Q (i.e., the appearance of $\alpha = 1$ does not depend on the particularities of a given $T < T^*$ state).

One can go a step further and address the above issues — which are related to competition of Coulomb interaction with thermal energy and disorder level — by probing another physical property of PANI–DBSA, a property both complementary to σ and sensitive to effects of electron (de)localisation. This property is static magnetisation which is described via **magnetic susceptibility** χ . For any conducting polymer, χ comprises a Curie-type contribution of localised electrons, i.e., spins, and a Pauli-

type contribution of delocalised, conducting electrons [16]. As $N(E)$ affects not only σ but also the contribution of conducting electrons to χ , the (de)localisation that leaves a fingerprint in σ is expected to influence χ as well.

Therefore, χ of our PANI–DBSA material has been investigated experimentally in the T range of 10 – 300 K. Pellets for magnetic measurements were made from the same material that was used in transport measurements. The obtained **results suggest that χ and σ are interrelated indeed**. Namely, it has been found that there is a temperature $T^*(Q)$ at which $\chi(T)$ undergoes a notable change, and this temperature agrees very well with that which marks the crossover from $\alpha < 1$ to $\alpha = 1$ in $\sigma(T)$. The mentioned change in $\chi(T)$ refers to a simultaneous enhancement (reduction) of the Pauli-type susceptibility χ_P and reduction (enhancement) of the Curie constant C at $T = T^*$ as T increases (decreases). This finding is consistent with a picture in which, at T^* , spins that disappear from C reappear in χ_P , and vice versa.

§ 5.2 Magnetisation and magnetic susceptibility

The volume magnetisation \mathbf{M}_V , defined as the volume density of a total magnetic moment μ_{total} , i.e.,

$$\mathbf{M}_V \equiv \frac{\mu_{\text{total}}}{V} = \frac{1}{V} \sum_k \mu_k \quad , \quad (5.1)$$

where V stands for sample volume, is a measure of the response of a material to an external magnetic field. The magnetising field \mathbf{H} , the magnetic induction \mathbf{B} , and \mathbf{M}_V are related by

$$\mathbf{B} = \mu_0(\mathbf{H} + \mathbf{M}_V) \quad , \quad (5.2)$$

where $\mu_0 = 4\pi \times 10^{-7} \text{ T}^2\text{m}^3/\text{J}$ is the vacuum permeability. If there is no magnetic ordering, \mathbf{M}_V is directed along \mathbf{H} , and we can write

$$\mathbf{M}_V = \chi_V \mathbf{H} \quad , \quad (5.3)$$

where χ_V is a dimensionless quantity called the volume magnetic susceptibility. Eqs. (5.2) and (5.3) lead to

$$\mathbf{B} = \mu_0(1 + \chi_V)\mathbf{H} \quad . \quad (5.4)$$

For materials with $\chi_V \ll 1$, which applies to PANI–DBSA, demagnetisation effects related to sample shape are negligible, and Eqs. (5.2) – (5.4) hold without further corrections. χ_V is dimensionless but traditionally it is expressed in a CGS unit emu/cm^3 , where $1 \text{ emu} = 1 \text{ gauss} \times \text{cm}^3$.

Alternatively, magnetisation can be defined not through volume density but instead through molar or mass density of the total magnetic moment:

$$\mathbf{M} \equiv \frac{1}{n} \sum_k \mu_k \quad , \quad \mathbf{M}_m \equiv \frac{1}{m} \sum_k \mu_k \quad , \quad (5.5)$$

where n and m stand for amount of substance and mass, respectively. Using the former of the two formulae in (5.5), one can define the **molar magnetic susceptibility**

$$\chi \equiv \frac{M}{H} = \mu_0 \frac{M}{B} \quad , \quad (5.6)$$

which will be used in the presentation of our results (see Section 5.6). The usual unit for χ is emu/mol, which is a CGS unit. The corresponding SI unit is m^3/mol .

§ 5.3 Magnetic susceptibility in the regime of linear $M(H)$

Many atoms and ions have a net magnetic moment, usually of the order of the Bohr magneton $\mu_B = e\hbar/2m_e$ which is close to the spin magnetic moment of a free electron. There are three principal sources of the magnetic moment of a free atom or ion: the electron spin, the orbital angular momentum of electrons in motion around the nucleus, and the change in the orbital motion of electrons when a magnetic field H is applied. The first two effects give paramagnetic contributions to M , and the third gives a diamagnetic contribution. Paramagnetism is not present in every material, in contrast to diamagnetism which is an inherent property of matter. In all our considerations, we assume H to be constant in space and time.

Magnetisation in solids is a quantum-mechanical effect. According to the Bohr – van Leeuwen theorem, a strictly classical system in thermal equilibrium cannot attain a magnetic moment even in a magnetic field [157]. The crucial part of this statement is that it pertains to solids. It is possible to have a magnetic effect if we have an isolated system — like a star held together by itself — which can start rotating if put in a magnetic field. But with a piece of material held in place so that it cannot start spinning, there will be no magnetic effects [158]. Nevertheless, classical physics can successfully describe magnetic properties, even magnetic ordering, if it includes certain quantum corrections [159].

Considerations in this section will be restricted to non-interacting electrons. The only interaction included is that with an applied magnetic field H . Thus, we shall remain within the regime of linear $M(H)$, which is relevant for our PANI–DBSA material. This restriction merely leads to M and χ containing a factor of N , the number of

atoms per either unit volume or unit amount of substance. Nonlinear $M(H)$ usually implies magnetic ordering, which rarely occurs in conducting polymers, and which has not been observed in PANI–DBSA.

There can be different contributions to M in the regime of linear $M(H)$: atomic and ionic diamagnetism, Curie paramagnetism, Pauli paramagnetism, van Vleck paramagnetism, Landau diamagnetism. The first three of them are of relevance for our PANI–DBSA, and are hence presented in more detail in Subsections 5.3.1 – 5.3.3..

The van Vleck paramagnetism is negligible in PANI–DBSA. It is an important contribution in ions with low-lying excited states, i.e., for some lanthanides and actinides [160]. It is also significant in ordered, tetrahedral semiconductors, which strongly deflect from spherically symmetric electron distribution [161]. None of these cases pertains to our system.

The Landau diamagnetism is also negligible in PANI–DBSA since the conduction therein is achieved by hopping, so it is hard to imagine in-plane loops of itinerant electrons in PANI–DBSA.

5.3.1 Diamagnetism of atoms and ions

Diamagnetism leads to a negative, small magnetic susceptibility. In a diamagnetic material, the induced magnetic moment opposes H . This effect is often discussed within the framework of classical electromagnetism: the action of H on the orbital motion of an electron causes a back electromotive force which by the Lenz law sets up a current opposing the local magnetic flux change. This shielding is always only partial (complete shielding can be achieved in type I superconductors, but these are different, macroscopic quantum systems).

Bearing in mind the Bohr – van Leeuwen theorem, one should be wary of approaches which attempt to show that the application of H to a classical system can induce a magnetic moment. Yet, the classical and the quantum theory can produce the same result if the classical theory adopts quantum corrections. These are the following: Electron orbits are stable quantum-mechanically [162], whereas classical electrons cannot move in a circular orbit round the atomic nucleus without radiating energy and collapsing into the centre of the atom [163]. Furthermore, according to the classical Faraday law, a magnetic flux must vary in time to induce an opposing current, whereas for an electron orbit within an atom, the induced current persists as long as a (constant) H is present.

To explain diamagnetism, the classical Langevin theory takes into account the Larmor theorem [22]: In an applied magnetic field H , the motion of an electron around a nucleus is, to the first order in H , the same as a possible motion in the absence of H except for the superposition of a precession of the electron with the angular frequency $\omega_{\text{Larmor}} = e\mu_0 H/2m_e$.

The Langevin’s classical calculation [22] gives the following result for the diamag-

netic susceptibility of a monatomic solid of an atomic number Z :

$$\chi_{\text{dia}} = -N \frac{e^2 \mu_0}{6m_e} \sum_{i=1}^Z \langle r_i^2 \rangle \quad , \quad (5.7)$$

where $\langle r_i^2 \rangle$ are the mean square distances of electrons from the nucleus. The problem of calculating χ_{dia} of an isolated atom is reduced to calculation of $\langle r_i^2 \rangle$. For closed-shell atoms or ions, Eq.(5.7) can be simplified as

$$\chi_{\text{dia}} \approx -N \frac{e^2 \mu_0 Z_{\text{eff}}}{6m_e} \langle r^2 \rangle \quad , \quad (5.8)$$

where $Z_{\text{eff}} \leq Z$ is the number of electrons in the outer shell of an atom or ion.

As T is increased above zero, states above the ground state become progressively more important in determining χ_{dia} , but this is a marginal effect and χ_{dia} is essentially T independent [157]. On the other hand, electrons in the outer shells may constitute chemical bonds, which modifies the diamagnetic response of a chemically bound atom. These modifications are taken into account through the Pascal constants, which will be explicated in Subsection 5.6.3.

The calculation of χ_{dia} that starts with quantum mechanical principles gives the same result as the classical Langevin's approach [22, 157].

5.3.2 Curie paramagnetism

Paramagnetism corresponds to a positive magnetic susceptibility. An applied magnetic field H induces a magnetisation M which aligns parallel with the H . Without H , these magnetic moments point in random directions and give no net magnetic moment. The application of H tends to line them up, the degree of the lining up (and hence the magnitude of M) depending on the magnitude of H .

Although an increase of H will tend to line up the magnetic moments, an increase of T will tend to randomise them. It is therefore expected that the magnetisation of a collection of atoms will depend on the ratio H/T . An atom in a magnetic field and with a total angular momentum quantum number j has $2j + 1$ equally spaced energy levels. It can be shown [157] that the paramagnetic response of such a system is given by

$$M(H/T) = M_{\text{sat}} B_j(X) = N g \mu_B j B_j(X) \quad , \quad (5.9)$$

where g stands for the Landé factor,

$$g = 1 + \frac{j(j+1) + s(s+1) - l(l+1)}{2j(j+1)} \quad ; \quad (5.10)$$

s is the spin quantum number, l the orbital quantum number, $X = g \mu_B j \mu_0 H / k_B T$, and $B_j(X)$ is the Brillouin function:

$$B_j(X) = \frac{2j+1}{2j} \coth\left(\frac{2j+1}{2j} X\right) - \frac{1}{2j} \coth\left(\frac{X}{2j}\right) \quad . \quad (5.11)$$

Except at very low T and/or in extremely high H , all experimental situations will correspond to $X \ll 1$ and, hence, $\chi \ll 1$. Utilising the fact that x is an analytic function, and thence can be expanded into a Maclaurin series [164], one obtains the Curie law

$$\chi = \frac{M}{H} = \frac{N\mu_0\mu_B^2 g^2 j(j+1)}{3k_B T} = \frac{N\mu_0\mu_{\text{eff}}^2}{3k_B T} = \frac{C}{T} \quad , \quad (5.12)$$

where C is the material-specific Curie constant. The magnetic moment per atom is in the above case given by $\mu_{\text{eff}} = g\mu_B \sqrt{j(j+1)}$. If $X \ll 1$ is not satisfied, the magnetisation saturates to M_{sat} , which corresponds to a magnetic moment of $g\mu_B j$ per atom.

The magnetic moment of a system of electrons in an atom or ion depends on the total angular momentum \mathbf{J} ,

$$\mu = -g\mu_B \mathbf{J} = -g\mu_B (\mathbf{L} + \mathbf{S}) \quad , \quad (5.13)$$

where \mathbf{L} and \mathbf{S} stand for the orbital and the spin magnetic moment, respectively. In materials without magnetic ordering, magnetisation (5.1) is directed along the axis of the magnetic field $\mathbf{H} = H\hat{\mathbf{H}}$. In solids, \mathbf{J} is very often contributed only by \mathbf{S} . This claim is trivial for s-electrons ($l = 0$), but it also holds for p- and d-electrons. The electric crystal field lifts (in the absence of \mathbf{H}) the degeneracy of the atomic orbitals. The orbital angular momentum of the atom is said to be quenched; $\mathbf{L} \cong 0$ [165]. The magnetic moment is thus given only by the value of s , i.e.,

$$\mu_{\text{eff}} = 2\mu_B \sqrt{s(s+1)} \quad . \quad (5.14)$$

For the electron, $s = 1/2$. The quenching of orbital angular momentum also applies to PANI–DBSA, because this material contains s- and p-electrons only. Combining (5.12) and (5.14), we obtain:

$$C = \frac{\mu_0\mu_B^2}{k_B} N_C \quad , \quad (5.15)$$

where, instead of N , we introduce N_C , the effective number of localised spins. So, the Curie paramagnetism is the paramagnetism of spatially localised electron spins. As our PANI–DBSA contains both localised and itinerant electrons, we still have to account for the latter ones, which is the topic of Subsection 5.3.3.

5.3.3 Pauli paramagnetism

We consider the electron gas. Each k -state in a band can be doubly occupied because of the two possible spin states of the electron. Each electron is therefore either spin-up or spin-down. When a magnetic field H is applied, the energy of an electron is raised or lowered depending on its spin. This change of energy with H gives rise to paramagnetic susceptibility of the electron gas — known as Pauli paramagnetism [157].

We neglect the orbital contribution and take $g = 2$. As shown in Fig. 5.1, in an applied magnetic field H , the electron band is spin-split into two spin subbands separated by

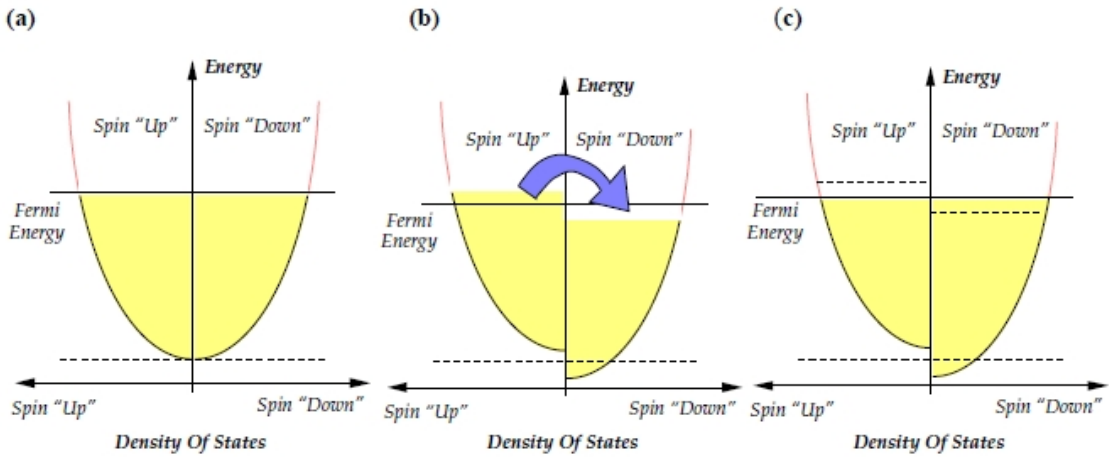


Figure 5.1: The origin of itinerant electron (Pauli) paramagnetism. In (a), $H = 0$, and the numbers of spin-up and spin-down electrons are the same. In (b), $H > 0$, and electrons with spins anti-parallel to H (spin-down) have a lower energy than spin-up electrons. This is because the spin-down electrons have a magnetic moment parallel to H . Albeit the system does not have a net magnetic moment yet, until the spin-up electrons lower their energy by reversing their spin and occupying the available spin-down states. In (c), there is now a net excess of spin-down electrons. This imbalance represents the paramagnetic response of itinerant electrons. (Reproduced from [166].)

$g\mu_B\mu_0H = 2\mu_B\mu_0H$. In comparison with the Fermi energy, $g\mu_B\mu_0H$ is very small, and the splitting of the energy bands is therefore a small perturbation. The number of extra electrons per unit volume with spin-up is $N_\uparrow = \frac{1}{2}N(E_F)\mu_B\mu_0H$, and the reduction of the number of electrons with spin-down per unit volume is $N_\downarrow = -\frac{1}{2}N(E_F)\mu_B\mu_0H$. Thus, the Pauli susceptibility is given by [167, 157]

$$\chi_P = \frac{M}{H} = \frac{\mu_B(N_\uparrow - N_\downarrow)}{H} = \mu_0\mu_B^2N(E_F) \quad . \quad (5.16)$$

So, χ_P is T independent. If we took into account the smearing of the Fermi surface due to finite T , we would obtain only a small correction to the result (5.16) [168].

Generally, Pauli paramagnetism is a weak effect, much smaller than typical paramagnetism observed in insulators due to the Curie law. This is because in paramagnetic insulators at least one electron on every magnetic atom in the material contributes to χ , whereas in electron gas, only electrons close to the Fermi surface play a role in the corresponding paramagnetism [157].

Up to now, we have been neglecting any correlation between the electrons. In many cases this would be an oversimplification. If we take into account the interaction potential of spin-up and spin-down electrons, \tilde{U} , we obtain the Stoner enhancement of the magnetic susceptibility of itinerant electrons [157, 169]:

$$\chi_{\text{Stoner}} = \frac{\chi_P}{1 - \tilde{U}N(E_F)} \quad . \quad (5.17)$$

So, the bare, non-screened, Coulomb interaction \tilde{U} may lead to itinerant ferromagnetism if the Stoner criterion, $\tilde{U}N(E_F) \geq 1$, is fulfilled. The Stoner model can be obtained from the Hubbard model* by applying the mean-field approximation.

The models of paramagnetism addressed above, serve as a starting point in the elucidation of experimental results for PANI–DBSA, which will be discussed later. But this system, where Curie (localised) and Pauli (delocalised) spins coexist, requires a more focused description based on more complex foundations. The Kamimura model, addressed in Section 5.4, seems to be appropriate for that purpose.

§ 5.4 Kamimura model

5.4.1 Basic notions

In this section, we describe the effects of electron-electron interactions (EEI's) in an disorder band. Our PANI–DBSA is a doped, disordered system with the Anderson localisation and EEI's, and its properties position it well on the insulating side of the metal-insulator transition (MIT).

The Kamimura model [171, 86] treats the coexistence of disorder and EEI's in the Anderson-localised regime on the insulating side of the MIT. The model is particularly suitable for the case where the localisation length is of the order of average dopant separation. We shall later see that this criterion is satisfied in our PANI–DBSA.

The Hamiltonian in TBA in the presence of both disorder and EEI can be generally written as

$$\begin{aligned} \mathcal{H} &= \mathcal{H}_0 + \mathcal{H}_1 \quad , \\ \mathcal{H}_0 &= \sum_{i\sigma} \lambda_i c_{i\sigma}^\dagger c_{i\sigma} + \sum'_{ij} \sum_{\sigma} I_{ij} c_{i\sigma}^\dagger c_{j\sigma} \quad , \\ \mathcal{H}_1 &= \frac{1}{2} \sum_{ijkl\sigma\sigma'} \langle ij | \hat{U} | kl \rangle c_{i\sigma}^\dagger c_{j\sigma'}^\dagger c_{l\sigma'} c_{k\sigma} \quad , \end{aligned} \quad (5.18)$$

where the operator $c_{i\sigma}^\dagger$ creates a state with a spin σ at the i -th dopant site with a single-electron energy λ_i , I_{ij} are transfer integrals, and \hat{U} is the operator of the EEI. \mathcal{H}_0

*The Hubbard model is widely used to investigate correlation effects. For example, it describes the transition from metallic to insulating behavior when \tilde{U} exceeds some threshold. The corresponding localisation of the electron wavefunctions is known as the Mott localisation. Strong Coulomb interactions result in an energy gap separating low-lying states with one electron per atom from states with two electrons per atom, and this level splitting is modified by an interatomic exchange interaction [170]. The Hubbard model is the simplest possible model of strongly-correlated materials [23], and is thus sometimes highly oversimplified [21] for real systems.

describes disorder, and \mathcal{H}_1 many-body interactions. In order to mimic the disorder, λ_i and I_{ij} are taken to be random variables. If we consider short-range interactions only and retain terms with $i = j = k = l$ in \mathcal{H}_1 , then the total \mathcal{H} corresponds to the Hubbard model for structurally random systems [171]. However, the Coulomb interaction between electrons generally gives rise to both intrastate and interstate interactions. We consider briefly this general case below.

We want to account explicitly for the Anderson-localised nature of the electron states, so we take eigenstates of \mathcal{H}_0 as the basis. This approach proves to be successful in describing disordered interacting systems, except those on the verge of the MIT. Since our PANI-DBSA is away from the MIT, we find it useful to consider this approach. So, in the transfer-diagonal representation, \mathcal{H} can be rewritten as:

$$\mathcal{H} = \sum_{\alpha\sigma} \varepsilon_{\alpha} \hat{n}_{\alpha\sigma} + \frac{1}{2} \sum_{\alpha\sigma} U_{\alpha} \hat{n}_{\alpha\sigma} \hat{n}_{\alpha,-\sigma} + \frac{1}{2} \sum'_{\alpha\beta\gamma\delta} \sum_{\sigma\sigma'} U_{\alpha\beta\gamma\delta} c_{\alpha\sigma}^{\dagger} c_{\beta\sigma'}^{\dagger} c_{\delta\sigma'} c_{\gamma\sigma} \quad , \quad (5.19)$$

where $\alpha, \beta, \gamma, \delta$ index the eigenstates of \mathcal{H}_0 with eigenvalues $\varepsilon_{\alpha}, \varepsilon_{\beta}, \varepsilon_{\gamma}, \varepsilon_{\delta}$. An eigenstate of \mathcal{H}_0 is given by a linear combination of the original Wannier functions,

$$|\alpha\rangle = \sum_i v_{i\alpha} |i\rangle \quad , \quad (5.20)$$

with unitary-matrix elements $v_{i\alpha}$. The other abbreviations stand for:

$$\hat{n}_{\alpha\sigma} \equiv c_{\alpha\sigma}^{\dagger} c_{\alpha\sigma} \quad , \quad U_{\alpha\beta\gamma\delta} \equiv \langle \alpha\beta | \hat{U} | \gamma\delta \rangle \quad , \quad U_{\alpha} \equiv U_{\alpha\alpha\alpha\alpha} \quad . \quad (5.21)$$

The dominant EEI's in (5.20) are the intrastate, on-site Coulomb interactions (OSCI's) [171]. The dominant interstate interactions — $U_{\alpha\beta\beta\alpha}$ (the direct exchange interaction) and $U_{\alpha\alpha\alpha\beta}$ (a kinetic-type exchange interaction) — may favour, respectively, ferromagnetic and antiferromagnetic spin configuration of two singly occupied Anderson-localised states. However, these exchange interactions are largely suppressed by spatial correlations of the VRH regime, and their importance is thus restricted mainly to low T . The other interstate interactions merely renormalise the single-electron energies or transfer integrals. Therefore, we will be concerned primarily with OSCI hereafter.

5.4.2 Spin susceptibility

Electron correlation effects on spin susceptibility in random systems were first studied in amorphous semiconductors [172] and in the metallic regime of doped semiconductors [173]. Here we give a general expression of spin susceptibility in the Anderson-localised regime in the presence of an OSCI [174].

When a magnetic field H is applied to a system, the single-electron energy levels are split and shifted by the Zeeman effect. Thus, Eq. (5.19) turns into

$$\mathcal{H} = \sum_{\alpha\sigma} (\varepsilon_{\alpha} - \sigma\mu_0\mu_B H) \hat{n}_{\alpha\sigma} + \frac{1}{2} \sum_{\alpha\sigma} U_{\alpha} \hat{n}_{\alpha\sigma} \hat{n}_{\alpha,-\sigma} \quad , \quad (5.22)$$

with the third term of Eq. (5.19), which accounts for the EEI's involving two or more eigenstates, being neglected for the reasons explicated in the preceding subsection. The general expression for χ in the case of Anderson localisation in the presence of OSCI is given by [86]

$$\chi(T) = \frac{2\mu_0\mu_B^2}{k_B T} \sum_{\alpha} \left[2 + \exp\left(\frac{E_F - \varepsilon_{\alpha} - U_{\alpha}}{k_B T}\right) + \exp\left(-\frac{E_F - \varepsilon_{\alpha}}{k_B T}\right) \right]^{-1}, \quad (5.23)$$

where the summation includes all localised states in the impurity band. Each of these states has four possible eigenenergies, depending on the occupancy of the eigenstate $|\alpha\rangle$:

- $E_{\alpha} = 0$ (unoccupied state)
- $E_{\alpha} = \varepsilon_{\alpha} - \mu_0\mu_B H$ (state occupied by a spin-down electron)
- $E_{\alpha} = \varepsilon_{\alpha} + \mu_0\mu_B H$ (state occupied by a spin-up electron)
- $E_{\alpha} = 2\varepsilon_{\alpha} + U_{\alpha}$ (doubly occupied state)

At low T , for which $k_B T < U$ (U is the average of all ε_{α} -dependent OSCI's U_{α}), the singly occupied states appear, and thus the spin susceptibility (5.23) when expanded in power series of T , obeys the Curie law [175]

$$\chi(T) = \frac{\mu_0\mu_B^2}{k_B T} N_S, \quad (5.24)$$

where N_S is the number of singly occupied states. This holds for any value of W/U , where W is the width of the disorder band. However, when $W > U$, an interesting feature occurs: the Curie-type behaviour becomes suppressed and gives rise to a Pauli-type behaviour as T increases (see Fig. 5.2). This crossover appears when $k_B T \sim U$, and results in a coexistence of the Curie-type and the Pauli-type contributions to the spin susceptibility. It will be shown later that we observe a similar behaviour in our samples.

At even higher temperatures, $k_B T \gg U, W$, the electrons become non-degenerate (hot), and the model predicts a Curie-type magnetic susceptibility where the number of contributing spins now equals the total number of electrons. This T region is beyond the T range of our measurements.

Let us now examine how the Pauli-type susceptibility appears in the Kamimura model. If an electron is in a localised state $|\alpha\rangle$ with the eigenenergy E_{α} , then the energy of a second electron with the opposite spin in the same state is $E_{\alpha} + U$. Thus, energy levels in the range between E_F and $E_F - U$ will be singly occupied, and the states lower in energy will be doubly occupied [171, 176]. At low temperatures, i.e., $T \ll U/k_B$, thermal excitations are weak and only singly occupied localised states will contribute to χ . In this case, Eq. (5.23) reduces to a Curie-type behaviour of Eq. (5.24), i.e., to Eq. (5.15) with N_C being the total number of singly occupied

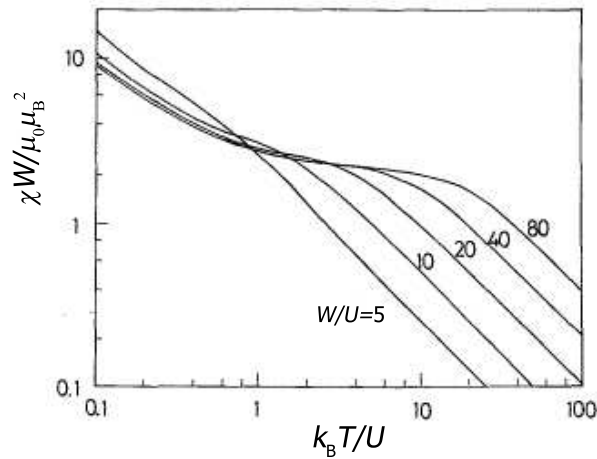


Figure 5.2: $\log \chi$ vs $\log T$ for various W/U , calculated within the Kamimura model. (Reproduced from [174].)

states. At higher temperatures, $T \gtrsim U/k_B$, thermal excitations lead to the appearance of doubly occupied states for which the energy of the second electron lays above E_F , thus giving rise to a Pauli-type susceptibility.

The Kamimura model is experimentally verified in a number of cases for doped semiconductors [171, 86]. It has also been applied to treat the coexistence of Pauli-type and Curie-type contributions to the paramagnetic susceptibility in conducting disordered PANI with weak EEI's [177, 70]. This treatment was done within the picture of the Fermi glass (finite DOS at E_F). In our PANI-DBSA, the strong Coulomb interaction results in opening of a soft gap at E_F , but the application of the Kamimura model is nevertheless suitable at finite T , due to the softness of the gap.

5.4.3 Comment on Coulomb interactions

After we have studied the impact of OSCI on χ , is natural to consider the effect of OSCI on the Mott VRH conduction. The Kamimura model predicts OSCI to have only a mild effect on the Mott VRH conductivity: the exponent $\alpha = 1/4$ of the Mott law (4.34) remains valid, only the dependence of T_0 on the localisation length ξ , (4.35), is altered [178]. $T_0(\xi)$ becomes more complicated in the presence of OSCI because ξ of doubly occupied states may be different from that of singly occupied states [179].

The Mott law does not describe well the conductivity of our PANI-DBSA, since it does not take into account the Coulomb interaction which leads to the appearance of the soft gap. At this point, it is appropriate to specify precisely which types of Coulomb interactions dominate in PANI-DBSA.

The Coulomb interaction that we have considered in Subsection 5.4.2, which is ab-

breviated as OSCI, is an on-site electron-electron interaction. The other relevant interaction for our PANI–DBSA material is the quasi-excitonic electron-hole interaction (QEEH) which results in a soft, Coulomb gap along with a variety of exponents α . Although some other Coulomb interactions are probably also present in PANI–DBSA (some of them have been mentioned in 5.4.1), these two (QEEH and OSCI) are the most important ones in the shaping of the electromagnetic properties of this material.

§ 5.5 Magnetism in conducting polymers

Magnetic properties of conducting polymers (CP's) are related to the presence of spins which are mainly correlated with the doping level and to a lesser extent with physical and chemical properties of the dopant. Doping is related to injecting charge carriers into polymer chains. These injected charges may or may not result in spin carriers, depending on the type of nonlinear excitations involved. Of these different types of nonlinear excitations, solitons appear in those CP's that have a degenerate ground state. In CP's where the ground-state degeneracy has been lifted by the molecular structure, we encounter confined soliton-antisoliton pairs, polarons, and bipolarons as the stable charge storage states [180]. The spin-charge relationships for different species of nonlinear excitations in CP's are summarised in Table 5.1.

Table 5.1: Spin-charge relationships for different nonlinear excitations in conducting polymers. Soliton has an inverse spin-charge relationship, that is, when a charge is present, there is no spin, and vice versa. Polaron has the usual spin-charge relationship of fermions: an injection of charge is accompanied by an appearance of spin. Polaron can be thought of as a bound state of a neutral soliton (contributing with spin) and a charged soliton (contributing with charge), the midgap states of which hybridise to form bonding and antibonding levels. Bipolaron has an inverse spin-charge relationship, and can be depicted as a bound state of two charged solitons of like charge, or as a bound state of two polarons (of like charge) the neutral solitons of which annihilate each other [47, 57]. Thus, positive bipolaron is a spinless dication, and negative bipolaron a spinless dianion. The two polarons in a bipolaron are bound together by the overlap of a common lattice distortion or enhanced geometrical relaxation of the bond lengths.

Nonlinear excitations	Charge [e]	Spin
neutral soliton	0	1/2
charged soliton	± 1	0
polaron	± 1	1/2
bipolaron	± 2	0

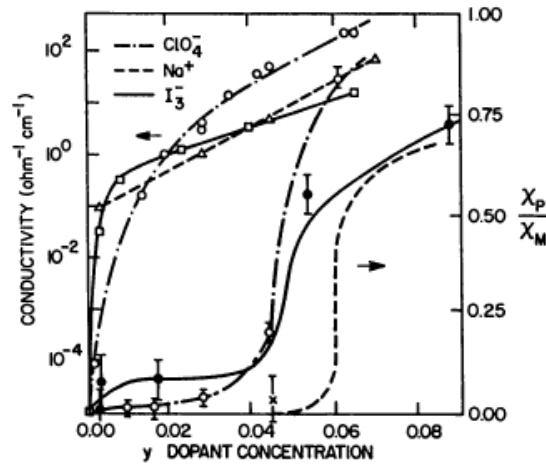


Figure 5.3: Dc electrical conductivity (left-hand scale) and Pauli magnetic susceptibility χ_P (right-hand scale) of PA, as functions of the dopant concentration y in percentage, for various dopants. χ_P data are normalized to the Pauli susceptibility of undimerised PA, χ_M . Such a PA does not undergo the Peierls transition, so has a wide (~ 10 eV) half-filled conduction band and is therefore a 1D metal. (Reproduced from [181].)

Intrinsic CP's are diamagnetic and become paramagnetic upon doping. An illustration of the correlation between the doping and magnetism (of itinerant electrons) in CP's is shown in Fig. 5.3.

PANI has a non-degenerate ground state, just as virtually all CP's have (except for PA). When a CP with a non-degenerate ground state is doped with an electron or a hole, a polaron is formed. CP's are often hole-doped by protonic acids.

As shown on Fig. 5.4a, the bonding of H^+ at the imine ($-N=$) sites that were previously lacking hydrogen, i.e., at two $-N=$ sites bypassed by the quinone ring, may result in a doubly charged spinless bipolaron site [182]. However, such a picture is inconsistent with results of magnetic measurements [183]. An ordered lattice of bipolarons centered on every fourth C_6 ring would form an empty band and this contradicts the measured χ_P which indicates the presence of itinerant electron spins. The transition of a bipolaron into two polarons (Fig. 5.4b) is energetically not favoured in the continuum theory [184, 185]. Yet, the formation of an ordered array of polarons centred on alternate nitrogen atoms, as shown schematically in Fig. 5.4c, can be stabilised by the energy gained through delocalisation and hence reduced (screened) Coulomb interaction [185].

Numerous experiments have confirmed [16, 169] that the paramagnetic part of the magnetic susceptibility in a vast majority of CP's — doped PANI being one of them [186] — is a superposition of a T -independent Pauli term and a $1/T$ Curie term:

$$\chi_{\text{para}}(T) = \chi_P + \chi_C(T) = \chi_P + \frac{C}{T} \quad (5.25)$$

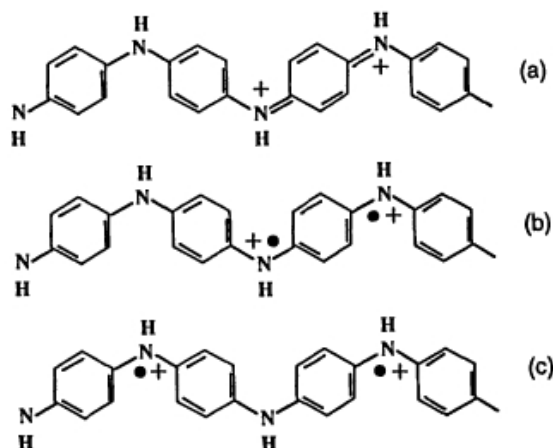


Figure 5.4: The formation of a polaron lattice in PANI: (a) emeraldine salt in the spinless bipolaron form; (b) dissociation of the bipolaron (of charge $2e$) into two positively charged polarons, each carrying a spin $1/2$; (c) rearrangement of the charges into a polaron lattice. (Reproduced from [186].)

It is interesting to mention three cases where either the usual correlation between itinerant electrons and a Pauli-type magnetic response has been broken, or an unexpected magnetic behaviour related to Pauli-type susceptibility has been found.

1. An exceedingly small Pauli-type magnetic susceptibility was observed in disordered PANI even in the absence of doping [187], which was ascribed to the following: Disorder can cause a decrease in the overlap between the p_z orbital of the imine nitrogen atom and the p_z orbital of the neighbouring carbon atom in the quinone ring. A bipolaron, which is a pair of polarons coupled by a strong exchange interaction, can thus be formed. A partial dissociation of such a disorder-induced bipolaron gives rise to spin-bearing polarons which are then responsible for the magnetic response. One pair of spins for every 200 rings was found, less than 10% of them being Curie spins. However, if the CP is heavily doped, two polarons are likely to merge again into a bipolaron [188].
2. In PPy films, highly disordered and heavily doped with polyanions [189], a non-Curie susceptibility has been attributed to thermal excitation of bipolarons from a singlet to a triplet state [190] rather than to a Pauli-type susceptibility.
3. Upon reducing disorder, an almost temperature independent magnetic susceptibility can be observed in many CP's [16]. This effect is also related to doping, but depends much more on the dopant itself. For example, PT doped with AsF_5 — which is a particularly strong Lewis acid [191] — shows a temperature independent Pauli susceptibility over the entire temperature range from ~ 10 K to RT, with only a hint of a Curie tail below 20 K [192].

As already mentioned in Section 5.3, CP's seldom exhibit effects of magnetic ordering. Yet, the possibility of a ferromagnetic or a ferrimagnetic behaviour in CP's has been proposed theoretically [193, 194], and experimental evidence of such interactions has been reported [195] even at RT. According to a theoretical calculation based on a 1D TBA method, a ferromagnetic (ferrimagnetic) state in poly(*m*-aniline) is more stable than the nonmagnetic one [196]. However, such extended ferromagnetic and ferrimagnetic interactions in CP's are generally weak. One will rather find indications of antiferromagnetic or ferromagnetic effects in restricted T intervals [197, 146].

§ 5.6 Magnetic susceptibility of PANI–DBSA

5.6.1 Measurements

A Quantum Design SQUID magnetometer of a resolution down to 10^{-6} emu was used to measure M in the temperature range 10 – 300 K. Samples of typically 100 mg were prepared by pressing the polymer powder into cylinders of 5 mm height and 5 mm in diameter. Samples were mounted onto a long polyethylene straw and placed into the magnetometer, where M was measured by using an isothermal 6 cm scan technique [198]. Measured background signal from the sample holder was subtracted from raw data.

5.6.2 Results

M was measured for all the values of Q that had previously been used in $\sigma(T)$ measurements. Results are henceforth presented in terms of molar magnetisation M and molar magnetic susceptibility χ , expressed per two rings of the PANI backbone.

Linearity of $M(H)$ was observed over the whole H range and for all of our samples, including the deprotonated one ($Q = 0$). This is exemplified in the inset to Fig. 5.5, where selected isothermal ($T = 10, 30, 80$ and 300 K) experimental $M(H)$ curves are shown for the $Q = 2.06$ sample ($Q = 2$ corresponding to the full protonation). Experimental magnetic susceptibility $\chi_{\text{exp}}(T)$ is extracted from the slopes of these curves and/or from $M(T)$ curves at $\mu_0 H = 2$ T after corrections for small (and T -independent) intercepts $M(H = 0)$ have been done. These (barely noticable) intercepts most probably originate in the presence of minuscule amounts of ferromagnetic impurities (Fe) originating from the chemicals used (this presence has been confirmed by the elemental analysis discussed in Subection 3.3.1).

χ_{exp} for the $Q = 2.06$ sample is plotted against T in the main panel of Fig. 5.5. One can observe a transition from diamagnetic to paramagnetic behaviour with decreas-

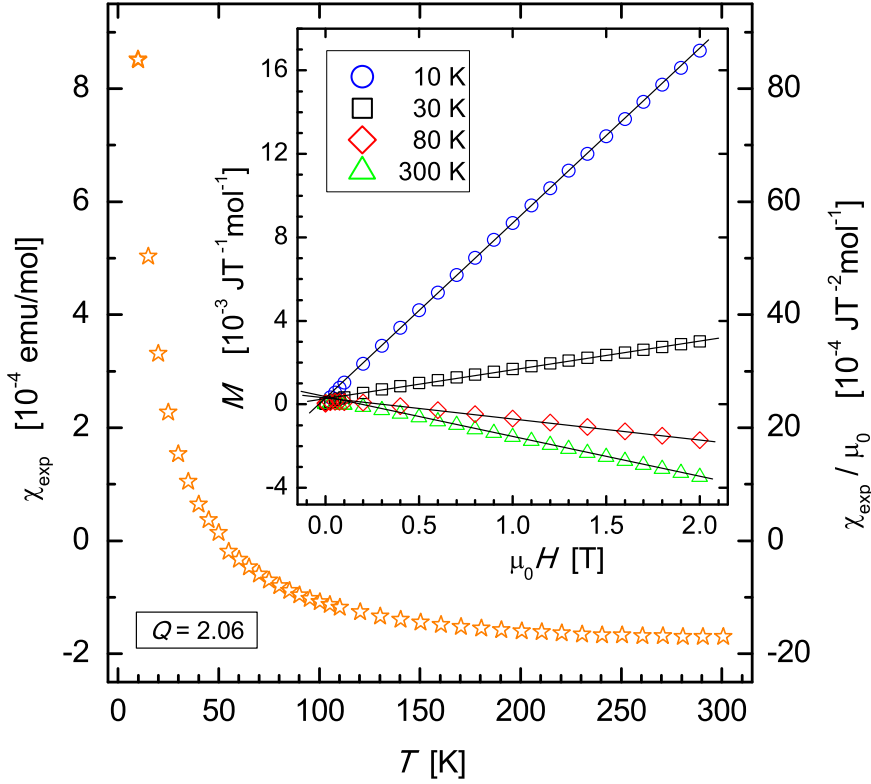


Figure 5.5: χ_{exp} vs T for the $Q = 2.06$ sample (main panel). At high temperatures, χ_{exp} shows a very weak T dependence. At low temperatures, $\chi_{\text{exp}}(T)$ becomes strongly paramagnetic with a dominant Curie-type behaviour. The left-hand scale gives the values of χ_{exp} in the CGS system, and the right-hand scale in the SI system. Inset: Linearity of $M(H)$ at selected temperatures for the $Q = 2.06$ sample. The solid lines are guides to the eye.

ing T , and a strong Curie-type behaviour below ~ 50 K. Error bars for M and χ data in this and subsequent plots are not shown since they are smaller than the symbol size.

Magnetic susceptibility of PANI–DBSA comprises the following contributions:

$$\chi_{\text{exp}}(T) = \chi_{\text{core}} + \chi_{\text{P}} + \frac{C}{T} \quad , \quad (5.26)$$

where χ_{core} corresponds to diamagnetism of atomic/ionic cores, χ_{P} to Pauli-type paramagnetism of conducting charge, and C/T to Curie-type paramagnetism of localised spins. Other contributions to χ_{exp} , originating in nuclear magnetism and orbital electron motion, are negligible or quenched (see Subsection 5.3.2). The paramagnetic parts of χ_{exp} are a consequence of the protonation: χ_{P} is related to the conducting charge — accounting for (dynamic) unoccupied, singly occupied, and doubly occupied states on the protonated N atoms — and C/T to unpaired localised spins (singly occupied states on the protonated N atoms). The diamagnetic contribution χ_{core} , on the other hand, arises from all the atoms present, and is independent of T .

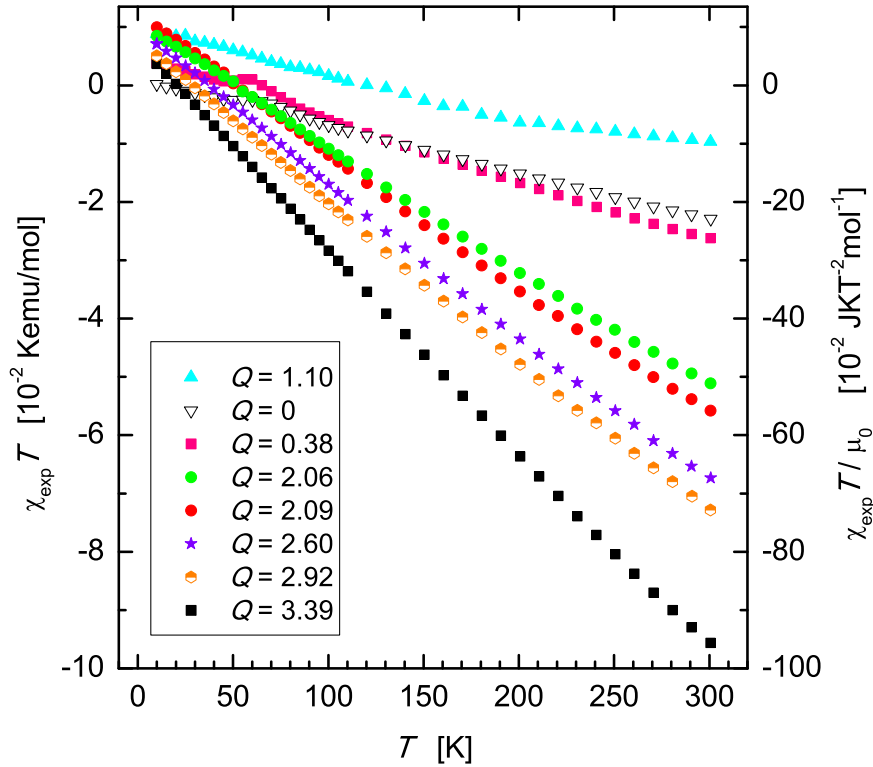


Figure 5.6: $\chi_{\text{exp}}T$ vs T for different Q . On left-hand scale, units of $\chi_{\text{exp}}T$ are in the CGS system, and on the right-hand scale, in the SI system.

In order to study different contributions to χ_{exp} , in Fig. 5.6 we plot $\chi_{\text{exp}}T$ vs T for different Q . According to (5.26), these plots are expected to be linear, with the Curie constant C being the intercept. Yet, a closer inspection of the data reveals that linearity of $\chi_{\text{exp}}T$ vs T with one intercept and slope actually does not hold over the whole T range. Instead, one can find two principal T ranges of linearity, except for the $Q = 0$ sample which has a single intercept and slope. Furthermore, for the $Q = 0$, and $Q = 0.38$ samples, one can observe an anomaly (a cusp) in the form of a departure from linear $\chi_{\text{exp}}T$ vs T in a certain restricted T range, which will be discussed separately in Section 5.7.

It is also discernible in Fig. 5.6 that the negative diamagnetic contribution to χ_{exp} grows faster with increasing Q than the positive paramagnetic contribution does. The only exception from this trend is the $Q = 1.10$ sample, which will be addressed separately in Subsection 5.6.4.

The observed trend in PANI–DBSA is exactly the opposite of that in PANI–HCl (produced from the same generic PANI base) where the positive paramagnetic contribution grows faster with increasing doping level than the negative diamagnetic contribution does [154]. Importantly, the protonation mechanism is known to be the same for both of these conducting polymers [47, 4]. Although the protonation level is not the only parameter which determines the paramagnetic response (for in-

stance, delocalisation of electrons is affected by local properties through the OSCI [86], and by extended disorder through the Coulomb gap [87, 88]), the opposite trends in PANI–DBSA and PANI–HCl can be safely ascribed to the diamagnetism of comparatively large DBSA molecules.

Because of this large diamagnetic contribution of DBSA, we do not analyse the curves in Fig. 5.6 in order to extract C and χ_p , since the sensitivity of such an analysis would be reduced. We rather calculate χ_{core} for each Q , subtract it from the corresponding χ_{exp} , and analyse the resulting paramagnetic part (χ_{para}) on the basis of $\chi_{\text{para}}T$ vs T plots.

The calculation of χ_{core} is somewhat cumbersome, so we dedicate Subsection 5.6.3 to explicating it in more detail.

5.6.3 Diamagnetic susceptibility of PANI–DBSA

The core susceptibility of the deprotonated sample is $\chi_{\text{core}}(Q = 0) = -80.3 \times 10^{-6}$ emu/mol, which is an experimentally found value with mole being defined per two-ring unit of PANI. The corresponding value in the SI units is $\chi_{\text{core}}(Q = 0)/\mu_0 = -8.03 \times 10^{-4}$ JT⁻²mol⁻¹. Since $\sigma(Q = 0) < 10^{-9}$ S/m, we assume that there is essentially no conducting charge, and hence $\chi_p(Q = 0) = 0$.

The estimated χ_{core} of other samples depends on Q , but can be worked out from the Pascal constants Π_i and their corrections due to constitutive chemical bonds h_j [199–201], utilising the following additive relation:

$$\chi = \sum_i v_i \Pi_i + \sum_j h_j \quad , \quad (5.27)$$

where v_i are the numbers of atoms/ions of the same kind in a molecule. The values for Π_i and h_j are taken from [202]. Changes of the constitutive chemical bonds upon the protonation of PANI, are taken into account and parameterised with Q .

The molar susceptibility χ (expressed in CGS units emu/mol) is related to the measured mass susceptibility χ_m (expressed in CGS units emu/g) by

$$\chi = \chi_m \frac{1}{2} (M_{\text{EB}} + Q M_{\text{DBSA}}) \quad , \quad (5.28)$$

where $M_{\text{EB}} = 362.43$ g/mol, and $M_{\text{DBSA}} = 325.74$ g/mol. The prefactor 1/2 is a consequence of Q and M_{EB} being defined per four rings of the PANI backbone, i.e., per mer of undoped PANI. We also note that the contributions of EB and of DBSA to χ_{core} can be written as

$$\chi_{\text{core}} = \chi_{\text{core,EB}} + \frac{1}{2} Q \chi_{\text{core,DBSA}} \quad , \quad (5.29)$$

where $\chi_{\text{core,EB}}$ and $\chi_{\text{core,DBSA}}$ are molar susceptibilities *per se* which can be calculated from Π_i and h_j . Our estimation gives

$$\chi_{\text{core,EB}} \approx \begin{cases} -(80.3 + 7.1Q) \times 10^{-6} \text{ emu/mol} & , \quad Q \leq 2 \\ -94.5 \times 10^{-6} \text{ emu/mol} & , \quad Q > 2 \quad , \end{cases}$$

where for the $Q = 0$ case we have taken the experimentally found value rather than the (slightly different) value obtained by calculation from Π_i and h_j . DBSA is responsible for a substantial part of χ_{core} even at moderate Q , as $\chi_{\text{core,DBSA}} \approx -225.1 \times 10^{-6}$ emu/mol.

5.6.4 Inferences

When we plot $\chi_{\text{para}}T$ vs T , we find (for all our PANI–DBSA samples) two principal T ranges of linearity, as exemplified in Fig. 5.7 for three samples which are selected to represent three distinct doping levels: $Q < 2$ (underdoped), $Q \approx 2$ (fully doped), and $Q > 2$ (overdoped). $Q = 2$ corresponds to 100% protonation, whereas $Q > 2$ designates a two-phase system comprising fully protonated PANI–DBSA with (chemically) unbound DBSA between the polymer chains (see Subsection 3.3.1).

The two ranges of linearity are separated by a crossover temperature T^* (indicated by the arrows; the straight solid lines depict the linear dependences). The Q -dependent crossover temperature $T^*(Q)$ found from $\chi_{\text{para}}T$ vs T plots is fairly the same as $T^*(Q)$ obtained from the $\sigma(T)$ data reported in Section 4.8 and [5]. From $\chi_{\text{para}}T$ vs T plots we extract the values of χ_{P} and C , which are different for $T < T^*$ and $T > T^*$. The extracted χ_{P} and C are listed, with some other inferred quantities that will be addressed later, in Table 5.2.

For the $Q = 3.39$ sample, which has two crossovers in $\sigma(T)$, one could expect three distinct regions of linearity in its corresponding $T\chi_{\text{para}}(T)$ curve. Although there are indications of three different slopes in $T\chi_{\text{para}}(T)$, these cannot be claimed with enough certainty. Therefore, two slopes are used to analyse $T\chi_{\text{para}}(T)$ for $Q = 3.39$ as well, and the mentioned indications result in larger error bars of the extracted quantities.

Figs. 5.8(a) and 5.8(b) show the obtained values of χ_{P} and C as functions of Q , at $T < T^*$ and $T > T^*$, respectively. The $Q=0$ sample has a small Curie constant $C/\mu_0 = 1.05 \times 10^{-2} \text{ JKT}^{-2}\text{mol}^{-1}$ in the whole T range, which is attributed to the presence of localised impurity spins. As already explained in Subsection 5.6.3, $\chi_{\text{P}}(Q = 0) = 0$.

In the protonation picture, $\chi_{\text{P}}(Q)$ and $C(Q)$ increase with increasing Q until the protonation is complete ($Q = 2$). For $Q \geq 2$, $\chi_{\text{P}}(Q)$ and $C(Q)$ should be constant. The above should hold both for $T < T^*$ and $T > T^*$. The results in Figs. 5.8a and 5.8b confirm this trend. There are discrepancies (e.g., the saturation seems to be shifted to below $Q = 2$) but these are neither critical nor entirely surprising. As discussed before, PANI–DBSA is a very complex system, with a huge dopant molecule which strongly increases the background diamagnetism and also complicates the structural properties, etc. Given this complexity, we can conclude that the results for $\chi_{\text{P}}(Q)$ and $C(Q)$ can be understood within the framework of the protonation picture (spin injection by doping).

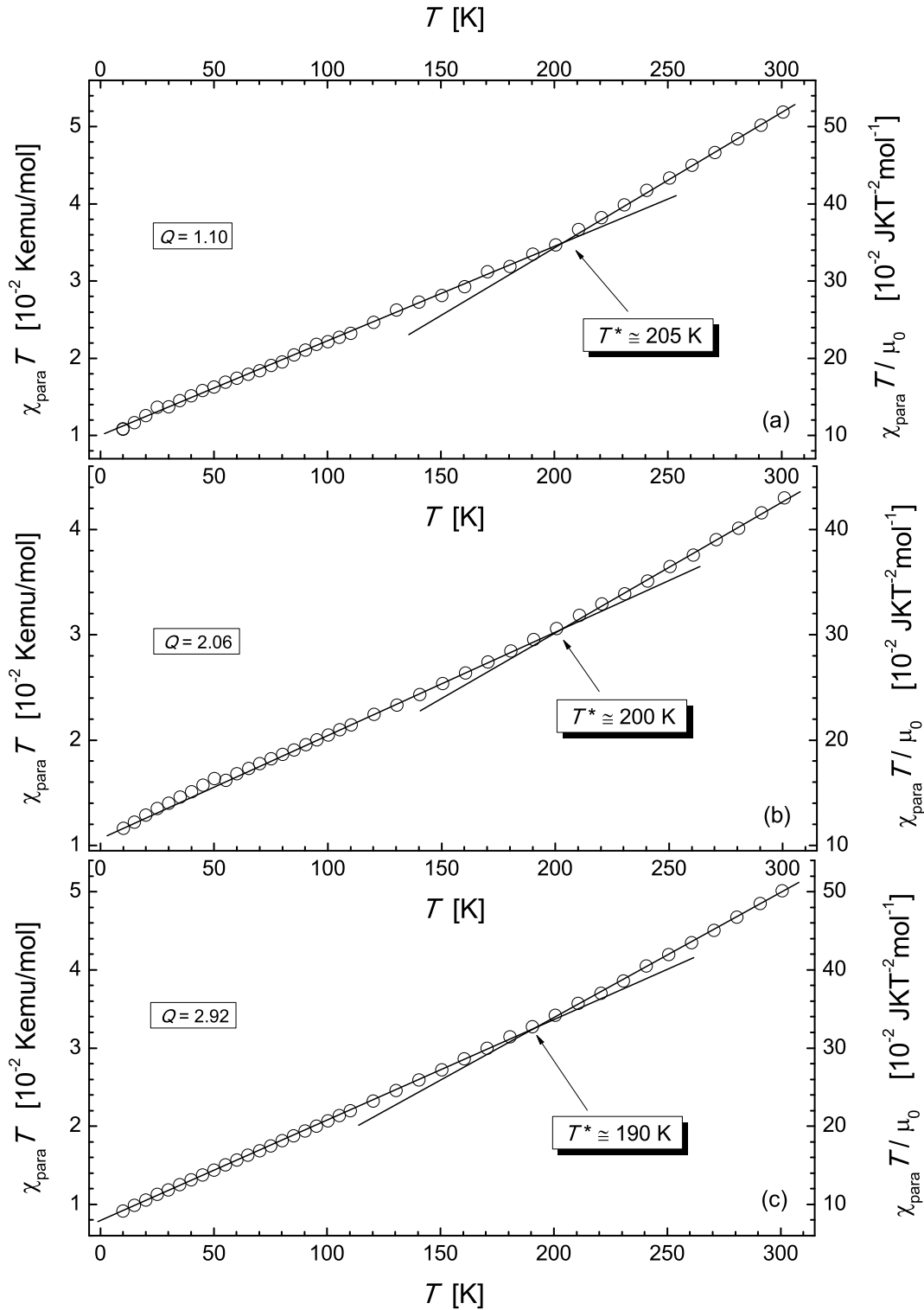


Figure 5.7: $\chi_{\text{para}}T$ vs T (symbols) for different Q . The plots are for clarity separated into panels. The chosen Q values represent three distinct doping levels (see the text): (a) $Q < 2$ (underdoped), (b) $Q \approx 2$ (fully doped), and (c) $Q > 2$ (overdoped). The arrows indicate positions of the crossover temperatures T^* , which agree with those in $\sigma(T)$ of the same material (see Section 4.8). The straight solid lines are guides to the eye, indicating regions of linearity. On the left-hand scale, units of $\chi_{\text{para}}T$ are in the CGS system, and on the right-hand scale, in the SI system.

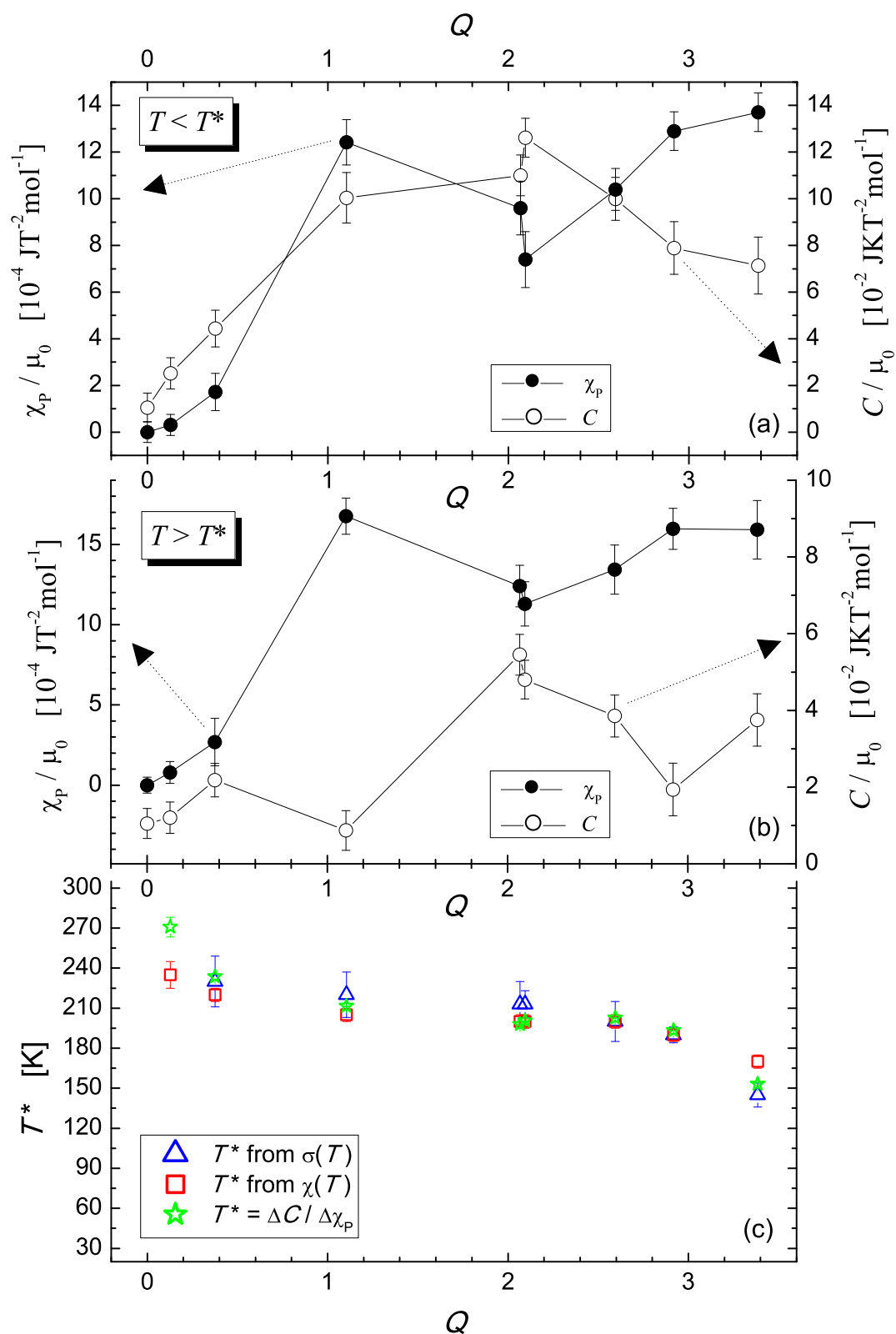


Figure 5.8: χ_p (left-hand scale, solid symbols) and C (right-hand scale, open symbols) as functions of Q at (a) $T < T^*$, and (b) $T > T^*$. (c) Crossover temperature T^* as a function of Q , determined by three independent methods as explained in the text.

Data in Figs. 5.8a and 5.8b contain information beyond general trends in the spin injection by protonation. In the $Q > 2$ region of the plots, one can note that χ_P and C , which both should be constant, seem to be correlated. An increase in χ_P is accomplished by simultaneous reduction in C , and vice versa. Such a simultaneity is observed even for the $Q = 1.10$ sample at $T > T^*$, where its C value represents the only departure from monotonicities in $Q < 2$ regions of the plots.

For the $Q = 1.10$ sample, the unexpectedly large values of χ_P at both $T < T^*$ and $T > T^*$, and an unexpectedly small value of C at $T > T^*$ may be explained by turning back to $\sigma(T)$ data.

In $\sigma(T)$, around $Q = 1$ there is a crossover in the VRH exponent from $\alpha = 1/2$ (holding for $Q \lesssim 1$) to $\alpha = 2/5$ (holding for $Q \gtrsim 1$) [5]. This crossover in α is the signature of a change in the structure of the Coulomb-gapped DOS, in our case from a quadratic to a linear Coulomb gap. A similar feature is found in PANI-HCl at about 60% of the full protonation [154]. Here, $Q = 1.10$ corresponds to 55% of the full protonation.

All the above features suggest that the same spins, injected by protonation, can behave either as Curie-type spins (contributing to C) or as Pauli-type spins (contributing to χ_P), depending on specific conditions. Furthermore, the results imply an interrelation between σ and χ in a way that a change in the electronic properties in the vicinity of E_F influences not just $\sigma(T)$ but $\chi(T)$ as well.

When values of χ_P and C (see Table 5.2) are analysed, one can note that, in all the samples, $\chi_P(T > T^*)$ is larger than $\chi_P(T < T^*)$, and, simultaneously, $C(T > T^*)$ is smaller than $C(T < T^*)$. This is consistent with a picture where the density of the delocalised electrons (represented by χ_P) at the expense of the localised ones (represented by C) is larger when the electrical transport occurs via NNH ($T > T^*$) than in the VRH regime ($T < T^*$).

After we have identified correlations between χ_P , C , and Q , we can calculate the following two parameters:

$$\begin{aligned} \Delta\chi_P(Q) &\equiv |\chi_P(Q, T > T^*) - \chi_P(Q, T < T^*)| = \\ &= \chi_P(Q, T > T^*) - \chi_P(Q, T < T^*) , \end{aligned} \quad (5.30)$$

$$\begin{aligned} \Delta C(Q) &\equiv |C(Q, T > T^*) - C(Q, T < T^*)| = \\ &= C(Q, T < T^*) - C(Q, T > T^*) . \end{aligned} \quad (5.31)$$

One can see from Table 5.2 that the ratio of the two parameters,

$$\frac{\Delta C(Q)}{\Delta\chi_P(Q)} \approx T^*(Q) , \quad (5.32)$$

yields a temperature, which is in very good agreement with the crossover temperature T^* found from both $\chi(T)$ and $\sigma(T)$. This exquisite threefold match is depicted in

Table 5.2: Experimentally obtained parameters χ_P/μ_0 and C/μ_0 , along with the derived parameters $N(E_F) = \chi_P/\mu_0\mu_B^2$, $N_C = Ck_B/\mu_0\mu_B^2$, and $L_{||} = \sqrt{\hbar^2\Delta N(E_F)/8m_e\Delta N_C}$. The mole (mol) is defined per two-ring unit of PANI.

Q	T range [K]	χ_P/μ_0 [10^{-4} JT $^{-2}$ mol $^{-1}$]	C/μ_0 [10^{-2} JKT $^{-2}$ mol $^{-1}$]	$N(E_F)$ [states (eV) $^{-1}$ (2 rings) $^{-1}$]	N_C [10^{-3} states (2 rings) $^{-1}$]	$L_{ }$ [Å]
3.39	10 – 170	13.71	7.14	4.24	19.03	8.50
	170 – 300	15.92	3.75	4.93	10.00	
2.92	10 – 190	12.90	7.89	3.99	21.02	7.56
	190 – 300	15.98	1.94	4.94	5.17	
2.60	10 – 200	10.40	10.02	3.22	26.64	7.38
	200 – 300	13.43	3.85	4.15	10.27	
2.09	10 – 200	7.39	12.62	2.29	33.63	7.43
	200 – 300	11.27	4.80	3.49	12.80	
2.06	10 – 190	9.60	11.00	2.97	29.32	7.48
	210 – 300	12.41	5.45	3.84	14.54	
1.10	10 – 200	12.42	10.04	3.84	26.77	7.23
	210 – 300	16.76	0.87	5.18	2.32	
0.38	10 – 220	1.72	4.44	0.53	11.83	6.88
	220 – 300	2.68	2.18	0.83	5.81	
0.13	10 – 210	0.31	2.52	0.10	6.71	6.39
	250 – 300	0.79	1.20	0.25	3.21	
0	10 – 300	0	1.05	0	2.80	

Fig. 5.8(c), where the following three series of independently determined crossover temperatures in PANI–DBSA are plotted against Q :

- T^* from $\sigma(T)$; blue triangles
- T^* from $\chi(T)$; red squares
- T^* calculated as $T^* = \Delta C/\Delta\chi_P$; green stars.

χ_P can provide information on the DOS for protonated samples. Properties of the DOS near E_F are at the heart of any problem associated with a soft [$N(E) = 0$ only at $E = E_F$] energy gap, so χ_P is a simple but powerful tool for studying this quantity. For Fermi liquids in the absence of exchange enhancement, χ_P can be expressed by (5.16), $\chi_P = \mu_0\mu_B^2 N(E_F)$, where $N(E_F)$ is thermal average of the DOS over a certain thermal window, approximately

$$E_F \pm k_B T \quad . \quad (5.33)$$

The calculated $N(E_F)$ for our PANI–DBSA samples are given in Table 5.2 together with the density of localised spins N_C , calculated from (5.15). One can see that, for $T > T^*$, values of $N(E_F)$ range from ~ 0.2 states $(\text{eV})^{-1}(2 \text{ rings})^{-1}$ up to ~ 5 states $(\text{eV})^{-1}(2 \text{ rings})^{-1}$, depending on Q . Simultaneously, N_C ranges from $\sim 145 \times 10^{-4}$ states $(2 \text{ rings})^{-1}$ down to $\sim 25 \times 10^{-4}$ states $(2 \text{ rings})^{-1}$. For $T < T^*$, the behaviour is similar, but due to the localisation being stronger, the values are somewhat lower for $N(E_F)$, and higher for N_C .

It is apparently confusing to have finite values of $N(E_F)$ in the VRH regime, where the Coulomb gap is present and $N(E_F)$ should vanish. However, since all our data correspond to a certain finite T , thermal smearing given by (5.33) applies, which results in the observation of a non-zero DOS at $T < T^*$ despite the presence of the Coulomb gap. So, in addition to its fingerprint in $\sigma(T)$, the Coulomb gap leaves a signature $\chi(T)$ as well — by the fact that at $T < T^*$ we observe a reduced DOS. This is consistent with the notion that the Coulomb gap models a reduction of the DOS for charge excitations in the vicinity of E_F .

The obtained values of $N(E_F)$ are in good agreement with those which other authors obtained for PANI doped with a similar surfactant acid, either from magnetic [203] or heat-capacity [204] measurements. In general, the reported values for $N(E_F)$ are within 1 – 10 states $(\text{eV})^{-1}(2 \text{ rings})^{-1}$ [149, 177, 183, 205, 206], regardless of the dopant or determination method (ESR, static magnetic measurements, calorimetry).

Having $N(E_F)$ and N_C , we can rewrite (5.32) more conveniently as

$$\frac{\Delta N_C}{\Delta N(E_F)} \approx k_B T^* . \quad (5.34)$$

Empiric relations (5.32) and (5.34) suggests that spins which disappear from χ_P reappear in C as localised spins when T is lowered below T^* , and vice versa. Such a scenario is predicted for certain values of the parameters of the Kamimura model (see Subsection 5.4.2). The observed (de)localisation of spins occurs when thermal energy becomes large enough to enable on-site pairing up of electrons which were at lower T unpaired due to the OSCI.

According to the Kamimura model, at low temperatures, i.e., $T \ll U/k_B$, thermal excitations are weak and only singly occupied localised states will contribute to χ , which gives a Curie-type response of Eq. (5.15) with N_C being the total number of singly occupied states. At higher temperatures, $T \gtrsim U/k_B$, thermal excitations lead to the appearance of doubly occupied states, and this gives rise to a Pauli-type susceptibility which eventually begins to dominate at higher T . Since our experimentally inferred T^* separates regimes of strong-to-moderate and weak electron localisation, it seems natural to assume that

$$T^* \sim \frac{U}{k_B} . \quad (5.35)$$

The assumption is further discussed below.

By combining results for $\chi(T)$ with those for $\sigma(T)$, we can extract electron localisation lengths in our samples. Since PANI–DBSA comprises coupled 1D elements (polymer chains), the longitudinal localisation length L_{\parallel} along the chain differs from the transversal localisation length L_{\perp} which is perpendicular to the chains. For the Anderson localisation, it holds that

$$L_{\parallel} \approx \sqrt{\frac{\hbar^2}{8m_e U_{\text{eff}}}} \quad , \quad (5.36)$$

where m_e is the free electron mass, and U_{eff} the effective strength of the OSCI [207, 100] We approximate $U_{\text{eff}} \approx k_B T^*$. This approach gives L_{\parallel} of about 7-8 Å, the exact values for all the samples being tabulated in Table 5.2. As expected intuitively, electrons become more delocalised as Q grows. The values of L_{\parallel} remain of the order of the PANI mer length [156, 90], which is consistent with the initial Anderson criterion for strong localisation, and which we also assume to be valid for our PANI–DBSA electronic system. Additionally, these values are consistent with the criterion of the Kamimura model that the localisation length is of the order of average dopant separation. Thus, these reasonable results for L_{\parallel} imply that our linking of T^* to $U_{\text{eff}} \sim U$ is justified. In this case, (5.36) combines with (5.34) to yield

$$L_{\parallel} \approx \sqrt{\frac{\hbar^2}{8m_e k_B T^*}} = \sqrt{\frac{\hbar^2 \Delta N(E_F)}{8m_e \Delta N_C}} \quad . \quad (5.37)$$

Furthermore, utilising the experimentally inferred values of $N(E_F)$ in the NNH regime (values corresponding to $T > T^*$ in Table 5.2), we can estimate the transversal localisation length L_{\perp} by assuming $N(E_F) \cong N_0$, where N_0 is the bare single-particle DOS at E_F in the Mott law [87]:

$$\ln \left[\frac{\sigma(T)}{\eta_{1/4}} \right] = - \left(\frac{T_{1/4}}{T} \right)^{1/4} = - \left[\frac{k}{N_0 L_{\parallel} L_{\perp}^2 T} \right]^{1/4} \quad . \quad (5.38)$$

We estimate $k \approx 150$ on the basis of a standard semi-phenomenological approach to VRH conductivity [100, 114, 87, 109]. We obtain L_{\perp} of the order of 1-2 Å, which is close to other reported values for CP's with similar σ_{RT} [154, 207–209].

§ 5.7 Cusps

Here we address the appearance of a positive deviation from linear $\chi_{\text{exp}} T$ vs T at low T in our samples which is exemplified in Fig. 5.9 for the $Q = 0.38$ sample. Similar cusps appear in some other samples, but are more pronounced in low- Q samples, possibly because they are hindered by the strong paramagnetic response in the high- Q

ones. A similar behaviour was observed by other authors too, in doped [146, 177] and undoped [210] PANI, but its origin has remained unclear. We believe that the effect may be suggestive of an ordering of localised spins due to their interaction.

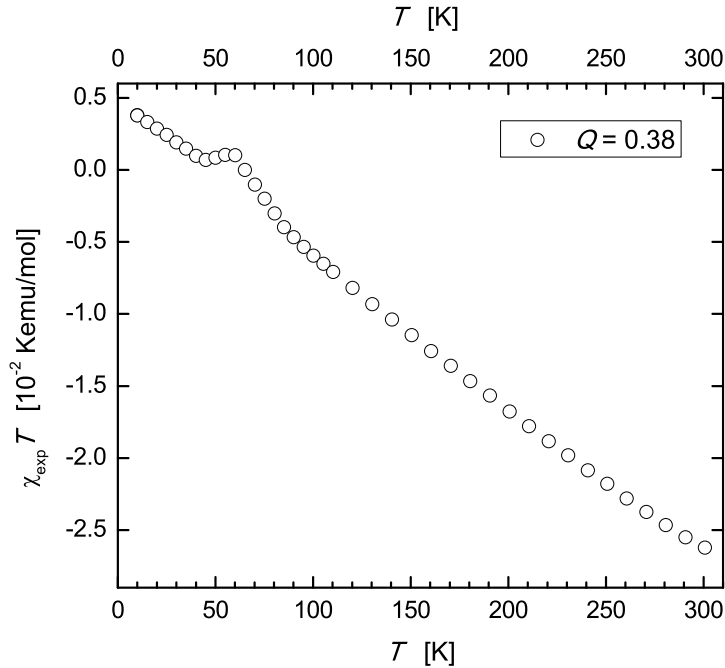


Figure 5.9: $\chi_{\text{exp}} T$ vs T for the $Q = 0.38$ sample. A cusp centred around ~ 60 K is observable. On the left-hand scale, units of $\chi_{\text{exp}} T$ are in the CGS system, and on the right-hand scale, in the SI system.

$\chi(T)$ of localised electrons follows the Curie law (5.15) at high T , but once T becomes comparable to or less than the typical spin-spin interaction strength, $\chi(T)$ may exhibit a different behaviour. There are several scenarios for the origin of the cusps [39], but we pay attention to a spin glass (SG) behavior in which $\chi(T)$ has a cusp at the temperature of a glass transition. SG's are not fully understood, and many of their properties are still controversial [39, 211, 212]. The basic feature of SG's is that the spins order, but differently than in a ferromagnet in which they all point in the same direction; the spins in a SG point in a random (but fixed) direction which varies from point to point. It is believed that SG's require spin-spin interactions of both ferromagnetic and antiferromagnetic signs which are sufficiently disordered to frustrate either of these ordering tendencies. As a result, the spins order in a novel state which can occur only in disordered systems.

The observed cusps in our PANI–DBSA could originate from the SG dynamics mentioned above, in particular since one of the two dominant interstate interactions of the Kamimura model favours ferromagnetic, whereas the other favours antiferromagnetic spin configuration of two singly occupied Anderson-localised states [213]. These in-

trastate interactions have been neglected in the derivation of the spin susceptibility (5.23). The picture of the competition between ferromagnetic and antiferromagnetic interactions is additionally supported by the fact that in PANI–HCl, produced from the same generic PANI, we have found both positive and negative cusps [154]. In general, glassy dynamics is a generic feature when disorder and interactions compete [214]. Glassy dynamics in relation to the Kamimura model has already been considered for doped PANI [177], albeit at considerably lower T .

Our PANI–DBSA is a paramagnet with interactions but without magnetic ordering. Clarification of the cusps calls for targeted measurements of local magnetisation [215]. In any case, the cusps are an interesting but marginal effect in the overall electromagnetic properties of PANI–DBSA.

§ 5.8 Coupling of spin and charge in PANI–DBSA

In this section, we discuss the interrelation between $\chi(T)$ (presented in Section 5.6) and $\sigma(T)$ (presented in Section 4.8) in PANI–DBSA.

In each of our PANI–DBSA samples, we have observed a coupling of spin and charge, the most direct manifestation of which is essentially the same temperature T^* found from both $\sigma(T)$ and $\chi(T)$. Temperature T^* has been found to be weakly dependent on Q , hence does not differ from sample to sample drastically. We believe that this coupling of spin and charge represents merely different manifestations of the same underlying physics, as explicated below.

Interaction effects (which classify our soft-matter material also as a strongly-correlated system) and thermal effects compete in PANI–DBSA, their relative strength depending on T . At low T , the interaction effects dominate over the thermal ones. As T increases, the thermal effects strengthen, and T^* is a particular temperature at which the thermal effects diminish the interaction effects in PANI–DBSA. This is demonstrated as follows:

1. **in electronic transport**, as a crossover from FTS-VRH regime to NNH regime. The depletion of the DOS for charge excitations, which is strongly pronounced at $T < T^*$, is at $T > T^*$ partly compensated by the delocalisation of the charge carriers. Hence, at $T > T^*$, all (or almost all) localised states (created by protonation) are available for hopping. In consequence, NNH within the disorder band ensues. The disorder is still present (slightly renormalised, though) in the NNH regime, but the thermal energy effectively diminishes its importance as the differences in the depths of the potential wells for charge carriers become unimportant.

However, the full physical picture for the cause of the onset of NNH, particularly why the crossover from VRH to NNH is not smeared out [132] (producing kinks at $T = T^*$, see Figs. 4.5c and 5.7), is yet to be revealed from $\chi(T)$.

2. **in magnetic response**, as a cessation of the importance of the OSCI U . Because of that, all the energy levels in the interval $[E_F - U, E_F]$ that were singly occupied at $T < T^*$ (and because of that were giving a Curie-type response), can at $T > T^*$ become also doubly occupied or empty, consequently giving a Pauli-type response. Thus, a portion of electrons that behaved as Curie-type spins at $T < T^*$, become Pauli-type spins at $T = T^*$.

It is plausible to assume $U \approx k_B T^*$. When U is relevant, most of the energy levels in the vicinity of E_F remain singly occupied and thus unavailable for hopping transport as long as $k_B T < k_B T^* \approx U$. If we assume that U ceases to be relevant at $T = T^*$, this implies that there are less restrictions for two spins being on the same site at higher T . Hence, the spins can pair up at $T > T^*$, and all the sites become available for the transport, which consequently leads to NNH. Namely, at $T \geq T^*$, the effects of OSCI are overcome by thermal effects; the Mott gap U closes at $T = T^*$. The disorder-induced soft gap Δ_C remains open at $T \geq T^*$, but the long-ranged QEEHI, which is responsible for Δ_C , is suppressed because of the enhanced screening of Coulomb interaction due to the strong thermal delocalisation of electrons. Because of this suppression of QEEHI, the soft gap is probably steeper at $T > T^*$ than at $T < T^*$.

Qualitatively, the electron physics in PANI–DBSA is at all T governed by the fact that, due to disorder, an electron cannot hop to any site but must choose those sites that are similar in energy. Additionally, at $T < T^*$, electron hops to singly occupied states cost energy and are therefore suppressed.

The measure of OSCI is U , which is, depending on Q , in the range $U \sim 15 - 20$ meV (equivalent of $T \sim 170 - 230$ K). The width of the soft gap, Δ_C , is the measure of QEEHI. It is, depending on Q , in the range $\Delta_C \sim 30 - 170$ meV (equivalent of $T \sim 350 - 2000$ K). Utilising the Kamimura model and taking into account the fact that in PANI–DBSA only a fraction of Curie-type electrons crosses over to Pauli-type electrons at T^* , we estimate (using Fig. 5.2) the width of the disorder band to be $W \sim 20 U$, i.e., $W \sim 300 - 400$ meV. Since the energy gap between the valence and the conducting band of PANI is $E_g \sim 2.5$ eV [216], we conclude that all the charge excitations in our PANI–DBSA happen within the disorder band. If it were not for the disorder band, which is created by protonation, our polymer would be a hard insulator.

From $\sigma(T)$ alone, we have inferred the importance of the long-ranged Coulomb interaction QEEHI in PANI–DBSA. From $\chi(T)$, we have inferred the importance of another type of Coulomb interaction in our PANI–DBSA — the on-site interaction OSCI. A local property U determines the spin dynamics whereas a collective property Δ_C is responsible for the charge dynamics, although U is not strictly a local property since it depends on Q weakly. At $T \geq T^*$, the energy difference between the

single and double occupancy of an Anderson-localised electron state in PANI–DBSA is thermally smeared out.

The energy scale that defines NNH regime of transport in PANI–DBSA is Δ_C , but the onset of NNH is enabled by closing the Mott gap U . So, we have a cooperative behaviour or coupling of spin and charge since U pertains to Coulomb correlations described in terms of spin only, whereas Δ_C is pertinent to spinless charge transport. The electronic conductivity in the NNH regime is given by an activation transport over the soft gap Δ_C (see Subsection 4.8.1),

$$\sigma_{\text{NNH}}(T) = \eta_1 \exp\left(-\frac{\Delta_C}{k_B T}\right), \quad (5.39)$$

where η_1 is a measure of disorder. The VRH regime of $\alpha = 1/2$ and $\alpha = 2/5$, on the other hand, correspond to a transport within the soft gap in the disorder band.

We observe the soft gap not only in $\sigma(T)$ but in $\chi(T)$ as well, since for all Q , $N(E_F, T < T^*) < N(E_F, T > T^*)$. If the soft gap were not detectable in $\chi(T)$, then the DOS for charge excitations would be equal in VRH and NNH. Furthermore, just as we can detect changes in the shape of the soft gap from the exponent α in $\sigma(T)$, we can also detect the same in $\chi(T)$. Namely, the change from a quadratic to a linear soft gap with increasing Q is observed as a sudden increase in $\chi_P(T > T^*)$, with a simultaneous decrease in $C(T > T^*)$, which occurs around $Q = 1.10$.

Our results suggest that PANI–DBSA is in its essence an Anderson–Mott insulator. Both disorder and Coulomb interactions govern its electromagnetic properties, and that holds at both $T < T^*$ and $T > T^*$. However, there are some quantitative and qualitative differences between these two T ranges even though both ranges contain conducting electrons as well as localised magnetic moments. According to modern approaches to MIT [217], T^* can be viewed as a temperature at which a Mott transition from an “insulator” to a “conductor” takes place[†]. At $T > T^*$, the Mott gap U is closed although a fraction of the sites still remain singly occupied with localised magnetic moments, but this is due to disorder. Because of the presence of a strong disorder, this Mott transition is (for any finite T) a smooth crossover, not a sharp first-order phase transition [217, 218]. Even though the Mott gap closes at T^* , the soft gap Δ_C remains open since the disorder remains present.

The relevance of U is also inferred [154] in the case of a PANI–HCl material produced from the same generic PANI as our PANI–DSBA, yet NNH is there seen in only one sample except for the as-synthesised one. Most of the crossovers in PANI–HCl are to $\alpha = 1/4$ (from either $\alpha = 1/2$ or $2/5$). The VRH $\alpha = 1/4$ regime also signifies a reduction of the depletion of the DOS for charge excitations, but this reduction is not as strong as in the case of the crossover to NNH. Therefore, in contrast to the situation in PANI–HCl where the crossover temperature T^* marks the transition within

[†]In spite of the delocalisation of a fraction of localised electrons at $T = T^*$, our PANI–DBSA is an insulator both below and above T^* since in PANI–DBSA $\sigma(T)$ increases with increasing T .

different VRH regimes, in PANI–DBSA, T^* marks a global process — transition to NNH where almost all sites in the vicinity of E_F are available for hopping transport of charge carriers. This reasoning is supported by the experimental fact that crossovers in PANI–DBSA are more pronounced than in PANI–HCl, both in $\sigma(T)$ and $\chi(T)$.

The interrelation between the spin dynamics and the electronic transport in PANI has already been observed [219], although not as directly as here. Other authors have also seen an increase in χ_P with a simultaneous decrease in C with increasing T [177, 205], but these findings were neither systematic nor could have been related to $\sigma(T)$ data.

We have established a strong correlation between the electronic-transport and thermodynamic properties of our material. Such an attainment is considered significant in studying fundamental properties of materials. Now we can set off for exploring the application potential of our PANI–DBSA.

Chapter 6

... towards application

The very selection of the complex material we have studied in the previous chapters, the properties of this material, and the procedures applied, together possesses an underlying layered simplicity in their complexity (see Section 1.1). This opens the gate towards application of PANI–DBSA. Let us list our layers of stacked simplicity which builds up a complexity. We believe that this stacked structure sets a firm basis for our PANI–DBSA polymer to become a real functional material.

1. The CP we deal with is PANI, a **common** CP. It is also the most studied CP, both in physics and chemistry. The main advantage of PANI in comparison with its immediate competitors in application (PPy, PT, PEDOT, PSS) are costs — PANI is the **cheapest** in the group. Perhaps this is the reason why PANI and PEDOT are the only CP's that have gained large-scale applications.
2. We have chosen DBSA as the dopant. There are other, similar surfactant acids which also enable solubility of PANI (CSA, DBNSA, AMPSA), yet DBSA is the **cheapest** among them. DBSA commercially comes not as a chemically pure substance but as a mixture of homologs and isomers. Nevertheless, we have chosen to dope PANI with a **commercially available** material and thus have avoided possible additional costs or/and unnecessary intricacies regarding possible application. DBSA is an ubiquitous material, it is one of the fractional distillates of oil.
3. Synthesis of PANI base is **facile**; it does not require a skilled chemist to perform one. Usually, stereoregular polymers are obtained in the presence of a Ziegler-Natta catalyst [220]. Stereoregularity of synthesised polymers is a necessity if one want to obtain isotactic, i.e., conjugated macromolecules. Since PANI does not have a doubly degenerate ground state, the equivalence of isotacticity in PANI is the alternation of fully-oxidised and fully-reduced monomers of the

PANI base, i.e., the requirement that PANI is in the emeraldine form. Anyhow, the rather complex **Ziegler-Natta catalysis is not required** in the synthesis we employed.

4. Synthesis of PANI base is such that it enables **versatility** of a consequent doping — the same generic PANI material can be used with any desired dopant.
5. We have invented an efficient and simple method of doping PANI with DBSA. The method **bypasses micellisation** of DBSA in aqueous solutions, and thus **enables a controllable and easy doping** with the complex dopant, resulting in highly-conducting CP.
6. The solubility of a CP is a prerequisite for their application. Our PANI–DBSA is **soluble in CHCl_3** , which is a common, uncostly solvent. By utilising this feature, we **avoid a more complex method (ROMP)** of achieving solubility of conjugated polymers, i.e., CP's.
7. We believe that by studying fundamental properties of our PANI–DBSA, we have achieved a **solid apprehension of its electromagnetic properties**. We also believe that such an apprehension is — as always on a route from fundamental to applied physics — if not a prerequisite, then at least an advantage in investigating the application potential of a material.

We reckon that all the above provides PANI–DBSA with a good building (stacking) potential.

The ever increasing demand for high-performance polymers has shifted the focus of recent studies in the area of polymer science from the development of novel homopolymers to the development of novel blends [221]. So, we employed the same route with our PANI–DBSA in an attempt to address the problem of its poor conductivity at low T . Namely, we blended PANI–DBSA with multiwall carbon nanotubes (MWCNT's). The choice of MWCNT's has emerged naturally for several reasons:

- PANI–DBSA is an organic conductor. It is natural to blend it with another organic conductor, and MWCNT's are such a material.
- PANI–DBSA is soluble in chloroform (CHCl_3). Since CHCl_3 is a common, uncostly solvent, the property that it dissolves PANI–DBSA enhances the application potential of this CP. Moreover, MWCNT's are also soluble in CHCl_3 . The existence of a common solvent for both components of the blend makes the blending procedure particularly facile.
- Blending PANI–DBSA with MWCNT's also enhances the application potential of the latter. In spite of their good conducting properties, MWCNT's are rarely used in bulk form, the reason being their peculiar mechanical properties that can be mitigated in blends.

The first polymer composites using carbon nanotubes as a filler were reported in 1994 [222]. Nowadays, the dominant approach in blending CP's with carbon nanotubes is via *in situ* polymerisation [223], which may also be accompanied by functionalisation of carbon nanotubes by polymer macromolecules [224], or carbon nanotubes can act as dopants themselves [225]. In both cases, *in situ* polymerisation has proven to distinctly enhance the conductivity of CP's. Yet, this method is neither simple nor controllable enough, therefore it is not very promising for large-scale applications. We believe that our simpler approach, which avoids *in situ* polymerisation, offers a better solution, as presented in Chapters 7 and 8.

Chapter 7

Blending PANI–DBSA with carbon nanotubes

§ 7.1 Treating PANI–DBSA with chloroform

PANI–DBSA is soluble in CHCl_3 [62]. Since CHCl_3 is a common solvent, the property that it dissolves PANI–DBSA enhances the application potential of this CP. However, treating PANI–DBSA with CHCl_3 might affect the properties of the pristine material. Therefore, the first step in blending PANI–DBSA with MWCNT's was to investigate how (if at all) the conductivity — which is the property of utmost interest — changes upon dissolving PANI–DBSA in CHCl_3 .

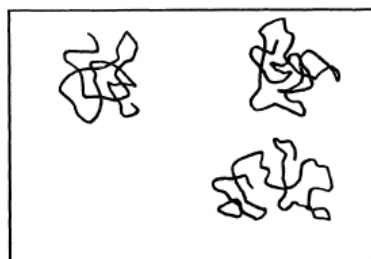


Figure 7.1: Schematic representation of polymer molecules in a dilute solution. (Reproduced from [226].)

For this purpose, we had chosen four previously synthesised PANI–DBSA powders of different doping levels ($Q = 3.39, 2.06, 1.10, 0.38$), and dissolved each of them in

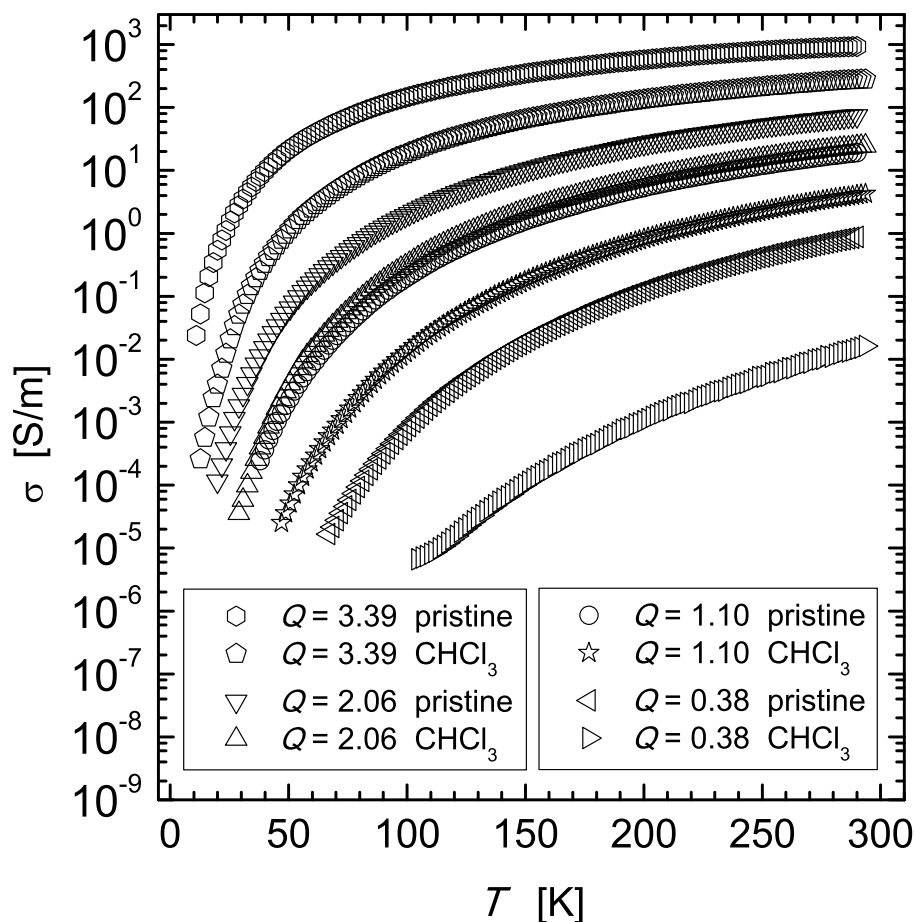


Figure 7.2: Comparison of $\sigma(T)$ for several chloroformed PANI–DBSA samples with the pristine samples of the same Q .

10 mL of CHCl_3 . Of course, these were more dispersions than real solutions, since the polymer macromolecules could not mix perfectly homogeneously with the solvent molecules [226, 45, 46]. In the case of a good solvent and a dilute solution, such mixtures form homogeneous suspensions of solid particles in a fluid [227], see Fig. 7.1. Nevertheless, it is customary to refer to dispersions of polymers as to solutions, so we will also use this terminology. Thus obtained solutions in beakers were mildly stirred and left covered by a filter paper. CHCl_3 eventually evaporated and the powders remained at the bottom of the beakers. We used these powders to produce pellets using the same procedure as that described in Subsection 4.8.2. Subsequently, $\sigma(T)$ of the pellets was measured using the same procedure as that described in Subsection 4.8.2.

Fig. 7.2 compares $\sigma(T)$ for several chloroformed PANI–DBSA samples with the pristine samples of the same Q . One can see that for each pair of PANI–DBSA samples, $\sigma_{\text{chloroformed}}(T) < \sigma_{\text{pristine}}(T)$, and that holds in the entire T range spanned. However, $\sigma_{\text{chloroformed}}$ and σ_{pristine} are not just scaled with a constant, their ratio is T dependent.

This ratio at RT is 3.3, 3.0, 4.8, and 88 for $Q = 3.39, 2.06, 1.10$, and 0.38, respectively. So, for the highly-conducting samples, σ_{RT} decreased by only about 3 times. This means that after a treatment in CHCl_3 , σ of PANI–DBSA decreases but still remains high enough for applicative purposes.

§ 7.2 Carbon nanotubes

Carbon nanotubes (CNT's) are allotropes of C with a cylindrical nanostructure. These cylindrical macromolecules have a hollow structure with the walls formed from graphene sheets. The sheets are rolled at specific discrete angles, and the combination of the rolling angle and radius determines the nanotube properties – for example, whether an individual nanotube shell is metallic or semiconducting. CNT's exceptional mechanical characteristics suppress Peierls instability, thus enabling a metallic behaviour. CNT's are subdivided into singlewall carbon nanotubes (SWCNT's) and multiwall carbon nanotubes (MWCNT's). MWCNT's consist of multiple coaxial rolled sheets of graphene (see Fig 7.3). Individual CNT's naturally appear as ropes held together by van der Waals forces [228].

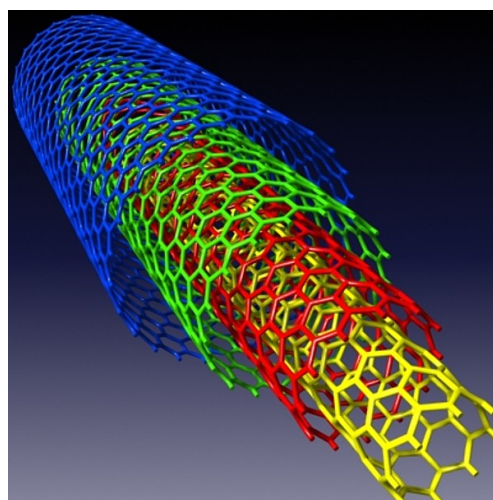


Figure 7.3: Schematic view of a MWCNT consisting of four concentric tubes.

CNT's have remarkable properties which are valuable for nanotechnology, electronics, optics and other fields of materials science and technology. In particular, owing to their extraordinary mechanical, thermal and electrical properties, CNT's find applications as additives to various structural and functional materials [229–231]. CNT's can also be made as yarn [232]. CNT yarn is probably the only feasible way of using pure CNT's in bulk form. Otherwise, CNT's are added to other materials — most

notably polymers — in a fraction of a few percent, usually in order to enhance mechanical strength of materials, or to increase their σ .

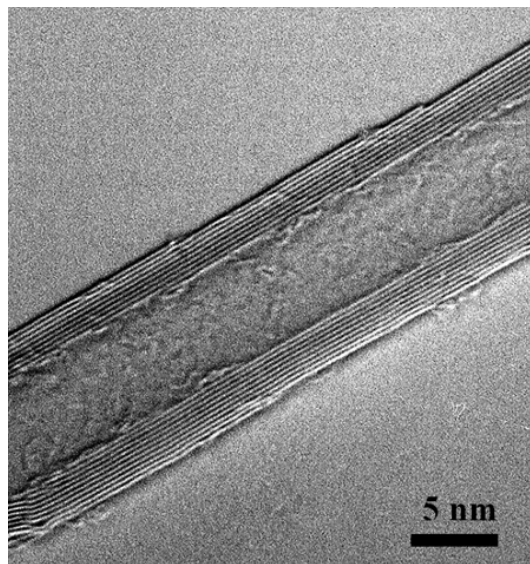


Figure 7.4: TEM image of Graphistrength[®] C100 MWCNT's. (Reproduced from [233].)

We used Graphistrength[®] C100 (Arkema) MWCNT's (see Fig 7.4) in our blending with PANI–DBSA. They have a thickness of 5-15 graphene layers (outer diameter: 10-15 nm), and length of 0.1-10 μm . Their $\sigma \approx 10^5$ S/m [234] is by two to three orders of magnitude higher than σ_{RT} of highly-doped PANI–DBSA samples. We have chosen these particular MWCNT's because they represent a reasonably pure and reasonably priced, commercially available product of a renowned CNT's manufacturer.

§ 7.3 Fabrication of blends and measuring their electrical conductivity

7.3.1 Initial steps

We produced blends of PANI–DBSA and MWCNT's by facilitating the fact that both components of the blend are soluble in CHCl_3 . These blends will be hereafter abbreviated as **PDMC (PANI-DBSA-MWCNT)**. The procedure was as follows. Both PANI–DBSA and MWCNT's are powders. We put both powders into a beaker and added 10 mL of CHCl_3 . The beaker was capped and put in an ultrasonic bath for a 5 h treatment. Afterwards, the beaker was uncapped and covered with a filter paper,

so CHCl_3 evaporated leaving the PDMC powder at the bottom of the beaker. This powder was then pressed into pellets using the same procedure as that described in Subsection 4.8.2.

Firstly, we wanted to find out what is the maximum fraction of MWCNT's that could be achieved in a PDMC. It turned out that

$$w_{\max} = 40 \% , \quad (7.1)$$

where w represents the mass fraction of MWCNT's in PDMC. The above holds regardless of the particular doping level Q of the PANI-DBSA material used in blending. A fraction higher than 40% could not have been achieved due to mechanical properties of MWCNT's. Namely, when we put more MWCNT's, the pressed pellets of PDMC would have disintegrated. It is known that pressing MWCNT's is like pressing steel nails, and this is the reason why MWCNT's are seldom used in bulk form. Hence the achieved mass fraction of MWCNT's of up to 40% is remarkable. To our knowledge, such a high fraction of MWCNT's has not been even closely achieved in

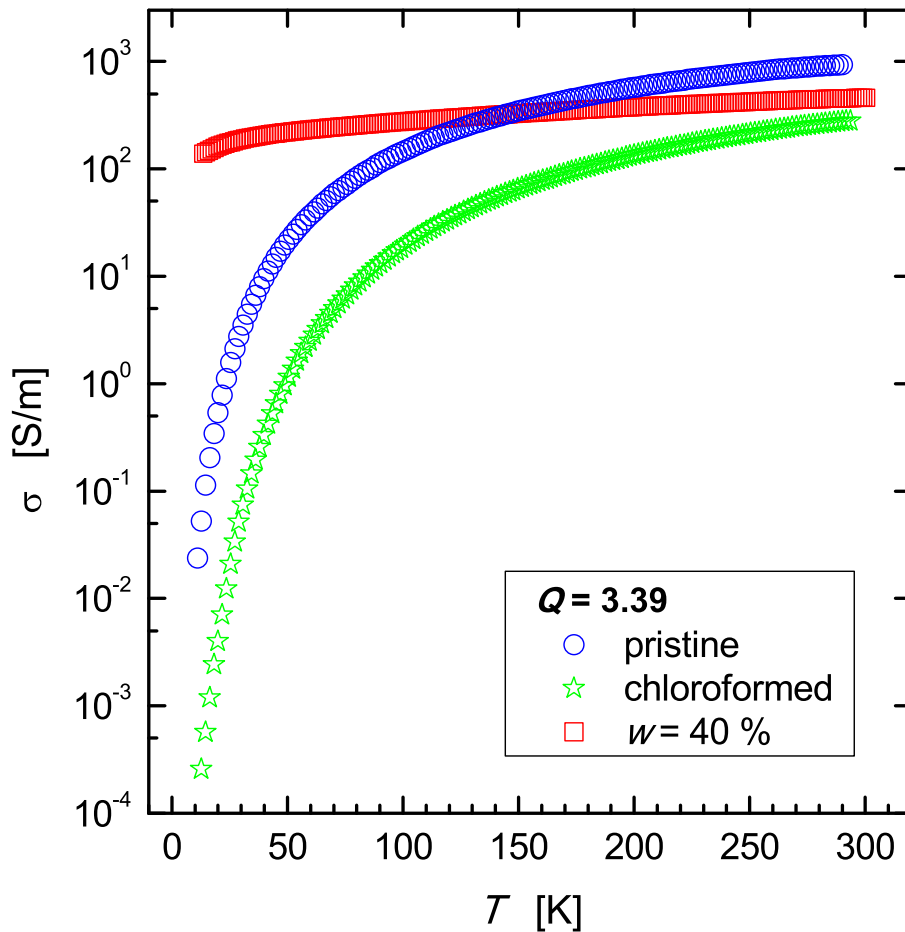


Figure 7.5: σ vs T for three different samples made from the $Q = 3.39$ PANI-DBSA material.

blends with CP's.

There is not much sense in using low-conducting PANI–DBSA for blending with MWCNT's since the goal has been to produce highly conducting composites. Therefore we started with the best conducting of all our PANI–DBSA materials, i.e., with $Q = 3.39$. Fig. 7.5 shows $\sigma(T)$ for three different samples made using the $Q = 3.39$ PANI–DBSA material:

- pristine sample - all the pristine samples that appear in this chapter have already been presented in Section 4.8,
- chloroformed sample - the one made only from PANI–DBSA material but treated in CHCl_3 as described in Section 7.1
- $w = 40\%$ blend sample, abbreviated as PD3.39MC40

One can see in Fig. 7.5 that σ of PD3.39MC40, in comparison with the non-blended samples, has almost lost its T dependence. However,

$$\sigma_{\text{RT}}(w = 40\%) < \sigma_{\text{RT}}(\text{pristine}) \quad . \quad (7.2)$$

Since $Q = 3.39$ is a two-phase material, there can be two explanations for this property. The first is that PD3.39MC40 is a mixture of two materials with similar σ_{RT} and that σ_{RT} of the blend sample can be either higher or lower than that of the pristine sample, depending on the structural properties over which we have no control. This argument certainly holds, but it does not take into account the role of extra DBSA (not bound to the PANI backbone by protonation, see Section 3.3) in the presence of MWCNT's. It has been shown in Section 3.3 that this extra DBSA most probably enhances 3D coupling and in this way enhances σ in PANI–DBSA without MWCNT's. However, by adding MWCNT's, a conducting material, to $Q = 3.39$ PANI–DBSA reduces σ_{RT} , which suggests that the enhancement of 3D coupling by the extra DBSA is no longer effective. In this picture, the extra DBSA in PD3.39MC40 acts as an insulator in the matrix of PANI–DBSA and MWCNT's.

In order to examine the feasibility of the above surmise we measured $\sigma(T)$ of PD2.06MC40 blend made from the best conducting single-phase (to be fully precise, almost single-phase) PANI–DBSA ($Q = 2.06$). Fig. 7.6 compares two $w = 40\%$ blends, one made from the $Q = 2.06$ PANI–DBSA material and the other from the $Q = 3.39$ one. It is discernible that

$$\sigma_{Q=3.39}^{w=40\%}(T) < \sigma_{Q=2.06}^{w=40\%}(T) \quad , \quad (7.3)$$

whilst

$$\sigma_{Q=3.39}^{w=0}(T) > \sigma_{Q=2.06}^{w=0}(T) \quad , \quad (7.4)$$

in the entire T range of the measurements. In order to avoid problems related to the role of extra DBSA in the presence of MWCNT's, we have chosen the best conducting single-phased PANI–DBSA material, $Q = 2.06$, to study the blends systematically.

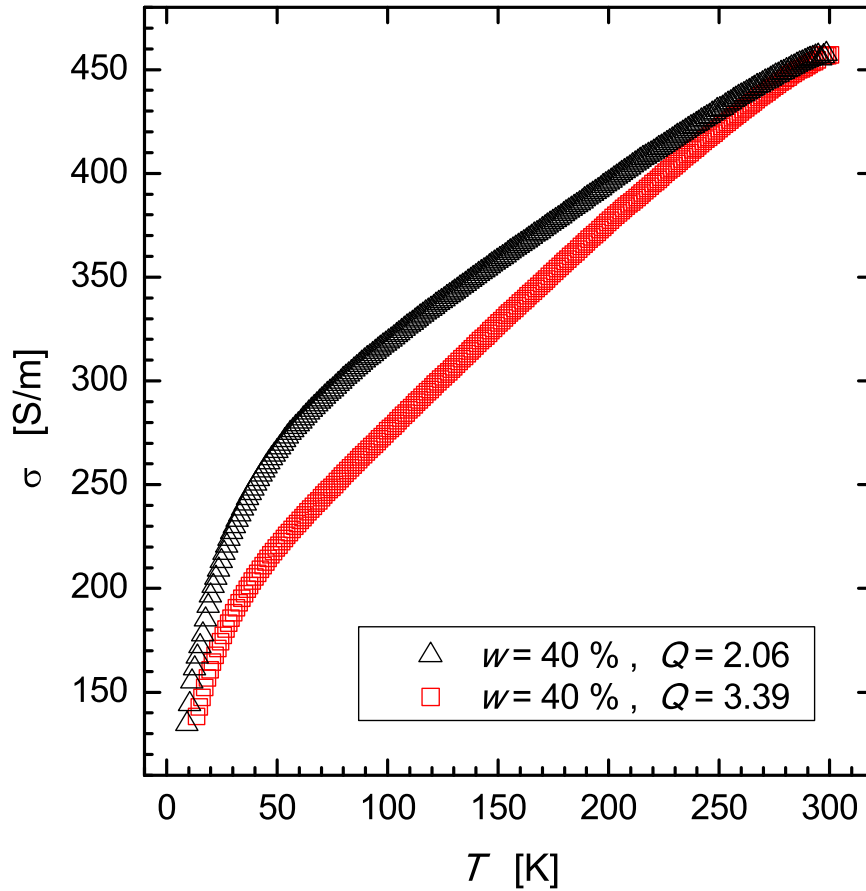


Figure 7.6: σ vs T for $w = 40\%$ blends made with $Q = 2.06$ and $Q = 3.39$ PANI–DBSA materials.

7.3.2 Systematic study of the blends

We made a series of PDMC blends with the best conducting single-phase PANI–DBSA material ($Q = 2.06$): PD2.06MC40, PD2.06MC20, PD2.06MC10, PD2.06MC6, PD2.06MC4.5, and PD2.06MC1. Fig. 7.7 shows $\sigma(T)$ for this series of blends together with the $w = 0$ samples (the pristine and the chloroformed ones). For all the blends, the T dependence gradually diminishes as w increases. For example, σ of the PD2.06MC40 sample decreases by only 2.25 times from RT to 20 K, whereas this decrease for the pristine PANI–DBSA with $Q = 2.06$ is by a factor of 10^6 . Thus, our blends simultaneously offer a solution to the problem of application of MWCNT's in bulk form, as well as to that of poor conductivity of PANI–DBSA at low T .

One can see from Fig. 7.7 that several PDMC samples have σ_{RT} lower than that of the pristine sample. As outlined before, the exact value of σ_{RT} depends on the morphology of a sample; i.e., on the arrangement of MWCNT molecules among PANI–DBSA molecules. Moreover, the pristine sample did not undergo treatment in an ultrasonic

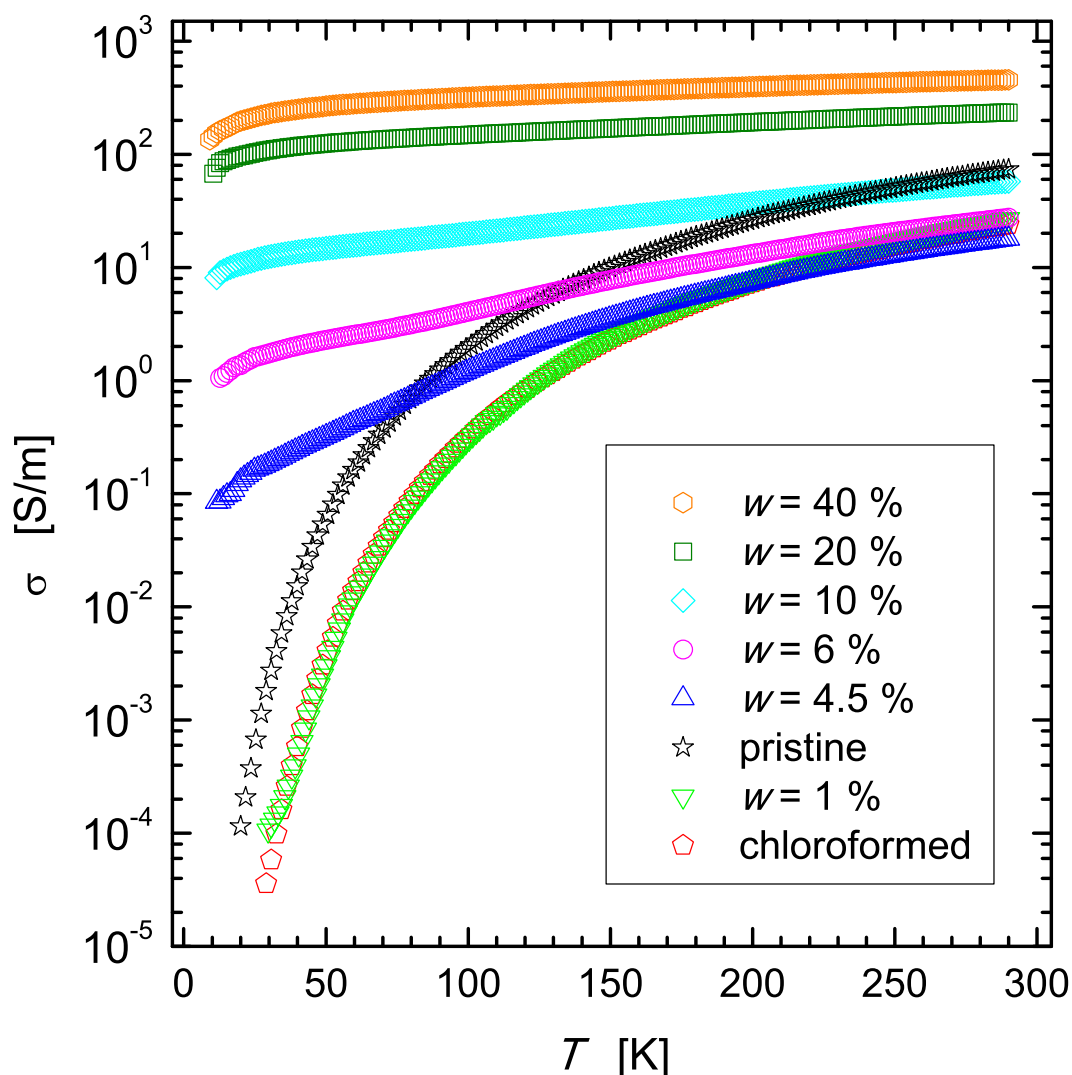


Figure 7.7: σ vs T for PDPMC blends made from the $Q = 2.06$ PANI–DBSA material, in comparison with the pristine and chloroformed samples ($w = 0$).

bath, in contrast to PDPMC samples. During the ultrasonication, a rearrangement of the morphological structure probably occurs, which is possibly one of the reasons for the decrease of σ of PANI–DBSA after ultrasonication (see Section 7.1). As shown in Chapter 4, disorder level plays a crucial role in σ , and in CP's it arises from a combination of molecular-scale disorder [134] and structural inhomogeneities at mesoscopic scale lengths [155], these properties being dependent on the treatment of a sample.

Furthermore, the $\sigma(T)$ curves of the PD2.06MC1 sample and the chloroformed sample nearly coincide, which suggests that addition of 1 % of MWCNT's is not enough for a substantial change to occur in chloroformed PANI–DBSA material.

The effects of the blending are best seen when we normalise the curves on Fig. 7.7 to $\sigma_{RT} = \sigma_{T=290\text{ K}}$, which eliminates the vertical shifts due to differences in the disorder level. These normalised curves are displayed in Fig. 7.8. One can see that the curves in Fig. 7.8 can be grouped into PANI-like type, MWCNT-like type, and intermediate ones, depending on the amount of the added MWCNT's, w . The curves of the pristine, the chloroformed, the $w = 1\%$, and the $w = 4.5\%$ sample are convex (PANI-like). The curves for the $w = 20\%$ and $w = 40\%$ samples are less steep (MWCNT-like). The curves for $w = 6\%$ and $w = 10\%$ have well defined inflexion points, and are in between the PANI-like and the MWCNT-like curves.

Somewhat similar results to ours (regarding the MWCNT's dominance in σ at low T , and $w_{\max} = 25\%$) have been reported [235], although they pertain to very thin samples produced from much more complicated *in situ* process.

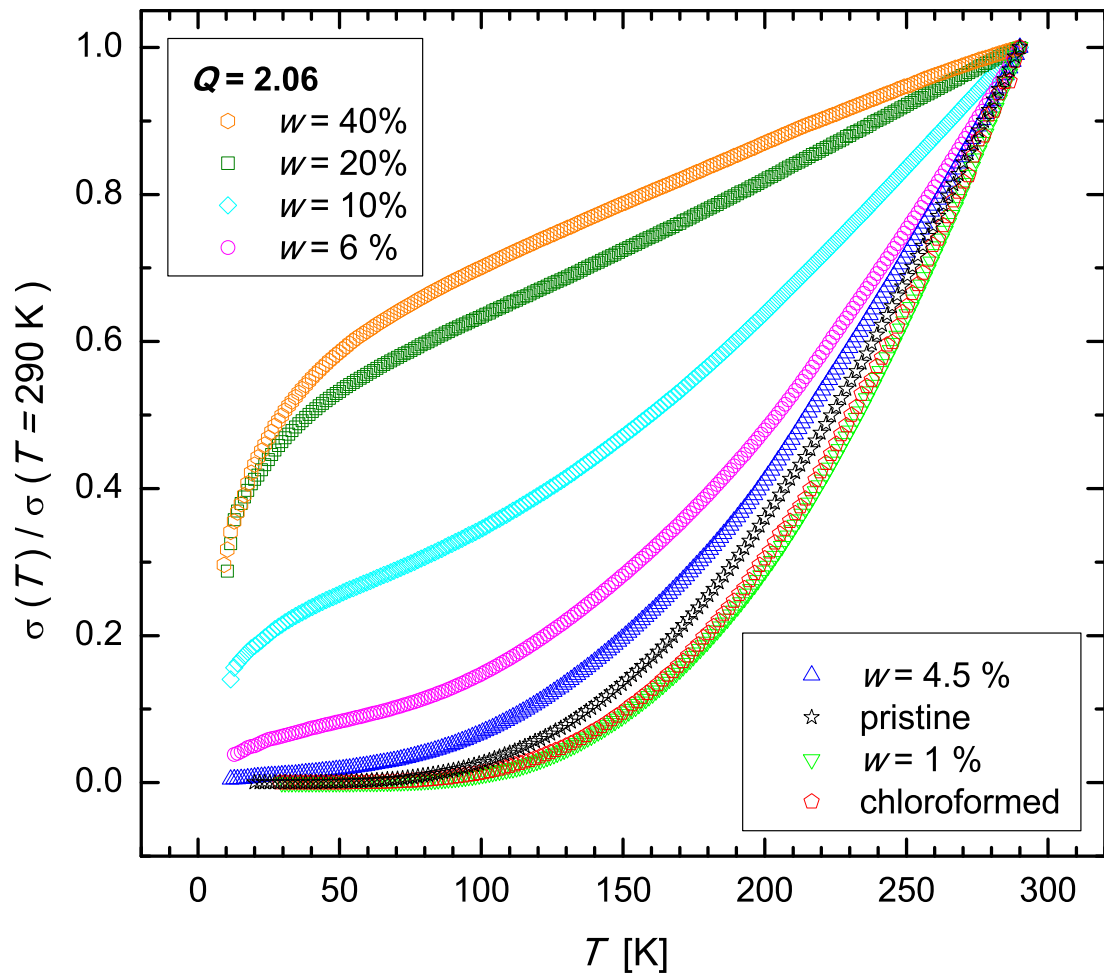


Figure 7.8: Normalised σ vs T for PDPMC blends made from the $Q = 2.06$ PANI-DBSA material, in comparison with the pristine and chloroformed samples ($w = 0$).

§ 7.4 Concluding remarks towards application

Blending of our PANI–DBSA with MWCNT's has proved successful. Utilising the fact that both components are soluble in CHCl_3 , we managed to produce a composite material with properties, altered in a desirable direction:

- Already good conducting properties of PANI–DBSA are remarkably enhanced by blending. Addition of MWCNT's mitigates the large decrease of σ with decreasing T , a hallmark of unblended PANI–DBSA. The mitigation can, for blends with a large fraction of MWCNT's, result in an almost complete loss of the T dependence of σ . This finding offers a solution to the problem of poor conductivity of PANI–DBSA at low T .
- In spite of their good conducting properties, MWCNT's rarely find use in bulk form, the reason being their peculiar mechanical properties. And even when they do appear in bulk structures, this is in composites with low fractions of MWCNT's. With our blends, composites with large fractions of MWCNT's (of up to 40 %) can be obtained. This finding offers a solution to the problem of application of MWCNT's in bulk form. Such applications would provide more comprehensive utilisation of good conducting properties, along with other physical properties, of MWCNT's.

Furthermore, these new, appealing properties have been achieved

- by simple and uncostly procedures,
- with complex yet uncostly materials.

Therefore, based on the concept of layered simplicity in complexity (see Section 1.1) we believe that our findings and their context open the gate towards application for both PDMC blends and unblended PANI–DBSA. We ourselves make the first step in that direction by setting off for examining the possibility of the use of our materials in planar structures, which are of particular interest for technology. The results are presented in Chapter 8.

Chapter 8

Outlook

We made two film samples: a film from the $Q = 2.06$ PANI–DBSA material, and a film from the PD2.06MC40 blend material. Both films were deposited onto an FR4 substrate (see Fig. 8.1) by a same simple method. A piece of the substrate board was put in the CHCl_3 solution of the material and left for the CHCl_3 to evaporate. By this method we obtained samples of homogeneous thickness and with no cracks. Thickness of the films was determined by a high-resolution optical microscopy.

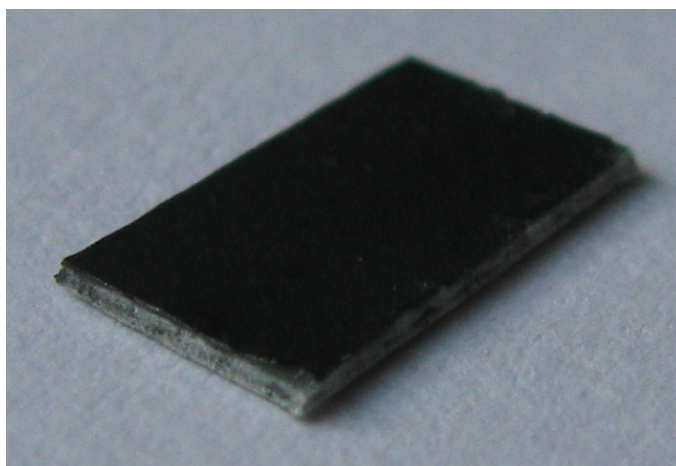


Figure 8.1: Film of the PD2.06MC40 blend on FR4 substrate board. The board is $350 \mu\text{m}$ thick, and the film thickness is $9 \mu\text{m}$.

FR4 is the most commonly used printed-circuit-board material in electronics industry, and it was selected because of its low cost, ease of processing, and a possible option

of future mounting of electronic components directly on to the substrate [236]. In addition, FR4 is chemically resistant to CHCl_3 .

Fig. 8.2 depicts $I - V$ characteristics of the films at RT, which exhibit linearity. σ of the films is as follows: $\sigma_{\text{RT}}(\text{PANI-DBSA}) = 20.43 \text{ S/m}$, and $\sigma_{\text{RT}}(\text{blend}) = 792.66 \text{ S/m}$. The former value represents a decrease of 1.17 times ($23.96 \text{ S/m} \rightarrow 20.43 \text{ S/m}$) in comparison with the same material in bulk form, whereas the latter value shows an increase of 1.74 times ($454.69 \text{ S/m} \rightarrow 792.66 \text{ S/m}$) times in comparison with the same material in bulk form. Hence, the materials do not undergo significant changes in their σ upon deposition onto the substrate.

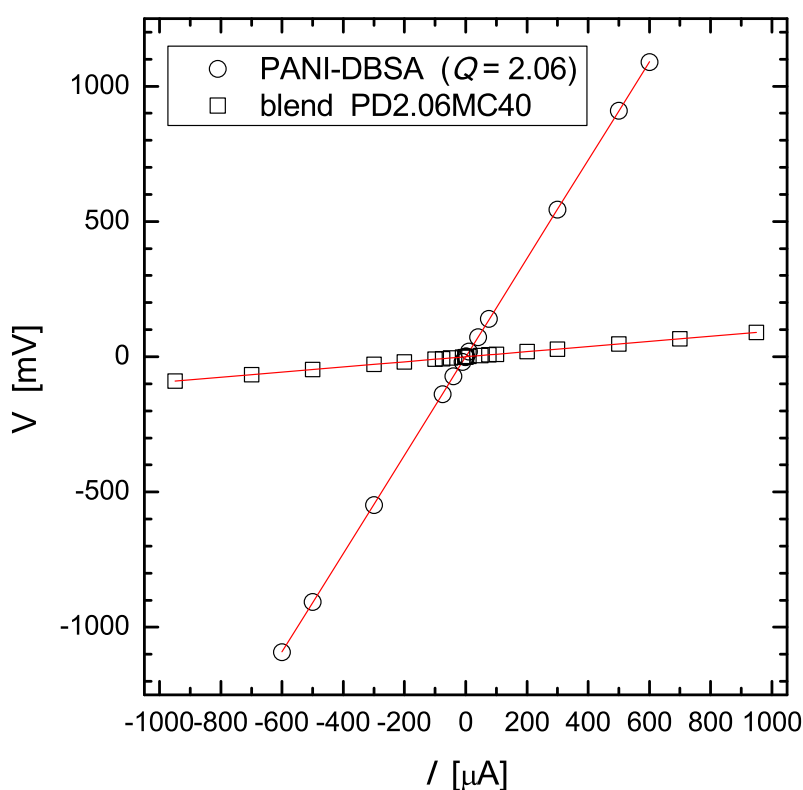


Figure 8.2: Measured $I - V$ characteristics (open symbols) of our films at RT. Straight lines are linear fits.

These results could be of interest for the production of supercapacitors, where an appropriate blend of carbon nanotubes and CP's has been sought for the electrodes [237]. CNT's and CP's have complementary properties. On their own, thin CP's films provide a high capacitance and reasonable response times, but they lack mechanical and chemical stability, and have low σ in the reduced or neutral states. When the thickness of the polymer film increases, charge transport in the polymer slows down. These drawbacks of CP's are addressed by the addition of CNT's. Their very high mechanical resilience, high σ , and large surface areas, are particularly relevant to their application in supercapacitors [238]. It has recently been found that the very

combination of PANI and MWCNT's combine in a flexible and efficient supercapacitor [239].

Since applications of planar structures are numerous, the described prototypes of the films of PANI-DBSA and its blends with MWCNT's may serve as a starting point in the design of other devices.

Chapter 9

Conclusion

We have carried out a comparative experimental study of the dc electrical conductivity σ and magnetic susceptibility χ of own-made polyaniline (PANI) pellets doped with dodecylbenzenesulphonic acid (DBSA), a long molecule with surfactant properties. For all samples, we find that σ at low temperatures (T) is governed by the variable-range hopping (VRH) in a homogeneously disordered three-dimensional (3D) system of coupled one-dimensional (1D) chains.

Depending on the doping and the corresponding disorder level, the VRH exponents are either $1/2$, $2/5$, or $1/4$. At higher T , in all samples, we find an exponent 1 that signifies nearest-neighbour hopping. All these exponents are predicted in a model by Fogler, Teber, and Shklovskii for the charge transport in quasi-1D Anderson-Mott insulators, and conditions for their appearance depend on disorder and T . We identified the presence of a soft (Coulomb) gap in our samples, which signifies a long-range Coulomb interaction.

Change from one exponent into another in $\sigma(T)$ appears at a crossover temperature T^* where there are also noticeable features in $\chi(T)$. This coupling of charge and spin is discussed in the spirit of $k_B T^*$ being the thermal energy which causes an enhancement of the density of delocalised (Pauli) spins at the expense of localised (Curie) spins as T rises above T^* . Utilising the observed correlation between spin dynamics and electronic transport, we estimate the energy scales in the electronic structure of PANI-DBSA.

Utilising a property that both PANI-DBSA and multiwall carbon nanotubes (MWCNT's) are soluble in chloroform, we have produced bulk blends of these two materials, the achieved mass fraction of MWCNT's being up to 40 %. This is as remarkable as the accompanying effective loss of the temperature dependence of σ :

it decreases by only 3 times from room temperature to 10 K, whereas this decrease for pure PANI–DBSA is by a factor of 10^6 . Thus, our blends simultaneously offer a solution to the problem of applications of MWCNT's in bulk form, as well as to that of poor conductivity of PANI–DBSA at low T . It is also possible to make thin films, both of PANI–DBSA and of the blends, on a commercial plastic substrate (FR4).

Appendices

Appendix A

Calculation of Coulomb gap from crossovers

In literature, expressions for various hopping laws usually just give proper exponents of the T -dependence without paying attention to actual factors of proportionality. Moreover, even when given, factors of proportionality from different sources are not intercomparable because different authors use different conventions in deriving a specific hopping law. However, these factors of proportionality are important if one wants to calculate values of the Coulomb gap, Δ_C , in real materials.

For that purpose, we have derived full expressions for hopping laws with an arbitrary* discrete exponent α . These expressions have a universal form (i.e., they do not depend on specific value of α), and are thus intercomparable. Consequently, we are able to calculate Δ_C in our PANI–DBSA from crossovers between two hopping laws.

Our derivation of the universal form of hopping laws follows the standard procedure enunciated by Mott (see Subsection 4.6.3), but different shapes of the DOSCE in the vicinity of E_F (constant DOSCE, linear soft gap, quadratic soft gap) have been accounted for. Our procedure is simple, but as such serves our purpose. We utilise the isotropic approximation of the Fermi sea, $\frac{4\pi}{3}R^3N_F = 1$, since our PANI–DBSA is a disordered system of polymer chains, so that all directions in space are equivalent. Our calculation addresses the following expressions for σ :

$$\sigma(T) = \eta_\alpha \exp \left[- \left(\frac{T_\alpha}{T} \right)^\alpha \right] , \quad (\text{A.1})$$

where T_α is related to the activation energy ε through

$$\varepsilon(T) = \alpha k_B T \left(\frac{T_\alpha}{T} \right)^\alpha . \quad (\text{A.2})$$

* α is arbitrary in the sense that it can assume any of the values prescribed by the shape of the DOSCE.

Crossover between different hopping transport regimes occurs at $T = T^*$. Δ_C can be calculated from a crossover utilising the relation

$$\Delta_C = \varepsilon^* = \varepsilon(T = T^*) \quad . \quad (\text{A.3})$$

Substituting for T^* , we obtain the relation for Δ_C in terms of exponents α and β (which correspond to hopping regimes for $T < T^*$ and $T > T^*$):

$$\Delta_C = k_B \left(\frac{\beta^{1-\alpha}}{\alpha^{1-\beta}} \right)^{\frac{1}{\beta-\alpha}} \left[\frac{\left(T_\beta^\beta \right)^{1-\alpha}}{\left(T_\alpha^\alpha \right)^{1-\beta}} \right]^{\frac{1}{\beta-\alpha}} \quad . \quad (\text{A.4})$$

In PANI–DBSA, we have identified the following discrete values of α : $1/2$, $2/5$, $1/4$ and 1 . Utilising Eq. (A.4), we list the specific expressions for Δ_C for all potential crossovers between the regimes characterised by this set of exponents:

$$\Delta_C \left(\frac{2}{5} \leftrightarrow \frac{1}{4} \right) = 2.621 \times k_B \frac{T_{2/5}^2}{T_{1/4}} \quad , \quad (\text{A.5})$$

$$\Delta_C \left(\frac{1}{2} \leftrightarrow \frac{1}{4} \right) = 2k_B \frac{T_{1/2}^{3/2}}{T_{1/4}^{1/2}} \quad , \quad (\text{A.6})$$

$$\Delta_C \left(\frac{1}{2} \leftrightarrow \frac{2}{5} \right) = 1.526 \times k_B \frac{T_{1/2}^3}{T_{2/5}^2} \quad , \quad (\text{A.7})$$

$$\Delta_C \left(\frac{1}{4} \leftrightarrow 1 \right) = k_B T_1 \quad , \quad (\text{A.8})$$

$$\Delta_C \left(\frac{2}{5} \leftrightarrow 1 \right) = k_B T_1 \quad , \quad (\text{A.9})$$

$$\Delta_C \left(\frac{1}{2} \leftrightarrow 1 \right) = k_B T_1 \quad . \quad (\text{A.10})$$

It is important to note that, although Δ_C can be mathematically calculated from the crossover $\left(\frac{1}{4} \leftrightarrow 1 \right)$, it does not have a physical meaning. Namely, already for $\alpha = 1/4$ the DOSCE has reached the constant value of the DOS, N_0 , the one that is assumed in the Mott model. Therefore, $\varepsilon(T) > \Delta_C$ in the $\alpha = 1/4$ regime, as it is in the $\alpha = 1$ regime, as well.

Prošireni sažetak

Polimeri

Polimer je tvar građena od polimernih makromolekula. Polimerna makromolekula je slijed gradivnih jedinica (monomera) uzajamno povezanih kovalentnom vezom. U golemoj većini slučajeva to su organske makromolekule. Polimerne makromolekule koje se sastoje od samo jedne vrste monomera grade homopolimer a one koje se sastoje od više vrsta monomera grade kopolimer. Budući da se kopolimer sastoji od barem dvije vrste gradivnih (a ne strukturnih) jedinica, kopolimere možemo klasificirati prema razmješčaju komonomera u kopolimernoj makromolekuli: razlikujemo periodičke, nasumične, blok-, i nacijspljene (engl. graft) kopolimere. Mer je gradivna jedinica kopolimera koja se sastoji od više vrsta monomera, uvijek u istom međusobnom rasporedu. U slučaju kopolimera s alternirajućim monomerima, mer, a ne monomer, predstavlja kristalnu bazu koja se pridijeljuje svakom čvorištu 1D Bravaisove rešetke polimerne makromolekule. Poznati primjer alternirajućeg kopolimera je poli(etilenglikol-tereftalat) (PET).

Bifunkcionalni monomeri daju lančaste makromolekule (polimerne lance) i poslijedično lančaste polimere. Svaki monomer u polimernom lancu, osim dviju terminalnih jedinica, vezan je s oba kraja na susjednu jedinicu. Ukoliko pak prekursorske molekule u reakciji polimerizacije mogu reagirati s tri ili više susjednih molekula, tada nastaju mrežaste makromolekule, a rjeđe i posve trodimenzionalne strukture. Takvi razgranati polimeri sadrže, uz bifunkcionalne, i neke polifunkcionalne monomerne jedinice (monomerne jedinice vezane kovalentnom vezom na više od dvije susjedne monomerne jedinice). Najjednostavniji razgranati polimer je polietilen niske gustoće, LDPE (engl. low-density polyethylene). On nastaje polimerizacijom samo jedne vrste molekula - etena, pa nije kopolimer, iako se očito sastoji od barem dvije vrste monomera, pri čemu svi bifunkcionalni monomeri pripadaju jednoj vrsti, a svi trifunkcionalni drugoj.

Glavna fizikalna svojstva polimera ovise o prirodi i rasporedu kovalentno vezanih monomernih jedinica. No, osim tih jakih (primarne interakcije) intramolekulskih interakcija monomera, za razumijevanje svojstava polimera treba uzeti u obzir i slabe (sekundarne interakcije) intermolekulske interakcije. U te sile između pojedinih polimernih makromolekula spadaju: van der Waalove sile između fluktuirajućih i

samoinducirajućih dipola, te elektrostatske multipolarne sile. Među elektrostatskim multipolarnim silama, dominira, naravno, interakcija permanetnih dipola, a među njima je najjača vodikova veza budući da je to jedini slučaj u kojem nema zasjenjenja naboja protona od strane pripadnih dubokoležećih elektrona elektropozitivnijeg atoma dipolne molekule. Energija kovalentne veze je reda veličine 10 eV po vezi. Vodikove veze su okvirno za red veličine slabije od kovalentne, a van der Waalsove veze za dva reda veličine slabije. Valja napomenuti da se u kemičarskoj literaturi energije veza izražavaju kao molarne entalpije pri standardnim uvjetima, pa su odgo-varajuće vrijednosti nešto niže. Na primjer, prosječna energija jednostruke veze C - C u poliatomnim molekulama iznosi $H_m^\ominus = 347 \text{ kJ/mol} = 3.6 \text{ eV}$.

Polimere, kao objekte promatranja fizike kondenzirane tvari, po stupnju uređenosti smještavamo između amorfni i mezomorfni materijala. Sekundarne interakcije imaju najvažniju ulogu u međusobnom rasporedu polimernih makromolekula u nekom polimernom materijalu. U polimeru uvijek postoji neka raspodjela Staudingero-vog indeksa n makromolekula (Staudingerov indeks je broj merova u makromolekuli). Povrh te razlike u molarnoj masi pojedinih makromolekula, postoji i razlika u strukturi makromolekula. Stoga polimeri ne mogu potpuno kristalizirati, nego samo mogu sadržavati, uz amorfna područja, i mnoga kristalinična područja - kristalite[†]. Stupanj kristalizacije znatno utječe na fizikalna svojstva polimera. Vodikove veze među nukleotidnim heterocikličkim bazama koje povezuju dvije uzvojnice u DNA ili RNA izvrstan su primjer utjecaja sekundarnih interakcija na uređenje i strukturu (ko)polimera. Valja još dodati da i intermolekulske interakcije mogu biti primarne. Tada govorimo o poprečnom povezivanju (engl. crosslinking) ili umrežavanju lančastih polimera. Kovalentne veze između pojedinih polimernih lanaca mogu nastati već pri prvotnoj polimerizaciji ili naknadno (bilo uvođenjem nekih malih molekula koje potiču umrežavanje i sudjeluju u njemu, bilo aktivacijom postojećih funkcionalnih skupina na polimernim lancima).

Polimeri se dijele na industrijske (sintetske) i prirodne. Polimerna makromolekula sintetskog lančastog polimera ima tipično $10^4 - 10^6$ monomera. Molekule veće molarne mase često nije potrebno (premda je moguće) sintetizirati, jer pri 10^6 monomernih jedinica ovisnost mehaničkih svojstava polimera o molarnoj masi doživljava saturaciju. Poznato je da su u ogromnoj većini slučajeva polimeri tvari niske gustoće, velikog omjera čvrstoće i mase, niske cijene proizvodnje, visoke stabilnosti (pri standardnim uvjetima), tvari koje se lako oblikuju, ne reflektiraju svjetlost, ne vode toplinu ni električnu struju. Zbog performansi koje zadovoljavaju veliki broj tehnoloških potreba, polimeri se konstantno nalaze u fokusu interesa znanosti o materijalima i njene potrage za poboljšanjima.

[†]Valja reći da je već 1957. dobiven prvi monokristal nekog polimera. A. Keller, P.H. Till i E.W. Fischer su međusobno neovisno sintetizirali monokristal polietena (PE), a uskoro je postojanje polimernog monokristala dobilo i uspješno teorijsko objašnjenje u modelu presavinutih makromolekula. No, monokristali polimera dobivaju se posebnim postupcima, te su kao takvi od ograničenog interesa u primijenjenoj fizici. To je fiziku polimera uvelike usmjerilo ka *ad hoc* istraživanjima s realnim polimernim materijalima.

Uspješno anticipiranje svojstava novih materijala pretpostavlja dobro razumijevanje strukture i fizikalnih procesa koji dominiraju u već postojećim materijalima. U slučaju polimera, to dugo vremena nije bio slučaj. Za razliku od razvijene kemijske tehnologije i industrije polimera, fizika polimera bila je do šezdesetih godina 20. stoljeća slabo razvijena. Zbog njihove kompleksnosti, smatralo se da je polimere gotovo nemoguće uspješno opisivati fizikalnim modelima. Začetnici moderne fizike polimera bili su H. Staudinger, P. Debye, W. Kuhn i H.A. Kramers. Najznačajniji doprinos u ranoj razvoju fizike polimera pružio je P.J. Flory razvojem eksperimentalnih i teorijskih postupaka za ispitivanje svojstava makromolekula. Novu fazu u razvoju fizike polimera omogućile su eksperimentalne metode: raspršenje neutrona i konstrukcije prvih lasera 1960. godine i 1962. godine. Sljedeći važan korak napravio je S.F. Edwards primijenivši sofisticirani matematički aparat fizike elementarnih čestica na izučavanje polimera. Preciznije, Edwards je pokazao postojanje korespondencije između konformacija polimernog lanca i trajektorija nerelativističkih čestica: statističkoj težini polimernog lanca odgovara propagator elementarne čestice. U nazočnosti vanjskog potencijala, oba fizikalna sustava opisana su istom Schrödingеровom jednačinom. Ovaj rezultat bio je ključan za kasniji razvoj statističke fizike polimera. No, najvažniji korak tek je trebao uslijediti. Koristeći klasičnu fiziku kao bazu, te uz uporabu najnovijih eksperimentalnih rezultata i teorijskih postignuća, Pierre-Gilles de Gennes preoblikovao je i dalje razvio fiziku polimera. Njegov najznačajniji doprinos je u razumijevanju dinamike polimernih lanaca te pravilnosti u njihovom geometrijskom rasporedu.

Poznato je da vrlo blago kemijsko tretiranje ili mala promjena fizikalnih parametara (npr. temperature) može dramatično promijeniti svojstva polimera. Ta fascinantna osobina tipična je za svu meku tvar (engl. soft matter), pod čime podrazumijevamo polimere, surfaktante, tekuće kristale i koloidna zrnca. Takve drastične promjene svojstava i prije su uočene u fizici, na znatno jednostavnijim sustavima. Poznati su fazni prijelazi iz normalnog u supravodljivo stanje, iz tekućeg u kruto stanje, iz neuređenog u uređeno stanje sustava magnetskih dipola, i slično. Uočavanje te analogije, te razrada modela baziranih na zakonima skaliranja koji uspješno opisuju prijelaze između reda i nereda za tako kompleksne (i naizgled posve neuređene) sustave koje tvori meka tvar priskrbila je de Gennesu Nobelovu nagradu iz fizike 1991. godine. Njegov doprinos je direktno, i na različite načine indirektno, otvorio vrata teorijskim i eksperimentalnim istraživanjima u fizici polimera, koja su uvijek preduvjet postavljanju čvršćih temelja za njihovu tehnološku primjenu.

Vodljivi polimeri

Neki polimeri nakon određenih modifikacija mogu postati vodljivi. Vodljivi polimeri pokazuju električna i optička svojstva metala ili poluvodiča, a istovremeno zadržavaju dobre mehaničke karakteristike, laganu oblikovnost i nisku cijenu proizvodnje klasičnih polimera. Vodljivost polimera, kao i mogućnost njihovog dopiranja u cijelom rasponu vodljivosti od izolatora do metala, otkrili su 1976. i objavili 1977. kemičari Alan G. MacDiarmid i Hideki Shirakawa te fizičar Alan J. Heeger. Od tada su vodljivi polimeri stali predmet istraživanja čiste i primijenjene fizike i kemije. Osim toga, već postoje mnoge važne praktične primjene vodljivih polimera. Za otkriće i razvoj vodljivih polimera gore navedeni znanstvenici primili su Nobelovu nagradu za kemiju 2000. godine.

Otkriće vodljivih polimera začelo je novo polje istraživanja na granici kemije i fizike kondenzirane tvari. Vodljivi polimeri otvorili su put za unapređenje fundamentalnog razumijevanja fizike i kemije makromolekula s π -vezama, otvorili su mogućnost da se nađu odgovori na pitanja poput: "Postoji li alternacija veza u dugačkim lančastim polienima?" ili "Kolika je relativna važnost elektron-elektron interakcije i elektron-rešetka interakcije u makromolekulama s π -vezama?". Oba ta pitanja bila su u središtu interesa kvantne kemije već desteljećima. Vodljivi polimeri omogućili su također i istraživanja od temeljnog interesa za fiziku čvrstog stanja, kao što su: metal-izolator prijelaz kako su ga opisali Mott i Anderson, ili strukturna nestabilnost 1D metala kako ju je opisao Peierls.

Polimeri se po prirodi kovalentnih veza između monomernih jedinica dijele na saturirane i nesaturirane. Kod saturiranih polimera, sukladno Paulingovom modelu, dolazi do sp^3 hibridizacije, te sva četiri valentna elektrona svakog C atoma sudjeluju u kovalencijama. Najjednostavniji linearni saturirani polimer je polieten, trivijalnog imena polietilen (PE). Nesaturirani polimeri kod kojih postoji alternacija jednostrukih i dvostrukih veza nazivaju se konjugiranim polimerima. Najjednostavniji linearni konjugirani polimer je *trans*-polietin, trivijalnog imena poliacetilen (PA).

Kod konjugiranih polimera, orbitale L -ljuske C atomâ imaju konfiguraciju sp^2p_z . To znači da su tri od četiri orbitale L -ljuske svakog C atoma hibridizirane, te njihovi elektroni ostvaruju σ -veze. Nehibridizirane p_z orbitale susjednih C atoma u lancu se preklapaju tvoreći tako π -vrpcu s delokaliziranim elektronima, odnosno jednu π -orbitalu zajedničku svim C atomima u kralješnici polimernog lanca kristaliničnog polimera. Takav PA može se zamisliti kao sinkronizirana vremenska visokofrekventna alternacija jednostrukih i dvostrukih veza, koja nakon uprosječivanja po bilo kojem vremenu većem od perioda rezonancije (alternacije veza) daje strukturu u kojoj su sve ugljik-ugljik veze jednake duljine (kraće od jednostrukih a dulje od dvostrukih). Sve spektroskopije veza daju upravo taj uprosječeni rezultat. Prema Heisenbergovoj relaciji neodređenosti za koordinate i impuls, ova delokalizacija elektrona snižava ukupnu energiju elektronskog podsistema (minimizacija ukupne en-

ergije postignuta je minimizacijom kinetičkog dijela ukupne energije), što strukturi (lancu PA) daje dodatnu stabilnost. Inače, svaka dvostruka veza sastoji se od jedne σ -veze (nastale preklapanjem dviju sp^2 hibridnih orbitala) i od jedne π -veze (nastale preklapanjem dviju p_z atomskih orbitala). Naravno, orbitale koje se preklapaju tvoreći kovalentnu vezu moraju biti centrirane na susjednim čvorištima Bravaisove rešetke.

Formula za PA s uniformnim vezama je $(-\text{CH}-)_n$. π -vrpca u PA je polupopunjena, budući da svaki C atom u polimernom lancu ima po jedan nesporeni elektron, a to je situacija idealna za vodljivost. No, ovo ne objašnjava električnu vodljivost u PA, čak ni u savršeno kristaliničnoj strukturi. Intrinzični (nedopirani) PA je poluvodič jer upravo opisana rezonantna struktura podliježe Peierlsovom prijelazu i postaje konjugirana struktura.

Naime, svi 1D sustavi građeni od istovrsnih gradivnih jedinica (U slučaju PA to su $(-\text{CH}-)_n$ monomeri, svaki duljine a .) nestabilni su prema statičkim deformacijama rešetke, valnog vektora $K = 2k_F$. Svaka nelinearna molekula s degeneriranim osnovnim elektronskim stanjem podliježe strukturnoj distorziji, kojom se uklanja degeneracija. Taj Peierlsov prijelaz je spontani loma simetrije prisutne kod stanja uniformnih C-C veza. PA prelazi iz strukture s vremenski alternirajućim jednostrukim i dvostrukim vezama u strukturu s prostorno alternirajućim jednostrukim i dvostrukim vezama, koja predstavlja (dvostruko degenerirano) osnovno stanje sustava. Kad je π -vrpca polupopunjena, tendencija za spontanom lomom simetrije je posebno jaka (za Peierlsov prijelaz nužna je komenzurabilnost nove kristalne rešetke sa starom), a strukturna distorzija se ostvaruje u vidu *dimerizacije*. Dimerizacijom se otvara energijski procijep na Fermijevoj plohi čime se snizuje energija zauzetih elektronskih stanja u blizini Fermijevo nivoa, te se stabilizira nastala strukturna distorzija u fononskom podsistemu. Periodičnost distorzije dana je s:

$$\Lambda = \frac{2\pi}{2k_F} = \frac{\hbar\pi}{p_F}, \quad (9.11)$$

gdje je k_F Fermijev valni broj, a p_F impuls fermiona u najvišem zaposjednutom stanju. U slučaju nedistordiranog PA, koji ima polupopunjenu π -vrpcu, vrijedi:

$$k_F = \frac{\pi}{2a} \quad \Rightarrow \quad \Lambda = 2a. \quad (9.12)$$

Dakle, došlo je do dimerizacije monomera *trans*-polietina, pa je nova formula $(-\text{HC}=\text{CH}-)_n$. Dimerizirani PA ima dvostruko manju prvu Brillouinovu zonu u odnosu na nedimerizirani PA. π -vrpca se rascijepila u dvije: posve popunjenu vrpcu (koju opet nazivamo π -vrpca) i posve praznu π^* -vrpcu. Obje imaju značajnu širinu od ≈ 5 eV. Budući da sada nema djelomično popunjene ni djelomično prazne vrpce, nema ni mogućnosti za vođenjem električne struje. Konjugirani polimeri tipično su poluvodiči ili izolatori. Širina procijepa E_G ovisi o molekularnoj strukturi monomerne jedinice. Između HOMO i LUMO stanja u PA postoji energijski procijep širine $E_G = 1.7$ eV, pa je intrinzični *trans*-polietin zbog Peierlsove nestabilnosti slabo vodljiv

poluvodič.

Polietin, osim u obliku *trans* izomera, postoji i u obliku *cis* izomera. *Cis*-polietin je primjer konjugiranog polimera koji nema degenerirano osnovno stanje. Ima znatno širi energijski procijep od *trans*-polietina. Posljedično, njegova intrinzična vodljivost je četiri reda veličine manja od intrinzične vodljivosti *trans*-polietina; intrinzični *cis*-polietin je izolator. *Cis*-polietin je termodinamički nestabilan; spontano izomerizira u *trans*-polietin.

Na primjeru *trans* i *cis* izomera polietina prikazano je da su intrinzični konjugirani polimeri poluvodiči ili izolatori, no jedino konjugirani polimeri imaju potencijal postati vodljivima.

Za postizanje vodljivosti konjugiranih polimera, potrebno je *dopiranje*, tj. potrebno je injektirati nositelje naboja u kralješnicu konjugiranog polimera. Njihovo gibanje duž polimernog lanca omogućit će već nazočan π -sistem polimernih makromolekula konjugiranog polimera. Injekcija nositelja naboja može se postići na nekoliko načina:

- kemijsko dopiranje: kemijskom reakcijom (bilo redoks-reakcijom, bilo kiselinsko-baznom reakcijom) polimernog lanca s dopantom injektiraju se nositelji naboja u kralješnicu polimera
- elektrokemijsko dopiranje: injekcija nositelja naboja u kralješnicu polimera događa se putem elektroda, a promjena naboja kralješnice polimera kompenzira se ionima elektrolita
- fotodopiranje: apsorpcijom kvanta elektromagnetskog zračenja u kralješnicu polimera, dolazi do lokalne oksidacije i redukcije (na nekom bliskom mjestu), te do separacije para elektron - šupljina u slobodne nositelje naboja
- injekcija nositelja naboja na granici vodljivog i poluvodičkog oblika polimera.

Samo u slučaju kemijskog i elektrokemijskog dopiranja postignuta je permanentna vodljivost. Fotovodljivost je tranzijentna - postoji samo do deekscitacije ili do zatočenja nositelja naboja. U slučaju injekcije nositelja naboja na granici vodljivog i poluvodičkog oblika polimera, elektroni postoje u π^* -vrpci (ili šupljine u π -vrpci) samo uz narinuti vanjski napon. U ovom radu ćemo se nadalje baviti isključivo kemijskim dopiranjem, a to je i dominantan način postizanja vodljivosti polimera.

Shirakawa i suradnici sintetizirali su 1974. godine korištenjem Ziegler-Nattinog katalizatora[‡] tanki film stereopravilnog PA koji je imao optička svojstva metala, ali je bio slabo vodljiv: vodljivost takvog materijala je reda veličine $\sigma \sim 10^{-4}$ S/m.

[‡]Od samih početaka sintetskih polimera znalo se da je mehanizam slobodnih radikala najvažniji mehanizam adicijskih reakcija polimerizacije, no bez kontrole slobodnoradikalnih reakcija, nastali adicijski polimeri su granasti te sadrže anomalije. Ziegler je otkrio novu metodu adicijske polimerizacije koja izbjegava neželjen utjecaj reakcija slobodnih radikala na produktne polimere. Korištenjem nekih organometalnih spojeva s Al kao katalizatora pri reakcijama polimerizacije dobivaju se lančasti polimeri željene duljine. Zieglerovi katalizatori danas se široko primjenjuju u znanosti i industriji.

Shirakawa, MacDiarmid i Heeger otkrili su da oksidacijom (dopiranjem kemijskom redoks-reakcijom) polietinskog filma s elementarnim halogenima Cl_2 , Br_2 ili I_2 , njegova vodljivost poraste $\approx 10^9$ puta — sintetiziran je prvi vodljivi polimer. Vodljivost takvog p-dopiranog filma PA bila je $\sigma \sim 10^5$ S/m, što predstavlja doista dramatičnu promjenu svojstava — a to je često u mekih tvarima.

Dopiranjem konjugiranih polimera uvodi se konačna gustoća stanja na Fermijevom nivou. Dopiranjem se uvode dodatni elektroni (redukcija ili *n-dopiranje*) ili se uklanjaju postojeći elektroni (oksidacija ili *p-dopiranje*). Fermijev nivo (elektrokemijski potencijal) u dotičnom se konjugiranom polimeru pomiče iz procijepa u područje velike gustoće elektronskih stanja, što dakle uzrokuje "metalizaciju" polimera. Uvođenjem šupljina otvaraju se slobodni energijski nivoi bliski Fermijevom nivou za elektrone π -vrpce, a koji su prije p-dopiranja bili popunjeni, te se time omogućava usmjereno gibanje elektrona π -sustava polimerne makromolekule pod djelovanjem razlike potencijala između dva kraja uzorka. U slučaju n-dopiranja, višak elektrona odlazi u π^* -vrpcu, prethodno posve praznu.

Vodljivost σ općenito ovisi o koncentraciji slobodnih nositelja naboja ζ , o njihovom naboju q i o njihovoj pokretljivosti (driftna brzina nositelja naboja po jedinici električnog polja) μ , pri čemu se moraju superponirati doprinosi svih vrsta nositelja naboja j :

$$\sigma = \sum_j q_j \zeta_j \mu_j \quad \mu_j = \frac{|v_{drift}|}{E}. \quad (9.13)$$

Vodljivost ovisi o temperaturi. σ se kod metala snižava porastom temperature, dok se kod poluvodiča i izolatora povećava. Porastom temperature povećava se broj termičkih fonona, te se pojačava raspršenje elektrona na fononima, što djeluje u smjeru smanjenja vodljivosti. No, porastom temperature povećava se i koncentracija elektrona u vodljivoj vrpici, što doprinosi vodljivosti. Kod poluvodiča i izolatora druga od dvije suprotne tendencije nadvladava, tako da σ ukupno raste s T .

Svi su vodljivi polimeri vodiči visoke anizotropije. Transport nosioca naboja uglavnom se odvija uzduž lanca, no budući da se lanac ne prostire od jednog kraja uzorka do drugog (kao što je slučaj s gradivnim jedinicama monokristala metala), za makroskopsku vodljivost polimera važan je i transport naboja između pojedinačnih lanaca. Stoga se kaže da su vodljivi polimeri kvazijednodimenzionalni vodiči.

Natta je otkrio da se dodatkom TiCl_4 u $(\text{C}_2\text{H}_5)_3\text{Al}$ dobiva koordinacijski katalizator, reakcije s kojim su stereoselektivne: mogu se dobiti stereopravilne polimerne makromolekule - izotaktične strukture. U našem slučaju to znači čisti stereomer *trans*-polietina, PA, a ne mješavina *trans* i *cis* izomera (ni u istoj makromolekuli, ni u volumnom polimernom materijalu). Karl Ziegler i Giulio Natta su za svoja otkrića na polju kemije i tehnologije viših polimera dobili Nobelovu nagradu za kemiju 1963. godine.

Procesibilnost i topivost vodljivih polimera

Za široku tehnološku primjenu nekog vodljivog polimera, ključan je preduvjet da ga se može lako procesirati nezahitjivim metodama. Godine 1976. dobiven je dobro vodljivi PA u obliku tankog filma, no PA je nestabilan. Problem stabilnosti ubrzo (1980.) je riješen sintezom poli(*p*-fenilena) (PPP) - prvog aromatski konjugiranog polimera koji se mogao prevesti u vodljivo stanje. Njegova aromatska struktura osigurava visoku otpornost na toplinsku i oksidativnu degradaciju. Problem procesibilnosti bilo je teže riješiti. Temperature taljenja i omekšavanja većine konjugiranih polimera iznad su temperature njihove degradacije, pa oni nisu procesibilni povećanjem temperature kao većina konvencionalnih plastika (koje su saturirani polimeri). Stoga je i procesiranje vodljivih polimera moguće jedino putem njihova otapanja. Čak do 1991. prikladno procesibilni vodljivi polimer nije bio poznat, kada je postignuta procesibilnost vodljivog polianilina u njegovom volumnom (engl. bulk) obliku, u vidu njegove topivosti u slabo polarnim organskim otapalima.

Polimerne otopine zapravo nisu prave otopine poput vodene otopine NaCl, gdje su Na^+ i Cl^- ioni homogeno raspoređeni među molekulama vode u svakom dijelu otopine. Polimerne otopine su disperzije. Dakle, iako se za polimere koristi termin otapanje, on zapravo označava dispergiranje. Osim o kemijskom sastavu monomera i električnom dipolnom momentu otapala, topivost polimera uvelike ovisi i o njihovoj topologiji. Nuždan uvjet za otapanje (dispergiranje) polimera jest da je interakcija između polimernih lanaca i otapala jača od slabih intermolekulskih interakcija među polimernim lancima. U protivnom će polimer u kontaktu s otapalom samo bubriti, te do otapanja (dispergiranja) neće dolaziti. Kristalinični polimeri, umreženi polimeri i polimeri čije su makromolekule vezane vodikovim vezama u pravilu su netopivi. Dobro otapanje polimera znači dobro izduživanje i razmotavanje statističkog klupka polimernog materijala. Svojstva polimernih otopina više ovise o konformaciji (te konformacije ovise kako o samom polimeru, tako i o međudjelovanju polimer-otapalo) polimernih lanaca u otopini, a manje o kemijskom sastavu monomerne jedinice. Entropije otapanja polimera su male i u slučaju najboljih otapala. Ipak, otapanje polimera u dobrom otapalu i ponovna solidifikacija redovito imaju za posljednicu strukturnu reorganizaciju volumnog materijala u odnosu na stanje prije otapanja, što može rezultirati i promjenom fizikalnih svojstava polimernog materijala bez promjene njegovog kemijskog sastava.

Primjena vodljivih polimera

Vodljivi polimeri koriste se ili se industrijski razvijaju s ciljem da služe kao: anti-statička zaštita fotografskog filma (derivati politiofena), antistatička zaštita u vidu plastičnih podova u uredima (dopirani polianilin), zaštita zaslona računala od elektromagnetskog zračenja, te za odvođenje prostornog naboja u litografiji elektronskim snopom (dopirani polianilin). Nadalje, vodljivi polimeri čija je vodljivost usporediva s vodljivošću poluvodiča koriste se u izradi LED dioda, fotonaponskih (solarnih)

ćelija, te kao zaslone mobilnih telefona (poli(*p*-fenilenvinilen)) i televizora malih dimenzija (polidialkilfluoreni). Elektroluminiscencija vodljivih polimera (emisija svjetlosti s tankog sloja polimera nakon pobuđivanja električnim poljem) koristi se u fotodiodama. Takve fotodiode su štedljivije od standardnih jer u pravilu daju više svjetlosti a razvijaju manje topline. LED diode, fotodiode i fotonaponske ćelije izrađuju se i od materijala koji su kompoziti vodljivog polimera i nekog drugog materijala, npr. fulerena. Vodljivi polimeri se koriste i kao antikorozijska zaštita (nedopirani polianilin). To je moguće jer je polianilin u elektrokemijskom nizu vrlo je blizu Ag, dakle kao metal plemenitiji je od Fe i Cu. Predviđa se i proizvodnja lasera od vodljivih polimera. Valja istaći da vodljivi polimeri ne samo da mogu služiti kao uspješna i jeftina zamjena postojećih materijala, već imaju i brojne prednosti pred materijalima čije zamjene sve češće postaju.

Velika prednost plastične mikroelektronike je brza i jeftina proizvodnja elektroničkih komponenata. Elektroničke komponente i integrirani krugovi bazirani na polimerima uskoro će naći svoje mjesto u onim potrošačkim artiklima gdje niska proizvodna cijena ima veću statističku težinu od velikih brzina (koje karakteriziraju silicijske čipove). Zanimljiva primjena plastičnih čipova leži u uporabi u supermarketima gdje bi se ugradnjom čipova u ambalažu proizvoda u jednom mahu putem računala na blagajni mogla očitati cijena koju je kupac dužan platiti, što je trenutno riješeno skupljim optičkim čitačima. Za ovu namjenu ne koriste se konvencionalni silicijski čipovi jer su skupi u usporedbi s cijenom optičkih čitača i projiciranom cijenom plastičnih čipova. Plastični čipovi ne natječu se s konvencionalnim silicijevim čipovima tamo gdje se traže vrhunske performanse, jer su silicijski čipovi brži i trajniji od plastičnih. Plastičnim čipovima namijenjeno je tržište koje traži masovnu produkciju po niskoj cijeni. Njihova dobra svojstva naslijeđena su od njihovog baznog materijala: fleksibilni su, jeftini i lagano se proizvode. Osim kao elektronički bar-kod, plastični memorijski čip mogao bi se ugrađivati u bankovne i telefonske kartice, koje danas sadržavaju Si čipove. Uporaba plastičnih čipova omogućit će izradu cijele kartice od plastike.

Istraživanje vodljivih polimera blisko je povezano i s brzim razvojem molekularne elektronike, iako je prijelaz s plastične mikroelektronike na molekularnu još dalek. Poluvodički konjugirani polimeri mogu se smatrati materijalima visoke čistoće. Kod njih, naime, nema zapinjanja Fermijeveg nivoa na površinskim stanjima. Stoga se, za razliku od konvencionalnih anorganskih poluvodiča, Fermijev nivo konjugiranih polimera može lako pomicati preko granica procijepa. Ta osobina znatno proširuje mogućnosti primjene tih materijala. Primjerice, oligomeri anilina potencijalni su materijal za reverzibilne senzore za detekciju hlapivih organskih spojeva zastupljenosti do nekoliko ppm.

Polianilin

Polianilin (PANI) je najproučavaniji materijal iz skupine vodljivih polimera, prema tome i jedan od najčešće korištenih vodljivih polimera u industrijske svrhe. Polianilin je bio i prvi stabilni vodljivi polimer koji se mogao dobiti u volumnom obliku. Polianilin postoji u dva osnovna kemijska oblika: u obliku baze (nedopirani i nevodljivi polianilin) i u obliku soli (dopirani i vodljivi polianilin). Polianilin nastaje oksidativnom polimerizacijom aminobenzena, trivijalnog imena anilin. Najstabilniji oblik PANI baze je emeraldin (EB).

EB osim u baznom obliku (PANI-EB), može postojati i u obliku soli (PANI-ES) neke protonirajuće kiseline. Ta protonirajuća kiselina je dopant polianilinske emeraldinske baze PANI-EB. U čestom slučaju kad je PANI-EB protoniran kloridnom kiselinom HCl, PANI-ES označava sol koja se naziva emeraldin-hidroklorid ili emeraldinij-klorid. Hidronij-ion (oksonij-ion ako se protonacija vrši u vodenoj otopini kiseline) veže se na nepodijeljeni elektronski par atoma N, pri čemu nastaje emeraldinij-polikation. Emeraldinij-polikation je nabijena konjugirana kiselina PANI-EB baze, te elektrostatski interagira s anionima - konjugiranim bazama dotične protonirajuće kiseline. U slučaju kloridne kiseline kao dopanta, anioni su Cl^- .

PANI se prevodi u vodljivo stanje protonacijom. Protonacija PANI baze je kiselinsko-bazna kemijska reakcija kojom se postiže p-dopiranje bez promjene broja elektrona u kralješnici polimera, što PANI čini jedinstvenim među vodljivim polimerima. Sam mehanizam dopiranja, objašnjen na Slici 9.1, ne ovisi o anionima parnjacima protonirajućih kiselina. Naravno, stupanj dopiranja i vodljivost ovise o anionima parnjacima.

Nakon protonacije PANI-a u emeraldinij-polikation, konjugiranu kiselinu PANI baze, dolazi do unutarnje redoks reakcije bez promjene ukupnog broja elektrona u kralješnici PANI-a. PANI iz izolatorskog stanja (nedopirani PANI) prelazi u vodljivo stanje (dopirani PANI). Za to je odgovoran (protonizacijom induciran) mehanizam rasparrivanja spinova. Konačni produkt protonacije je poli(semikinon) radikal kation. Nastala struktura ima dvostruko manji monomer u odnosu na PANI bazu, ima jedan nesparni spin po monomeru (jednostruko pozitivno nabijenom). Ovo rasparrivanje spina ima za posljedicu stvaranje polupopunjene polaronske vrpce — potencijalno metalno stanje poli(semikinon radikal kationa). Gustoća relevantnih lokaliziranih stanja (lokaliziranih nazočnošću aniona — konjugiranih baza dotične protonirajuće kiseline) proporcionalna je koncentraciji primijenjenog dopanta, odnosno vrijednosti pH dopanta, ako je ta koncentracija mala i ako se pretpostavi da lokalizacijska duljina vrlo malo ovisi o stupnju dopiranosti. Inače, jača dopiranost PANI-a rezultira boljom vodljivošću. Povećanjem koncentracije dopanta vodljivost dopiranog PANI-a raste sve do saturacije zbog potpune protonacije.

Dopirani PANI je konjugirani polimer koji nema degenerirano osnovno stanje, pa kod njega ni nema solitonske vodljivosti. Očekuje se da pozitivni naboj monomera

Figure 9.1: p-dopiranje PANI baze protonacijom. Prijelaz iz izolatorskog u vodljivo stanje bez promjene broja elektrona. (a) PANI baza (emeraldin). (b) Protonacijom iminskih atoma nastaje jedan bipolaron po meru emeraldinij-polikationa. (c) Kinonski prsten prelazi u benzenski — nastaju 2 polarona. Ovdje dolazi do unutarnje redoks reakcije u kojoj iminski N atomi (treći i četvrti N atom s lijeva) mijenjaju oksidacijsko stanje iz $m = -3$ u $m = -2$, dok C atomi kinonskog prstena koji su kovalentno vezani na iminske N atome, mijenjaju oksidacijsko stanje iz $m = +2$ u $m = +1$. (d) Redistribucija naboja i spina — nastaju 2 odvojena polarona, odnosno jedan po monomernoj jedinici poli(semikinon radikal kationa).

poli(semikinon radikal kationa) bude ravnomjerno raspoređen između oba N atoma, no i da djelomično bude delokaliziran preko oba C_6H_4 benzenska prstena monomera.

Mottov model skočne vodljivosti

Model skočne vodljivosti (variable-range hopping, VRH) je model široko korišten u opisu niskotemperaturne vodljivosti u jako neuređenim sustavima s Anderson-lokaliziranim stanjima, kao što je naš PANI-DBSA. Razvio ga je N. F. Mott. Skočni transport naboja se događa između nasumično smještenih dopantskih stanja (u vrpci nereda), koja se čine superrešetku unutar matične rešetke. Važan postulat koncepta skočne vodljivosti je pretpostavka da su praktički sva stanja različita u energiji: dva ekvivalentna stanja su beskonačno udaljena. Stoga je skočni transport naboja praćen emisijom ili apsorpcijom fonona.

Razmotrimo dva elektronska stanja, i i j , u vrpici nereda. Stanja su udaljena za R , a njihove svojstvene energije su E_i i E_j . Možemo, bez smanjenja pune općenitosti, uzeti da vrijedi $W \equiv E_j - E_i > 0$. Elektron može skočiti s mjesta i na mjesto j apsorpcijom fonona energije W . Odgovarajuća vjerojatnost preskoka je dana s

$$P_{ij} = e^{-2R/\xi} f_i (1 - f_j) b_W \quad , \quad (9.14)$$

gdje je ξ lokalizacijska duljina valne finkcije elektrona, b_W Bose-Einsteinova raspodjela za fonone energije W , i f_i Fermi-Diracova raspodjela za stanje i :

$$b_W = \frac{1}{e^{W/k_B T} - 1} \quad , \quad f_i = \frac{1}{e^{(E_i - \mu_i)/k_B T} + 1} \quad , \quad (9.15)$$

gdje je μ_i lokalni kemijski potencijal u nazočnosti električne struje. f_i in (9.14) označava vjerojatnost da je stanje i puno, dok $(1 - f_j)$ označava vjerojatnost da je stanje j prazno. Faktor $e^{-2R/\xi}$ predstavlja kvantnomehaničko tuneliranje, elektrona između preklapljenih stanja i i j . U 1D sustavu, ξ jednostavno opisuje eksponencijalno trnjenje elektronske valne funkcije u potencijalnoj barijeri i direktno je povezana s visinom te barijere. U višedimenzionalnim sustavima, značenje ξ je manje očito. Ono je određeno integracijom preko svih mogućih puteva tuneliranja između dva stanja, čime se odražava kakva okolina okružuje dotično skočno mjesto.

Vjerojatnost za obrnuti skok, od mjesta j do mjesta i , je dana s

$$P_{ji} = e^{-2R/\xi} f_j (1 - f_i) (b_W + 1) \quad , \quad (9.16)$$

i praćena je emisijom fonona energije W . Odgovarajuće skočne brzine su

$$\frac{1}{\tau_{ij}} = \omega_0 P_{ij} \quad , \quad \frac{1}{\tau_{ji}} = \omega_0 P_{ji} \quad , \quad (9.17)$$

gdje je ω_0 frekvencija pokušaja, dana tipičnom fononskom frekvencijom.

Uz pretpostavku da nema korelacija između vjerojatnosti zaposjednuća različitih lokaliziranih stanja, tok elektrona između dva stanja je

$$\mathcal{J}_{ij} = eR \left(\frac{1}{\tau_{ij}} - \frac{1}{\tau_{ji}} \right) \propto \omega_0 e^{-2R/\xi} \frac{\sinh \frac{\mu_j - \mu_i}{2k_B T}}{\sinh \frac{W}{2k_B T} \cosh \frac{E_i - \mu_i}{2k_B T} \cosh \frac{E_j - \mu_j}{2k_B T}} \quad . \quad (9.18)$$

Taj izraz se može pojednostavniti (razvojem u red do linerenih članova) ukoliko se pretpostavi da se sve energijske razlike u (9.18) veće od ili usporedive s $k_B T$. U režimu slabog električnog polja, što se odnosi na mali pad napona preko skočne duljine ($\mu_j - \mu_i \ll k_B T$), gornja pretpostavka rezultira sljedećim izrazom za električnu vodljivost ($\Delta\mu \equiv \mu_j - \mu_i$):

$$\sigma_{ij} \equiv \lim_{\Delta\mu \rightarrow 0} \frac{\mathcal{J}_{ij}}{\Delta\mu} \propto \exp \left[-\frac{2R}{\xi} - \frac{|E_i - \mu| + |E_j - \mu| + W}{2k_B T} \right] \quad . \quad (9.19)$$

uz $\Delta\mu \ll \mu_i, \mu_j$.

Mottov pristup pretpostavlja dominantni doprinos skočnoj struji od stanja koja su unutar $k_B T$ oko kemisjkog potencijala $\mu \equiv E_F$. Tada izraz (9.19) postaje

$$\sigma_{ij} \propto e^{-W/k_B T} e^{-2R/\xi} . \quad (9.20)$$

Na niskim T , gdje postoji oskudica fonona, elektronski transport favorizira dulje skokove varijabilnog dosega. Konačno, može se pokazati da Mottova razmatranja i račun daju sljedeću temperaturnu ovisnost skočne vodljivosti:

$$\sigma_{\text{VRH}}(T) = \sigma_0 \exp \left[- \left(\frac{T_0}{T} \right)^{\frac{1}{4}} \right] , \quad (9.21)$$

što se u d dimenzija generalizira u

$$\sigma_{\text{VRH}}(T) = \sigma_0 \exp \left[- \left(\frac{T_0}{T} \right)^{\frac{1}{1+d}} \right] . \quad (9.22)$$

Fogler - Teber - Shklovskii model

Efros - Shklovskii (ES) model uzima u obzir kulonsku interakciju, ali se odnosi na izotropne sustave, kao i Mottov model. Budući da su vodljivi polimeri na mikroskopskim skalama vrlo anizotropni 3D sustavi, očekujemo da bi složeniji model VRH vodljivosti bolje opisivao fiziku vodljivih polmera. Dobar kandidat za to je Fogler-Teber-Shklovskii model (FTS) model skočne vodljivosti, koji se odnosi na 1D vezane sustave, te uključuje kulonsku interakciju u smislu ES modela.

Interakcije imaju važnu ulogu u određivanju svojstava 1D i kvazijednodimenzionalnih (Q1D) vodiča jer je u tim materijalima bezdimenzionalna jakost kulonske interakcije vrlo velika, $r_s \gg 1$, za razliku od gustog elektronskog plina gdje je $r_s \ll 1$. Zato se 1D i Q1D vodiči ponašaju kao izolatori i ne posjeduju metalno zasjenjenje, pa su coulombske interakcije i jake i dugodosežne, te mogu otvarati kulonski procijep. Matrični elementi transverznog tuneliranja (u slučaju vodljivih polimera to je interlančani transport naboja) su konačni, ali i snažno atenuirani u odnosu na longitudinalne matrične elemente. Folger, Teber i Shklovskii su istražili utjecaj takvih interakcija na prirodu niskoenergijskih nabojnih pobuđenja i na njihovu statičku vodljivost u Ohmskom režimu. Rezultati tih teorijskih istraživanja objedinjeni čine Fogler-Teber-Shklovskii model vodljivosti skočnim mehanizmom promjenjivog dosega.

Središnje obilježje FTS modela je neuniverzalni diskretni eksponent α u potisnutno-eksponencijalnoj ovisnosti dc električne vodljivosti, $\sigma(T) \propto \exp \left[- (T_{\text{FTS}}/T)^\alpha \right]$. α implicitno ovisi o kulonskoj interakciji i neredu. To je generičko svojstvo Q1D Anderson-Mott izolatora koje se ne pojavljuje u uobičajenim poluvodičima ili zapetom Wignerovom kristalu.

Vrlo anizotropno zasjenjenje kulonskog potencijala predviđa neuobičajene VRH zakone. Npr. eksponent α može poprimiti različite diskretne vrijednosti: 1/2, 2/5, 1/4

i 1 (u 3D Q1D slučaju), te $1/2$, $3/5$, $5/11$, $1/4$ i 1 (u 2D Q1D slučaju). Eksponent 1 označava NNH, dok ostali eksponenti označavaju VRH. Stoga, vidimo da se unutar FTS modela mogu pojaviti Mottov slučaj, ES slučaj, NNH slučaj, ali i da FTS uvodi dodatne eksponente međurežima.

Kao i u ES modelu, i u FTS modelu se javlja meki kulonski procijep u gustoći stanja niskoenergijskih nabojnih pobuđenja oko E_F . U 3D Q1D slučaju, gustoća stanja za nabojna pobuđenja pokazuje potencijalnu ovisnost o energiji ϵ :

$$N_v(\epsilon) \propto |\epsilon|^v, \quad (9.23)$$

gdje se $v = 0, 1, 2$ odnosi na slučajeve bez procijepa, s linearnim procijepom, i s kvadratičnim procijepom, respektivno. Posljedično, FTS model daje sljedeće VRH zakone, parametrizirane s α :

$$\sigma_{\text{VRH}}(T) = \eta_\alpha \exp \left[- \left(\frac{T_\alpha}{T} \right)^\alpha \right], \quad \alpha = \frac{1+v}{1+v+d}. \quad (9.24)$$

U slučaju 3D Q1D sustava, $d = 3$. Ovisno o obliku kulonskog procijepa (9.23), $\alpha = 1/2$, $2/5$ ili $1/4$.

Karakterizacija uzoraka PANI–DBSA

Table 9.1: Numeričke vrijednosti važnih parametara našeg PANI–DBSA materijala.

V [cm ³]	c_{DBSA} [mol/m ³]	P	Q	σ_{RT} [S/cm]	χ_{RT} [10 ⁻⁶ emu/mol]
80	134.8	29.90	3.385	9.314	-640.6
80	44.51	9.532	2.918	3.373	-491.9
200	19.19	9.781	2.595	2.177	-449.6
80	26.52	3.085	2.095	0.7386	-357.9
800	4.950	10.14	2.067	0.7065	-347.0
80	8.941	1.054	1.104	0.1918	-64.98
80	2.855	0.3454	0.3766	8.765×10^{-3}	-175.5
80	0.8903	0.1103	0.1282	9.235×10^{-6}	-164.9
80	0.2072	0.03987	0.0536	1.352×10^{-8}	
80	0.05760	0.01107	0.0248	2.241×10^{-9}	
80	0.02878	0.002920	0.0117	1.871×10^{-10}	

Provedeno je ravnotežno dopiranje praška nedopiranog polianilina (PANI) u vodenj otopini dodecilbensulfonske kiseline (DBSA), u širokom rasponu. Dopirani materijal je amorfan, a pripadni udio dopanta — određen nuklearnom spektroskopijom — ukazuje na dva režima dopiranja. Kada je množina dopanta u reakcijskoj otopini manja od množine iminskih atoma u nedopiranom polimeru, sav dopant je iskorišten u protonaciji. Pri većim množinama dopanta dopiranje rezultira dvofaznim sistemom, koji se sastoji od potpuno protoniranog polimera i kemijski nevezanog dopanta između polimernih lanaca. Taj zaključak potkrepljuje magnetska susceptibilnost odabranih uzoraka na sobnoj temperaturi. Istosmjerna električna vodljivost na sobnoj temperaturi povećava se s povećanjem udjela dopanta, čak i u dvofaznom sistemu, te se proteže u rasponu $\sim 10^{-8} - 10^3$ S/m. Za taj porast u jednofaznom sistemu odgovorno je stvaranje vodljivog naboja protonacijom, dok se u dvofaznom sistemu taj porast tumači prirodnom transporta naboja na mikroskopskoj skali. Glavni eksperimentalni podaci su prikazani u Tablici 9.1.

Elektronski transport u PANI-DBSA

Transport čestica u neuređenom potencijalu koji se sastoji od dubokih, lokalizirajućih potencijalnih jama je desetljećima bio zagonetan. Transport u takvom potencijalu se obično događa putem termički potpomognuto preskakivanja s jednog lokaliziranog mjesta na drugo, za što su dobri primjeri transport elektrona u jako neuređenim vodičima i puzanje vrtloga u supravodičima druge vrste. Ako dubina jame jako varira u prostoru, čestica skače na mjesto određeno ravnotežom između duljine preskoka i energijske razlike između uključenih lokaliziranih stanja. Kad je termička aktivacija dovoljno jaka da se zanemari važnost prostorno varirajućih dubina jama, gornji mehanizam — koji se naziva skočni mehanizam promijenjivog dosega (VRH) — se zamjenjuje mehanizmom preskoka do najbližih susjeda (NNH). Najprikladnija opservabla za istraživanje ove pojave je električna vodljivost σ . To je fizikalna veličina linearnog odgovora koja može pružiti dovoljno informacija o prirodi elektronskog skočnog transporta (HET). Taj pristup je bio dominantan sve od ranih radova Andersona i Motta na lokaliziranim elektronskim stanjima u krutinama i njihovoj termički potpomognutoj delokalizaciji. HET električna vodljivost σ općenito ovisi o T kao

$$\sigma(T) = \eta_{\alpha} \exp \left[- \left(\frac{T_{\alpha}}{T} \right)^{\alpha} \right], \quad (9.25)$$

gdje η_{α} , T_{α} , i $\alpha \leq 1$ sadrže informacije o mikroskopskim mehanizmima. Ovi parametri mogu ovisiti o dimenzionalnosti (d), interakcijama relevantnima za transport, stupnju nereda, lokalizacijskoj duljini elektrona, itd. Za VRH, $\alpha < 1$, dok NNH poštuje Arrheniusov zakon ($\alpha = 1$).

VRH neinteragirajućih elektrona rezultira Mottovim zakonom $\alpha = (1 + d)^{-1}$. Kulonska interakcija vodi na $|E - E_F|^{\nu} \equiv |\epsilon|^{\nu}$ energijsku (E) ovisnost DOS-a u blizini Fermijeve energije E_F , gdje je ν konstanta. To otvara meki (kulonski) procijep u DOS-u, te rezultira u Efros - Shklovskii (ES) zakonu gdje je $\alpha = 1/2$ univerzalan. Navedeni modeli se odnose na izotropne sustave, primjerice na neuređene poluvodiče. Međutim, HET se pojavljuje i u drugim materijalima, od kojih mi obraćamo pozornost na vodljive polimere. Za mnoge od njih, (9.25) se izvanredno slaže s eksperimentalnim podacima, u slučaju $\alpha = 1/4$ i $\alpha = 1/2$. Ostali $\alpha < 1$ su pronađeni također, uključujući i $\alpha = 2/5$ koji se ne može objasniti tradicionalnim modelima. NNH je, s druge strane, puno rjeđi u vodljivim polimerima, a $\alpha = 1$ se rijetko opaža, vjerojatno zato što su uvjeti za njegovu pojavu rijetko uspostavljeni na T nižoj od temperatura degradacije materijala.

Model s potencijalom da obuhvati svu složenost $\sigma(T)$ u vodljivim polimerima, razvili su je Fogler, Teber i Shklovskii (FTS). Oni su proučavali HET u vezanim lančastim vodičima u prisutnosti kulonske interakcije ovisne o neredu koja utječe na DOS slično kao i u ES modelu. FTS model predviđa $\alpha = (1 + \nu) / (1 + \nu + d)$, što za jako vezane lance ($d = 3$) i $\nu = 0, 1, 2$ vodi na $\alpha = 1/4, 2/5, 1/2$, respektivno. Na niskim T , vrlo neuređeni uzorci bi trebali pokazivati $\alpha = 1/2$, a uređeniji uzorci $\alpha = 2/5$. U

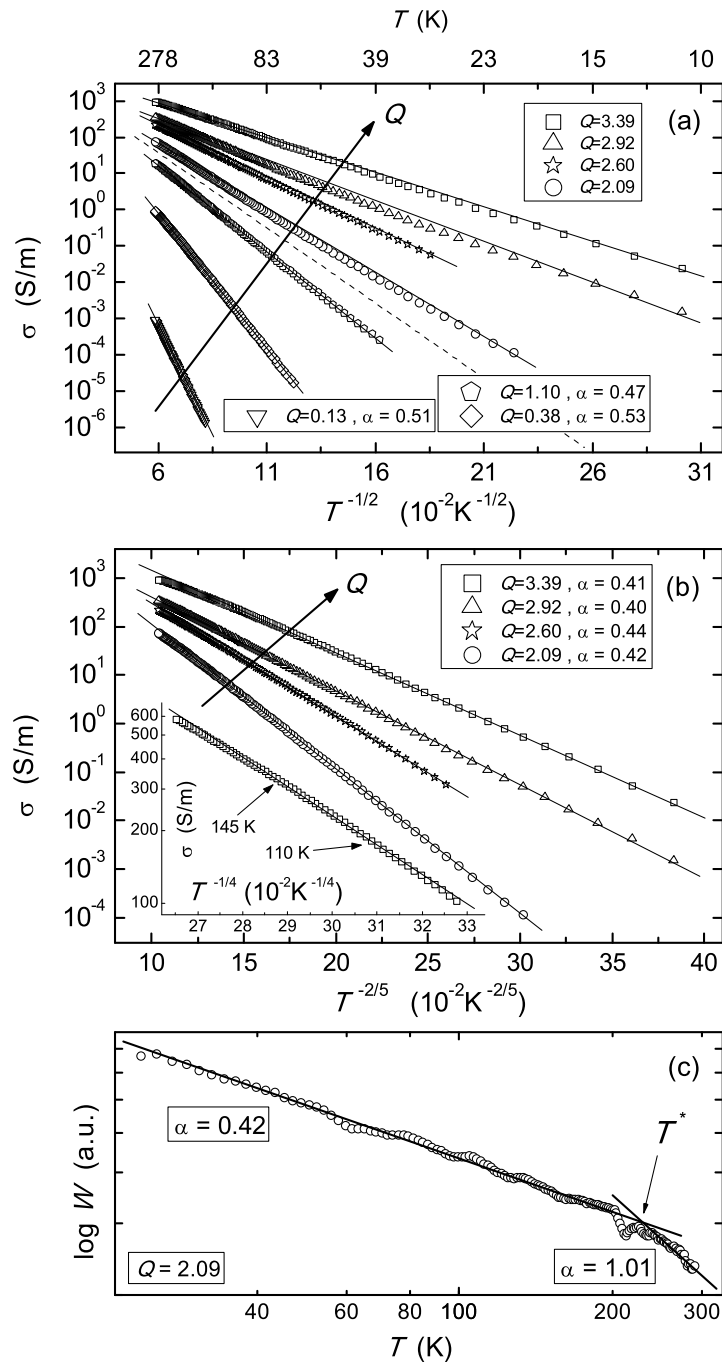


Figure 9.2: (a) Eksperimentalni $\log \sigma$ vs $T^{-1/2}$ (simboli). Pune linije su [ovdje i u (b)] vodilje za oko. (b) Podaci iznad crtkane linije u (a), prikazani kao $\log \sigma$ vs $T^{-2/5}$ (simboli). Inset u (b): $\log \sigma$ vs $T^{-1/4}$ za $Q = 3.39$, pokazuje linearnost $110 \lesssim T \lesssim 145$ K. Pripadajući α određen numerički [kao što je prikazano u (c)] je 0.27. (c) $\log W$ vs $\log T$ odabranih uzoraka (simboli), pokazuju dva odvojena područja linearnosti s prijelazom na T^* . Pune linije predstavljaju linearne prilagodbe iz kojih se α dobiva numerički. α dobivene tim postupkom su navedene u legendama u (a) i (b).

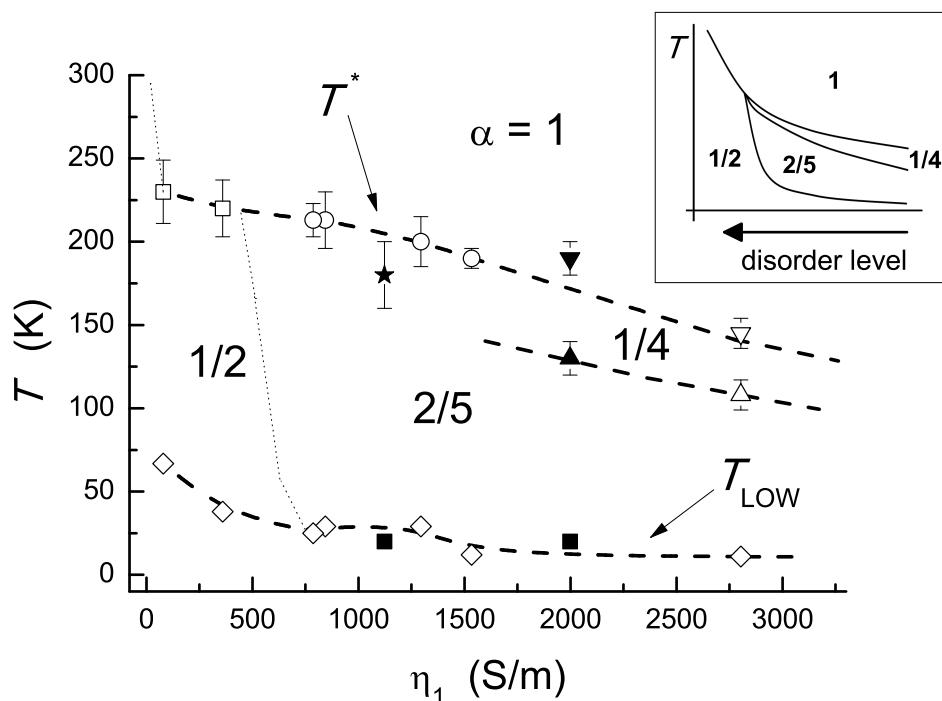


Figure 9.3: Područja različitih α , prikazana u T vs η_1 ravni. Prazni simboli odgovaraju PANI-DBSA uzorcima, a puni dvama PANI-HCl uzorcima koji pokazuju $\alpha = 1$ ispod RT. Linije su vodilje za oko. Najgornji simboli odgovaraju T^* , dok najdonji simboli prikazuju T_{LOW} što je najniža T na kojoj je σ mjerena. Središnji simboli za dva uzorka s najvećim η_1 vrijednostima označavaju prijelaze između $\alpha = 2/5$ i $\alpha = 1/4$. Skica teorijski predviđenog dijagrama je prikazana u insetu.

prvom slučaju, prijelaz u NNH s povećanjem T bi trebao biti izravan, tj. $\alpha = 1/2 \rightarrow 1$, dok bi se u drugom slučaju trebalo opaziti $\alpha = 2/5 \rightarrow 1/4 \rightarrow 1$. Temeljem tih razmatranja, FTS su predložili dijagram za $d = 3$ gdje su temperature prijelaza između različitih α prikazane u ovisnosti o prikladno parametriziranom stupnju nereda.

Glavni rezultati mjerenja σ i posljedično izvrijednjenih parametara su dani na Slici 9.2 i 9.3. Mjerenjem elektronskog transporta potvrdili smo važnost kulonske interakcije u našem PANI-DBSA materijalu ispod određene temperature T^* koja blago ovisi o stupnju dopiranja Q : $T^* = T^*(Q)$. Naše proučavanje temperaturne (T) ovisnosti električne vodljivosti σ u PANI-DBSA tabletama pokazalo je razvučenu eksponencijalnu ovisnost $\sigma(T)$, s neuniverzalnim i diskretnom eksponentom – *alpha*. Pojava različitih eksponenata α je posljedica različitih oblike gustoće stanja $N(E)$ za naboja pobuđenjima oko Fermijeve energije. Različiti oblici $N(E)$ proizlaze iz ovisnosti kulonske interakcije o stupnju nereda. Prijelazi iz $\alpha < 1$ u $\alpha = 1$, sustavno nađeni u $\sigma(T)$ naših PANI-DBSA uzoraka, sugeriraju da efekti kulonskog procijepa nisu isti za $T < T^*$ i $T > T^*$, budući da je $\alpha = 1$ nađen za sve Q (tj. pojava $\alpha = 1$ ne ovisi o specifičnostima danog stanja pri $T < T^*$).

Magnetska svojstva PANI-DBSA

Table 9.2: Eksperimentalno dobiveni parametri χ_P/μ_0 i C/μ_0 , zajedno s izvrijednjenim parametrima $N(E_F) = \chi_P/\mu_0\mu_B^2$, $N_C = Ck_B/\mu_0\mu_B^2$, i longitudinalnom lokalizacijskom duljinom $L_{||} = \sqrt{\hbar^2\Delta N(E_F)/8m_e\Delta N_C}$. Mol is definiran po dva prstena PANI-ja.

Q	T range [K]	χ_P/μ_0 [10^{-4} JT $^{-2}$ mol $^{-1}$]	C/μ_0 [10^{-2} JKT $^{-2}$ mol $^{-1}$]	$N(E_F)$ [states (eV) $^{-1}$ (2 rings) $^{-1}$]	N_C [10^{-3} states (2 rings) $^{-1}$]	$L_{ }$ [Å]
3.39	10 – 170	13.71	7.14	4.24	19.03	8.50
	170 – 300	15.92	3.75	4.93	10.00	
2.92	10 – 190	12.90	7.89	3.99	21.02	7.56
	190 – 300	15.98	1.94	4.94	5.17	
2.60	10 – 200	10.40	10.02	3.22	26.64	7.38
	200 – 300	13.43	3.85	4.15	10.27	
2.09	10 – 200	7.39	12.62	2.29	33.63	7.43
	200 – 300	11.27	4.80	3.49	12.80	
2.06	10 – 190	9.60	11.00	2.97	29.32	7.48
	210 – 300	12.41	5.45	3.84	14.54	
1.10	10 – 200	12.42	10.04	3.84	26.77	7.23
	210 – 300	16.76	0.87	5.18	2.32	
0.38	10 – 220	1.72	4.44	0.53	11.83	6.88
	220 – 300	2.68	2.18	0.83	5.81	
0.13	10 – 210	0.31	2.52	0.10	6.71	6.39
	250 – 300	0.79	1.20	0.25	3.21	
0	10 – 300	0	1.05	0	2.80	

Natjecanje kulonske interakcije s termičkom energijom i neredom u PANI-DBSA se može sondirati ispitujući njegovu magnetsku susceptibilnost χ . To svojstvo je komplementarno sa σ , te je osjetljivo na efekte (de)lokalizacije elektrona. Za bilo koji vodljivi polimer, χ obuhvaća doprinos Curiejevog tipa od lokaliziranih elektronskih spinova, i doprinos Paulijevog tipa of delokaliziranih, vodljivih elektrona. Budući $N(E)$ utječe ne samo na σ nego i na χ (preko vodljivih elektrona), očekujemo da (de)lokalizacija koja ostavlja trag u σ bude vidljiva i u χ .

Dakle, eksperimentalno smo istražili χ našeg PANI-DBSA materijala u temperaturnom rasponu 10-300 K. Dobiveni rezultati ukazuju na to da su χ i σ dosita međusobno povezani. Naime, našli smo temperaturu $T^*(Q)$, na kojoj $\chi(T)$ doživljava značajnu promjenu, a ta temperatura se vrlo dobro slaže s temperaturom koja označava prijelaz iz $\alpha < 1$ u $\alpha = 1$ u $\sigma(T)$. Spomenuta promjena u $\chi(T)$ se odnosi na istodobno

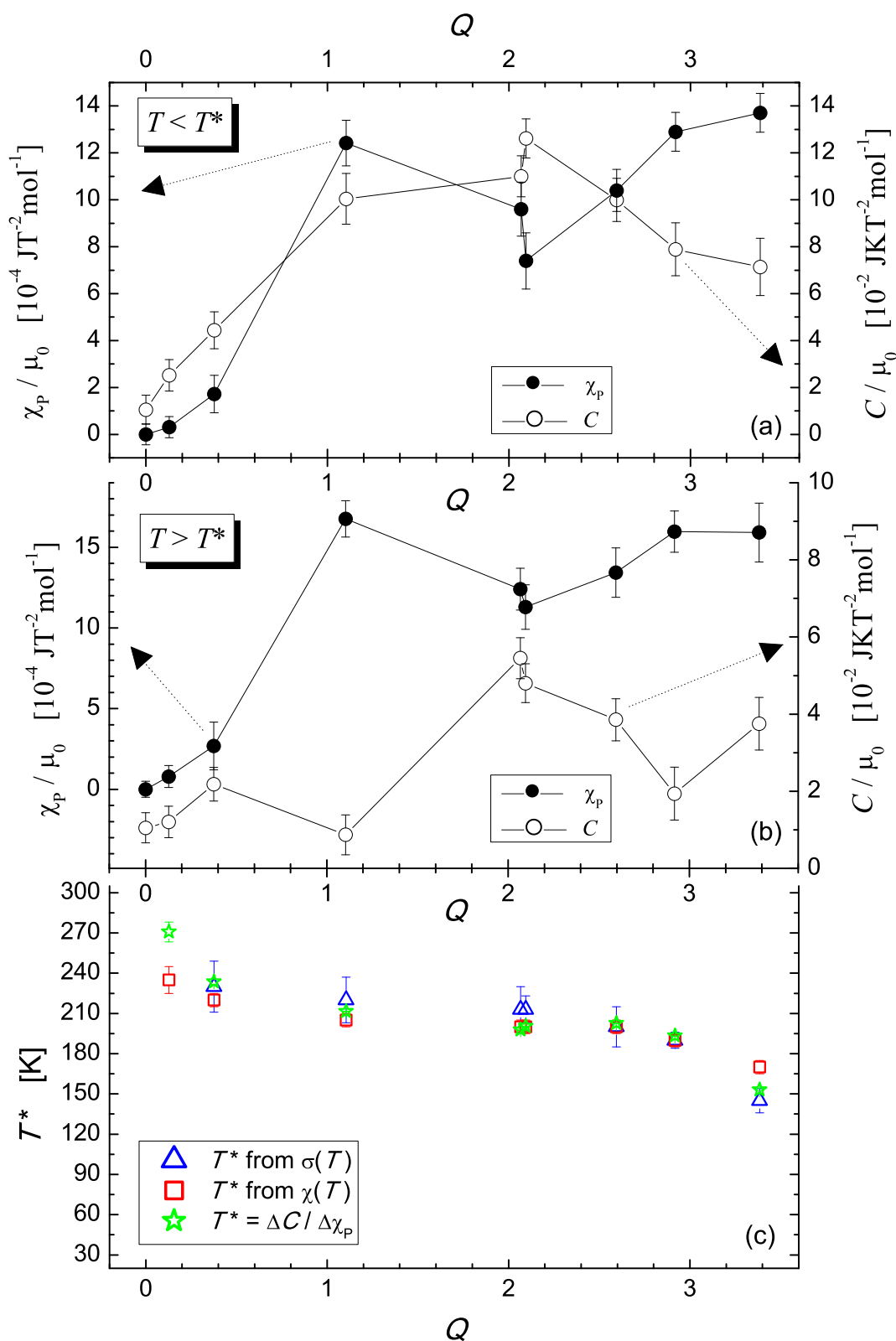


Figure 9.4: χ_p (lijeva skala, puni simboli) and C (desna skala, prazni symbols) kao funkcije of Q pri (a) $T < T^*$, i (b) $T > T^*$. (c) Temperature prijelaza T^* kao funkcije od Q , određene trima nezavisnim metodama, kao što je objašnjeno u tekstu.

povećanje (smanjenje) susceptibilnosti Paulijevog tipa χ_P i smanjenje (povećanje) Curiejeve konstante C na $T = T^*$ s povećanjem (smanjenjem) T . Ovaj nalaz je u skladu sa slikom u kojoj se, na T^* , spinovi koji nestaju iz C pojavljuju u χ_P , i obrnuto. Glavni rezultati su prikazani na Slici 9.4 i u Tablici 9.2.

Vezanje spina i naboja u PANI-DBSA

U ovom poglavlju diskutiramo međusobnu povezanost $\chi(T)$ i $\sigma(T)$ u PANI-DBSA. U svakom od naših PANI-DBSA uzoraka opazili smo vezanje spina i naboja, koje se najizraženije očituje u približno istoj temperaturi T^* nađenoj i u $\sigma(T)$ i u $\chi(T)$. T^* blago ovisi o Q , stoga se ne razlikuje od uzorka do uzorka drastično. Vjerujemo da ovo vezanje spina i naboja predstavlja samo različite manifestacije iste fizike, kao što je objašnjeno u nastavku.

Efekte interakcije (koji svrstavaju naš soft-matter materijal i među jako korelirane sustave) natječu se u PANI-DBSA s termičkim efektima. Njihova relativna jakost ovisi o T . Na niskim T , efekti interakcije dominiraju nad termičkim efektima. Kako se T povećava, termički efekti jačaju. T^* je temperatura na kojoj termički efekti nadjačaju efekte interakcije u PANI-DBSA. To se očituje u sljedećem:

1. **u elektronskom transportu**, kao prijelaz iz FTS-VRH režima u NNH režim. Osiromašenje DOS-a za nabojna pobuđenja, koje je snažno naglašeno pri $T < T^*$, je pri $T > T^*$ djelomično kompenzirano delokalizacijom nositelja naboja. Dakle, pri $T > T^*$, sva (ili skoro sva) lokalizirana stanja (stvorenja protonacijom) su slobodna za preskoke. Kao posljedica toga, javlja se NNH unutar vrpce nereda. Nered je i dalje nazočan (doduše, ponešto je renormaliziran) u NNH režimu, ali termička energija učinkovito umanjuje njegovu važnost kako razlike u dubinama potencijalnih jama za nositelje naboja postaju nevažne.

Međutim, punu fizikalnu sliku uzroka pojavljivanja NNH, tek treba izvući iz $\chi(T)$.

2. **u magnetskom odgovoru**, kao prestanak važnosti on-site kulonske interakcije U . Zbog toga, svi energijski nivoi u intervalu $[E_F - U, E_F]$ koji su bili jednostruko popunjeni pri $T < T^*$ (i zbog su davali odgovor Curiejevog tipa), mogu pri $T > T^*$ postati i dvostruko okupirani ili prazni, dajući posljedično odgovor Paulijevog tipa. Dakle, dio elektrona koji su se ponašali kao spinovi Curiejevog tipa na $T < T^*$, postaju spinovi Paulijevog tipa na $T = T^*$.

Plauzibilno je pretpostaviti $U \approx k_B T^*$. Kad je U relevantan, većina energijskih nivoa u blizini E_F ostaje jednostruko zauzeta i time nedostupna za skočni transport dokle god je $k_B T < k_B T^* \approx U$. Ako pretpostavimo da U prestaje biti relevantan na $T = T^*$, to implicira da ima manje ograničenja za nazočstvo dva spina na istom mjestu na višoj T . Dakle, spinovi se mogu upariti pri $T > T^*$, i sva mjesta postaju dostupna za transport, što posljedično vodi na NNH. Naime, pri $T \geq T^*$, efekti od U su nadvladani

termičkim efektima; Mottov procijep U se zatvara na $T = T^*$. Neredom inducirani kulonski procijep Δ_C ostaje otvoren i pri $T \geq T^*$, ali dugodosežna elektron-šupljina interakcija, koja je i odgovorna za Δ_C , je potisnuta zbog povećanog zasjenjenja kulonske interakcije uslijed jake termičke delokalizacijske elektrona. Zbog ovog potisnuća elektron-šupljina interakcije, kulonski procijep je strmiji pri $T > T^*$ negoli pri $T < T^*$.

Kvalitativno, fizika elektrona u PANI-DBSA je na svim T određena činjenicom da, zbog nereda, elektroni ne mogu skočiti na bilo koje mjesto već moraju birati energijski slična mjesta. Dodatno, na $T < T^*$, elektroni ne mogu doskočiti u jednos-truko okupiranja stanja.

Mjera on-site kulonske interakcije je U , koji je, ovisno o Q , u rasponu $U \sim 15 - 20$ meV (ekvivalentno $T \sim 170 - 230$ K). Širina kulonskog procijepa, Δ_C , je mjera elektron-šupljina interakcije. Ona je, ovisno o Q , u rasponu $\Delta_C \sim 30 - 170$ meV (ekvivalentno $T \sim 350 - 2000$ K). Koristeći Kamimurin model, i uzimajući u obzir činjenicu da u PANI-DBSA samo dio elektrona Curiejevog tipa prelazi u elektrone Paulijevog tipa na T^* , procijenili smo da je širina vrpce nereda $W \sim 20 U$, tj., $W \sim 300 - 400$ meV. Budući da je energijski procijep između valentne i vodljive vrpce u PANI $E_g \sim 2.5$ eV, možemo zaključiti da se sve nabojna pobuđenja u našem PANI-DBSA događaju unutar vrpce nereda. Kada ne bi bilo vrpce nereda, koja se stvorila protonacijom, naš polimer bi bio tvrdi izolator.

Iz mjerenja elektronskog transporta, zaključili smo o važnosti dugodosežne elektron-šupljina interakcije u PANI-DBSA. Iz $\chi(T)$, zaključili smo o važnosti druge vrste kulonske interakcije u našem PANI-DBSA — on-site kulonske interakcije. Lokalno svojstvo U određuje dinamiku spina dok je kolektivno svojstvo Δ_C odgovorno za dinamiku naboja, iako U nije striktno lokalno svojstvo, budući da blago ovisi o Q . Na $T \geq T^*$, energijska razlika između jednostruke i dvostruke popunjenosti Anderson-lokaliziranog elektronskog stanja u PANI-DBSA je termički izbrisana.

Energijska skala koju definira NNH režim prometa u PANI-DBSA je Δ_C , ali pojavljivanje NNH je omogućeno zatvaranjem Mottov procijepa U . Dakle, imamo kooperativno ponašanje ili vezanje spina i naboja jer se U odnosi na kulonske korelacije opisane isključivo preko spina, dok se Δ_C odnosi na spinski nepolarizirani transport naboja. Elektronska vodljivost u NNH režimu je dana aktivacijskim transportom preko mekog procijepa Δ_C ,

$$\sigma_{\text{NNH}}(T) = \eta_1 \exp\left(-\frac{\Delta_C}{k_B T}\right), \quad (9.26)$$

gdje je η_1 mjera nereda. VRH režim s $\alpha = 1/2$ ili $\alpha = 2/5$ odgovara transportu unutar mekog procijepa vrpce nereda.

Kulonski procijep vidimo ne samo u $\sigma(T)$, nego također i u $\chi(T)$, budući da je za sve Q , $N(E_F, T < T^*) < N(E_F, T > T^*)$. Da kulonski procijep nije bio detektiran u $\chi(T)$, tada bi DOS za nabojna pobuđenja bii jednak u VRH i NNH. Osim toga, baš

kao što možemo detektirati promjene u obliku kulonskog procijepa iz exponenta α u $\sigma(T)$, također možemo također detektirati iste promjene u $\chi(T)$. Naime, primijetili smo promjenu iz kvadratnog u linearni kulonski procijep s povećanjem Q kao nagli porast nagli porast u $\chi_P(T > T^*)$, uz istodobno smanjenje $C(T > T^*)$, oko $Q = 1.10$.

Naši rezultati ukazuju na to da PANI-DBSA u svojoj suštini Anderson-Mottov izolator. Elektromagnetska svojstva PANI-DBSA su određena i neredom i kulonskim interakcijama, te to vrijedi i pri $T < T^*$ i pri $T > T^*$. Međutim, postoje neke kvantitativne i kvalitativne razlike između ova dva T raspona, iako oba sadrže vodljive elektrone kao i lokalizirane magnetske momente. Prema suvremenim pristupima MIT-u, T^* se može promatrati kao temperatura na kojoj se događa Mottov prijelaz iz “izolatora” u “vodič”[§]. Na $T > T^*$, Mottov procijep U je zatvoren, iako dio mjesta i dalje ostaje jednostruko okupiran s lokaliziranim magnetskim momentima, ali to je zbog nereda. Zbog prisutnosti jakog nereda, taj Mottov prijelaz je (za svaki konačni T) glatki prijelaz, nije oštri fazni prijelaz prvog reda. Iako se Mottov procijep zatvara na T^* , kulonski procijep Δ_C ostaje otvoren budući da nered ostaje prisutan.

Relevantnost energijske skale U je također utvrđena i u slučaju PANI-HCl materijala proizvedenog iz istog generičkog PANI kao naš PANI-DSBA, pa ipak NNH je u PANI-HCl viđen u samo jednom uzorku isključujući as-synthesised uzorak. Većina prijelaza u PANI-HCl su u $\alpha = 1/4$ (bilo iz $\alpha = 1/2$ ili $2/5$). VRH režim s $\alpha = 1/4$ također indicira ublažavanje osiromašenja DOS-a za nabojna pobuđenja, ali to ublažavanja nije tako jako kao u slučaju prijelaza u NNH. Stoga, za razliku od situacije u PANI-HCl gdje temperatura prijelaza T^* označava prijelaz unutar različitih VRH režima, u PANI-DBSA T^* obilježava globalni proces — prijelaz na NNH gdje su gotovo sva mjesta u blizini E_F dostupna za skočni transport naboja. U prilog ovakvom razmatranju ide i činjenica da su prijelazi u PANI-DBSA izraženiji negoli u PANI-HCl, kako u $\sigma(T)$ tako i u $\chi(T)$.

Međuodnos spinske dinamike i elektronskog transporta u PANI je bila uočena i ranije, iako ne tako izravno kao ovdje. Drugi autori su detektirali povećanje u χ_P uz istodobno smanjenje u C s povećanjem T , ali ta opažanja nisu bila sustavna, niti su mogla biti povezani s $\sigma(T)$.

Uspostavili smo snažnu korelaciju između svojstava elektronskog transporta i termodinamičkih svojstava našeg materijala. Takvo postignuće smatra se značajnim pri proučavanju temeljnih svojstava materijala. Sada možemo krenuti u istraživanje potencijala primjene našeg pani-DBSA .

[§]Unatoč delokalizaciji dijela lokaliziranih elektrona na $T = T^*$, naš PANI-DBSA je izolator i ispod i iznad T^* budući da se u PANI-DBSA $\sigma(T)$ povećava s povećanjem T .

Kompoziti od PANI–DBSA i ugljikovih nanocjevčica

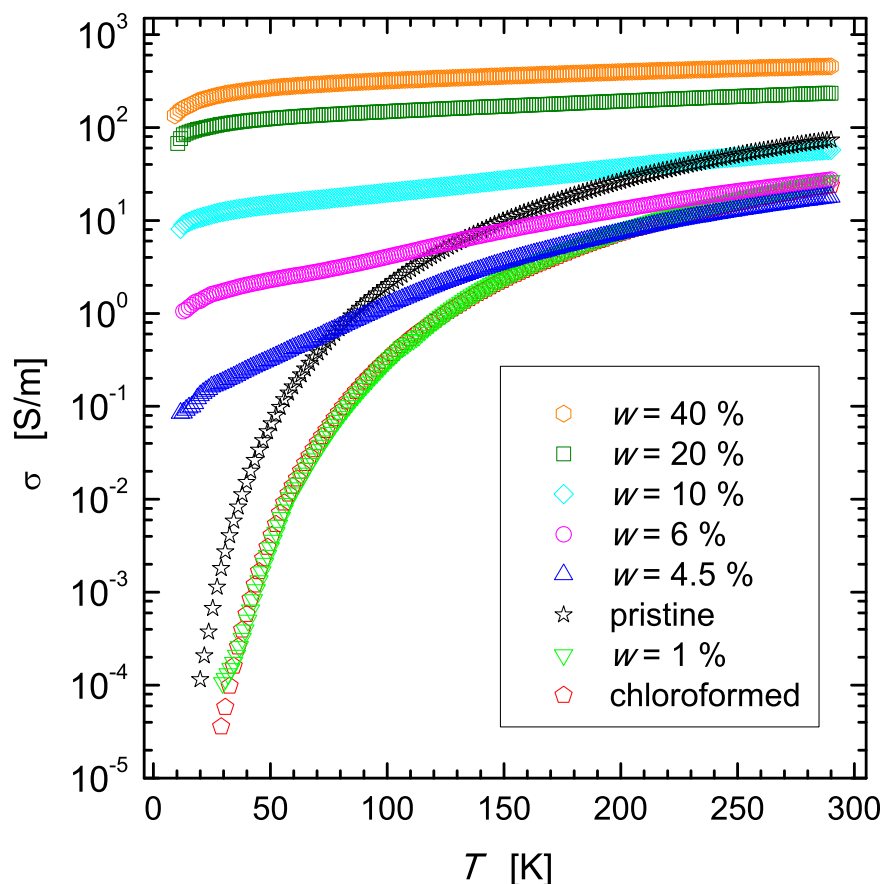


Figure 9.5: σ vs T za PDMC kompozite načinjene od $Q = 2.06$ PANI–DBSA materijala, u usporedbi s čistim and kloroformiranim PANI–DBSA uzorcima ($w = 0$).

Načinili smo volumne kompoziti od PANI–DBSA i višezidnih ugljikovih nanocjevčica (MWCNT), koristeći svojstvo topivosti u kloroformu CHCl_3 , koje je zajedničko i PANI–DBSA polimeru i MWCNT. Postignut je značajan maseni udio MWCNT od do 40 %. Značajan je i prateći efektivan gubitak temperature ovisnosti σ : smanji se svega 3 puta od sobne temperature do 10 K, dok je to smanjenje za čisti PANI–DBSA za faktor 10^6 . Tako naši blendovi istovremeno nude rješenje problema primjene MWCNT u volumnom obliku, te problema loše vodljivosti PANI–DBSA na niskim T . Također je moguće raditi tanke filmove, i od PANI–DBSA i od blendova, na komercijalnom plastičnom supstratu (FR4). Glavni rezultati su prikazani na Slici 9.5 i 9.6.

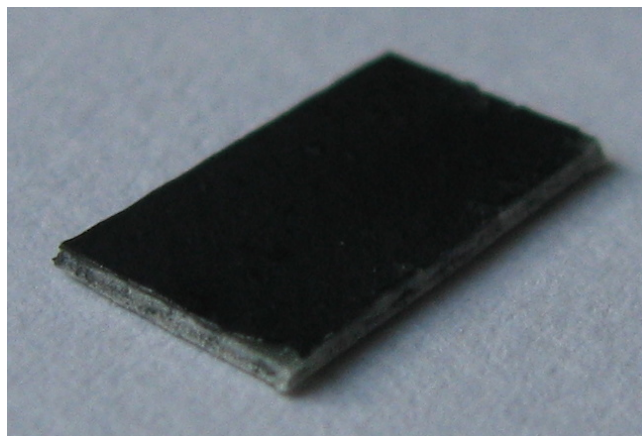


Figure 9.6: Film od PD2.06MC40 kompozita na pločici od FR4 supstrata. Pločica je debela $350 \mu\text{m}$, a film $9 \mu\text{m}$.

Zaključak

Provedeno je komparativno eksperimentalno istraživanje temperaturne (T) ovisnosti istosmjerne električne vodljivosti σ i magnetske susceptibilnosti χ na tabletama polianilina (PANI) dopiranog s dodecilbenzensulfonskom kiselinom (DBSA), koja je dugačka molekula sa surfaktantskim svojstvima. Niskotemperaturno ponašanje u svim uzorcima karakterizirano je skočnom vodljivošću promjenjivog dosega (VRH) u homogeno neuređenom trodimenzionalnom (3D) sustavu vezanih jednodimenzionalnih (1D) lanaca.

Ovisno o dopiranju i pripadnom stupnju nereda u materijalu, VRH eksponenti su $1/2$, $2/5$ ili $1/4$, dok je na višim T u svim uzorcima nađen eksponent 1, koji ukazuje na redukciju srednjeg dosega skokova na prve susjede. Svi ti eksponenti anticipirani su u teoriji Foglera, Tebera, i Shklovskijia za transport naboja u kvazi-1D Anderson-Mott izolatorima, a uvjeti za njihovo pojavljivanje ovise o neredu i T . Utvrdili smo prisustvo mekog (kulonskog) procijepa, što ukazuje na postojanje dugodosežne kulonske interakcije u našim uzorcima.

Promjene s jednog eksponenta na drugi zbivaju se u $\sigma(T)$ na temperaturama prijelaza T^* , gdje su također zamjetne i promjene u $\chi(T)$ krivuljama, što ukazuje na vezanje naboja i spina. Diskutirano je kako $k_B T^*$ ima ulogu termičke energije koja uzrokuje povećanje gustoće delokaliziranih (Paulijevih) spinova na račun lokaliziranih (Curiejevih) spinova pri porastu T iznad T^* . Uočena korelacija između spinske dinamike i elektronskog transporta omogućila nam je procjenu energijskih skala u elektronskoj strukturi PANI-DBSA.

Koristeći svojstvo topivosti u kloroformu, koje je zajedničko i PANI-DBSA polimeru i višezidnim ugljikovim nanocjevčicama (MWCNT), načinili smo volumne kom-

pozite ta dva materijala. Postignut je značajan maseni udio MWCNT od do 40 %. Značajan je i prateći efektivni gubitak temperaturne ovisnosti σ : smanji se svega 3 puta od sobne temperature do 10 K, dok je to smanjenje za čisti PANI–DBSA za faktor 10^6 . Tako naši blendovi istovremeno nude rješenje problema primjene MWCNT u volumnom obliku, te problema loše vodljivosti PANI–DBSA na niskim T . Također je moguće raditi tanke filmove, i od PANI–DBSA i od blendova, na komercijalnom plastičnom supstratu (FR4).

References

- [1] L. C. Epstein, *Thinking Physics*, 2nd ed. (Insight Press, San Francisco, 1995).
- [2] S. P. Jobs, Stanford Report **Jun 14, 2005**,
<http://news.stanford.edu/news/2005/june15/jobs-061505.html> (Accessed 6 Aug, 2012).
- [3] M. Baćani, D. Babić, M. Novak, I. Kokanović, and S. Fazinić, *Synth. Met.* **159**, 2584 (2009).
- [4] D. Babić, M. Baćani, M. Novak, and I. Kokanović, *Croat. Chem. Acta* **83**, 1 (2010).
- [5] M. Baćani, M. Novak, I. Kokanović, and D. Babić, *Synth. Met.* **172**, 28 (2013).
- [6] G. M. Whitesides, *Toward a Science of Simplicity*, TED talk, Feb 2010, Long Beach CA, http://www.ted.com/talks/george_whitesides_toward_a_science_of_simplicity (Accessed 23 Jun, 2011).
- [7] G. M. Whitesides, *Complexity and Simplicity*, Harvard University,
<http://gmwgroup.harvard.edu/research/index.php?page=13> (Accessed 18 Sep, 2011).
- [8] A. W. Martinez, S. T. Phillips, M. J. Butte, and G. M. Whitesides, *Angew. Chem. Int. Ed.* **46**, 1318 (2007); A. W. Martinez, S. T. Phillips, G. M. Whitesides, and E. Carrilho, *Anal. Chem.* **82**, 3 (2010); G. M. Whitesides, *Lab Chip* **13**, 11 (2013).
- [9] A. W. Martinez, S. T. Phillips, B. J. Wiley, M. Gupta, and G. M. Whitesides, *Lab Chip* **8**, 2146 (2008); H. Bruus, *Theoretical Microfluidics* (OUP, Oxford, 2008).
- [10] W. Brian Arthur, *The Nature of Technology: What It Is and How It Evolves* (Free Press, New York, 2009).
- [11] R. Dawkins, *The Selfish Gene*, 2nd ed. (OUP, Oxford, 1999).
- [12] A. J. Leggett, *Nature Phys.* **2**, 134 (2006).
- [13] P. W. Anderson, *Science* **235**, 1196 (1987).
- [14] M. Cyrot, *Nature* **330**, 115 (1987), and references therein.
- [15] R. B. Laughlin, *Phys. Rev. B* **89**, 035134 (2014).
- [16] A. J. Heeger, N. S. Sariciftci, and E. B. Namdas, *Semiconducting and Metallic Polymers* (OUP, Oxford, 2010).

- [17] S. Bhadra, D. Khastgir, N. K. Singha, and J. H. Lee, *Prog. Polym. Sci.* **34**, 783 (2009), and references therein.
- [18] M. Geoghegan and G. Hadziioannou, *Polymer Electronics* (OUP, Oxford, 2013).
- [19] Z. Bao and J. Locklin, *Organic Field-Effect Transistors* (CRC Press, Boca Raton FL, 2007).
- [20] T. A. Skotheim and J. R. Reynolds, eds., *Handbook of Conducting Polymers*, 3rd ed. (CRC Press, Boca Raton FL, 2007).
- [21] N. W. Ashcroft and N. D. Mermin, *Solid State Physics* (Holt, Rinehart and Winston, New York, 1976).
- [22] C. Kittel, *Introduction to Solid State Physics*, 8th ed. (Wiley, New York, 2005).
- [23] J. Quintanilla and C. Hooley, *Phys. World* **June**, 32 (2009).
- [24] G. M. Whitesides and J. Deutch, *Nature* **469**, 21 (2011).
- [25] R. B. Laughlin, *A Different Universe* (Basic Books, New York, 2005).
- [26] UNESCO, *History of Humanity, Vol. VII: The Twentieth Century*, edited by S. Gopal, S. L. Tikhvinsky, I. A. Abu-Lughod, G. Weinberg, I. D. Thiam, and W. Tao (UNESCO, Paris, 2008).
- [27] F. A. Hayek, *The Constitution of Liberty* (University of Chicago Press, Chicago, 2011).
- [28] F. Bourguignon and C. Morrisson, *Am. Econ. Rev.* **92**, 727 (2002).
- [29] R. J. Shiller, *Finance and the Good Society* (PUP, Princeton, 2012).
- [30] N. G. Mankiw, *Principles of Economics*, 6th ed. (South-Western Cengage Learning, Mason OH, 2011).
- [31] J. Bardeen and W. H. Brattain, *Phys. Rev.* **74**, 230 (1948); W. B. Shockley, *US Patent 2569347* (1951) assignee: Bell Telephone Labor.
- [32] J. S. Kilby, *IEEE Trans. Electron Dev.* **23**, 648 (1976); R. N. Noyce, *US Patent 2981877* (1961) assignee: Fairchild Semiconductor.
- [33] T. Berners-Lee, *Sci. Am.* **303** (6), 80 (2010).
- [34] P. Coles, T. Cox, C. Mackey, and S. Richardson, *The Toxic Terabyte* (IBM United Kingdom, London, 2006).
- [35] T. L. Friedman, *The New York Times* **Feb 22, 2014**, <http://www.nytimes.com/2014/02/23/opinion/sunday/friedman-how-to-get-a-job-at-google.html> (Accessed 23 Feb, 2014).
- [36] D. I. Bower, *An Introduction to Polymer Physics* (CUP, Cambridge, 2002).
- [37] G. Strobl, *The Physics of Polymers*, 3rd ed. (Springer, Berlin, 2007).

- [38] R. Zallen, *The physics of amorphous solids* (Wiley, New York, 1998); J. M. Ziman, *Models of Disorder* (CUP, Cambridge, 1979); P. T. Erslev, Ph.D. thesis, University of Oregon, Eugene (2010).
- [39] C. Nayak, *Quantum Condensed Matter Physics* (University of California at Santa Barbara, Santa Barbara, 2011).
- [40] P. W. Anderson, *Basic Notions in Condensed Matter Physics* (Benjamin Cummings, Menlo Park CA, 1984).
- [41] R. B. Laughlin, *Rev. Mod. Phys.* **71**, 863 (1999).
- [42] R. A. L. Jones, *Soft Condensed Matter* (OUP, Oxford, 2002).
- [43] P.-G. de Gennes, *Rev. Mod. Phys.* **64**, 645 (1992).
- [44] G. Gompper and M. Schick, in *Soft Matter*, Vol. 1, edited by G. Gompper and M. Schick (Wiley-VCH, Weinheim, 2006) Chap. An Introduction to Soft Matter, pp. 1–16.
- [45] P.-G. de Gennes, *Scaling Concepts in Polymer Physics* (Cornell University Press, Ithaca, 1979).
- [46] J. des Cloizeaux and G. Jannink, *Polymers in Solution* (Clarendon Press, Oxford, 1990).
- [47] A. J. Heeger, *Rev. Mod. Phys.* **73**, 681 (2001).
- [48] J. C. W. Chien, *Polyacetylene: Chemistry, Physics, and Material Science* (Academic Press, Orlando, 1984).
- [49] H. Shirakawa, *Rev. Mod. Phys.* **73**, 713 (2001), and references therein.
- [50] D. J. Berets and D. S. Smith, *Trans. Faraday Soc.* **64**, 823 (1968).
- [51] T. Ito, H. Shirakawa, and S. Ikeda, *J. Polym. Sci. A Polym. Chem.* **12**, 11 (1974).
- [52] H. Shirakawa, E. J. Louis, A. G. MacDiarmid, C. K. Chiang, and A. J. Heeger, *J. Chem. Soc., Chem. Commun.*, 578 (1977); C. K. Chiang, C. R. Fincher, Y. W. Park, A. J. Heeger, H. Shirakawa, E. J. Louis, S. C. Gau, and A. G. MacDiarmid, *Phys. Rev. Lett.* **39**, 1098 (1977); C. K. Chiang, M. A. Druy, S. C. Gau, A. J. Heeger, E. J. Louis, A. G. MacDiarmid, Y. W. Park, and H. Shirakawa, *J. Am. Chem. Soc.* **100**, 1013 (1978).
- [53] H. Naarmann, *Synth. Met.* **17**, 223 (1987).
- [54] N. Basescu, Z.-N. X. Liu, D. Moses, A. J. Heeger, H. Naarmann, and N. Theophilou, *Nature* **327**, 403 (1987).
- [55] J. Tsukamoto, A. Takahashi, and K. Kawasaki, *Jpn. J. Appl. Phys.* **29**, 125 (1990).
- [56] J. Tsukamoto, *Adv. Phys.* **41**, 509 (1992).
- [57] A. J. Heeger, S. Kivelson, J. R. Schrieffer, and W.-P. Su, *Rev. Mod. Phys.* **60**, 781 (1988).

- [58] S. Barišić, J. Labbé, and J. Friedel, *Phys. Rev. Lett.* **25**, 919 (1970); S. Barišić, *Phys. Rev. B* **5**, 932 (1972); S. Barišić, *Phys. Rev. B* **5**, 941 (1972).
- [59] W. P. Su, J. R. Schrieffer, and A. J. Heeger, *Phys. Rev. Lett.* **42**, 1698 (1979); W. P. Su, J. R. Schrieffer, and A. J. Heeger, *Phys. Rev. B* **22**, 2099 (1980).
- [60] L. W. Shacklette, H. Eckhardt, R. R. Chance, G. G. Miller, D. M. Ivory, and R. H. Baughman, *J. Chem. Phys.* **73**, 4098 (1980).
- [61] W. J. Feast and R. H. Friend, *J. Mater. Sci.* **25**, 3796 (1990).
- [62] Y. Cao, P. Smith, and A. J. Heeger, *Synth. Met.* **48**, 91 (1992).
- [63] C. B. Gorman, E. J. Ginsburg, and R. H. Grubbs, *J. Am. Chem. Soc.* **115**, 1397 (1993).
- [64] J. Janata and M. Josowicz, *Nature Mater.* **2**, 19 (2003); H. Hoppe and N. S. Sariciftci, *J. Mater. Res.* **19**, 1924 (2004); T. Mäkelä, Ph.D. thesis, Åbo Akademi University, Åbo (2008).
- [65] R. H. Friend, R. W. Gymer, A. B. Holmes, J. H. Burroughes, R. N. Marks, C. Taliani, D. D. C. Bradley, D. A. Dos Santos, J. L. Brédas, M. Lögdlund, and W. R. Salaneck, *Nature* **397**, 121 (1999).
- [66] G. Malliaras and R. Friend, *Phys. Today* **58** (5), 53 (2005); G. Yu, J. Gao, J. C. Hummelen, F. Wudl, and A. J. Heeger, *Science* **270**, 1789 (1995).
- [67] A. G. MacDiarmid, *Rev. Mod. Phys.* **73**, 701 (2001), and references therein.
- [68] A. G. MacDiarmid, J.-C. Chiang, A. F. Richter, and A. J. Epstein, *Synth. Met.* **18**, 285 (1987).
- [69] J.-C. Chiang and A. G. MacDiarmid, *Synth. Met.* **13**, 193 (1986).
- [70] F. Wudl, R. O. Angus, F. L. Lu, P. M. Allemand, D. Vachon, M. Nowak, Z. X. Liu, H. Schaffer, and A. J. Heeger, *J. Am. Chem. Soc.* **109**, 3677 (1987).
- [71] S. Stafström, J. L. Brédas, A. J. Epstein, H. S. Woo, D. B. Tanner, W. S. Huang, and A. G. MacDiarmid, *Phys. Rev. Lett.* **59**, 1464 (1987), and references therein.
- [72] M. Gosh, A. Barman, A. K. Meikap, S. K. De, and S. Chatterjee, *Phys. Lett. A* **260**, 138 (1999).
- [73] Y. Haba, E. Segal, M. Narkis, G. I. Titelman, and A. Siegmann, *Synth. Met.* **106**, 59 (1999); M. G. Han, S. K. Cho, S. G. Oh, and S. S. Im, *Synth. Met.* **126**, 53 (2002); Y.-G. Han, T. Kusunose, and T. Sekino, *Synth. Met.* **159**, 123 (2009).
- [74] P. Atkins and J. de Paula, *Physical Chemistry*, 8th ed. (W. H. Freeman and Co., New York, 2006); D. Myers, *Surfactant Science and Technology*, 3rd ed. (Wiley, Hoboken NJ, 2006).
- [75] T. F. Tadros, *Applied Surfactants* (Wiley-VCH, Weinheim, 2005).
- [76] B.-H. Lee, *J. Kor. Chem. Soc.* **40**, 420 (1996).

- [77] K. Tsujii, N. Saito, and T. Takeuchi, *J. Phys. Chem.* **84**, 2287 (1980).
- [78] M. J. Rosen, *Surfactants and Interfacial Phenomena*, 3rd ed. (Wiley, Hoboken NJ, 2004).
- [79] P. Mukerjee and K. J. Mysels, *Critical Micelle Concentration of Aqueous Surfactant Systems*, Tech. Rep. NSRDS-NBS 36 (National Bureau of Standards, Washington DC, 1971).
- [80] W.-K. Chu, J. W. Mayer, and M.-A. Nicolet, *Backscattering Spectroscopy* (Academic Press, New York, 1978).
- [81] *SIGMACALC calculator*, available at <http://www.surreyibc.ac.uk/sigmacalc/>.
- [82] IAEA, *Instrumentation for PIXE and RBS*, Tech. Rep. IAEA-TECDOC 1190 (International Atomic Energy Agency, Vienna, 2000).
- [83] A. F. Gurbich, *Nucl. Instrum. Meth. B* **229**, 157 (2005).
- [84] A. F. Gurbich, *Nucl. Instrum. Meth. B* **266**, 1193 (2008).
- [85] A. F. Gurbich, *Nucl. Instrum. Meth. B* **261**, 401 (2007).
- [86] H. Kamimura, in *Electron-Electron Interactions in Disordered Systems*, Modern Problems in Condensed Matter Sciences, Vol. 10, edited by A. L. Efros and M. Polak (North Holland, Amsterdam, 1985) Chap. Electron-electron interactions in the Anderson-localised regime near the metal-insulator transition, pp. 555–617, and references therein.
- [87] M. M. Fogler, S. Teber, and B. I. Shklovskii, *Phys. Rev. B* **69**, 035413 (2004).
- [88] M. Novak, I. Kokanović, D. Babić, M. Baćani, and A. Tonejc, *Synth. Met.* **159**, 649 (2009).
- [89] R. Guinebretière, *X-ray Diffraction by Polycrystalline Materials* (ISTE, London, 2007).
- [90] M. Novak, Ph.D. thesis, Sveučilište u Zagrebu, Zagreb (2010).
- [91] H. Alloul, *Introduction to the Physics of Electrons in Solids* (Springer, Berlin, 2011).
- [92] P. W. Anderson, *Phys. Rev.* **109**, 1492 (1958).
- [93] R. Abou-Chacra, D. J. Thouless, and P. W. Anderson, *J. Phys. C* **6**, 1734 (1973).
- [94] T. Giamarchi, *Chem. Rev.* **104**, 5037 (2004).
- [95] K. Byczuk, W. Hofstetter, and D. Vollhardt, *Phys. Rev. Lett.* **94**, 056404 (2005).
- [96] N. F. Mott, *Metal-Insulator Transitions*, 2nd ed. (Taylor & Francis, London, 1990).
- [97] N. F. Mott and W. D. Twose, *Adv. Phys.* **10**, 107 (1961).
- [98] P. W. Anderson, *Rev. Mod. Phys.* **50**, 191 (1978).

- [99] P. A. Lee and T. V. Ramakrishnan, *Rev. Mod. Phys.* **57**, 287 (1985).
- [100] N. F. Mott and E. A. Davis, *Electronic Processes in Non-Crystalline Materials*, 2nd ed. (Clarendon Press, Oxford, 1979).
- [101] J. Fröhlich and T. Spencer, *Commun. Math. Phys.* **88**, 151 (1983).
- [102] A. F. Ioffe and A. R. Regel, *Prog. Semicond.* **4**, 237 (1960).
- [103] P. W. Anderson, *Comments Solid State Phys.* **2**, 193 (1970).
- [104] N. F. Mott, *Adv. Phys.* **16**, 49 (1967).
- [105] B. Simon, *J. Stat. Phys.* **38**, 65 (1985); W. Kirsch and B. Simon, *J. Stat. Phys.* **42**, 799 (1986).
- [106] E. Abrahams, P. W. Anderson, D. C. Licciardello, and T. V. Ramakrishnan, *Phys. Rev. Lett.* **42**, 673 (1979).
- [107] T. Giamarchi and H. J. Schulz, *Phys. Rev. B* **37**, 325 (1988).
- [108] S. Roth and D. Carroll, *One-Dimensional Metals: Conjugated Polymers, Organic Crystals, Carbon Nanotubes*, 2nd ed. (Wiley-VCH, Weinheim, 2004).
- [109] S. Teber, *Eur. Phys. J. B* **49**, 289 (2006).
- [110] A. A. Gogolin, V. I. Mel'nikov, and E. I. Rashba, *Sov. Phys. JETP* **42**, 168 (1975).
- [111] C. L. Kane and M. P. A. Fisher, *Phys. Rev. B* **46**, 15233 (1992).
- [112] D. M. Basko, I. L. Aleiner, and B. L. Altshuler, *Ann. Phys.* **321**, 1126 (2006).
- [113] B. Sapoval and C. Hermann, *Physics of Semiconductors* (Springer, New York, 1995).
- [114] B. I. Shklovskii and A. L. Efros, *Electronic Properties of Doped Semiconductors* (Springer, Berlin, 1984).
- [115] B. D. Simons, *Quantum Condensed Matter Physics, Michaelmas Term 2004*, Lecture Notes: University of Cambridge, <http://www.tcm.phy.cam.ac.uk/~bds10/grad.lec.html> (Accessed 22 Mar, 2008).
- [116] P. A. Lee, *8.512 Theory of Solids II, Spring 2009*, MIT OpenCourseWare: Massachusetts Institute of Technology, <http://ocw.mit.edu/courses/physics/8-512-theory-of-solids-ii-spring-2009> (Accessed 5 Feb, 2012).
- [117] V. F. Gantmakher, *Electrons and Disorder in Solids* (OUP, Oxford, 2005).
- [118] J. J. van Hapert, Ph.D. thesis, Universiteit Utrecht, Utrecht (2002).
- [119] A. Miller and E. Abrahams, *Phys. Rev.* **120**, 745 (1960).
- [120] M. Pollak and I. Riess, *J. Phys. C* **9**, 2339 (1976).
- [121] N. F. Mott, *J. Non-Cryst. Solids* **1**, 1 (1968).
- [122] N. F. Mott, *Philos. Mag.* **19**, 835 (1969).

- [123] S. Baranovski and O. Rubel, in *Charge Transport in Disordered Solids with Applications in Electronics*, edited by S. Baranovski (Wiley, Chichester, 2006) Chap. Description of Charge Transport in Amorphous Semiconductors, pp. 49–96; N. F. Mott, *J. Phys. C* **13**, 5433 (1980).
- [124] N. Apsley and H. P. Hughes, *Philos. Mag.* **30**, 963 (1974).
- [125] J. Kurkijärvi, *Phys. Rev. B* **8**, 922 (1973).
- [126] A. J. Epstein, W.-P. Lee, and V. N. Prigodin, *Synth. Met.* **117**, 9 (2001).
- [127] V. K. S. Shante, C. M. Varma, and A. N. Bloch, *Phys. Rev. B* **8**, 4885 (1973).
- [128] V. Ambegaokar, B. I. Halperin, and J. S. Langer, *Phys. Rev. B* **4**, 2612 (1971).
- [129] A. L. Efros and B. I. Shklovskii, *J. Phys. C* **8**, L49 (1975).
- [130] A. L. Efros, B. Skinner, and B. I. Shklovskii, *Phys. Rev. B* **84**, 064204 (2011).
- [131] A. I. Larkin and D. E. Khmel'nitskii, *Sov. Phys. JETP* **56**, 647 (1982).
- [132] S. Teber, *private communication* (2013).
- [133] R. Menon, C. O. Yoon, D. Moses, and A. J. Heeger, in *Handbook of Conducting Polymers*, edited by T. A. Skotheim, R. L. Elsenbaumer, and J. R. Reynolds (Marcel Dekker, New York, 1998) 2nd ed., Chap. Metal-Insulator Transition in Doped Conducting Polymers, pp. 27–84.
- [134] A. J. Heeger, *Phys. Scr.* **2002**, 30 (2002).
- [135] W. L. McMillan, *Phys. Rev. B* **24**, 2739 (1981).
- [136] A. S. Rodin and M. M. Fogler, *Phys. Rev. Lett.* **105**, 106801 (2010).
- [137] A. N. Aleshin, H. J. Lee, Y. W. Park, and K. Akagi, *Phys. Rev. Lett.* **93**, 196601 (2004).
- [138] A. Rahman and M. K. Sanyal, *J. Phys. Condens. Matter* **22**, 175301 (2010).
- [139] J. D. Yuen, R. Menon, N. E. Coates, E. B. Namdas, S. Cho, T. H. Scott, D. Moses, and A. J. Heeger, *Nature Mater.* **8**, 572 (2009).
- [140] J. H. Worne, J. E. Anthony, and D. Natelson, *Appl. Phys. Lett.* **96**, 053308 (2010).
- [141] K. Lee, S. Cho, S. H. Park, A. J. Heeger, C.-W. Lee, and S.-H. Lee, *Nature* **441**, 65 (2006).
- [142] S.-H. Lee, D.-H. Lee, K. Lee, and C.-W. Lee, *Adv. Funct. Mater.* **15**, 1495 (2005).
- [143] G. Blatter, M. V. Feigel'man, V. B. Geshkenbein, A. I. Larkin, and V. M. Vinokur, *Rev. Mod. Phys.* **66**, 1125 (1994).
- [144] A. B. Kaiser, *Rep. Prog. Phys.* **64**, 1 (2001).
- [145] A. N. Aleshin, S. R. Williams, and A. J. Heeger, *Synth. Met.* **94**, 173 (1997).

- [146] D. Chaudhuri, A. Kumar, R. Nirmla, D. D. Sarma, M. García-Hernández, L. S. S. Chandra, and V. Ganesan, *Phys. Rev. B* **73**, 075205 (2006).
- [147] S. Maji, S. Mukhopadhyay, R. Gangopadhyay, and A. De, *Phys. Rev. B* **75**, 073202 (2007).
- [148] P. Sheng, B. Abeles, and Y. Arie, *Phys. Rev. Lett.* **31**, 44 (1973).
- [149] Z. H. Wang, C. Li, E. M. Scherr, A. G. MacDiarmid, and A. J. Epstein, *Phys. Rev. Lett.* **66**, 1745 (1991); Z. H. Wang, E. M. Scherr, A. G. MacDiarmid, and A. J. Epstein, *Phys. Rev. B* **45**, 4190 (1992).
- [150] L. Zuppiroli, M. N. Bussac, S. Paschen, O. Chauvet, and L. Forró, *Phys. Rev. B* **50**, 5196 (1994).
- [151] M. Novak, I. Kokanović, D. Babić, and M. Baćani, *J. Non-Cryst. Solids* **356**, 1725 (2010).
- [152] C. C. Bof Bufon and T. Heinzl, *Phys. Rev. B* **76**, 245206 (2007); M. Ghosh, A. K. Meikap, S. K. Chattopadhyay, and S. Chatterjee, *J. Phys. Chem. Solids* **62**, 475 (2001).
- [153] A. G. Zabrodskii and K. N. Zinov'eva, *Sov. Phys. JETP* **59**, 425 (1984).
- [154] M. Novak, I. Kokanović, M. Baćani, and D. Babić, *Eur. Phys. J. B* **83**, 57 (2011).
- [155] A. B. Kaiser, *Adv. Mater.* **13**, 927 (2001).
- [156] J. P. Pouget, M. E. Jozefowicz, A. J. Epstein, X. Tang, and A. G. MacDiarmid, *Macromolecules* **24**, 779 (1991).
- [157] S. Blundell, *Magnetism in Condensed Matter* (OUP, Oxford, 2001).
- [158] R. P. Feynman, R. B. Leighton, and M. Sands, *The Feynman Lectures on Physics, Vol. 2* (Addison-Wesley, Reading MA, 1977).
- [159] A. Aharoni, *Introduction to the Theory of Ferromagnetism*, 2nd ed. (OUP, Oxford, 2000).
- [160] J. M. D. Coey, *Magnetism and Magnetic Materials* (CUP, Cambridge, 2009).
- [161] A. V. Nikolaev and B. Verberck, in *Carbon-Based Magnetism – An Overview of the Magnetism of Metal Free Carbon-Based Compounds and Materials*, edited by T. Makarova and F. Palacio (Elsevier, Amsterdam, 2006) Chap. Diamagnetism of Diamond and Graphite, pp. 245–278; S. Hudgens, M. Kastner, and H. Fritzsche, *Phys. Rev. Lett.* **33**, 1552 (1974).
- [162] G. Auletta, M. Fortunato, and G. Parisi, *Quantum Mechanics* (CUP, Cambridge, 2009).
- [163] J. D. Jackson, *Classical Electrodynamics*, 3rd ed. (Wiley, Hoboken NJ, 1999).
- [164] A. Mattuck, *Introduction to Analysis* (Prentice Hall, Upper Saddle River NJ, 1999).

- [165] C. P. Slichter, *Principles of Magnetic Resonance*, 3rd ed. (Springer, Berlin, 1989).
- [166] M. de Podesta, *Understanding the Properties of Matter*, 2nd ed. (Taylor & Francis, London, 2002).
- [167] R. Kubo, *Statistical Mechanics*, 2nd ed. (North Holland, Amsterdam, 1988).
- [168] J. Kübler, *Theory of Itinerant Electron Magnetism* (OUP, Oxford, 2010).
- [169] P. K. Kahol, W. G. Clark, and M. Mehring, in *Conjugated Conducting Polymers*, Springer Series in Solid-State Sciences, Vol. 102, edited by H. G. Kiess (Springer, Berlin, 1992) Chap. Magnetic Properties of Conjugated Polymers, pp. 217–304.
- [170] R. Skomski, *Simple Models of Magnetism* (OUP, Oxford, 2008).
- [171] H. Aoki and H. Kamimura, *The Physics of Interacting Electrons in Disordered Systems* (Clarendon Press, Oxford, 1990), and references therein.
- [172] T. A. Kaplan, S. D. Mahanti, and W. M. Hartmann, *Phys. Rev. Lett.* **27**, 1796 (1971).
- [173] M. A. Kanehisa and H. Kamimura, *J. Phys. Soc. Jpn.* **34**, 44 (1973); H. Aoki and H. Kamimura, *J. Phys. Soc. Jpn.* **39**, 1169 (1975).
- [174] H. Kamimura and E. Yamaguchi, *Solid State Commun.* **28**, 127 (1978); E. Yamaguchi, H. Aoki, and H. Kamimura, *J. Phys. C* **12**, 4801 (1979); E. Yamaguchi, H. Aoki, and H. Kamimura, *J. Non-Cryst. Solids* **35-36**, 47 (1980).
- [175] V. Čápek, *Phys. Status Solidi B* **55**, K55 (1973).
- [176] P. Phillips, *Phys. Rev. B* **49**, 4303 (1994).
- [177] N. S. Sariciftci, A. J. Heeger, and Y. Cao, *Phys. Rev. B* **49**, 5988 (1994).
- [178] A. Kurobe and H. Kamimura, *J. Phys. Soc. Jpn.* **51**, 1904 (1982).
- [179] A. Natori and H. Kamimura, *Prog. Theor. Phys. Suppl.* **69**, 353 (1980).
- [180] A. J. Heeger, *Polym. J.* **17**, 201 (1985), and references therein. S. A. Brazovskii and N. N. Kirova, *JETP Lett.* **33**, 4 (1981); K. Fesser, A. R. Bishop, and D. K. Campbell, *Phys. Rev. B* **27**, 4804 (1983).
- [181] A. J. Epstein, R. W. Bigelow, H. Rommelmann, H. W. Gibson, R. J. Weagley, A. Feldblumt, D. B. Tanner, J. P. Pouget, J. C. Pouxviel, R. Comes, P. Robin, and S. Kivelson, *Mol. Cryst. Liq. Cryst.* **117**, 147 (1985).
- [182] S. Stafström, J. L. Brédas, A. J. Epstein, H. S. Woo, D. B. Tanner, W. S. Huang, and A. G. MacDiarmid, *Phys. Rev. Lett.* **59**, 1464 (1987).
- [183] J. M. Ginder, A. F. Richter, A. G. MacDiarmid, and A. J. Epstein, *Solid State Commun.* **63**, 97 (1987).
- [184] Y. Onodera, *Phys. Rev. B* **30**, 775 (1984).
- [185] S. Kivelson and A. J. Heeger, *Phys. Rev. Lett.* **55**, 308 (1985).

- [186] M. Nechtschein, in *Organic conductors: fundamentals and applications*, edited by J.-P. Farges (Marcel Dekker, New York, 1994) Chap. Doped Conjugated Polymers: Conducting Polymers, pp. 647–689.
- [187] P. K. Kahol, *Solid State Commun.* **124**, 93 (2002); P. K. Kahol, A. Raghunathan, and B. J. McCormick, *Synth. Met.* **140**, 261 (2004).
- [188] F. Genoud, M. Guglielmi, M. Nechtschein, E. Genies, and M. Salmon, *Phys. Rev. Lett.* **55**, 118 (1985).
- [189] O. Chauvet, S. Paschen, L. Forró, L. Zuppiroli, P. Bujard, K. Kai, and W. Wernet, *Synth. Met.* **63**, 115 (1994).
- [190] O. Chauvet, S. Paschen, M. N. Bussac, and L. Zuppiroli, *Europhys. Lett.* **26**, 619 (1994); M. N. Bussac and L. Zuppiroli, *Phys. Rev. B* **47**, 5493 (1993); P. K. Kahol, W. R. Spencer, N. J. Pinto, and B. J. McCormick, *Phys. Rev. B* **50**, 18647 (1994).
- [191] G. A. Olah, *Angew. Chem. Int. Ed. Engl.* **34**, 1393 (1995); G. L. Miessler and D. A. Tarr, *Inorganic Chemistry*, 3rd ed. (Prentice Hall, Upper Saddle River NJ, 2003); G. A. Olah, G. K. S. Prakash, and J. Sommer, *Science* **206**, 13 (1979).
- [192] F. Moraes, D. Davidov, M. Kobayashi, T. C. Chung, J. Chen, A. J. Heeger, and F. Wudl, *Synth. Met.* **10**, 169 (1985).
- [193] H. Fukutome, A. Takahashi, and M. Ozaki, *Chem. Phys. Lett.* **133**, 34 (1987).
- [194] A. M. S. Macêdo, M. C. dos Santos, M. D. Coutinho-Filho, and C. A. Macêdo, *Phys. Rev. Lett.* **74**, 1851 (1995), and references therein.
- [195] J. N. Devine, J. A. Crayston, and J. C. Walton, *Synth. Met.* **103**, 2294 (1999); K. Yoshizawa, K. Tanaka, T. Yamabe, and J. Yamauchi, *J. Chem. Phys.* **96**, 5516 (1992); A. A. Correa, L. Walmsley, L. O. S. Bulhões, W. A. Ortiz, A. J. A. de Oliveira, and E. C. Pereira, *Synth. Met.* **121**, 1836 (2001); O. R. Nascimento, A. J. A. de Oliveira, A. A. Correa, L. O. S. Bulhões, E. C. Pereira, V. M. Souza, and L. Walmsley, *Phys. Rev. B* **67**, 144422 (2003); O. R. Nascimento, A. J. A. de Oliveira, E. C. Pereira, A. A. Correa, and L. Walmsley, *J. Phys. Condens. Matter* **20**, 035214 (2008).
- [196] K. Yoshizawa, A. Takata, K. Tanaka, and T. Yamabe, *Polym. J.* **24**, 857 (1992).
- [197] A. Rajca, J. Wongsriratanakul, and S. Rajca, *Science* **294**, 1503 (2001).
- [198] M. McElfresh, *Fundamentals of Magnetism and Magnetic Measurements - Featuring Quantum Design's Magnetic Property Measurement System* (Quantum Design, San Diego, 1994).
- [199] G. A. Bain and J. F. Berry, *J. Chem. Educ.* **85**, 532 (2008), and references therein.
- [200] J. H. van Vleck, *The Theory of Electric and Magnetic Susceptibilities* (Clarendon Press, Oxford, 1932).
- [201] L. Pauling, *Proc. R. Soc. A* **114**, 181 (1927).
- [202] G. Foëx, in *Tables de Constantes et Données Numériques* (Masson, Paris, 1957) Chap. Constantes Sélectionnées Diamagnétisme et Paramagnétisme, pp. 222–226.

- [203] P. K. Kahol, *Phys. Rev. B* **62**, 13803 (2000).
- [204] A. Raghunathan, P. K. Kahol, J. C. Ho, Y. Y. Chen, Y. D. Yao, Y. S. Lin, and B. Wessling, *Phys. Rev. B* **58**, R15955 (1998).
- [205] D. Chaudhuri, A. Kumar, D. D. Sarma, M. García-Hernández, J. P. Joshi, and S. V. Bhat, *Appl. Phys. Lett.* **82**, 1733 (2003).
- [206] Y. Cao and A. J. Heeger, *Synth. Met.* **52**, 193 (1992).
- [207] N. J. Pinto, P. K. Kahol, B. J. McCormick, N. S. Dalal, and H. Wan, *Phys. Rev. B* **49**, 13983 (1994).
- [208] J. A. Reedijk, H. C. F. Martens, H. B. Brom, and M. A. J. Michels, *Phys. Rev. Lett.* **83**, 3904 (1999).
- [209] Q. Li, L. Cruz, and P. Phillips, *Phys. Rev. B* **47**, 1840 (1993).
- [210] A. J. Epstein, J. M. Ginder, F. Zuo, R. W. Bigelow, H.-S. Woo, D. B. Tanner, A. F. Richter, W.-S. Huang, and A. G. MacDiarmid, *Synth. Met.* **21**, 63 (1987).
- [211] D. L. Stein and C. M. Newman, *Spin Glasses and Complexity* (PUP, Princeton, 2013).
- [212] D. L. Stein and C. M. Newman, *Complex Syst.* **20**, 115 (2011).
- [213] T. Takemori and H. Kamimura, *Solid State Commun.* **41**, 885 (1982).
- [214] V. Dobrosavljević, D. Tanasković, and A. A. Pastor, *Phys. Rev. Lett.* **90**, 016402 (2003).
- [215] B. Batlogg and K. Prša, *private communication* (2011).
- [216] W. Barford, *Electronic and Optical Properties of Conjugated Polymers* (Clarendon Press, Oxford, 2005).
- [217] V. Dobrosavljević, in *Conductor-Insulator Quantum Phase Transitions*, edited by V. Dobrosavljević, N. Trivedi, and J. M. Valles Jr. (OUP, Oxford, 2012) Chap. Introduction to Metal-Insulator Transitions, pp. 3–63.
- [218] E. Miranda and V. Dobrosavljević, in *Conductor-Insulator Quantum Phase Transitions*, edited by V. Dobrosavljević, N. Trivedi, and J. M. Valles Jr. (OUP, Oxford, 2012) Chap. Dynamical mean-field theories of correlation and disorder, pp. 161–243.
- [219] K. Mizoguchi, M. Nechtschein, J.-P. Travers, and C. Menardo, *Phys. Rev. Lett.* **63**, 66 (1989).
- [220] E. V. Anslyn and D. A. Dougherty, *Modern Physical Organic Chemistry* (University Science Books, Sausalito CA, 2005).
- [221] S. Lee, *Polymer Blend and Composites*, Ohio University, <http://www.ohio.edu/people/lees1/pblend.html> (Accessed 25 Oct, 2013).
- [222] P. M. Ajayan, O. Stephan, C. Colliex, and D. Trauth, *Science* **265**, 1212 (1994).

- [223] M. Moniruzzaman and K. I. Winey, *Macromolecules* **39**, 5194 (2006); Y. Li, H. Wang, X. Cao, M. Yuan, and M. Yang, *Nanotechnology* **19**, 015503 (2008); P. Yao, J. Xu, Y. Wang, and C. Zhu, *J. Mater. Sci. Mater. Electron.* **20**, 891 (2009); T.-M. Wu and Y.-W. Lin, *Polymer* **47**, 3576 (2006); J. Deng, X. Ding, W. Zhang, Y. Peng, J. Wang, X. Long, P. Li, and A. S. C. Chan, *Eur. Polym. J.* **38**, 2497 (2002); T.-M. Wu, Y.-W. Lin, and C.-S. Liao, *Carbon* **43**, 734 (2005); W. Feng, X. D. Bai, Y. Q. Lian, J. Liang, X. G. Wang, and K. Yoshino, *Carbon* **41**, 1551 (2003).
- [224] B. Philip, J. Xie, J. K. Abraham, and V. K. Varadan, *Polym. Bull.* **53**, 127 (2005).
- [225] G. Z. Chen, M. S. P. Shaffer, D. Coleby, G. Dixon, W. Zhou, D. J. Fray, and A. H. Windle, *Adv. Mater.* **12**, 522 (2000).
- [226] P. J. Flory, *Principles of Polymer Chemistry* (Cornell University Press, Ithaca, 1953).
- [227] T. A. Witten and P. A. Pincus, *Structured Fluids: Polymers, Colloids, Surfactants* (OUP, Oxford, 2010).
- [228] L. Forró and C. Schönenberger, in *Carbon Nanotubes*, edited by M. S. Dresselhaus, G. Dresselhaus, and P. Avorius (Springer, Berlin, 2001) Chap. Physical Properties of Multiwall Nanotubes, pp. 329–391.
- [229] M. F. L. De Volder, S. H. Tawfick, R. H. Baughman, and A. J. Hart, *Science* **339**, 535 (2013); A. Krueger, *Carbon Materials and Nanotechnology* (Wiley-VCH, Weinheim, 2010).
- [230] B. P. Grady, *Carbon Nanotube-Polymer Composites* (Wiley, Hoboken NJ, 2011).
- [231] L. Forró, *Nature* **441**, 414 (2006).
- [232] K. Jiang and S. Li Q. & Fan, *Nature* **419**, 801 (2002); M. Zhang, K. R. Atkinson, and R. H. Baughman, *Science* **306**, 1358 (2004); M. Miao, *Carbon* **49**, 3755 (2011).
- [233] T. P. McAndrew, P. Laurent, M. Havel, and C. Roger, in *Nanotechnology 2008: Materials, Fabrication, Particles, and Characterization - Technical Proceedings of the 2008 NSTI Nanotechnology Conference and Trade Show, Vol. 1* (2008) pp. 47–50.
- [234] S. Bordere, J. M. Corpart, N. E. El Bounia, P. Gaillard, N. Passade-Boupat, P. M. Piccione, and D. Plée, *Industrial Production and Applications of Carbon Nanotubes*, Arkema Inc, <http://www.graphistrength.com> (Accessed 18 Nov, 2013).
- [235] Y. Long, Z. Chen, X. Zhang, J. Zhang, and Z. Liu, *Appl. Phys. Lett.* **85**, 1796 (2004).
- [236] I. Žura, D. Babić, M. D. Steinberg, and I. M. Steinberg, *Sens. Actuat. B* **193**, 128 (2014).
- [237] C. Peng, S. Zhang, D. Jewell, and G. Z. Chen, *Prog. Nat. Sci.* **18**, 777 (2008).
- [238] M. Wu, G. A. Snook, V. Gupta, M. Shaffer, D. J. Fray, and G. Z. Chen, *J. Mater. Chem.* **15**, 2297 (2005).
- [239] H. Lin, L. Li, J. Ren, Z. Cai, L. Qiu, Z. Yang, and H. Peng, *Sci. Rep.* **3**, 1353 (2013).

Curriculum Vitæ

First name | Surname : Mirko Baćani

Address

Physics Department, Faculty of Science, University of Zagreb
Bijenička cesta 32, P.O. Box 331
HR-10002 Zagreb, Croatia

e-mail: mbaćani@phy.hr | telephone: +385 1 460 5550

Born 06 August 1979, in Varaždin, Croatia

Education

1986-1994 Elementary school (in Varaždin)
1994-1998 High school (in Varaždin)
1998-2007 Faculty of Science, University of Zagreb
Jun 2007 **MSc**, Diploma thesis: *Conducting properties of polyaniline doped with 4-dodecylbenzenesulphonic acid*, supervisor: Dr Dinko Babić
2008-2014 PhD student, University of Zagreb
Mar 2014 **PhD** thesis completed and submitted

Research interests

conducting polymers; variable-range hopping; Coulomb gap; applied physics

Position

Since 2008 research and teaching assistant at Physics Department of the Faculty of Science, University of Zagreb.

Teaching experience

Teaching assistant in courses:

- Materials Physics (3rd year course)
- Introduction to Materials Physics (3rd year course)
- General Physics (1st year course)
- Laboratory Exercises in General Physics 1 (2nd year course)
- Laboratory Exercises in General Physics 2 (2nd year course)
- Statistics and Fundamentals of Physical Measurements (1st year course)

Dissemination

3 invited talks at international research institutions:

- Electromagnetic properties of DBSA-doped polyaniline: from fundamentals towards application
Université Paris-Sud 11, Orsay, France (24 June 2013)
- Effects of the Coulomb gap on electrical transport and magnetic properties of doped polyaniline
EPFL, Lausanne, Switzerland (07 June 2011)
- Effects of the Coulomb gap on electrical transport and magnetic properties of doped polyaniline
ETH, Zurich, Switzerland (06 June 2011)

2 contributing talks at a scientific conference / summer school:

- Coupling of spin and charge in polyaniline pellets doped with DBSA
3rd EuroMagNET Summer School, Insel Rügen, Germany (01 October 2012)
- Vežanje spina i naboja u tabletama polianilina dopiranog s HCl ili s DBSA
7th Scientific Meeting of the Croatian Physical Society, Primošten, Croatia (14 October 2011)
This talk was awarded 1st prize in the category “Best talk given by a young scientist”.

List of publications

- 1) M. Baćani, M. Novak, I. Kokanović, D. Babić, *Hopping electron transport in doped polyaniline: An experimental verification of the Fogler-Teber-Shklovskii model*, Synth. Met. **172**, 28 (2013).
- 2) M. Novak, I. Kokanović, M. Baćani, D. Babić, *Interplay of Curie-type and Pauli-type magnetic susceptibilities in HCl-doped polyaniline pellets*, Eur. Phys. J. B **83**, 57 (2011).
- 3) M. Novak, I. Kokanović, D. Babić, M. Baćani, *Influence of disorder on electrical transport and magnetic properties of HCl-doped polyaniline pellets*, J. Non-Cryst. Solids **356**, 1725 (2010).
- 4) D. Babić, M. Baćani, M. Novak, I. Kokanović, *New aspects of variable-range-hopping conductivity in doped polyaniline*, Croat. Chem. Acta **83**, 1 (2010).
- 5) M. Baćani, D. Babić, M. Novak, I. Kokanović, S. Fazinić, *Equilibrium doping of polyaniline by dodecylbenzenesulfonic acid*, Synth. Met. **159**, 2584 (2009).
- 6) M. Novak, I. Kokanović, D. Babić, M. Baćani, A. Tonejc, *Variable-range-hopping exponents 1/2, 2/5 and 1/4 in HCl-doped polyaniline pellets*, Synth. Met. **159**, 649 (2009).

Conference proceedings

- 1) M. Baćani, I. Kokanović, M. Novak, D. Babić, *Effects of the Coulomb gap on electrical transport and magnetic properties of doped polyaniline*, International Conference "Physics of Low-Dimensional Conductors: Problems and Perspectives", Zagreb, 25-28 March 2012 (eds. I. Balog, O. S. Barišić, A. Smontara), 49-49, Institute of Physics, Zagreb (2012)
- 2) M. Baćani, I. Kokanović, M. Novak, D. Babić, S. Fazinić, *Vežanje spina i naboja u tabletama polianilina dopiranog s HCl ili s DBSA*, 7th Scientific Meeting of the Croatian Physical Society, Primošten 2011 (eds. A. Gajović, V. Tokić, M. Zorić, T. Marušćak), 72-72, Croatian Physical Society, Zagreb (2011)

- 3) M. Baćani, M. Novak, I. Kokanović, D. Babić, Coupling of spin and charge in polyaniline pellets doped with HCl or DBSA, 2nd International Symposium: Frontiers in Polymer Science, Lyon, 29-31 May 2011 (eds: B. Charleux, S. S. Z. Cheng, J.-F. Gérard, A. H. E. Müller), 95-95, Elsevier, Oxford (2011)
- 4) M. Baćani, D. Babić, M. Novak, I. Kokanović, S. Fazinić, Karakterizacija polianilina dopiranog dodecilbenzensulfonskom kiselinom, 6th Scientific Meeting of the Croatian Physical Society, Primošten 2009 (eds. H. Buljan and D. Horvatić), 120-120, Croatian Physical Society, Zagreb (2009)
- 5) M. Novak, I. Kokanović, D. Babić, M. Baćani, Usporedba magnetskih i električnih svojstava PANI-HCl-a, 6th Scientific Meeting of the Croatian Physical Society, Primošten 2009 (eds. H. Buljan and D. Horvatić), 103-103, Croatian Physical Society, Zagreb (2009)
- 6) D. Babić, I. Kokanović, M. Novak, M. Baćani, New aspects of variable-range hopping in doped polyaniline, Croatian - Japanese Workshop on Materials Science, Zagreb, 29-30 June 2009 (eds. B. Gumhalter and T. Tadić), 21-21, Institute of Physics and Ruđer Bošković Institute, Zagreb (2009)
- 7) D. Babić, M. Baćani, M. Novak, I. Kokanović, New aspects of variable-range-hopping conductivity in doped polyaniline, Frontiers in Complex Metallic Alloys CMA-Zagreb '08 (ed. A. Smontara), 23-23, Institute of Physics Zagreb and European Network of Excellence, Zagreb (2008)
- 8) M. Novak, I. Kokanović, D. Babić, M. Baćani, Influence of disorder on variable-range-hopping exponents in HCl-doped polyaniline pellets, Ampere NMR School, Poznan/Wierzba, 19-28 June 2008 (ed. S. Jurga), 65-65, Faculty of Physics "Adam Mickiewicz", Poznan (2008)
- 9) M. Novak, M. Baćani, D. Babić, I. Kokanović, Utjecaj strukturalnog nereda na vodljivost dopiranog polianilina, 5th Scientific Meeting of the Croatian Physical Society, Primošten 2007 (eds. A. Dulčić and Z. Glumac), 52-52, Croatian Physical Society, Zagreb (2007)